HARD AND SOFT NANOCOMPOSITES ENABLED BY RATIONALLY DESIGNED NONLINEAR COPOLYMERS DERIVED FROM HIGH FUNCTIONALITY POLYOLS

A Dissertation
Presented to
The Academic Faculty

By

James Iocozzia

In Partial Fulfillment
of the Requirements for the Degree
Doctor of Philosophy in the
School of Materials Science and Engineering

Georgia Institute of Technology

August 2018

HARD AND SOFT NANOCOMPOSITES ENABLED BY RATIONALLY DESIGNED NONLINEAR COPOLYMERS DERIVED FROM HIGH FUNCTIONALITY POLYOLS

Dr. Zhiqun Lin, Advisor
School of Materials Science and Engineering
Georgia Institute of Technology

Dr. Vladimir Tsukruk
School of Materials Science and Engineering
Georgia Institute of Technology

Dr. Dong Qin
School of Materials Science and Engineering
Georgia Institute of Technology

Dr. John Zhang
School of Chemistry and Biochemistry
Georgia Institute of Technology

Dr. Paul Russo
School of Materials Science and Engineering
Georgia Institute of Technology

Date Approved: June 5, 2018

To make a prairie it takes a clover and one bee,

One clover, and a bee.

And revery.

The revery alone will do,

If bees are few.

-Emily Dickinson

To my family, my friends, and my better half

for supporting me in my one and only marathon

…*Nike!*

ACKNOWLEDGMENTS

I wish to thank my advisor, Professor Zhiqun Lin, for his unending support, encouragement, and above all else fairness. Day by day and year by year, Dr. Lin's hard work both in the group and for the group have seen it grow and flourish both in terms of talented researchers, technical capabilities, and ultimate impact within the fields of polymers, nanomaterials, and energy capture and storage among others. He has given me many opportunities to contribute to and participate in the entire academic experience in the form of proposals, reviews, conferences, and visiting fellowships while simultaneously giving me the freedom and flexibility to work on areas that interest me.

I would also like to thank the National Defense Science and Engineering Graduate Fellowship for supporting me as an NDSEG Fellow during my doctoral program and the National Science Foundation-East Asian Summer Pacific Institute Fellowship (NSF-EAPSI) for supporting me as a visiting doctoral fellow in Japan.

I thank my thesis committee; Professor Dong Qin, Professor Paul Russo, Professor Vladimir Tsukruk, and Professor John Zhang for their time and advice throughout my doctoral work.

I thank the members of my research group for their mentoring during my doctoral research. Professor Xinchang Pang and Professor Hui Xu were especially helpful with teaching me various essential chemical techniques including ATRP and click chemistry. I thank Dr. Chaowei Feng, Dr. Beibei Jiang, Dr. Yanjie He, Young Jun Yoon, Zewei Wang, Dr. Yihuang Chen, and Professor Jaehan Jung for their support and help addressing problems.

TABLE OF CONTENTS

LIST OF TABLES

LIST OF FIGURES

LIST OF SYMBOLS AND ABBREVIATIONS

^{1}H-NMR	Proton nuclear magnetic resonance imaging
4BMBC	4-bromomethylbenzoyl chloride
5CB	4-cyano-4'-pentylbiphenyl
AFM	Atomic force microscopy
AIBN	Azobisisobutyronitrile
ALD	Atomic layer deposition
ARGET	Activator regenerated by electron transfer
ATRP	Atom-transfer radical polymerization
BA	Benzyl alcohol
BDY	2,2-bipyridyl
BIBB	2-bromo-2-methylpropionyl bromide
BTBA	Borane *tert*-butylamine complex
CNBP	4-isocyano-4'-(prop-2-yn-1-yloxy)biphenyl
CTAB	Cetyltrimethylammonium bromide
CuAAC	Copper-catalyzed azide-alkyne coupling
CVD	Chemical vapor deposition
D	Dendritic unit
DB	Degree of branching
DCM	Dichloromethane
DI	Deionized water
DLS	Dynamic light scattering
DMF	Dimethylformamide
DMSO	Dimethylsulfoxide
DP	Degree of polymerization
eATRP	Electrochemical atom-transfer radical polymerization
EtOAc	Ethyl acetate
FT-IR	Fourier transform infrared spectroscopy
GPC	Gel permeation chromatography
HPG	Hyperbranched polyglycerol
HPG-4BMBe	HPG-4-bromomethyl benzoyl ester
HPG-4-N_3-MBE	HPG-azidomethyl benzoyl ester
HPG-*b*-PS	Star-like hyperbranched polyglycerol-*block*-polystyrene
HPG-Br	Brominated hyperbranched polyglycerol
IG^{13}CNMR	Inverse-gated carbon nuclear magnetic resonance imaging
L_{13}	Linear-13 unit
L_{14}	Linear-14 unit
LbL	Layer-by-layer
LC	Liquid crystal
LSPR	Local surface plasmon resonance
MALDI-TOF	Matrix-assisted laser desorption ionization spectroscopy-time of flight

MeOH	Methanol
MI	Macroinitiator
M-IPA	1-methoxy-2-propanol
M_n	Number average molecular weight
M_w	Weight average molecular weight
NaOMe	Sodium methoxide
NMP	Nitroxide mediated polymerization
NP	Nanoparticle
NP-LC	Nanoparticle-liquid crystal nanocomposite
P3EEET	2,2-(ethoxyethoxy)ethoxy-modified polythiophene
P3HT	Poly(3-hexylthiophene)
P4VP	Poly(4-vinyl pyridine)
PAA-CNBP	Poly(acrylic acid-CNBP)
PDI	Polydispersity index
PEG	Poly(ethylene glycol)
PEO	Poly(ethylene oxide)
PET	Petroleum ether
PI-2555	Polyimide
PLA	Poly(L-lactic acid)
PMDETA	N,N,N',N'',N''-pentamethyldiethylenetriamine
PMMA	Poly(methyl methacrylate)
POSS	Polyhedral oligomeric silsesquioxane
PRE	Persistent radical effect
PS	Polystyrene
P*t*BA	Poly(*tert*-butyl acrylate)
PVA	Poly(vinyl alcohol)
QD	Quantum dot
RAFT	Reversible addition fragmentation chain transfer polymerization
ROMBP	Ring opening multibranching polymerization
SARA	Supplemental activators and reducing agents
SCVP	Self-condensing vinyl polymerization
SFRP	Stable free radical polymerization
SMA	Slow monomer addition
Styrene	St
T	Terminal unit
*t*BA	*Tert*-butyl acrylate
TEM	Transmission electron microscopy
THF	Tetrahydrofuran
TFA	Trifluoroacetic acid
TMP	1,1,1-tris(hydroxymethyl)propane
TMS	Tetramethylsilane
T_{NI}	Nematic-to-isotropic transition temperature
UV-vis	Ultraviolet-visible spectroscopy
XRD	X-ray diffraction
β-CD	Beta-cyclodextrin

SUMMARY

Controlled living polymerization techniques, such as atom-transfer radical polymerization (ATRP) and reversible addition-fragmentation chain transfer polymerization (RAFT), have enabled the synthesis of well-defined monodisperse polymer structures possessing many different compositions including telechelic (chain end) and pendant (side chain) functionality amenable to post polymerization modification by various approaches. One such approach is the immensely useful class of reactions known as “click” chemistry that enables many different materials to be easily connected to each other in high yield and under mild conditions. The most popular click chemistry approach is copper-catalyzed azide-alkyne click chemistry (CuAAC).

In parallel, the rational design and synthesis of high functionality polyols such as cyclodextrins and hyperbranched polyglycerols (HPG) has offered the opportunity to produce many new, complex and highly nonlinear polymer architectures. Only in the last fifteen years have the techniques for producing HPG via anionic ring-opening multibranching polymerization (ROMBP) improved to the point where samples of sufficiently controlled molecular weight and low polydispersity have been realized. Consequently, these and related high functionality polyols can be used as polymer macroinitiators in conjunction with ATRP to produce densely-packed polymer and copolymer structures spanning multiple dimensions and length scales with useful shapes and retained functionalities with many immediate applications in nanoscale materials science and technology.

HPG, and related polyol-based star-like copolymers, can be used as nanoreactors for the synthesis of varied nanocrystalline (hard) and wholly polymeric (soft) nanomaterials. This is because the globular structure, dense surface arms, and retained functionality naturally lend themselves to the production of nanoparticle structures of various types. More importantly, HPG carries several advantages over established polyols including the ability to control the degree of functionality and polymer size. In addition, HPG possesses inherent biocompatibility and functionality owing to the numerous ether groups present within its structure.

This dissertation investigates the synthesis of well-defined β-cyclodextrin and HPG-based star-like polymers and copolymers produced by ATRP in conjunction with CuAAC click chemistry and other surface chemistries for applications in three key areas: (1) Promesogen-capped β-cyclodextrin-based star-like polymer templates for improved inorganic dispersion in liquid crystal solution; (2) HPG-based dense star-like polymer templates for the production of functional inorganic (hard) nanomaterials with retained nanoscale properties and solubility; (3) Azido-HPG hyperbranched polymers for producing biocompatible, wholly polymeric (soft) nanoparticles. These areas of fundamental research are related through their use of high functionality polyols, ATRP and simple, robust linker chemistries to produce novel and useful nanomaterials for applications in displays, optics, ferroelectrics, and biomaterials among others by varying the types of polymers grown, the surface moieties attached and the methods of crosslinking. The specific details of each of these research areas are summarized below.

First, a β-cyclodextrin-based promesogen-capped star-like polymer template (21-arm star-like poly(acrylic acid)-CNBP) was produced by a combination of ATRP and

click chemistry. The CNBP capping moiety (4-isocyano-4'-(prop-2-yn-1-yloxy)biphenyl) is structurally similar to cyanobiphenyl-type liquid crystals, such as 5CB, commonly encountered in LCD displays. The inner poly(acrylic acid) (PAA) core of the polymer is used to template superparamagnetic iron oxide nanoparticles (Fe_3O_4) within the core. This leads to iron oxide nanoparticles capped with the CNBP promesogen molecules. The advantages of this approach to producing liquid crystal-capped nanoparticles are twofold. First, the resulting CNBP-capping molecules are covalently tethered to the inner core. This improved the stability of the overall nanocomposite as the ligands cannot readily detach under elevated temperatures or changes in pH. Second, the inner PAA core can be used to template many other inorganic nanomaterials in the future making this approach highly generalizable. This star-like polymer template successfully enabled the formation of superparamagnetic iron oxide nanoparticles and showed good dispersion in liquid crystal solvents at useful loading percentages for property improvement. The aim of this polymer-based templating strategy is to incorporate such templated nanomaterials into LC displays to reduce the switching voltage and increase the switching speed, thus producing low energy, high performance display technologies.

Second, an HPG-*b*-polystyrene star-like polymer template (HPG-*b*-PS) was produced using ring-opening multibranching polymerization (ROMBP) and ATRP. Various batches were crafted possessing different numbers of arms with different lengths. The templating abilities of the various batches were investigated under different reaction conditions. HPG-based templates can successfully template Au nanoparticles through coordination between the inner ether moieties of HPG and the inorganic precursor molecules while the outer PS-arms stabilize and isolate the nanoparticles during

formation and thereafter. By adjusting these parameters it was discovered that a critical arm length is required to stabilize templated Au nanoparticles of a given size in solution. It was also found that an optimal solvent composition existed wherein distinct and well-dispersed nanoparticles can be produced. Nanomaterials templated herein demonstrated excellent long term solubility and stability in organic solvents while also retaining their desirable nanoscale properties. The HPG-*b*-PS template has been successfully applied to directing the growth of Ag and Fe_3O_4 nanoparticles as well with similar stability measures. The aim of the solution-based HPG-*b*-PS templating strategy is to extend its use to templating other well-defined industrially-relevant metal oxides that currently can only be produced in energy intensive hydrothermal techniques yielding irregular shapes.

Third, azide-functionalized HPG is synthesized (HPG-4-N_3-MBE) for use in the production of wholly polymeric soft nanoparticles. This is achieved by UV-induced activation of azides to highly reactive nitrene intermediates that can combine with each other to form stable azo crosslinks. By performing the UV-induced crosslinking in a dilute regime, it is possible to promote intramolecular crosslinking to yield small unimolecular and multimolecular particles that remain well dispersed in solution. Particle formation occurs fairly quickly over less than 40 minutes. The aim of this work is to produce biocompatible soft nanoparticles that can serve as nanocarriers for drugs and other functional molecules for targeted drug delivery and water remediation.

From only a few simple, robust reactions including ATRP, click chemistry and nitrene homocoupling, and high functionality polyols such as β-CD and HPG, it is possible to craft a diverse array of both hard and soft nanocomposite structures easily and at low cost. By understanding how polymer architecture and chemical functionality

inform on the resulting nanostructures, several different interesting materials have been realized by applying different post polymerization modification strategies to high functionality polyols to yield polymer-tethered inorganic nanoparticles, promesogen-capped nanoparticles and wholly polymeric soft nanoparticles. These materials have potential applications in optoelectronics, surface/film modification, antifouling and biotechnology among many others.

CHAPTER 1. INTRODUCTION

Polymers have found ever-increasing use across many different fields of science, engineering and medicine. Once considered an impossibility by leading members of the academic community, it is evident to all that polymers have become not only an ubiquitous but essential component of everything we see in our lives spanning many length scales from the largest of structural and building components to the smallest perceivable structures present in drugs, electronics, energy, and even our very genetic makeup. Within this immense realm of active research, recent efforts have been directed towards the use of polymers for the construction of nanostructures of many different shapes, sizes, functionalities, and compositions. By combining only a small set of polymerizable materials, polymerization techniques and other post-polymerization chemistries one can craft many complex and interesting nanocomposite structures.

The great wave that is nanotechnology has since broke upon the world of academic research. Often behaving fundamentally different from their bulk counterparts, nanoscopic materials have enabled the realization of materials with new and interesting properties and applications. In addition, the interaction among materials on the nanoscale has enabled researchers to interact with systems in ways previously impossible. It is at the intersection of novel nanoscale properties and new nanoscale interactions where one finds nanocomposites. To that end, star-like copolymers derived from Beta-cyclodextrin (β-CD) and hyperbranched polyglycerols (HPG) and their application in hard and soft nanocomposite templating are the focus of this work. Several variations on this central

idea will be introduced, presented and summarized for future research in the areas of hard and soft nanoparticle synthesis with applications in optics, energy and drug delivery among others.

Unlike hard templating techniques, of which there are many, soft templating techniques based on polymers offer better control over final surface functionality and therefore have greater applicability in a wide range of organic, polar, nonpolar and biological media. The generally milder conditions encountered in the soft templating of inorganic and organic nanostructures allow for the retention of many capping ligands and/or the subsequent covalent attachment of additional surface functionalities (post polymerization modification). In the case of hard templating, it is common to use high temperatures, pressures, and harsh chemicals essentially leading to bare inorganic structures. Consequently, the focus of this dissertation lies in strictly soft polymer-mediated templating strategies of inorganic and organic structures.

Details regarding the current state-of-the-art in relevant polymer templating strategies, controlled living polymerization techniques, small molecule organic synthesis, inorganic synthesis, post-polymerization modification techniques, and prospective applications are herein addressed. The motivation as well as the objectives and outcomes of this work with as they relate to the greater body of related research are also summarized accordingly.

1.1 Techniques in Polymer-mediated Nanocomposite Preparation

Myriad techniques are available for polymer-mediated templating. Within this large group, it is natural to divide it into several groups including biologically-sourced

templating techniques[1-8] hard templating techniques,[9] linear block copolymer micelle templating techniques,[10-15] and unimolecular nanoreactor templating techniques.[16-21] Within the context of nanocomposites, templating can be described as using a scaffold to either direct or contain the formation or exclusion of some added material components in a fashion analogous to how fine wire meshes selectively contain water droplets within the pores. In the case of polymer templating, the scaffold material is the polymer and added materials are both chemically directed and physically contained by this scaffold to form different nanostructures. The focus of this work lies within the last group of templating techniques, unimolecular nanoreactors, and will be the primary subject of further elaboration throughout this work.

1.1.1 Star-like Polymer Templates

Star-like polymers have been of academic interest since the formulation of macromolecular theory. Owing to their fundamentally different physical, rheological and chemical properties, they have applications in areas including but also in addition to those of their linear counterparts. Star polymers can take on many forms, but the simplest definition assumes a single multi-functional core molecule from which polymerization takes place radially outward. **Figure 1.1** provides a general illustration of useful star polymer architectures.[22]

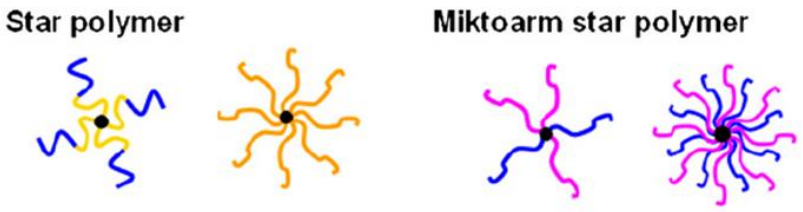

Figure 1.1 (Left) A generic representation of a star polymer and star copolymer. (Right) A generic representation of a mixed-arm (miktoarm) star polymer. The star block copolymer on the left is the basis for many nanoscale templating strategies and the focus for part of this dissertation. Reproduced with permission[22] copyright 2009 Elsevier.

In addition to single-component star polymers, there are also copolymers and heteroarm (miktoarm) polymers which contain two or more different polymer chains attached to the central core.[23] From this it can be seen that many different combinations and therefore many different properties can be obtained depending on the different copolymers employed as well as the size of polymer chains. Details of polymerization techniques are addressed in a subsequent section. Many different core molecules can serve as macroinitiators, but the most common types are β-cyclodextrin (β-CD),[17, 19, 24-26] polyhedral oligomeric silesquioxanes (POSS),[21, 27] and small molecule polyols such as calixarenes and aliphatic alcohols,[28, 29] derivatives of 1,3,5-tris(4-iodophenyl)benzene[30] and 1,3,5-tris(3,5-dimethyl-4-pyradinyl)benzene[31] as well as new tritritylbenzene-based molecules,[32] dipyridamole,[33] and cyclophosphazine derivatives.[34] There are also macromolecular star polymer macroinitiators including single chain cyclized/knotted nanoparticles (SCKPs)[35] composed of a randomly crosslinked polymer core with residual unreacted functional groups such as terminal vinyl units; and hyperbranched poly(siloxysilane) systems (HBPS)[36] composed of siloxy units containing vinyl groups amenable to polymerization. Many of these macroinitiators possess hydroxyl groups

which can be further functionalized to become polymer macroinitiators. In addition, these macroinitiators are readily available, and generally inexpensive to either purchase or produce. **Figure 1.2** summarizes the most commonly encountered low and high molecular weight star polymer macroinitiators.

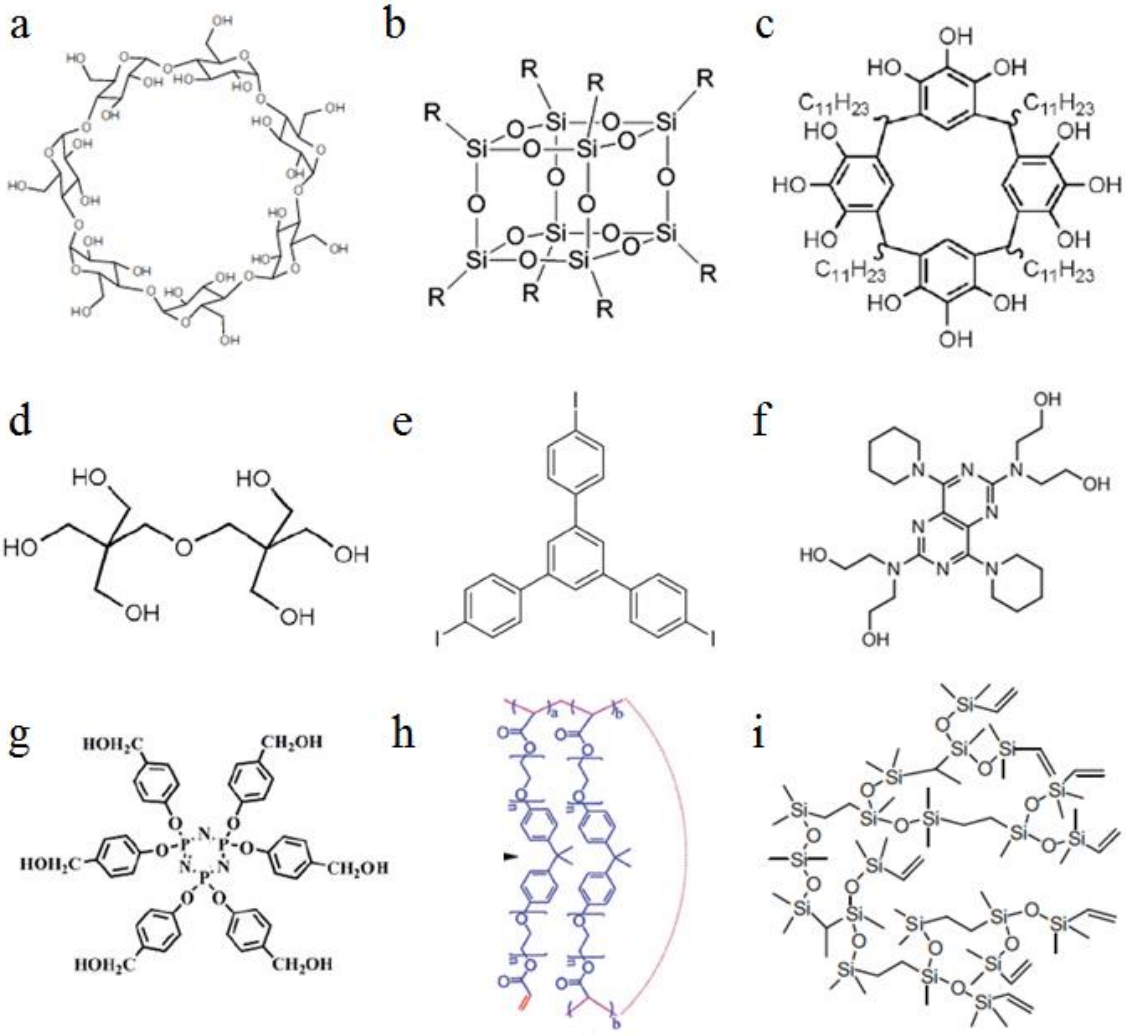

Figure 1.2 Commonly encountered star-like polymer macroinitiator starting materials. (a) β-cyclodextrin (f = 21). Reproduced with permission[20] copyright 2013 Springer Nature. (b) Polyhedral oligomeric silsesquioxanes (POSS) (f = variable). Reproduced with permission[27] copyright 2012 Royal Society of Chemistry. (c) Calixarene derivatives (f = variable). Reproduced with permission[29] copyright 2009 Elsevier. (d) Dipentaerythritol (f = 6). Reproduced with permission[29] copyright 2009 Elsevier. (e) Derivatives of 1,3,5-tris(4-iodophenyl)benzene (f = 3). Reproduced with permission[30]

copyright 2017 American Chemical Society. (f) Dipyridamole (f = 4). Reproduced with permission[33] copyright 2017 American Chemical Society. (g) Cyclophosphazine derivatives (f = 6). Reproduced with permission[34] copyright 2016 Wiley. (h) SKCP star polymer core with residual vinyl groups capable of additional polymerization (f = variable). Reproduced with permission[35] copyright 2017 Wiley. (i) Hyperbranched poly(siloxysilane) systems (HBPS) (f = variable). Reproduced with permission[36] copyright 2010 Elsevier. Note that the above molecules typically go through different additional reactions at functional groups to become macroinitiators for several different types of polymerizations.

Many factors must be considered when using star polymers as nanoparticle templates. These include the functionality of the macroinitiator (*f*), the degree of polymerization of different block components (DP_n), polydispersity of the polymers (PDI), the chemical structure of block components (hydrophilicity, hydrophobicity, amphiphilicity), and the nature of the reaction solvent (mixed or pure). All of these parameters influence the shape of star polymers in solution and thus influence how easily such materials can be used to template hard and soft nanoparticles.

The functionality defines the number of reactive sites on the macroinitiator. In other words, it defines the maximum number of polymers that can be grown from a core if 100% initiation is achieved. The higher functionalities result in larger polymer grafting densities on the resulting star polymer. Since nanoparticles are commonly produced from inorganic precursors coordinating with certain components of the star polymer on the inner/outer/intermediate surfaces, higher functionalities are essential to achieving uniformly-shaped particles at lower molecular weights per arm.[20] For example, **Figure 1.2a** has a functionality of 21, **Figure 1.2b** can have a variable functionality, and **Figure 1.2c** has a functionality of 12 each of which will impact the overall appearance of particles templated from copolymers. Tradeoffs do exist when going to higher functionalities. Polyols with higher functionality are typically more difficult to dissolve

due to intermolecular and intramolecular hydrogen bonding. This makes functionalization into macroinitiators more challenging. Assuming successful macroinitiator synthesis, one can then focus on the resulting polymer structure and size considerations.

Once polymers have been grown from the macroinitiator core, attention to the degree of polymerization (DP_n), or size, of the as synthesized polymer should be considered. Also referred to as molecular weight or length, degree of polymerization is the number of repeat units in the polymer, and it is essential to defining the size of polymers.[37] The molecular weight of a polymer controls the size of the different components of resulting nanotemplated structures such as the size of the core, the thickness of the shell or the size of a hollow space. **Figure 1.3** shows how different copolymer structures can lead to different inorganic and organic hybrid nanostructures including hollow, core@shell, and solid core varieties.

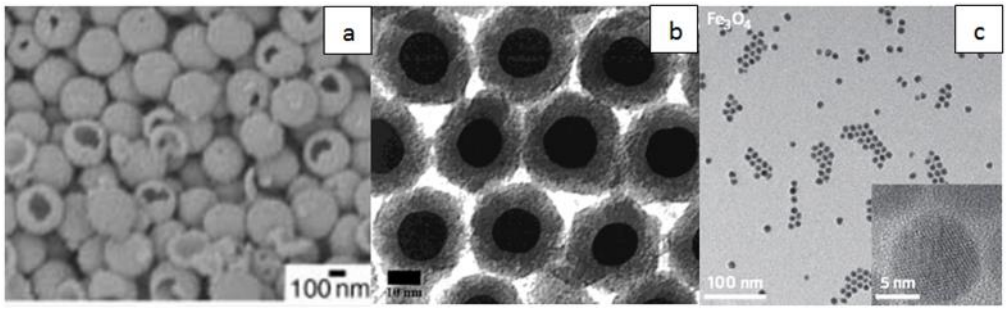

Figure 1.3 (a) Hollow titania nanoparticles synthesized via templating onto the surface of polymer a template. Reproduced with permission[38] copyright 2003 Wiley. (b) Core@shell gold-silica nanoparticles made by selective coordination with star copolymer sections. Reproduced with permission[39] copyright 2000 American Chemical Society. (c) Polymer-coated iron oxide nanoparticles made by metal ion precursor coordination within the inner polymer phase. Reproduced with permission[20] copyright 2013 Springer Nature.

In addition to the size of the polymers, their size distribution about some average is also important. Called the polydispersity index (PDI), it is a number that is defined mathematically as the quotient of the weight-average molecular weight (M_w) and number-average molecular weight (M_n). This number has a lower bound of unity (perfectly monodisperse) where all the polymer chains in a sample have exactly the same size. Higher PDI values result in larger size variations between chains and a corresponding reduction in the size regularity of resulting templated nanostructures for example. It is not yet possible to achieve perfectly monodisperse samples by synthetic means; however chemistry has gotten very good at coming quite close. Details of low PDI synthesis techniques are detailed in subsequent sections.

The greatest variability and, arguably, difficulty in the use of star block copolymer templates centers on the chemical composition and behavior of different polymers. There are many different materials that can undergo polymerization and by many different mechanisms. The scope of this work is limited to a relatively narrow group of polymers and polymerization techniques; however, a general understanding of how different polymers behave based on their chemical composition is nonetheless warranted.

Generally, polymers can be divided into three categories: hydrophilic, hydrophobic and amphiphilic. Hydrophilic polymers such as poly(L-lactic acid) (PLA), poly(vinyl alcohol) (PVA), and poly(ethylene glycol) (PEG) typify this group with their hydrogen bonding and generally polar character. Hydrophobic polymers include polystyrene (PS), poly(methyl methacrylate) (PMMA), and poly(tert-butyl acrylate) (P*t*BA) which lack hydrogen bonding and do not form charged species under and pH

when in solution. In general, hydrophilic polymers tend to be soluble in water and other hydrogen bonding, protic or polar solvents. Hydrophobic polymers tend to dissolve better in organic, nonpolar solvents. In mixed solvents, a complex interaction with star copolymer templates can occur; leading to preferential swelling and contraction of different constituent blocks. This behavior can be used to produce cage-like polymeric structures in solution to serve as nanoreactors.[19, 20, 40] **Figure 1.4** shows three different combinations of mixed solvent and the simplified effect on a generic diblock star copolymer. In general, a bad solvent for a polymer causes it to reduce its free volume and essentially collapse down whereas a good solvent causes a polymer to swell and expand. Depending on the proportion of good and bad solvent for one or several blocks of a copolymer; contraction, swelling, or both can be observed.

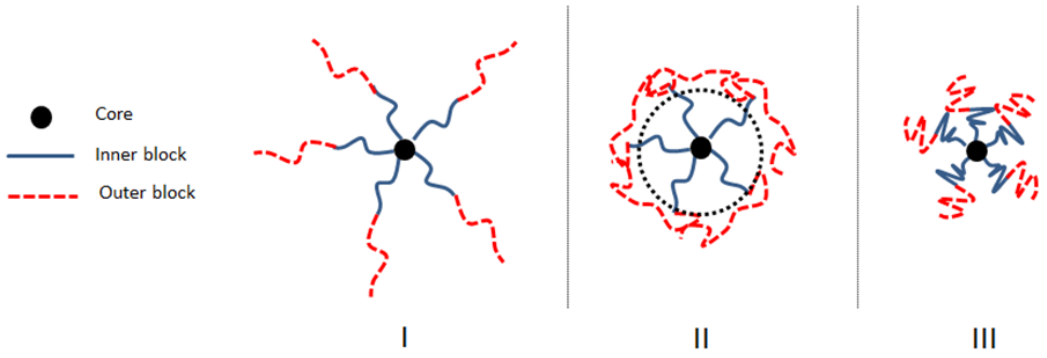

Figure 1.4 (I) Two-component solvent where both are good solvents for both blocks (both blocks swelled). (II) Two-component solvent where one is a good solvent for both blocks and the other is a bad solvent for the outer block (swelling of inner block and contraction of outer block). (III) Two-component solvent where both are bad solvents for both blocks (both blocks contracted with likely precipitation of copolymer).

As is the case for micellar systems, the optimum proportions of mixed solvents are essential for obtaining the desirable nanoreactor conformation shown in **Figure 1.4(II)**. However, unlike micellar systems, unimolecular star copolymer templates are

covalently linked and hence are less sensitive to changes in temperature, pH, iconicity, and concentration.

A key point yet to be addressed is the order of synthesis of star polymer templates of all sorts. Up to this point, the procedure described is what is called a "core-first" methodology. Essentially, this means that polymer chains are grown from a central core outward. This method has several advantages including higher yields, lower inherent PDI and reduced need for post-polymerization purification via fractionation.[41] Several other methods exist including "coupling-onto" and "arm-first" which will be discussed next. **Figure 1.5** provides a general description of the three main star copolymer synthesis approaches.

As one might expect, "coupling-onto" is essentially the opposite of the core-first method in that one adds a multifunctional core into a sample of mono-functionalized linear polymer arms which can then react with complimentary groups on the core. In this case, typically an excess of linear polymer is required in order to achieve high core attachment due to the low coupling efficiency of the reactive chain ends of linear polymers. It also requires additional purification though some control is possible in terms of the maximum number of arms obtainable. It should be noted that the other end of the linear chain can be reactive so long as it does not participate in the polymerization.

The "arm-first" approach brings the ends of several arms together by a small molecules crosslinker (typically a divinyl derivative) to form the central core.[41] This approach is inherently more complicated because the nature of the crosslinking resulting in the core formation is typically less controlled and can lead to star-star coupling if proper stoichiometry and reaction conditions are not maintained. Nonetheless, the "arm-

first" method is capable of producing the miktoarm star polymers described earlier. The "core-first" approach will be primarily used throughout this work.

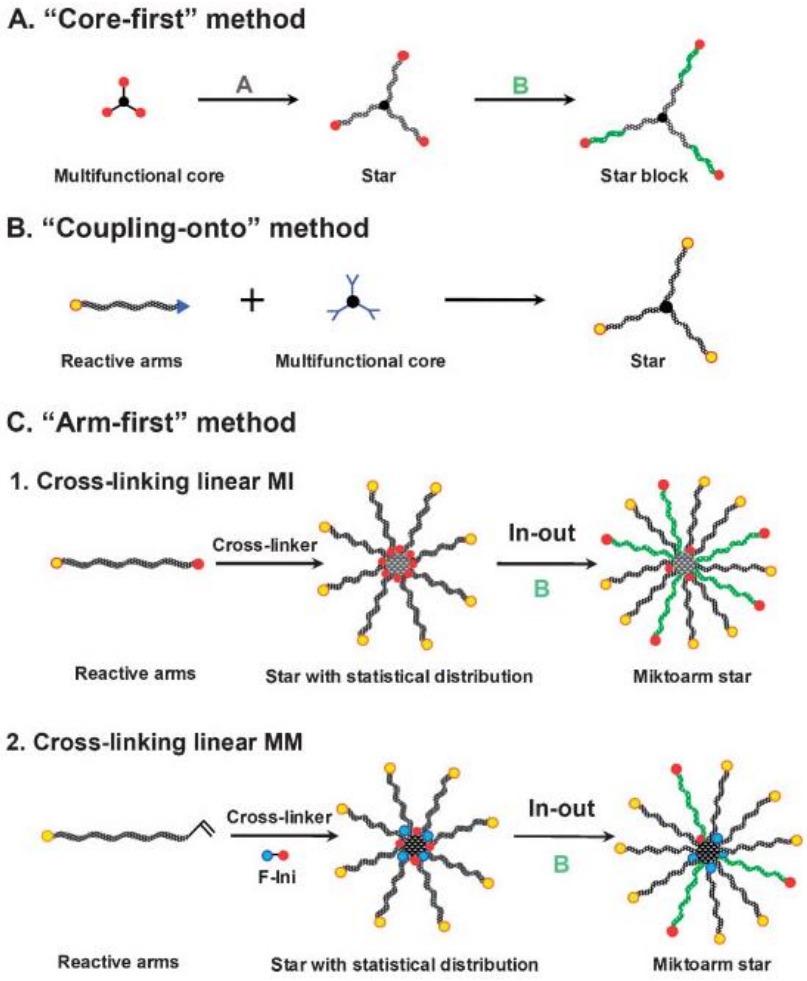

Figure 1.5 The three main approaches to growing star polymers. (A) In the "core-first" method one starts with a macroinitiator core from which polymer arms are grown to produce a star-like polymer. (B) In the "coupling-onto" method one prepares the core and the arms separately and then combined to form star polymers by some covalent linking chemistry. (C) In the "arm-first" method one stars with linear telechelic polymer chains. In one approach, the ends of the chains coalesce and are then crosslinked by the addition of chemical crosslinker to produce a core. In a second approach, a macromonomer (MM) is employed where again the ends of the polymerizable side coalesce and are then crosslinked via initiation of polymerization to produce a core. Reproduced with permission[41] copyright 2007 Wiley.

To date, several different inorganic structures have been crafted through the use of star polymer templates (Au, Ag, TiO_2, Cu_2O, $BaTiO_3$, SnO, CdSe and ZnO among

others).[20] Some of the typical applications of these nanoparticles include plasmonics,[42, 43] superparamagnetics,[16, 44] semiconductors,[45] drug delivery,[46, 47] catalysis,[48, 49] and ferroelectrics.[50] It is important to note that such examples are limited to particles synthesized by soft, polymeric templating approaches and not template-free or sol-gel like processes of which there are many more examples and ultimately many more applications to be reviewed. In addition, layer-by-layer approaches are considered a separate group of soft templating because they employ several layers of different polymers and are not strictly unimolecular.

A key point in justifying polymer-templated methods as a viable strategy for making inorganic structures is the often present polymer capping layer on the exterior of templated nanostructures. That is, a surface coating which enables the materials to remain soluble in particular solvents (organic, inorganic, ionic, polar or nonpolar) dependent on the nature of the polymer layer. Since most nanoscale structures are dealt with in solution, this is an essential consideration for many applications and a method for avoiding the aggregation of prepared nanostructures and subsequent loss of desirable nanoscale properties.

Unlike template-free processes, templated nanoparticles offer several distinct advantages in certain applications. For example, an understanding of the plasmonic phenomena of nanoscale noble metal particles requires a systematic variation in the size, shape and thickness of plasmonically-active layers as well as other inorganic components that may be present in the structure. Variation in these properties can be used, for example, to control the plasmonic peak intensity, position, and width in various gold multicomponent nanocomposites. **Figure 1.6** shows this variation in polymer templated

Au and Au@Fe_3O_4 nanocomposites.[51] Although several examples of polymer templated inorganic nanoparticles have been reported, they are relatively few when compared to template-free and hard templating methods (templating in/on inorganic wires, mesoporous silica, carbon nanotubes, and anodic aluminum oxide). The particles synthesized in **Figure 1.6** are also covalently capped with hydrophilic or hydrophobic polymers to facilitate their solubility in common solvents such as water, chloroform and toluene. This is important for preventing aggregation and is one of the reasons that precisely controlled size-dependent properties can be realized in these systems.

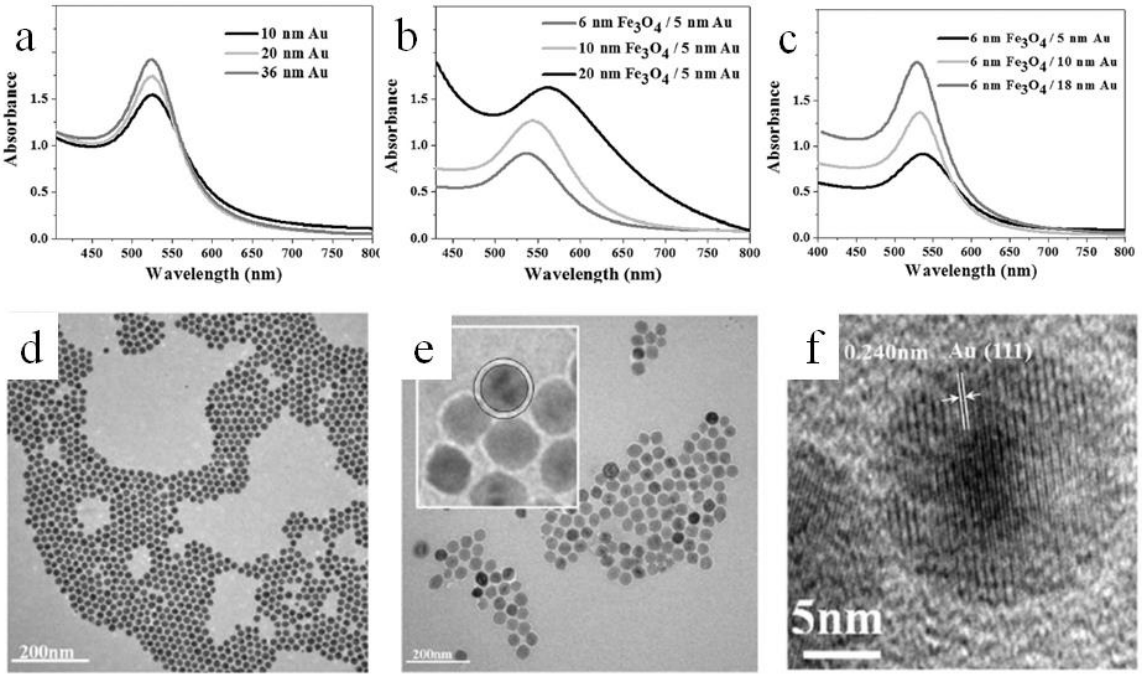

Figure 1.6 (Top) UV-Vis spectra of different core@shell nanostructures with varying core or shell sizes. (a) Control gold nanoparticles showing expected plasmonic behavior. (b) Red-shift in plasmonic peak measured in core@shell nanoparticles with fixed outer Au shell and increasing diameter Fe_3O_4 core. (c) Blue-shift in plasmonic peak of core@shell nanoparticles with fixed Fe_3O_4 core and increasing Au shell thickness. (d) TEM showing the regularity of the templated core@shell nanoparticles (Scale bar = 200 nm). (e) TEM showing the well-defined interface between the dissimilar core and shell materials (Scale bar = 200 nm). (f) High resolution TEM showing the interface between the Au and Fe_3O_4 crystal lattices. Reproduced with permission[51] copyright 2015 Wiley.

The hysteresis behavior of superparamagnetic nanoparticles (saturation magnetization, susceptibility and blocking temperature) is also highly size dependent (**Figure 1.7**).[44] In fact, superparamagnetism is a strictly sub-micron phenomenon in iron oxide so size control is paramount. It is important to note that the size variation of the resulting inorganic particles is highly dependent on the type of polymerization(s) employed.

Controlled radical polymerizations are by far the best suited to achieving highly monodisperse star polymer templates (see section on Relevant Chemistries in Nanocomposite Synthesis). The ability to produce superparamagnetic nanoparticles is clearly demonstrated in the literature.[52-54] The challenge is making use of them in applications including ferrofluids (magneto-rheology) and medical applications (imaging, and therapy). This is primarily dictated by the type of surface capping to maintain solubility and/or appropriate uptake into cells. Subsequent ligation is often susceptible to chemical or thermal attack once particles are introduced into different environments which can greatly affect their performance and residence time within the body. Having covalently-attached ligands on the surface is ideal for avoiding this problem.

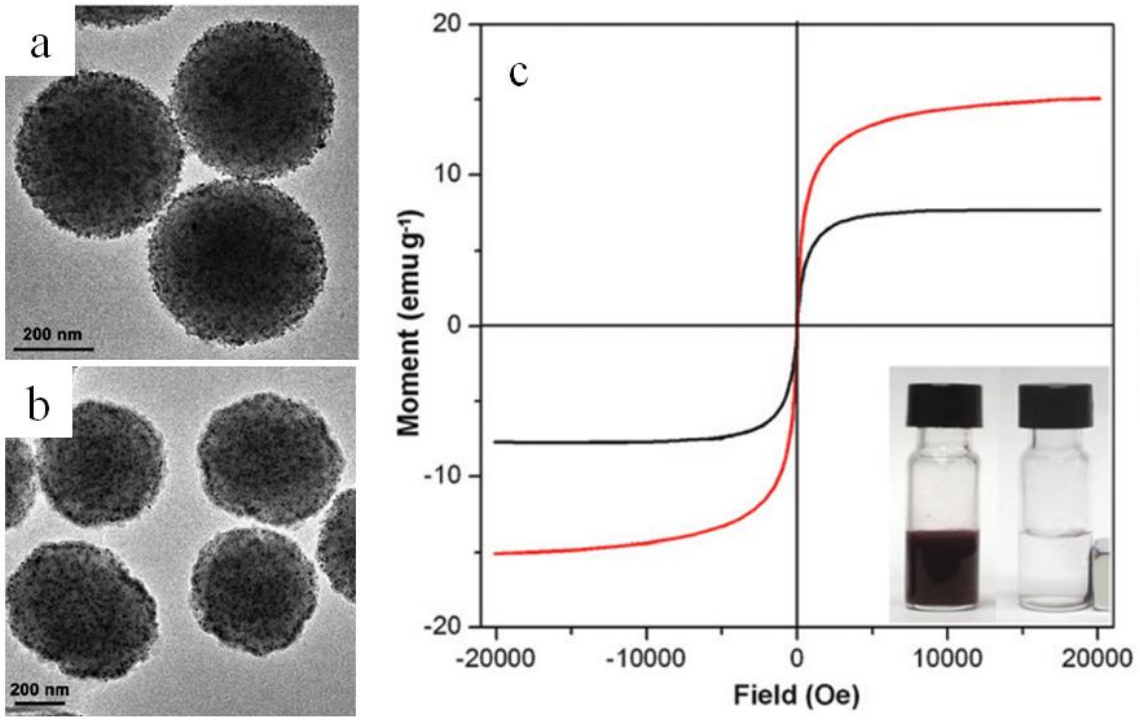

Figure 1.7 (a, b) Two different iron oxide nanocomposites of different sizes and compositions synthesized by templating on poly(dopamine) spheres. The magnetic performance of the two materials (c) is clearly different with each showing a different saturation magnetization value and different susceptibility (hardness) with no remnant magnetization (y-intercept) or magnetic coercivity (x-intercept). Reproduced with permission[44] copyright 2015 Royal Society of Chemistry.

In addition to hard inorganic nanoparticles synthesized by polymer templates, relatively new examples of soft polymeric nanoparticles have been reported.[46, 47] Instead of serving as a nanoreactor for the incorporation of inorganic precursors, the polymer template can be crosslinked in some fashion to serve as a capsule for holding active species and/or as a soft surface to be subsequently coated with functional chemical or biological species for cell recognition, uptake, and transport. Microcapsules have been investigated and reported for such purposes using conventional layer-by-layer (LbL)[55] techniques; however the similarity is only superficial in terms of how to go about making similar structures on the nanoscale. The potential advantage of using smaller drug loading species is greater ease of access in different cellular environments and the option for smaller drug loading amounts for improved safety. **Figure 1.8** provides representative

examples of the types of degradable organic nanoparticles that have been reported to date. In one case, a drug analog is released at different rates by varying the shell diffusivity (i.e. crosslinking density)[47] and the other is regulated by in vivo degradation by enzymes (i.e. burst delivery).[46]

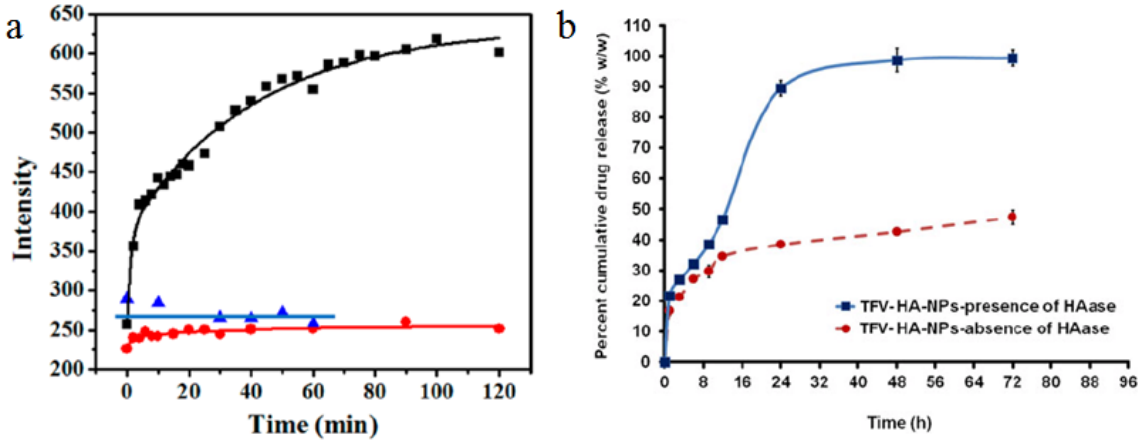

Figure 1.8 (a) Controlled release of a drug analogue regulated by diffusion out of hollow nanoparticles of different crosslinking densities. There is an inverse relationship between drug release rate and crosslinking density. Reproduced with permission[47] copyright 2014 American Chemical Society. (b) Experiment showing controlled release of drug due to enzyme-specific degradation (HAse) of polymer particle. Reproduced with permission[46] copyright 2013 American Association of Pharmaceutical Scientists.

Drug delivery triggering mechanisms and fine control are a particularly important aspect of such systems. By far the most common mechanism of delivery is local injection and simple diffusion. This strategy, however, is not always useful or safe depending on the types of drugs used and the loading amount. It is for this reason that additional diffusion-triggering mechanisms developed using LbL approaches (pH,[56] temperature,[57] ionicity, enzymatic,[58] and magnetic[59] triggers) need to be translated into unimolecular star polymer templating approaches. The rationalization for this is that it eliminates the problematic issue of using such triggers for drug release from microcapsules whose stability is also dependent on these parameters. A very precise control and understanding

of which triggers are available and over what range without fully compromising the integrity of the microcapsule are fundamental in such works. Particles need to stay intact at least up until the location of intended drug release. In covalently crosslinked systems (i.e. unimolecular star-templated structures) less concern need be given to particle degradation. This has the potential to greatly simplify dealing with such drug delivery systems and triggers. Furthermore, the cycling behavior and longevity of LbL systems is problematic because of the nature of particle association (i.e. non-covalent). This makes repetitive and reliable on/off cycling behavior a challenge.

Transitioning from medical applications to energy applications, polymer templated inorganic structures have shown new promise in ferroelectrics.[50] Most ferroelectric nanocrystal synthesis routes to date have relied on inorganic templating approaches[60] or sacrificial polymer templates.[61] Ferroelectric materials are of particular interest for high capacitance, small size capacitors and other energy storage devices. In order to raise electrical storage, it is often necessary to increase the dielectric constant of a material (among other changes), which is also size dependent. **Figure 1.9** shows an example of ferroelectric nanocomposites produced using star polymer templates and their subsequent spatial organization into a complimentary domain of a block copolymer dielectric film. Such precise size and spatial control is not generally possible with conventional hard templating, template-free, and sol-gel approaches.

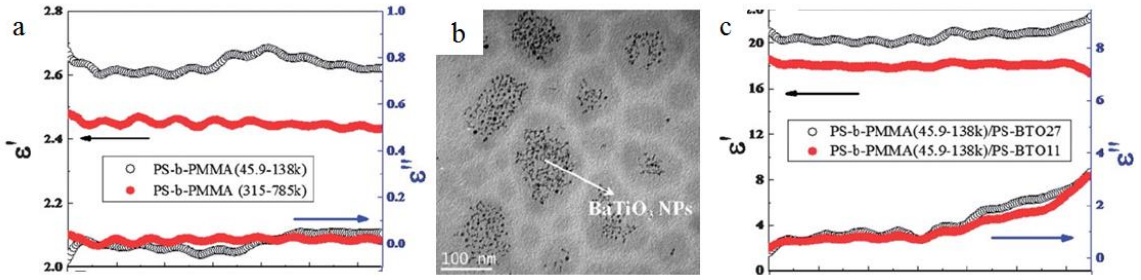

Figure 1.9 (a) Block copolymers without $BaTiO_3$ nanoparticles showing relatively low dielectric constant values over a 2-16 GHz frequency range. (b) PS-capped $BaTiO_3$ particles dispersed selectively in the PS domains of a PS-PMMA copolymer film. (c) Improved dielectric performance resulting from the incorporation of PS-capped $BaTiO_3$ particles into a PS-PMMA copolymer film. Reproduced with permission[50] 2013 Royal Society of Chemistry.

The size uniformity and solubility of nanoparticles can heavily influence their ultimate performance and reliability by reducing the tendency for aggregation. In the case of thin film devices, aggregation is particularly a problem because interfacial resistance and trapping can lead to poor electron flow and higher resistances (heat generation) and high current densities. By far the vast majority of ferroelectric nanoparticles are produced though the three established techniques previously mentioned. To that end, there is little available literature on this topic but there are a lot of directions that new research can take in this area.

The current state-of-the-art in star-like polymer-mediated nanoparticle synthesis covers many different areas to varying degrees. In situations where size control, size uniformity, strong surface functionality (or potential for strong surface functionality) and low inherent degradability are desired it is clear that star-like polymer templates have several advantages. This same rationale is present when discussing the bottlebush-like polymer-mediated organic and inorganic structures addressed in the following section.

1.1.2 Bottlebrush Polymer Templates

In most ways, the strategies associated with constructing star-like block copolymer templates are similar to those of bottlebrush templates. The key difference between these approaches is the overall shape associated with the template and the resulting structures. In the case of bottlebrush templates, higher dimensional templating structures can be produced depending on the identity of the macroinitiator. One dimensional brushes are attached to a central linear polymer chain. Two dimensional brushes are attached to a planar surface. Finally three-dimensional brushes are attached to a spherical particle. This dissertation is limited to one dimensional polymer brushes (cylindrical) polymers which have side chains grafted onto a central linear core. **Figure 1.10** provides a general description of the different brush structures possible.[62]

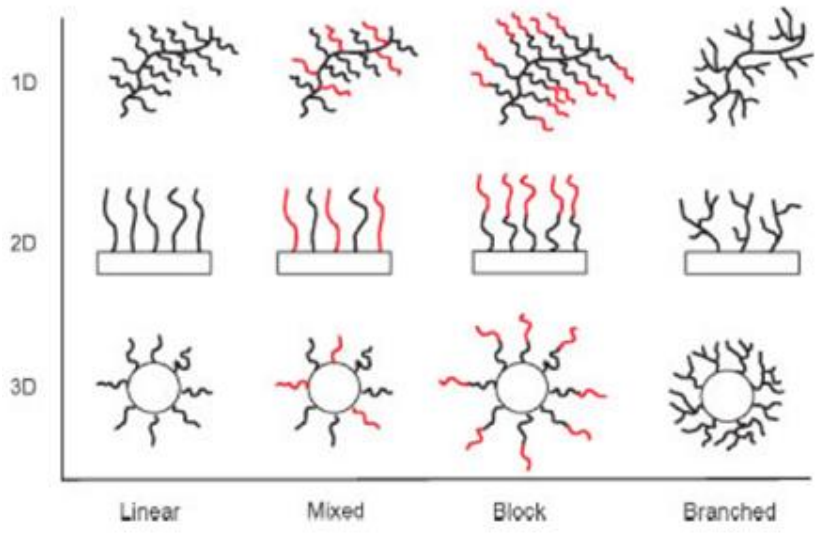

Figure 1.10 One, two and three dimensional brush structures. Types of brushes can include single-chain, copolymer chains, miktoarm and branched (dendritic) among others. Reproduced with permission[62] copyright 2005 Wiley.

It should be noted that copolymer or mixed-arm (miktoarm brush) structures mirroring their star polymer analogues are also possible. Several features that make bottlebrush polymer structures interesting and useful originate in the high grafting density of the side chains from the backbone linear polymer chain. Essentially, a coil-like linear polymer chain can be made to be more rigid by the addition of densely grafted side chains. This is a result of the excluded volume of the side chains which prefer to minimize contact. A consequence of this contact minimization is to straighten the backbone to which they are all attached. This property coupled with the type and arrangement of the different bottlebrush components makes them particularly useful for applications in both hard and soft research areas. Some interesting areas include molecular actuators,[63] nanomagnetics and magnetoviscocity,[64] semiconducting nanowires for nanoelectronics applications, and anisotropic plasmonic structures. Depending on the size and type of polymer backbone and side chain, many different stimuli-responsive materials can be generated (i.e. thermo-responsive, pH-responsive, magneto-responsive). When discussing polymer brushes, several parameters are useful for characterizing their structure and size.

Similarly for star polymers, the molecular weight and molecular weight distributions are essential to understanding how large brush components are. Unlike for star polymers, there is a highly skewed molecular weight different between the backbone and the side chains. That is the backbone polymer is typically much longer than the grafted chains. The length variation of the graft chains verses the length variation of the backbone (and their ratio) can have significant effects on the overall structure and rigidity. Rigidity in polymer brushes can be expressed in several ways however the most

commonly used parameter is the persistence or Kuhn length of a polymer.[65] The Kuhn length essentially defines the distance over which the chain can be considered effectively rigid. It is illustrative to think of chains composed of rigid Kuhn monomer spheres connected though kinks where the monomer length is the Kuhn length.[66] Thus, highly flexible chains tend to have low Kuhn lengths whereas one dimensional brush structures tend to have large Kuhn lengths relative to the bare backbone polymer. This is due to the side chains repelling one another and thereby straightening the backbone chain to some extent.

Similarly to star-like polymer templates, bottlebrush polymers can be produced in several different ways of which there are three dominant approaches.[67] The three general strategies for synthesizing one dimensional bottlebrush polymers are summarized in **Figure 1.11**.[62] The first is the "grafting through" strategy which is where macromonomers (polymer chains with one end polymerizable) are initiated and polymerized in a similar fashion as small molecule monomers.[68] The polymer chains on each macromonomer ultimately constitute the side chains on the resulting bottlebrush polymer. This strategy has the advantage of producing very large grafting density bottlebrush structures with high persistence length backbones. The drawback of this technique is the relatively small number of polymerizable end groups in the reaction mixture and the steric hindrance of accessing them. This leads to relatively low degrees of polymerization of the resulting bottlebrush chains. Methods to boost the degree of polymerization have been investigated, however, they have not been successful nor have they relied heavily on living or controlled polymerization techniques, leading to poor molecular weight control.

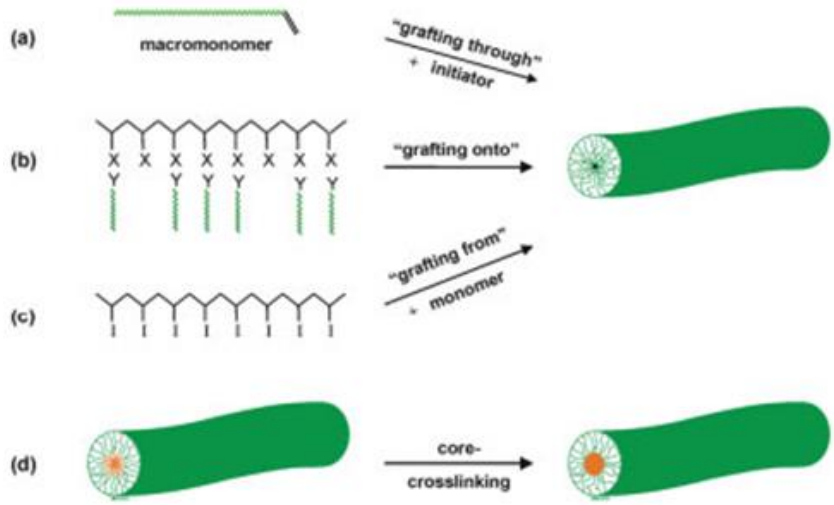

Figure 1.11 (a) The "grafting through" approach starts with a single-end-polymerizable macromonomer. (b) The "grafting onto" approach first polymerizes a pendant-reactive main-chain polymer to which side chains are attached by a coupling reaction between the side chain and pendant groups. (c) The "grafting from" approach first synthesizes a main-chain polymer with initiator groups in the backbone from which an additional polymer is grown. (d) Certain copolymers form micellar structures in which the core can be cross-linked to also yield brush structures. Reproduced with permission[62] copyright 2005 Wiley.

In an attempt to improve on the limitations of the "grafting through" strategy, researchers have developed a related technique called "grafting onto."[69, 70] This approach involves two steps: main-chain monomer polymerization and side chain attachment. First, a monomer is selected which possesses some latent or overt pendant reactivity once polymerized. Side groups such as alcohols, vinyl halides and double bonds are some common examples.[62] Next, the side-chain polymer is separately synthesized and functionalized on one or both ends in a way to compliment the main-chain pendant reactivity. Examples of such coupling reactions include thiol-ene,[71] azide-alkyne,[72] Hay/Glaser coupling (alkyne-alkyne heterocoupling),[73] and Diels-Alder coupling.[67] More details on relevant click chemistries are provided in a subsequent section. The "grafting

onto" approach has several advantages. First, the main chain degree of polymerization can be well-controlled and adjusted to very large molecular weights. Second, the grafting density of the side chains can be controlled if the main chain is copolymerized with non-reactive monomer units in an alternating fashion as well as in block fashion or with monomers capable of different coupling reactions. What this translates to is a greater variability of potential brush polymers that can be produced.

There is also the possibility of copolymers forming core-shell micellar structures under certain conditions (**Figure 1.11d**). In such cases, the core can possess a cross-linkable core which can also lead to the formation of bottlebrush polymeric structures. Different challenges are at play in this scenario, specifically what parameters allow such micellar structures to form and considerations of stability during crosslinking as they are quite sensitive to external perturbations. The core-crosslinking technique also has relatively low achievable degrees of polymerization but can be achieved in many different ways including chemical crosslinking and UV photo-crosslinking.

Müller et al. have investigated several different types of bottle-brush structures and their potential use as inorganic nanocrystal templates.[62, 74, 75] In most cases, the resulting inorganic structures were wormlike in appearance and did not possess long range rigidity. To date many different functional inorganic materials have been successfully synthesized within block copolymer templates including semiconductors (cadmium sulfide, silica),[76] encapsulated f-block metal cations (Ln^{3+}, Gd^{3+}),[75] plasmonic materials (Au, Ag),[20] and materials for photocatalysis (titania)[77] among several others. **Figure 1.12** provides representative examples of flexible bottlebrush templated inorganic materials including silica[76] (left), titania[77] (center) and rare earth cations (right).[75] The

general procedure for obtaining inorganic structures typically involves at least one copolymerization of an overt or latent metal-ion-coordinating polymer such as poly(tert-butyl acrylate) (PtBA), a latent example, or poly(4-vinyl pyridine) (P4VP), an overt example, followed by polymerization of a covering polymer such as poly(methyl methacrylate) (PMMA) or polystyrene (PS). Subsequently inorganic precursors are added to the template bottlebrush which selectively coordinate to the inner block of the template and nucleate to form the appropriate inorganic material typically by hydrolysis, reduction, or oxidation.

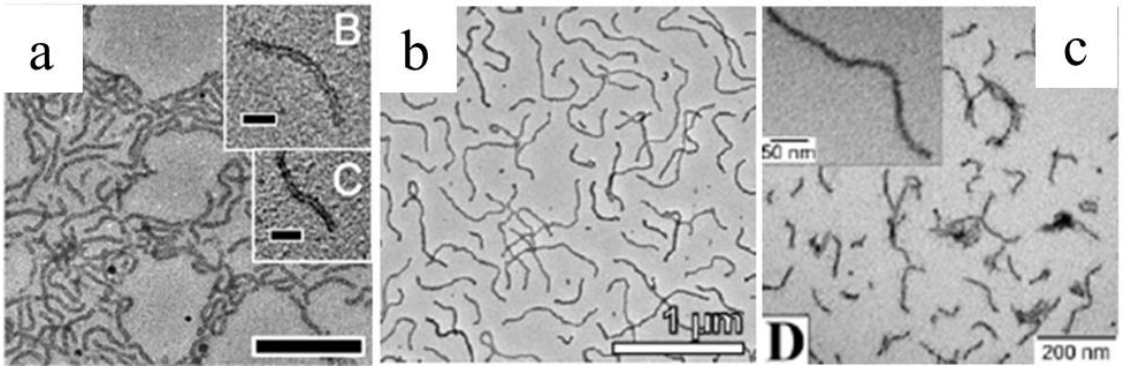

Figure 1.12 (a) Polymer-templated flexible silica wires. Reproduced with permission[76] copyright 2010 American Chemical Society(Scale bar = 200 nm) (Insets scale bars = 100 nm). (b) Polymer-templated titania nanowires. Reproduced with permission[77] copyright 2012 American Chemical Society. (c) Silica nanowires containing rare earth metal ions templated with cylindrical polymer brushes (Inset scale bar = 50 nm). Reproduced with permission[75] copyright 2013 American Chemical Society. Note that different length scales can be realized by polymer templating techniques to fit many different applications.

It is interesting to note that because the backbone is not very rigid, the subsequent grafting only somewhat improved the persistence length of the main chain. This is why the resulting inorganic structures appear to be wormlike rather than rod-like or wire-like.

Consequently, researchers have also looked into backbone materials that can be used to produce nanorod and nanowires with higher rigidity.

Templating strategies for more rigid polymers, such as cellulose, have relied more on sol-gel mineralization processes whereby such templates are coated with precursors and allowed to react. This approach can yield either irregularly-coated nanorod structures[78, 79] or nanoparticle-decorated cellulose.[80, 81] Subsequently, the cellulose is removed. These structures are not particularly uniform, tend to aggregate and are highly irregular in length, thickness and morphology. Indeed, cellulose and its derivatives are highly useful as rigid backbone materials; however they suffer greatly in all attempts to use them due to their poor solubility in all but the harshest or difficult-to-use solvents (concentrated acids and ionic liquids). They are also generally polydisperse. This leads to fluctuations in overall length and thickness. **Figure 1.13** provides a summary of the two principle types of inorganic structures obtained when using cellulose templating strategies.

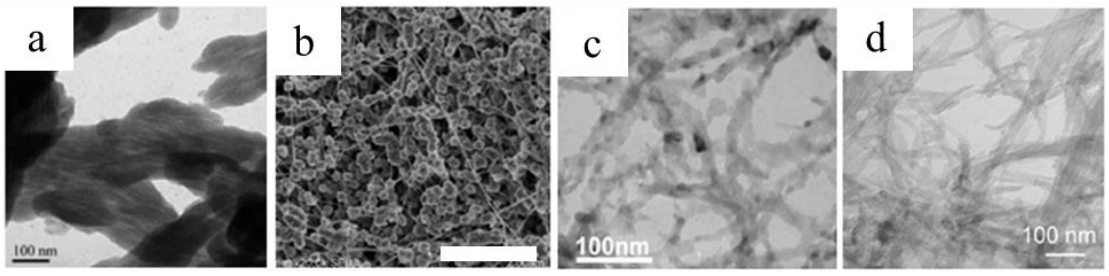

Figure 1.13 (a) silica nanowires produced on surface of cellulose (Scale bar = 100 nm). Reproduced with permission[78] copyright 2013 American Chemical Society. (b) ZnS nanoparticles templated onto the surface of cellulose (Scale bar = 2 μm). Reproduced with permission[81] copyright 2014 Wiley. (c) Titania nanowires templated onto the surface of cellulose. Reproduced with permission[80] copyright 2005 RSC. (d) Different silica nanowires grown on the surface of cellulose. Reproduced with permission[79] copyright 2009 Materials Research Society.

Figures 1.13a, **1.13c** and **1.13d** show the typical appearance of wires created by reacting adsorbed inorganic precursors on the surface of the polymer. The variation in length, thickness and coverage is quite large and the samples tend to aggregate. **Figure 1.13b** shows semiconducting nanoparticles grown on the surface of cellulose fibers. The coverage is also quite varied and the particle size is not controlled. The use of cellulose is motivated primarily for its higher rigidity in comparison to more flexible polymer templates discussed earlier. Thus, the arrangement of formed inorganic material is, in some sense, straighter but at the expense of control within the structure. An important distinction to be made is that polymer templates can be from either synthetic or biological origins. In addition to cellulose, several other soft biological materials have been used to template rod and wire-like inorganic structures. A brief description of these methods is provided below.

Virus capsids of various linear shapes have been used by researchers to template a variety of inorganic structures.[4] The capsid, or protein shell, of many viruses possesses a cylindrical or rod-like structure with functional groups on it that can be subjected to chemical modification. Some of the nanostructures that can be templated by viruses such as M13 include ZnS nanowires, Co_3O_4, and other metal oxides.[4, 5] Many different rod-like virus capsids can be used to template inorganic structures. The drawback of these approaches is the relatively limited number of inorganic materials that can be templated as well as the inability to modify the thickness of the resulting inorganic structures. This is because the capsids are specific sizes as determined by their biology. Virus capsid template inorganic structures are indeed useful for producing a relatively large number of the same type of structure, but completely different lines and procedures are required to

make anything different. In addition, there may not be virus structures that exist for desirable sizes of the resulting inorganic structures. Lastly, subsequent functionalization is not readily achievable as the resulting structures are essentially bare.

Virus capsids can be classified as unimolecular templates. This signifies that each individual template molecule can result in a single templated inorganic structure. In contrast to virus capsids, lipids can be classified as micellar templates. That is, they are capable of templating inorganic structures through coordinated interactions of many small components. Unlike all templating strategies discussed before, micelle approaches are at a disadvantage. This is because micelle formation is highly dependent on concentration, temperature, pH and ionicity of the system. Thus harsh reaction conditions can destroy all micellar assemblies and make inorganic templating difficult, irregular or impossible. However, some interesting inorganic structures can be made with this procedure including complex helical inorganic structures (**Figure 1.14**).[15]

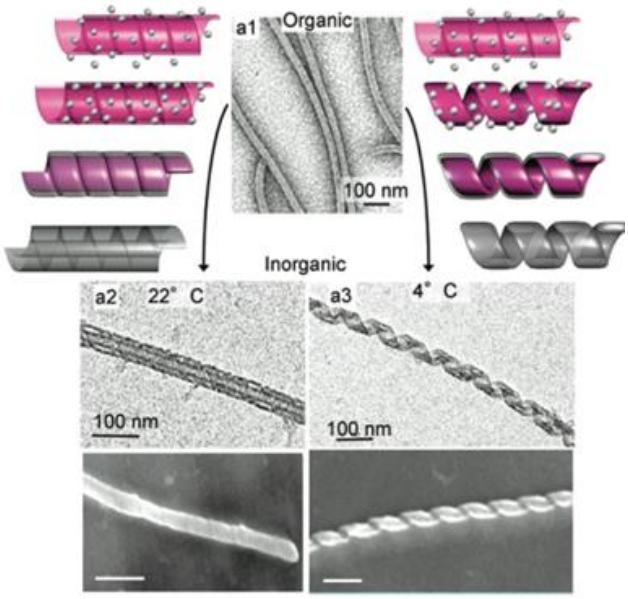

Figure 1.14 Helical inorganic silica templated by bis-quaternary ammonium gemini (two alkyl tails) surfactants and tartarate. Reproduced with permission[15] copyright 2008 American Chemical Society.

Indeed, such biologically-sourced materials have many applications in templating; however the advantages of availability are countered by lack of control of the possible structures made. Thus, synthetic means offer a clear advantage if specific and precise control over size, shape, solubility and properties are desired. The various wire/rod-like inorganic nanostructures described have applications across many different fields in engineering, science and medicine.

All of the previous background has focused on a particular group of primarily synthetic templating approaches. Indeed they possess several advantages including well-defined macroinitiator cores, excellent solubility in organic solvents and a diverse assortment of different polymers and small molecules capable of complex functionalization. Despite this, limitations in such approaches do exist and have the

potential to be mitigated by a different polymer templating approach. The following section introduces hyperbranched polyglycerol systems which are the primary focus of all work outlined in this dissertation due to their potential advantages in many applications to be discussed in detail despite being relatively poorly understood and investigated.

1.1.3 Hyperbranched Polyglycerol Templates

Branching in polymers can occur in many different ways.[28, 82] In the case of previously-described star polymer template strategies, a branched polymer is created via polymerization from a macroinitiator core to ultimately produce an x-arm star polymer structure. Similarly, a macroinitiator polymer backbone is used to produce a branched linear structure known as a bottlebrush polymer. In the case of hyperbranching this concept is again adopted; however the branching continues in a repetitive fashion throughout the polymerization. What this means is that the number of branches from a macroinitiator core is not fixed at the outset as in the previous examples. This work focuses specifically on the use of polyglycerol-based hyperbranched polymers (HPGs) and to lesser extent β-CD-based templates. Details regarding the polymerization mechanism, polymerization control, properties, and current state-of-the-art are herein addressed.

First pioneered by Suzuki et al. in 1992, the concept of a polymerization driven by the ring opening isomerization of highly strained cyclic species is a relatively new strategy for crafting interesting polymeric structures.[83, 84] Dubbed ring-opening multibranching polymerization (ROMBP), it remained largely unexplored until the turn of the last century when substantial efforts were put forth by Sunder and Frey into

understanding specifically the polylycerol-based hyperbranched system.[85, 86] ROMBP is one of three typical branching polymerization techniques described as a ring-opening polymerization from a latent AB_x monomer.[85] The other two are step-growth polycondensation of AB_x monomers and self-condensing vinyl polymerization (SCVP) of AB* monomers.[87, 88] **Figure 1.15** shows a simplified mechanism for the three branching techniques described. The top two pathways represent polycondensation and ROMBP and the bottom pathway represents SCVP. Each strategy has its own set of advantages and disadvantages. For ROMBP, it is possible to achieve narrower molecular weight distributions and higher degrees of polymerization due to the absence of a small molecule condensate as well as the high ring strain driving polymerization. The drawback is that few latent monomers are commercially available which makes application of this method more challenging as all monomers must be produced in-house. Also intra and intermolecular cyclization can be a problem for certain systems.[89]

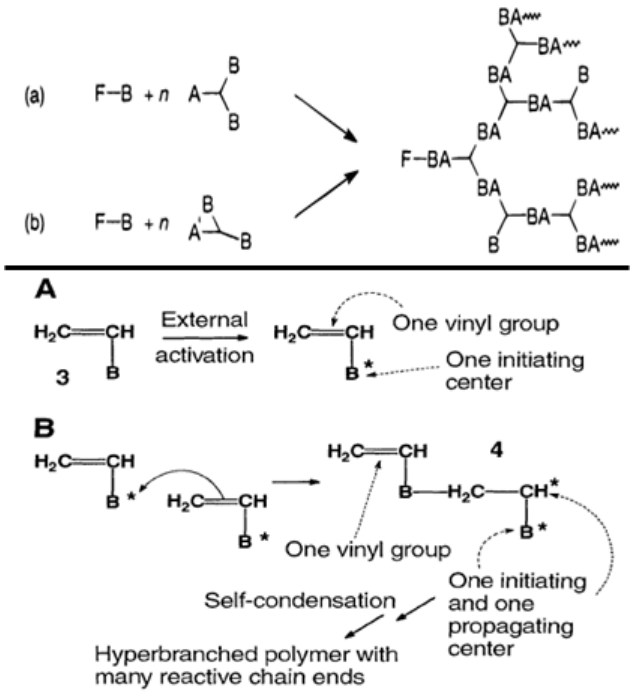

Figure 1.15 (Top) General schematic for polycondensation-branching polymerization from an AB_x monomer and ROMBP polymerization from a latent AB_2 monomer. Reproduced with permission[87] copyright 1999 American Chemical Society. (Bottom) General schematic for self-condensing vinyl polymerization (SCVP). Reproduced with permission[88] copyright 1995 American Association for the Advancement of Science.

SCVP is a more elegant technique in the sense that polymerization occurs through "inimers" which are monomeric units containing both a vinyl group and an initiator that can be activated externally and also initiate polymerization though the vinyl double bond. This also facilitates a more controllable polymerization. More materials can readily undergo SCVP compared to ROMBP which makes it more accessible. Traditional polycondensation branching has by far the largest number of polymers to choose from which makes it the most versatile. However, it has the problem of low degrees of polymerization due to the formation of small molecule condensation products in many situations. Also, nearly quantitative conversion is required in most cases to see high molecular weight polymers.

Polyglycerols proceed by the ROMBP mechanism of a commercially-available latent AB_2 monomer called glycidol. It can proceed either in a cationic or anionic fashion, but the focus of this dissertation is strictly anionic ROMBP due to greater availability in the literature as well as complications associated with the former in terms of yield, solvent limitations and a more complex and less understood polymerization mechanism.[90, 91] **Figure 1.16** shows the specific mechanism for the anionic ring-opening multibranching polymerization of glycidol monomer.[92]

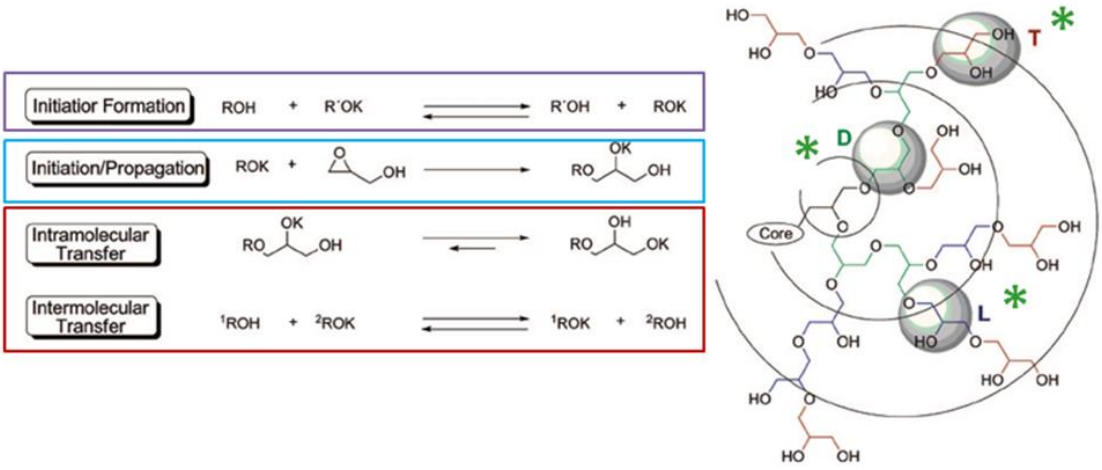

Figure 1.16 Schematic representation of the key stages in anionic ROMBP of glycidol monomer (left) into a generic hyperbranched polyglycerol structure (right). ROMBP proceeds first through an initiation stage followed by propagation (ring-opening) and inter/intramolecular anion transfer prior to additional propagation. The last two stages alternate during the main stage of polymerization. Note the four different types of repeat units present in this random structure: L_{13}, L_{14}, D, and T. The ability to characterize such random structures relies heavily on accounting for the relative population of these fundamental building blocks (analogous to the repeat units of a well-defined linear polymer or dendrimer). Reproduced with permission[92] copyright 2012 Wiley.

The mechanism can be broken down into four key stages. In the first stage, a small molecule polyol initiator, typically 1,1,1-tris(hydroxymethyl)propane (TMP), is partially deprotonated (10%) by a strong base such as potassium or sodium methylate (NaOMe or KOMe). Low deprotonation percentages are typically used to maintain

solubility of the initiator. Investigations into maintaining the solubility of polyol initiators of higher percent deprotonation are greatly needed. Upon deprotonation, the in situ fored methanol is removed by evaporation.

In the second stage, monomer is slowly added via a syringe pump and the deprotonated initiator attacks the glycidol monomer ring, initiating the ring-opening polymerization and forming a negative alkoxide species. The reactivity of the anionic alkoxide is highly dependent on several factors including counter-ion, solvent dielectric constant, volume, and temperature. Since this polymerization isn't overtly controlled by a catalyst these parameters play a much greater role in polymerization control. The slow monomer addition (SMA) technique employed during this polymerization is a compromise necessary to control the polymerization and maximize the percentage of polymer initiated from the initiator as opposed to auto-initiated polymerization. The tradeoff is that the reactions take longer to complete.

In the third stage, this alkoxide species can undergo two different types of rapid proton transfer between the anionic end and an available hydroxyl proton nearby prior to initiating another monomer. These are either intermolecular proton transfers or intramolecular proton transfers. This step is the most critical in defining the hyperbranching character of these polymers as it is the origin of branch point formation. Since the proton transfer is fast, there is an equal probability of either occurring in theory. This means that on average an equal number of both types of proton transfer will occur. Proton transfer creates a branch point on a growing polyglycerol chain. This leads directly to either an L_{13} or L_{14} type linear unit or a dendritic branch point (D) depending on the type of transfer that occurred immediate prior. A succession of the same type of

alkoxide initiation yields linear groups whereas an alternation yields a dendritic group. Once the last of the monomer is consumed the final ring-opening yields a terminal group containing two hydroxyl groups (T). Terminal units can also form anytime a ring opening does not initiate another ring opening. Ring cyclization is an unintended reaction that can occur if the amount of glycidol in the reaction is much larger than the number of initiating alkoxide groups. This is because the hydroxyl proton of monomers can be deprotonated and react to form stable six-membered rings. It is for this reason that the SMA technique is used to keep the number of monomers present low with respect to the initiating species and ensure that the growing chains are properly initiated throughout the course of the polymerization.

Figure 1.17 shows the deprotonation as a function of molecular weight/time and underscores just how important having a small amount of monomer present is.[93] It can be seen that even for 100% deprotonation, once the molecular weight gets above 10 kDa, there are less than 10% active chain end remaining. With respect to the size of the molecule there may still be a large absolute number, but their density is extremely low. Thus, if a large amount of monomer is present, it is as if a sea of monomer exists and auto-initiated polymerization among monomers dominates leading to large PDIs. Cyclization leads to low degrees of branching (as it essentially eliminates them) and reduces the availability of hydroxyl groups. The takeaway is that the polymerization of hyperbranched polyglycerols is extremely easy to achieve, but the controlled polymerization of hyperbranched polyglycerols of desired molecular weight and low polydispersity in a reliable fashion is extremely difficult. Though depending on the intended applications, the importance of this point is variable. In fact, it was only recently

that any kinetic study of such hyperbranched polymers was undertaken by Haag et al. and supports the fact that a low feed ratio (i.e. SMA condition) is ideal for achieving high molecular weight and low PDI hyperbranched polymers.[94, 95]

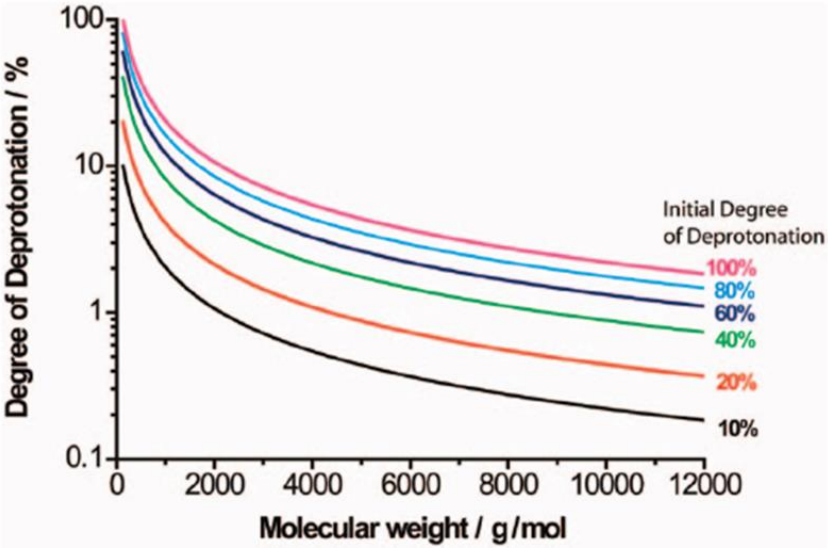

Figure 1.17 Molecular weight-dependent decrease in active chain concentration at all initiation degrees of deprotonation (DD_0). Reproduced with permission[93] copyright 2009 American Chemical Society.

Polyglycerols are an interesting type of hyperbranched polymer with many distinct advantages over the other hyperbranched polymer systems available. Essentially the branched equivalent of polyethylene glycol (PEG) and poly(vinyl alcohol) (PVA), they possess a large number of ether linkages and hydroxyl groups. But unlike PEG, whose ratio of hydroxyl groups decreases with increasing molecular weight, the opposite effect is observed for polyglycidol. And, unlike PVA, it is much more soluble in water and other polar or ionic solvents at much higher degrees of polymerization. As can be seen in the polymerization mechanism, there is an abundance of hydroxyl groups both at the surface as well as within the structure to a slightly lesser degree. Compared to perfectly dendritic structures, HPGs offer the advantage of a large volume one-pot

synthesis route which avoids the tedious iterative generational synthesis procedure employed for dendrons. The tradeoff is that the polymerization mechanism is highly sensitive to water, the hyperbranched structures are far less uniform and require more complex methods of characterization and purification.

HPGs are primarily characterized by a combination of NMR, GPC and MALDI-TOF to determine primarily the molecular weight, polydispersity, degree of branching (DB), number of hydroxyl groups, and degree of cyclization. Molecular weight and PDI have already been reviewed and the same meaning is employed here. The degree of branching is a term used to quantify the relative branching of a given structure, and thus serve as a basis of comparison between different branched structures particularly of similar degrees of polymerization. Degree of branching can be defined by equation (1) below.[92]

$$DB = \frac{D + T}{D + T + L_{13} + L_{14}} \qquad (1)$$

The variables *D, T,* and *L* refer to the relative percentages of the different types of hyperbranched polyglycerol units mentioned earlier (dendritic, terminal and linear respectively). The extremes of this equation are [0, 1], where 0 refers to a linear polymer (i.e. $D = T = 0$) and 1 is a perfectly branched true dendrimer (i.e. L = 0), respectively. Hyperbranched polymers typically occupy the range between 0.5 and 0.67 when strictly the SMA anionic ROMBP technique is employed. Higher DB values can be reached by post polymerization modification. The method for determining the relative contributions of each unit is a specialty NMR spectroscopy technique called inverse gated (IG) ^{13}CNMR spectroscopy. Traditional ^{1}HNMR spectroscopy cannot be used because the

protons are all of relatively similar relaxation times so their signals are convoluted together. Fortunately, the carbon signals for each component are resolvable and studies have been done to identify these pairings.[85] This technique enables quantitative resolution of carbon signal intensity. **Figure 1.18** shows a representative IG^{13}CNMR and ^{1}HNMR spectra of HPG with the unit assignments. Note in the left spectrum that each of the carbon repeat unit peaks is resolvable whereas the proton peaks in the right spectrum are convoluted. The chemical shift of each carbon for the respective units is indicated at the bottom.

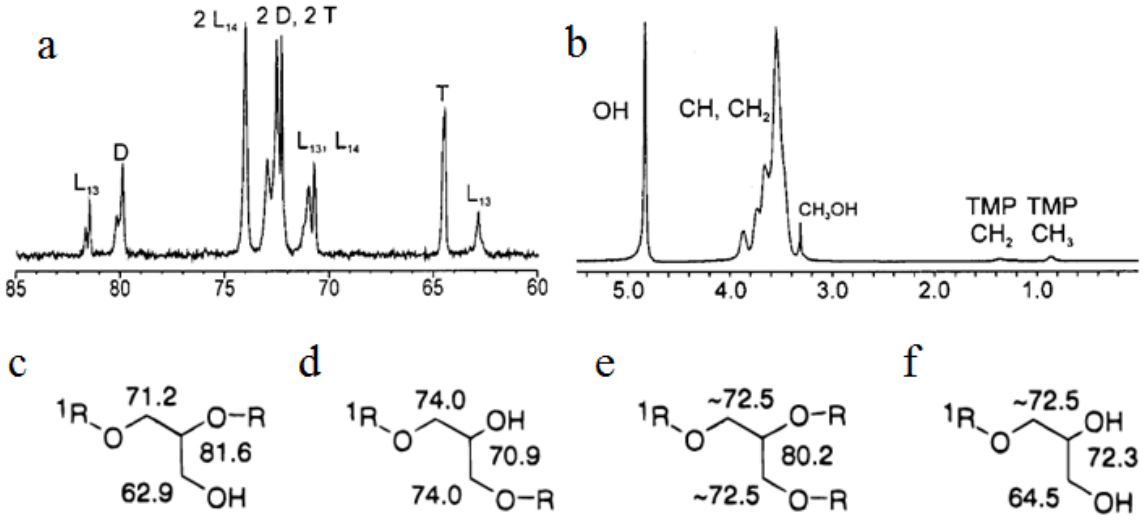

Figure 1.18 (a) IG^{13}CNMR spectra of typical HPG sample showing individual resolution of all peak types. (b) ^{1}HNMR signal spectra of a typical TMP-initiated HPG showing signals from the initiator core and HPG backbone. Carbon chemical shift assignments for the different fundamental units of hyperbranched polyglycerol: (c) Linear type 1,3 (L_{13}), (d) Linear type 1,4 (L_{14}), (e) Dendritic (D), and (f) Terminal (T). Reproduced with permission[85] copyright 1999 American Chemical Society.

The molecular weight of HPG polymers can be determined from ^{1}HNMR by integrating the core TMP methyl or methylene proton signals with respect to the

backbone proton signal. It becomes difficult to determine the molecular weight accurately for large molecular weights due to the low relative intensity of the core protons. Gel permeation chromatography is also used to evaluate the molecular weight distribution and calculate the PDI. However, depending on the calibration standards used and the general structure of HPGs they typically results in poor agreement with the molecular weights measured in NMR. Once the molecular weight (DP_n) is determined the number of hydroxyl groups n(-OH) can be determined by equation (2).

$$n(-OH) = DP_n + f \cong DP_n \quad for\ n \rightarrow large \qquad (2)$$

Note that this gives the total number and cannot make a distinction between exterior terminal hydroxyl groups (more reactive) and internal linear hydroxyl groups (less reactive). To make this distinction the relative percentages of each fundamental unit can be multiplied by the total number of hydroxyl groups.

The last major consideration when characterizing hyperbranched polyglycerols is the degree of cyclization. Since cyclization cannot be distinguished by NMR, its presence is typically verified by matrix-assisted laser desorption ionization-time of flight spectroscopy (MALDI-TOF). This is because cyclic species have an offset in the molecular weight of non-cyclized species which is resolvable in MALDI plots. **Figure 1.19** shows a comparison between an HPG sample where there is an absence of cyclization and one where there is cyclization. Depending on the reaction conditions, cyclization can be minimized. However, at long reaction times or outside of the SMA regime, cyclization can dominate.

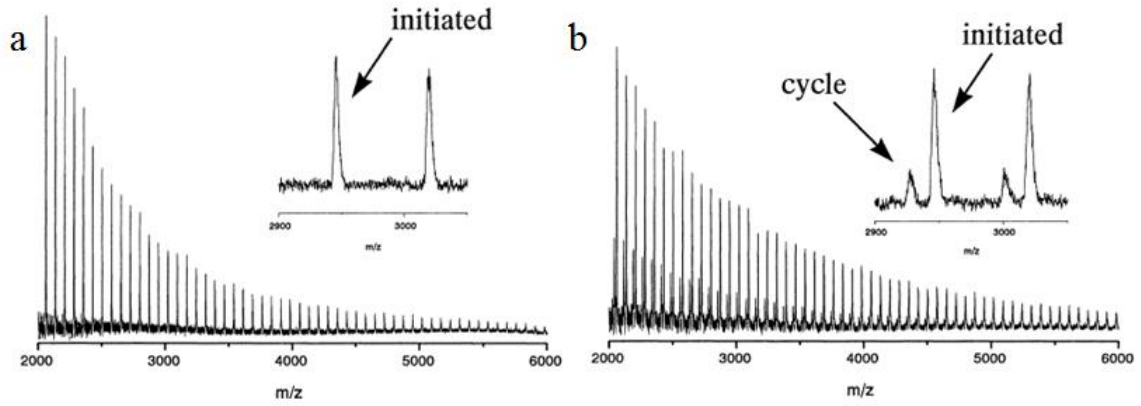

Figure 1.19 (a) MALDI plot of an HPG sample showing no cyclization (low molecular weight example). (b) MALDI plot of an HPG sample showing partial cyclization at a higher molecular weight. The challenges associated with HPG center around pushing the boundary of controlled polymerization to higher molecular weights while maintaining low polydispersity and minimal cyclization. Reproduced with permission[86] copyright 2001 Wiley.

It is important to note that MALDI cannot be used to determine the molecular weight distribution of hyperbranched systems because the sensitivity is very low above 10 kDa. The essential aspects are cyclization verification and the appropriate repeat unit value. The above details highlight the essential characterization aspects of hyperbranched polyglycerols. In addition, there are several commonly-referenced aspects associated with the synthesis procedure which are detailed in **Table 1.1**. These parameters are referenced when outlining the synthesis route for HPG proceeding via anionic ROMBP.[96]

Table 1.1 Key parameters governing anionic ROMBP of hyperbranched polyglycerols

Parameter	Description
Monomer to Initiator Ratio (molar)—M:I	Ratio of glycidol to polyol initiator—This ratio corresponds to the theoretical molecular weight of the final product under ideal SMA conditions.
Solvent to Monomer ratio (v/v)—S:M	Volume ratio of dispersing solvent to latent glycidol monomer—This ratio controls the viscosity of the solution and regulates the relative concentration of monomer to initiator species. SMA and high dilutions keeps monomer ratio to active site concentration low.

Table 1.1 continued

Stirring Speed (rpm)	The highly viscous nature of the polymerization requires external mechanical stirring to uniformly disperse the mixture, reduce agglomerations, and also keep local monomer concentration low.
Temperature (C)	Has effects on the rate of reaction and greatly reduces the viscosity.
Percent Deprotonation (% -H^+)	The amount of hydroxyl groups deprotonated at the beginning of the polymerization. Higher deprotonations can theoretically lead to larger molecular weights and more uniforms shapes. However, the solubility of highly deprotonated initiator is poor. This leads to incomplete dissolution and poorly-controlled polymerization.
Solvent dielectric constant	This is important in controlling the coordination of the counter-ion of the base used in deprotonating the initiator. The reactivity of the growing alkoxide anions is affected by this coordination.
Base	The polyol initiator is deprotonated by a strong alkali methoxide (MOMe). Depending on the cation, the degree of deprotonation can be affected as well as the activity of the as-formed alkoxide anions and growing alkoxide chain ends
Reaction time (hours)	The length of time the system is allowed to react determines the molecular weight. However, the longer it reacts the greater the likelihood that cyclization and crosslinking can occur and raise the PDI.
Monomer injection rate (ml/hr)	The rate of addition of monomer (may be diluted in syringe) to the reactor via dosing pump. This controls the concentration of monomer present in the reactor and is essential to having a controlled anionic ROMBP polymerization.

Hyperbranched polyglycerols are truly an exciting area of chemistry which has received surprisingly little interest despite the wealth of applications to be had. All applications of HPG structures follow a simple recipe of synthesis and derivatization.[97] Granted this is not so simple to execute, but the separation between fundamental study and end use is remarkably short for HPG-based materials. With applications in immense and diverse fields including biomedicine (proteomics,[98] drug conjugation/delivery,[99-104] biomineralization,[105] antifouling,[106, 107] biocompatibility,[97, 108-110] synthetic biology[111, 112]) and nanomaterials (batteries,[113] catalysis,[114, 115] block-copolymers,[116-121] nanoparticles[122-124]). **Figure 1.20** summarizes the key areas of biomedical applications motivated by the

comparable, if not improved, biocompatibility of HPG compared to PEG. Bioconjugation to biomolecules is made possible by the ease of differentiation of the surface hydroxyl groups.[101]

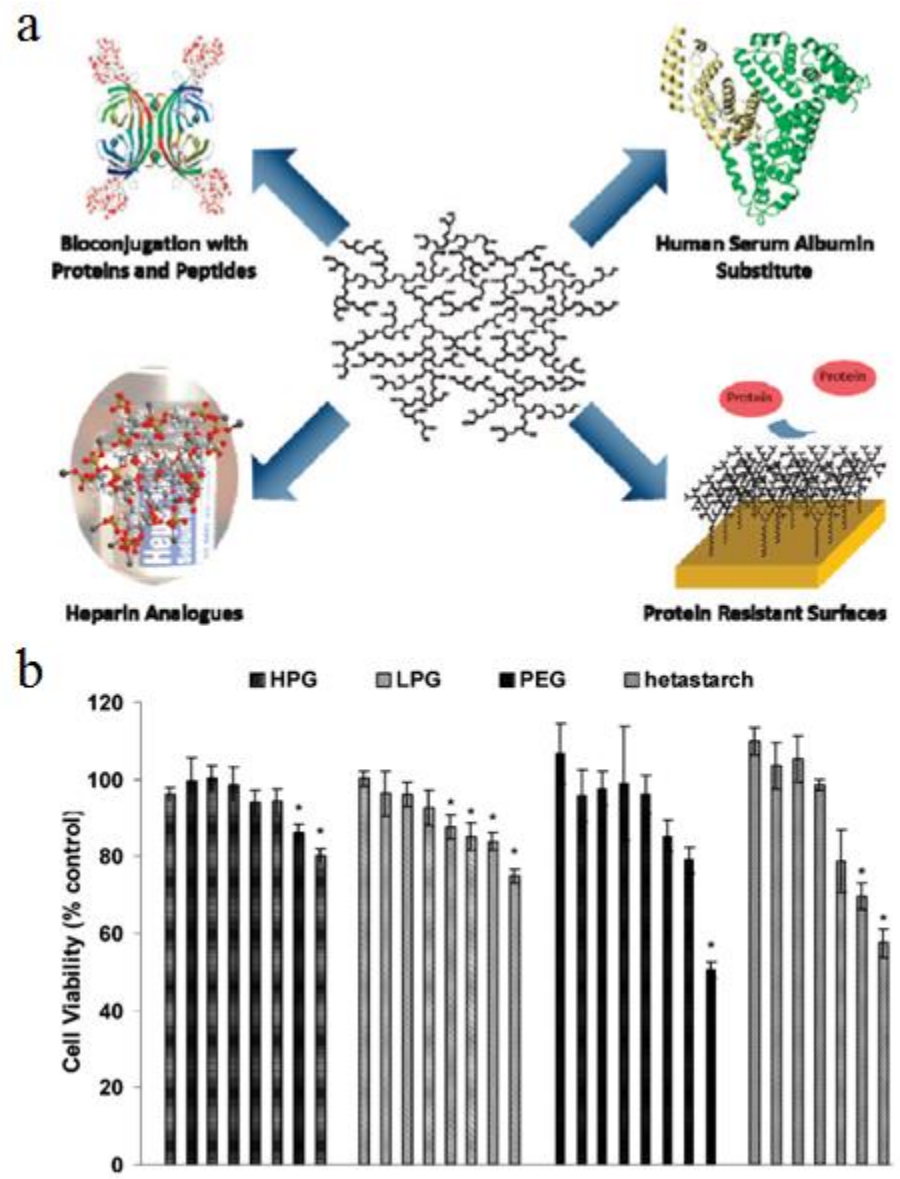

Figure 1.20 (a) Hyperbranched polyglycerols have applications in proteomics, synthetic biological materials, drug alternatives and bio-resistant coatings for myriad applications. Reproduced with permission[97] copyright 2010 American Chemical Society, https://pubs.acs.org/doi/10.1021/ar900158p. Further permission relating to this material should be directed to the ACS. (b) The cell viability of different biocompatible polymers supports the claim that HPG possesses good, if not improved, biocompatibility compared to the PEG industry standard. Reproduced with permission[108] copyright 2006 American Chemical Society.

Furthermore, covalent attachment of different biological molecules or charged species coupled with the internal hydrophilic core allows HPG to coordinate many biological molecules including fats, proteins and of course water. This has led to research into HPG synthetic biologicals including the anticoagulant heparin[111] and blood plasma.[112] The advantage of using HPG for these applications is the likely lower costs and risks compared to biologically sourced materials (bovine serum albumin).

The potential for unimolecular amphiphilic core-shell like structures also enables HPG to serve as a carrier for many different active materials including water-soluble and organic-soluble drug compounds. Since such materials can be further crosslinked, they serve as mechanically strong soft carriers for use in high shear environments such as the blood stream. The HPG structure thus facilitates uptake and retention of many different dyes[102] and drug molecules[100] for both imaging and therapeutic applications. Despite efforts in this area, little attention has been given to produce highly regular HPG capsules for these applications. In addition, most of the particles have relatively small, single-component loading structures. Investigation into co-loaded, larger volume and reversible HPG-based nanocapsules is a relatively unexplored area of research.

The biocompatibility of HPG extends it use beyond just a benign nanoscopic drug carrier to include coating small and large surfaces for antifouling purposes. This is particularly a problem in the body where adhesion of proteins and other biomolecules to polymeric components inserted into the body (stents, catheters, implants, artificial valves/organs)[106] as well as cell microarrays is a problem.[125] Since HPG has excellent film casting properties and a lower viscosity compared to linear PEG, it represents an ideal alternative for bio-resistant coatings.

In addition to applications in soft, biological and medical fields, hyperbranched polyglycerols also have many applications across nanotechnology. Many of these applications stem from the ability of HPG to function as a macroinitiator for many different types of polymerization and/or small-molecule functionalization. Since the number of hydroxyl groups can be controlled in HPG systems from only a few to several hundred (with several tradeoffs as previously mentioned) the degree of functionality can be readily optimized. It is also important to note that depending on the application, the necessity for having highly monodisperse HPG may be lessened. An interesting application of HPG that has the potential to become very useful lies in its use as a polymeric binder in batteries.[113] One of the biggest problems in battery research is pushing the performance to higher cycle times while minimizing electrode pulverization during the high volume change often associated with lithium cycling. Hyperbranched polyglycerols offer a low Tg (flexible) binder that can hold electrode materials together in a cage-like fashion but also reform intimate contacts with electrode active materials (silica, barium titanate) to maintain the performance characteristics. A systematic study of their use in the many different battery applications is still yet to be undertaken. **Figure 1.21** compares the typical polymeric binder behavior to that of a recently-reported HPG based binder. In the case of batteries and many of the biomedical applications, HPG on its own has proved to be quite useful. The amazing potential of this material in both areas is unlocked when it is used as a macroinitiator to grow useful star polymer structures.

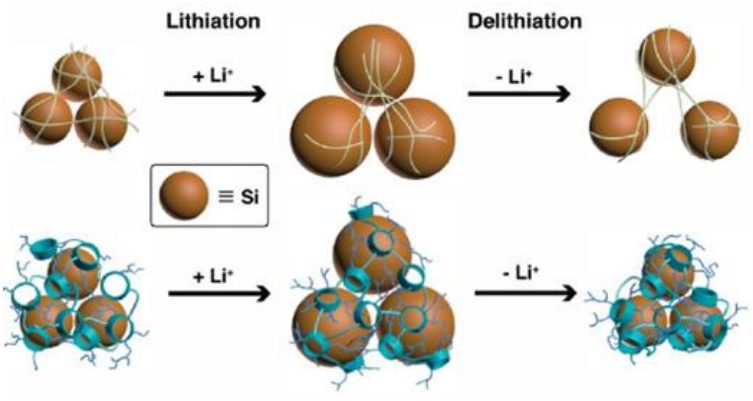

Figure 1.21 (Top) Typical lithium cycling with linear polymer binder resulting in dissociation of electrode materials. (Bottom) HPG-based binder that holds the electrode material together during lithium cycling thus improving the battery lifetime. Reproduced with permission[113] copyright 2014 American Chemical Society.

The use of HPG to encapsulate catalytically actice metal atoms has shown promise in recent years for applications in *in situ* catalysis in aqueous and organic solutions.[48, 114, 126, 127] The basic premise is to take an HPG molecule and functionalize it with hydrophobic chains to create an amphiphilic HPG-g-alkyl chain molecule. These molecules can then form micelle structures where metal colloids can be coordinated on the inside of the structure. These approaches yield very irregular structures which have poorly-defined shapes, though for the application of catalysis this is less of an issue. The materials to be catalyzed essentially diffuse into the structure and react, with products diffusing out. Stability is also a concern in such systems over time, temperature and environmental variations which can lead to aggregation and sedimentation. Nonetheless these approaches are useful in that they show the ability of the HPG core to corrdinate metal ions (albeit not as strongly as other chemical species). It also shows that metal ions can diffuse through the short hydrophobic exterior into the core. Lastly, it motivates the

use of acyl chlroide-functionalized molecules for derivitizing HPG due to the high reactivity between primary alcohols and acyl chlorides (as of yet minimally reported). **Figure 1.22** summarizes the general approach to creating amphiphilic micelle structures based on HPG.

The approaches to encapsulate catalytically-active metal precursors are certainly an interesting application of HPG chemistry. But the results are ill-defined and are not developed more than this. The use of HPG-based molecules for crafting a greater diversity of hard inorganic structures is clearly lacking but certainly suggestive as a next step based on the literature. HPG copolymers have been developed and researched, but strictly as interesting and complex macromolecular architectures and less so for templating.

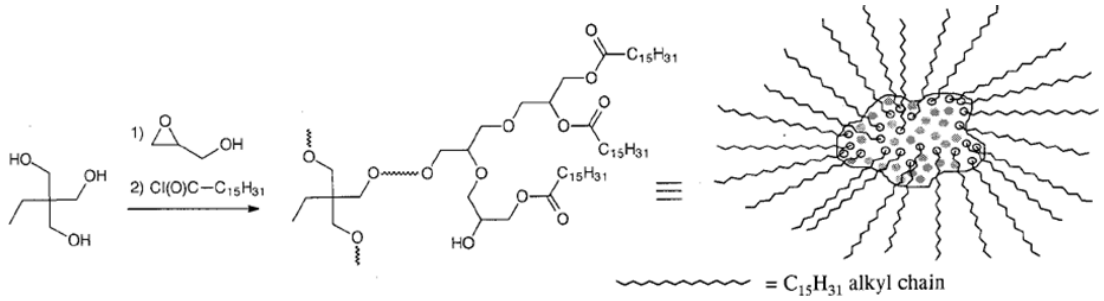

Figure 1.22 General synthetic route for producing amphiphilic HPG-b-alkyl chain molecules. The inner hydrophilic core can preferentially coordinate with metal ions. Reproduced with permission[114] copyright 2000 American Chemical Society.

Significant efforts in the past decade have been directed toward boosting the molecular weight of hyperbranched polyglycerols while maintaining low polydispersities. To date, the threshold for reliably producing monodisperse HPG (PDI <1.5) is around 10 kDa by using the established approach previously outlined.[86] Attempts to produce higher molecular weights have succeeded; however, the polymerizations generally proceed with

little control. The result is larger PDI values. Strangely, higher molecular weight HPG (greater than 80 kDa) have been reported with low PDIs; however, there is much debate as to the reason for this and the nature of the polymerization occurring.[128, 129] What remains is the challenge of creating high and intermediate molecular weight HPG (20-50 kDa) possessing low PDI via controlled ROMBP.

From such structures, additional chemistry has been performed; particularly sequential polymerizations of one form or another. The result is several different types of HPG block copolymers[130-132] and miktoarm type polymer structures.[133] In the case of these pure polymeric structures the motivation for investigating them hinges on the tunability of several properties including Tg, crystallization, and degree of hydrophobicity/hydrophilicity/amphiphilicity. One of the most common types of copolymer structures investigated is that of a combination of hyperbranched polyglycerol and poly(ethylene glycol); essentially a copolymer of a linear and branched polymer of the same kind. This is motivated by the fact that such structures are extremely soluble in water and lower alcohols and thus have no aggregation issues. Systems which possess nonpolar hydrocarbon components (aromatic rings) are not nearly as effective for biological combinations.

Block copolymers have primarily been investigated for their micelle-like behavior[132] and potential to form crosslinkable organic structures that can complex with various drugs or chelate metal ions.[97] This process can be further developed and used to produce HPG-based inorganic and organic templates of greater complexity and uniformity. Owing to the abundance of surface hydroxyl groups, virtually any type of post synthetic chemistry can be performed on hyperbranched polyglycerol structures. In

the next sections, details regarding the relevant chemistries employed throughout this work are reviewed.

1.2 Relevant Chemistries in Nanocomposite Synthesis

The work in this dissertation relies on a small set of simple, robust and generalizable orthogonal organic synthesis techniques applied in different sequences to achieve different results. To that end, this work heavily relies on two classes of organic chemistry. The first is several types of polymerization techniques including anionic ring-opening multibranching polymerization (as previously described), atom-transfer radical polymerization (ATRP).[134, 135] In addition, reversible addition fragmentation chain transfer polymerization (RAFT)[136] and nitroxide-mediated polymerization (NMP), while not employed, are reviewed for completeness.[136] The second is the extremely popular and reliable class known as "click" chemistry. Each of the three radical polymerization techniques falls into a broader subgroup of controlled/living radical polymerization techniques ATRP (its own category), degenerative transfer (RAFT) , and stable free radical polymerization (NMP).

1.2.1 Atom-Transfer Radical Polymerization (ATRP)

Since its independent discovery by Krzysztof Matyjaszewski and Mitsuo Sawamoto in 1995, atom-transfer radical polymerization has emerged as one of the most important chemical techniques in both industry and research.[137] The ATRP technique is best classified as a radical polymerization mediated by an equilibrium between an

activator and deactivator state of the growing polymer chains.[138] That is, a polymer chain (P_m) is considered active ($P_m^{\bullet}$) if it can attack a monomer and thereby grow, and inactive (P_m-X) if it cannot. This equilibrium is defined by specific rate constants for activation (k_a) and deactivation (k_d). Since all chains are initiated quickly and then promptly deactivated apart from a small number at any given time, it allows only a small number of chains to polymerize at any one time and thus reduce undesirable termination events.

The key ingredients in a typical ATRP reaction include the catalyst, co-catalyst, initiating species, and monomer to be polymerized. The catalyst for activating and deactivating the polymer chains is typically a metal halide (most commonly copper) with an appropriate chelating ligand (M_t^n/L) typically composed of multiple primary amine units that can coordinate with the metal ion. The catalyst activates a dormant polymer chain via oxidation from a lower to higher state upon accepting the deactivating halide from the dormant polymer chain (X-M_t^{n+1}/L). At this point the polymer chain can then undergo radical polymerization defined by polymerization rate (k_p) or terminated by exposure to air, radical quencher (k_t) or removal of co-catalyst complex. **Figure 1.23** shows a representative schematic of the general ATRP reaction as defined by the variables already introduced.[138]

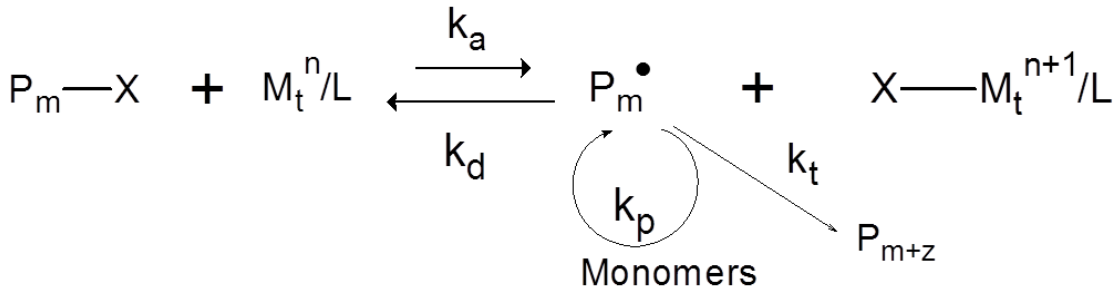

Figure 1.23 General mechanism for an ATRP polymerization controlled by an activator/deactivator equilibrium.

Figure 1.24 provides a summary of the variety of acrylate and methacrylate monomers that can be polymerized via ATRP.[138] In general, ATRP is insensitive to the chemical composition of the side groups so long as they do not interfere with the catalyst employed. It is remarkable just how many different types of polymers can be produced via ATRP. There are of course a few disadvantages associated with ATRP that necessitate the development of other controlled radical polymerization techniques. The most evident is that ATRP cannot be used to polymerize halide-containing monomers as these can serve as initiating sites as well leading to poorly controlled branch polymerization. Moreover, depending on the monomer used, it may be difficult to completely remove the catalyst/co-catalyst complex (as is the case for P4VP).

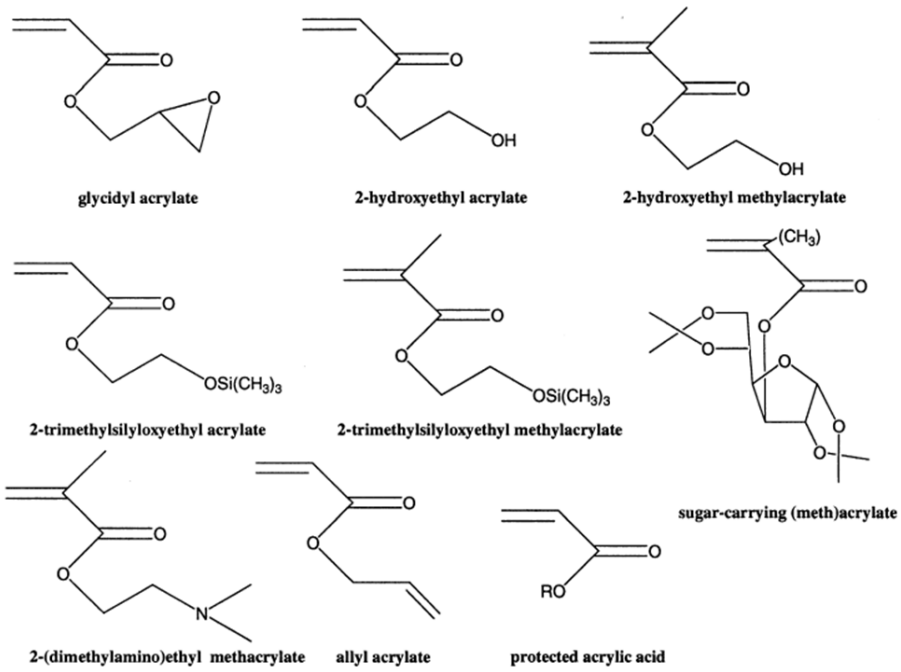

Figure 1.24 A representative group of functional acrylic and methacrylic monomer derivatives that can be directly polymerized by traditional ATRP (i.e. no need for a protecting group). Reproduced with permission[138] copyright 2001 Elsevier.

In comparison to previously-developed radical or ionic polymerization techniques, ATRP offers several significant advantages as follows:

- A wide range of vinyl monomers can be polymerized including functional monomers capable of undergoing subsequent reaction (i.e. orthogonal chemistry)
- Reactions are performed under mild conditions including neutral pH, low temperature
- Reactions are relatively insensitive to water or oxygen
- Affords living polymers that can be easily copolymerized with other monomers
- Inexpensive and readily available variety of co-catalysts
- Inexpensive and safe initiators
- Low polydispersities (PDI<1.1) are possible

ATRP is a major polymerization technique used in this work for the reasons above. In addition to the above general description for ATRP, several additional modifications of this basic procedure have been developed. These include reverse ATRP, ARGET, Zerovalent metal ATRP, Electrochemical ATRP, aqueous ATRP and metal-free ATRP.[24, 137, 139, 140] In reverse ATRP, the transition metal/ligand complex is introduced in the elevated oxidations state from the beginning which is then converted to the activating species by a typical free radical initiator (AIBN). This technique is useful for polymerizing more reactive species that are stabilized in the oxidative state. The drawback is that copolymerization is not possible for this approach and it can only be applied to homopolymer synthesis.

Activator regenerated by electron transfer (ARGET) ATRP is a polymerization technique utilizing extremely low catalyst concentrations.[141-143] In this approach the small amount of catalyst that is added is continuously regenerated by a reducing agent. This approach is often touted as a "green" polymerization technique because such a small amount of catalyst is used that it often does not require subsequent removal after the reaction is completed. Also the small catalyst concentration greatly reduces the frequency of side reactions.

Zerovalent metal ATRP, also known as supplemental activators and reducing agents (SARA) ATRP, involves using metal atoms in their M(0) state as a reducing agent (typically Cu or Fe).[144-146] This process has the advantage of rate control mediated by surface area and ease of removal of solid M(0). This procedure does introduce more metal into the system as a tradeoff. This technique is very much at odds with others which are tending toward the reduction of metal catalyst.

Electrochemical ATRP (eATRP) offers the first example of an ATRP technique where the reduction occurs via electric potential and not from an added chemical.[147, 148] Thus a new handle is achieved for ultimately controlling the polymerization (ratio of X(1) to X(2) catalyst oxidation states) via externally-adjustable variables such as applied current, potential and total charge. This technique also retains the livingness of traditional ATRP and is a relatively unexplored area within controlled radical polymerization techniques.

Aqueous ATRP is also an interesting technique particularly because it has immediate applications in industry which often make use of aqueous environments for many large-scale reactor syntheses. These are essentially emulsion-based ATRP methods in which the addition of a surfactant enables the polymerization of either organic-soluble or water-soluble polymers via ATRP at a large scale.[149] This technique is particularly important for polymerizations involving biologically-relevant materials and/or processes.[150, 151]

The most recent development in controlled radical polymerization is that of metal-free ATRP in which the metal halide/ligand complex is replaced by a UV activated organic small molecule such as phenothiazine derivatives. This allows the rate to be controlled by the intensity of UV light as well as halted at any time by removal of UV source.[152-154] This recent development is very interesting and will likely constitute a large area of research in the near future.

1.2.2 Reversible Addition-Fragmentation Chain Transfer Polymerization (RAFT)

Discovered a few years after ATRP by Thang et al., reversible addition-fragmentation chain transfer (RAFT) has also become an extremely powerful and well-studied controlled polymerization technique.[155] Unlike ATRP, RAFT is defined as a degenerative transfer process. This means that any one chain is activated simultaneously with another chain being deactivated and that both chains form an intermediate of approximately twice their respective molecular weights before alternatively fragmenting off. Thus activation/deactivation occurs via chain transfer, not atom transfer, in a see-saw like process. This process is regulated by a chemical called a chain-transfer agent (or RAFT agent).[156] The RAFT process generally proceeds via five separate steps; initiation, reversible chain transfer, reinitiation, chain equilibrium and termination. The initiation step is essentially the same as for ATRP in that a conventional initiator (AIBN) creates the first free radical/oligomer radical ($P_n^{\bullet}$). In reversible chain transfer, the radical combines with the RAFT agent (ZC(=S)SR) and produces another radical initiator ($R^{\bullet}$). This radical initiator then proceeds to reinitiate a monomer and form another oligomer radical ($P_m^{\bullet}$). Eventually enough initiated radicals are formed and the primary phase of RAFT polymerization begins in which a chain equilibrium is developed between all growing polymer chains and the RAFT agent. This equilibrium is what leads to the even buildup of all chains and thus the low PDI upon completion. Retention of RAFT moieties upon completion is also typically observed.

In general, RAFT agents have been developed based on several groups of thiocarbonylthio compounds including trithiocarbonates, xanthates and dithiocarbamates. The rationalization for this is due to the requirements associated with what a RAFT agent

needs to do. To that end RAFT agents must have reactive C=S bonds, intermediate radicals that form must quickly fragment, the coupled intermediate in the equilibrium must preferably fragment to produce growing monomers and the R-group initially expelled must effectively reinitiate the polymerization in stage two.[156] Similar to the co-catalyst in ATRP, the precise structure of the RAFT agent must be compatible with the monomer which is desired to be polymerized. The thiocarbonylthio RAFT agent kinetics can be tuned by substitution of the R- and Z-groups. The main role of the Z-group is to control the degree of activation/deactivation of the C=S towards a radical. The R-group is primarily a good leaving group but also must be able to reinitiate polymerization. It is difficult to generalize which Z and R groups are ideal as it is highly dependent on the monomer of interest. The Z-group tends to dominate in determining the overall activity whereas the R-group can be thought of as a fine tuning component. **Figure 1.25** provides a general description of commonly-encountered RAFT agents based on the above description.[157] RAFT agents can also be bifunctional and facilitate RAFT polymerization initiation sites on the surface of particles[158] or other macromolecular and biological materials.[121]

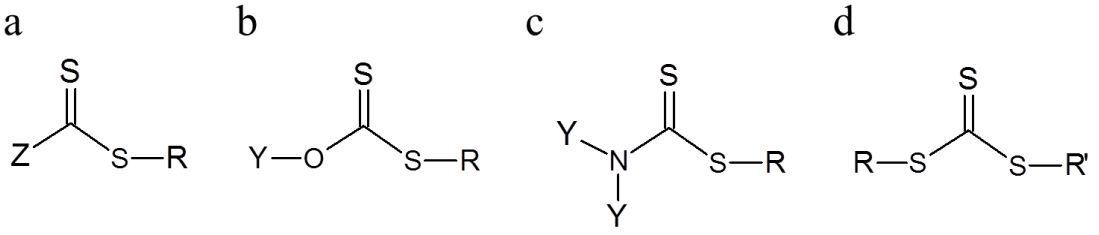

Figure 1.25 General structure of the most commonly encountered RAFT agents: (a) dithioesters, (b) xanthates, (c) dithiocarbamates, and (d) trithiocarbonates. In each case the choice of Z and R/Y will drastically affect the kinetics of RAFT polymerization for a particular monomer.

As with ATRP, RAFT possesses several distinct advantages which have motivated its research and development as follows:

- Many functional monomers can be polymerized by RAFT (including halogenated, nonionic, anionic, cationic and zwitterionic) that cannot be polymerized by ATRP
- Many different RAFT agents exist allowing precise control to be achieved in very specific cases
- RAFT can be performed directly in aqueous media and on hydrophilic monomers (in addition to hydrophobic monomers)
- Acid-containing monomers can be directly polymerized (polyelectrolytes)

RAFT polymerization also has limitations and disadvantages inherent in the nature of its mechanism. In certain combinations the polymerization can be greatly retarded or inhibited due to the nature of the RAFT intermediate formed. In aqueous reactions, there is a possibility of RAFT agent hydrolysis leading to undesired side product formation and poor control of the polymerization. Ultimately, what these problems can lead to are long reaction times and the need for elevated temperatures during the reaction.

1.2.3 Nitroxide-Mediated Polymerization (NMP)

Nitroxide-mediated polymerization is the last major type of polymerization to be reviewed. Unlike both ATRP and RAFT, NMP is a stable free radical polymerization (SFRP) technique. This technique is interesting from the standpoint that the equilibrium between activation and deactivation of the living polymer chains is strictly temperature controlled.[159] The distinguishing feature of NMP is the unusual nature of the nitroxide/alkoxyamine which can form a long-lived radical in solution due to the stabilization of the N—O bond (persistent radical effect, PRE). Moreover, the nitroxide can reversibly couple with the growing chain end but is sufficiently stable to not initiate polymerization on its own via monomer coupling. **Figure 1.26** shows the complete NMP mechanism. The nitroxide is usually the sole initiator of polymerization because at elevated temperatures it undergoes a hemolytic cleavage of the C—O bond resulting in an initiating carbon radical and a persistent nitroxide radial in a 1:1 stoichiometry. Bimolecular initiators can be used but they proceed with less control as the exact ratio of initiating species is not well controlled. During propagation, the nitroxide radical quickly couples and decouples with the growing active chain end of the monomer (reversible). This limits the possibility of irreversible termination by chain coupling and facilitates only monomer addition to the growing chains which cannot permanently couple with the nitroxide radical.[160]

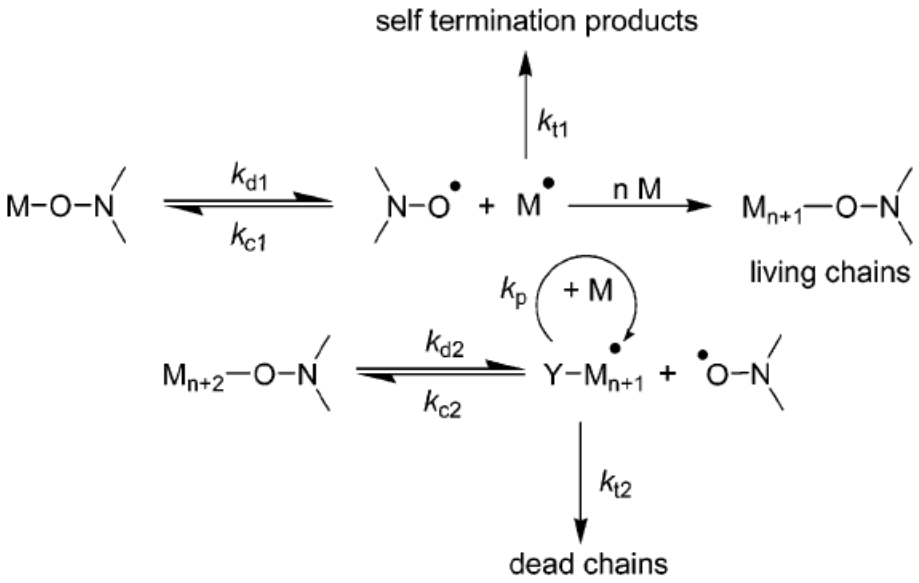

Figure 1.26 General reaction scheme for nitroxide mediated polymerization (NMP). The persistent radical effect (PRE) is the main inhibitor to irreversible termination by coupling and what facilitates primarily monomer addition to the growing radical chains. The nitroxide radical must be able to reversibly couple to the growing chain but also be stable enough to not initiate polymer chains on its own. Reproduced with permission[161] copyright 2006 American Chemical Society.

What makes NMP particularly attractive is the lack of metal catalyst and the wide range of monomer types that it can polymerize. In addition, the tunability of nitroxides enables initiation in many different systems and from many different starting materials.[41] This has the further advantage of eliminating extra purification steps which are present in both ATRP and RAFT.[162] Furthermore, the somewhat prohibitive cost of NMP has been addressed by several methods which generate nitroxides (alkoxyamines) in situ. Of all the controlled radical techniques discussed, NMP is the least developed and hence general procedures associated with how to perform such reactions and optimize them are not as abundant.

1.2.4 Click Chemistry

Among all the chemistry detailed herein, the notion of "click" chemistry warrants a bit of personal embellishment. Arguably the holy grail of all organic chemists, click chemistry is precisely that, the simple, strong connection of two lock-and-key type functional groups. Moreover, it is the robustness, mild conditions, high yield, air and water insensitivity, inexpensive materials and almost unwillingness of these reactions to misbehave that makes them so popular. Furthermore, the types of functional groups capable of undergoing click chemistry are easily incorporated (if not already naturally present) into many different synthetic schemes in drug development, inorganic chemistry, biology and polymer chemistry.

It is with respect to the last group, polymer chemistry, that click chemistry becomes especially useful for this work. This is because many of the controlled/living radical polymerizations employed in this dissertation naturally lead to participation in click chemistry reactions, particularly copper-catalyzed azide-alkyne coupling (CuAAC) due to the presence of halogen atoms on growing chain ends or in pendent groups of certain monomers. CuAAC in particular plays a key role in this work. In the case of hyperbranched polyglycerols, the many hydroxyl groups can be readily functionalized with alkyne and/or azide moieties.

Sharpless et al.[72] first discovered and coined the term "click" chemistry in 2001 and provided a strict set of requirements for a reaction to be considered a click-type chemistry as defined below:

- Reaction must be modular in nature
- Wide in scope of applicability
- Proceed to high conversion and yields
- Generate only inoffensive byproducts that can be easily removed

- Stereospecific
- Simple reaction conditions (ideally insensitive to water and oxygen)
- Readily available starting materials and reagents
- Require the use of no solvent or solvent that is benign or easily removed
- Simple product isolation

The reactions detailed in **Figure 1.27** are representative of the different types of chemistry that satisfy all of the above requirements. Depending on the type, they can either require catalyst (CuAAC) or be catalyst free (thiol-ene). In many cases, click reactions involve attack at various types of unsaturated carbon-carbon bonds (terminal alkenes and alkynes) often with the formation of a stable ring structure.

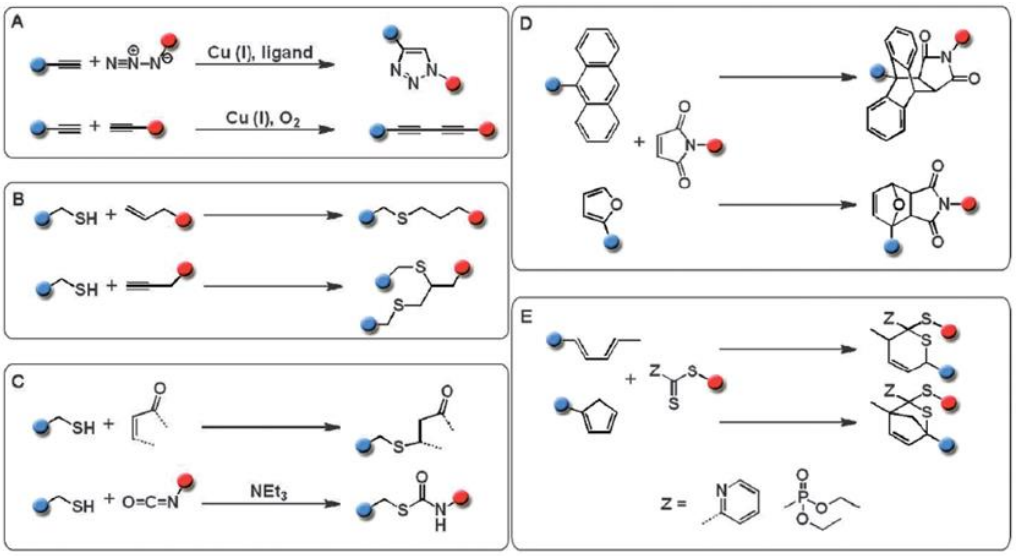

Figure 1.27 Representative reaction schemes for the most commonly-encountered click chemistries: (A) Azide-alkyne and Hay/Glaser homocoupling, (B) Thiol-ene/yne coupling, (C) Thio-isocyanate coupling, (D), (E) Diels-Alder coupling. Reproduced with permission[67] copyright 2012 Royal Society of Chemistry.

By far the most famous and well-researched type of click chemistry is the copper-catalyzed azide-alkyne click reaction (CuAAC)[163] This reaction is a modification of a Huisgen 1,3 dipolar cycloaddition type reaction resulting in the formation of a stable,

aromatic five-membered triazole ring. **Figure 1.27** presents many of the other equally-useful click chemistries available.[67] **Figure 1.27A** shows the classic azide-alkyne and Hay/Glaser homocoupling reactions. **Figure 1.27B** shows the biologically-relevant thiol-ene/yne reactions. **Figure 1.27C** shows thiol-isocyanate and thiol-enone click reactions. **Figure 1.27D**, **1.27E** depicts two variations on a Diels-Alder click reaction with some being reversible (retro Diels-Alder) and others being irreversible.

The applications of click chemistry, like controlled/living radical polymerization and HPG, span many different fields from biomedical to materials science to drug delivery. Indeed, there is virtually an endless possibility of clicking-onto reactions which can bring many seemingly incompatible materials together through strong covalent bonds. Some interesting applications in biomedicine include click derivatization of proteins (human and virus) for sorting (assays), separation, conjugation and manipulation (**Figure 1.28**).

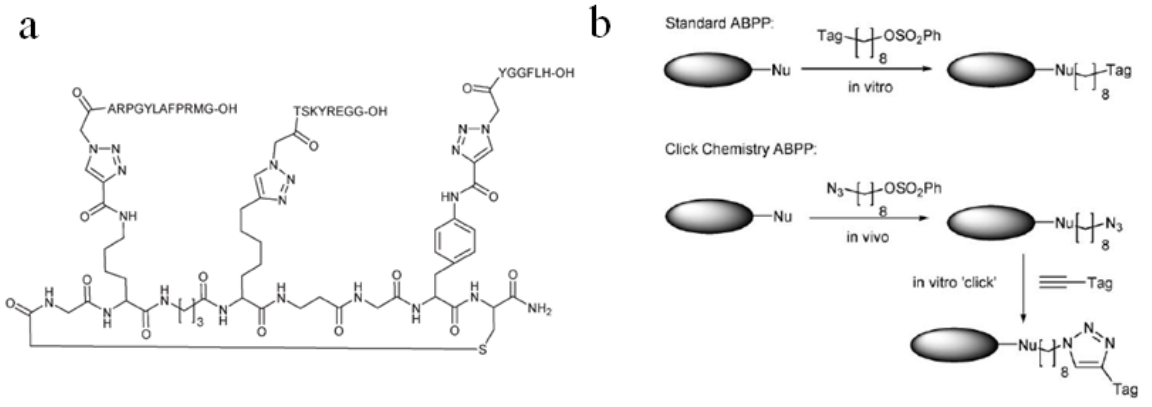

Figure 1.28 (a) Click-functionalized peptides useful for protein editing. (b) Click-enabled protein tagging for imaging and diagnostics. Reproduced with permission[164] copyright 2007 Royal Society of Chemistry.

Click chemistry is particularly useful when dealing with biological systems because it is generally insensitive to water and can react with common biological functional groups. This allows for click chemistry-modified bioconjugation and biorecognition, both *in vitro* and *in vivo* of electrophoretic or chromatographic materials for improved separation of biologicals by conventional techniques as well as selective tagging with fluorescent molecules or peptide modification to produce modified protein conformations. Click-chemistry can also be used to tag virus capsids with myriad surface molecules or influence how they interact in biological systems. Click chemistry has also been touted as a useful technique for the development of new drugs by essentially pulling together all the final components rather than by conventional, complex and multi-step approaches.[164]

Click-chemistry also has applications in material science as well, especially in polymer research. Some major areas include the synthesis of click-functionalized star, hyperbranched and linear copolymers.[67, 69] Click chemistry allows monomers that are incapable of being copolymerized to still be combined via click-functionalization to produce amphiphilic polymer structures of well-defined molecular weights. Since ATRP naturally produces exposed halogen atoms, it is an ideal method to couple with CuAAC for which ATRP-synthesized polymers are inherently telechelic. Click chemistry can also be used to crosslink polymeric structures to produce stable, unimolecular organic nanostructures.[20, 47]

CHAPTER 2. MOTIVATION, GOALS AND ORGANIZATION

2.1 Motivation

The use of polymers in crafting various nanoscale materials is an attractive and flexible approach to producing many interesting and useful materials of various sizes, shapes and functionalities. Owing to the immense variety of materials that can be polymerized in different ways, the potential of polymer-based nanomaterials design is truly unlimited. Techniques such as click chemistry and atom-transfer radical polymerization have made it possible to craft extremely low PDI polymers of immense variety and perform precision coupling reactions with high yield and under mild conditions. Consequently, there are many areas within this greater field that remain largely unexplored. In this work, star-like polymers possessing a large number of hydroxyl groups (polyols) are investigated as the starting point for many useful non-linear polymer architectures capable of significant and broad chemical diversification through post polymerization modification. The key polymers to be investigated in this work are cyclodextrins and hyperbranched polyglycerols (HPG). Unlike cyclodextrins which are established and well-defined in shape, HPG has only recently been successfully produced in well-defined and low PDI varieties, making it more useful in the development of novel polymeric materials. This presents an opportunity to develop a new class of complex non-linear polymer architectures to be applied across numerous fields.

The overarching ***goal*** of this work is to use cyclodextrins and HPG in the development of non-linear polymer architectures for the solution-based production (templating) of hard and soft spherical nanocomposites. The specific areas of

investigation within which these types of non-linear polymer architectures will be applied are: (**CHAPTER 3**) cyclodextrin-based templated liquid crystal-capped inorganic nanoparticles, (**CHAPTER 4**) HPG-based templated polymer-capped inorganic nanoparticles, and (**CHAPTER 5**) HPG-based wholly-polymeric soft nanoparticles. The specific motivations for each of these research areas are subsequently presented.

(CHAPTER 3) Cyclodextrin-based templated liquid crystal-capped inorganic nanoparticles: The use of liquid crystals in display devices has made them one of the most ubiquitous classes of materials encountered and interacted with in daily life. However, the largest energy drain in most devices is also the LC display. Therefore they consume a large portion of stored energy in batteries in mobile devices. To address this limitation, efforts are being made to increase the energy density of batteries. However, this is challenging and has physical limitations. In addition to better batteries, one can also investigate strategies for reducing the energy consumption of LC displays. This can be achieved by reducing the switching voltage of LC pixels by doping functional materials into liquid crystals. This can be challenging because liquid crystals do not generally solubilize many materials as dopants typically introduce high energy defects which are pushed to the interface. It is for this reason that non-linear liquid crystal-caped polymer templated nanocomposites are being investigated in **CHAPTER 3**. The rationale is to template inorganic nanoparticles within a star-polymer capped with liquid crystals that mimic the structure of the surrounding liquid crystal solvent. The capping materials are intimately and strongly attached to the surface, thus preventing them from being dislodged.

(CHAPTER 4) HPG-based templated polymer-capped inorganic nanoparticles: The production of various nanoparticles is made possible by numerous cleanroom techniques. However, these methods are expensive and tedious. Furthermore, they often produce bare nanomaterials possessing no surface functionalities. An alternative approach involves the use of polymer-based templates to produce inorganic and metallic nanoparticles in solution. Previous work has employed linear and self-assembled linear polymers to template nanoparticle formation. These techniques often produce irregularly-sized nanomaterials or require precise control of synthesis conditions. Other spherical materials, such as dendrimers, have also been investigated but they are difficult and tedious to make. As a compromise of the previous strategies for solution-based templating, HPG-based techniques are investigated. HPG can be produced in large quantities and with sufficiently low PDI to be useful for templating. In the present work, HPG-based star-like polymers have been developed to template nanoparticles in a unimolecular fashion in solution. In this way, the synthesis conditions do not need to be precisely controlled and the size of the nanoparticles can be controlled by adjusting the size of the HPG core. The solubility of the resulting nanocomposite can also be easily adjusted by varying the type of capping polymer.

(CHAPTER 5) HPG-based wholly-polymeric soft nanoparticles: The synthesis of polymeric nanoparticles has become an attractive vehicle for the loading of functional molecules for applications in drug encapsulation/delivery and water remediation. However, typical approaches involve the formation of micelle structures which are generally less stable to deviations in environmental conditions. Such problems have been mitigated by chemically crosslinking metastable micelles at the expense of

producing irregular sizes and the need for purification to remove unreacted crosslinker molecules. Hard templating has also been used whereby a polymer is coated onto a sacrificial particle and crosslinked with the particle then removed typically by dissolution. This strategy improves size control but it necessitates having well-defined hard particles of a deliberate size. In the present work, azide-functionalized HPG is used to produce wholly-polymeric soft nanoparticles without the need for chemical crosslinking or hard nanoparticle templating. By using UV-induced crosslinking, there is no need for subsequent polymerization. Furthermore, by performing crosslinking in a dilute regime it is possible to produce soft nanoparticles of fairly uniform size while avoiding large scale macromolecular aggregation and irregular sizes. Since HPG is also biocompatible, the resulting nanoparticles may be well-suited for drug delivery, water purification and surface antifouling applications.

All of the above areas of work are motivated by the clear drawbacks and limitations of established methods for producing hard and soft nanoparticles. By capitalizing on high functionality polyols, click chemistry and ATRP, it is possible to produce stable, well-defined polymeric templates of deliberate size. Striving for simplicity by using a small assortment of robust reactions, the diverse range of applications of polyol-based non-linear polymer architectures are realized with clear directions on further future development made clear.

2.2 Goals

For CHAPTER 3, the aims are to (1) develop a liquid crystal-capped cyclodextrin star-like polymer through a combination of ATRP and CuAAC. This

polymer is to be used for templating inorganic nanoparticles to produce nanocomposites composed of an inorganic Fe_3O_4 intimately and permanently capped with the liquid crystal moieties. This is achieved by the preferential growth of nanoparticles within the inner cyclodextrin core of the star-like polymer template. (2) Successful demonstration of template capabilities while also retaining the liquid crystal capping species is essential in this effort.

For **CHAPTER 4**, the aims are to (1) develop HPG-based star-like copolymers of well-defined sizes, arm numbers and arm lengths through a combination of ROMBP and ATRP; (2) demonstrate the capabilities of the HPG-*b*-PS star-like copolymers in templating an array of different inorganic nanomaterials including noble metals (Au, Ag) and metal oxides (Fe_3O_4); (3) understand the optimal conditions for producing well-defined aggregate-free nanoparticles by varying the solvent conditions, arm length, and arm number.

For **CHAPTER 5**, the aims are to (1) develop an azide-functionalized HPG polymer; (2) demonstrate its ability to form wholly-polymeric soft nanoparticles via UV-induced homocoupling of reactive nitrene intermediate groups to produce stable azo crosslinked HPG while avoiding the formation of reactive aziridine crosslinks.

2.3 Organization

CHAPTER 1 is a general overview of the current state-of-the-art and background related to strategies for hard and soft templating of various nanostructures. First, star-like polymers derived from micelles and moderate functionality macroinitiators are reviewed. The various synthesis strategies including grafting-from, grafting-to, and grafting-through

are summarized. The efficacy of different polymer and copolymer compositions in coordinating inorganic precursors are also detailed with key advantages and drawbacks of the different approaches highlighted.

Next, bottlebrush block copolymer synthesis strategies derived from a rigid cellulose backbone as well as semi-flexible polymer backbones are reviewed with key strategies including grafting-from, grafting-to, grafting-through and core crosslinking summarized. Biologically-derived templating approaches based on spherical and rod-like virus capsids and DNA are also briefly reviewed.

Third, the key aspects of well-defined hyperbranched polyglycerol synthesis and characterization are detailed including the ROMBP mechanism, slow monomer addition technique and IG^{13}CNMR characterization. Key parameters of HPG synthesis are outlined and explained with respect to their influence on molecular weight control, PDI and subunit composition. Applications of HPG as well as the current-state-of-the art in HPG-based copolymers are reviewed

Lastly, the key details of other relevant chemistries are reviewed. The most important chemistry employed in this work is controlled living/radical polymerization. Different types of controlled/living polymerization, including ATRP, RAFT and NMP, are detailed. Aspects of their kinetics, polymerizable monomers advantages and drawbacks are discussed with an emphasis placed on ATRP. Click chemistry strategies including CuAAC, thiol-ene, Diels-Alder, and Hay/Glaser coupling are reviewed with an emphasis on their mechanisms and selectivity.

CHAPTER 2 describes the motivation as well as the specific goals of this work. In brief, this work is motivated by the lack of high functionality polyols being

investigated for use in polymer templating for which HPG-based polymer templates offer a new and highly generalizable solution. The goals of this work relate to developing well-defined non-linear polymer architectures and demonstrating their ability to template inorganic nanoparticles for applications in liquid crystal doping, solution-stable polymer-capped functional inorganic nanoparticles, and wholly-polymeric soft nanoparticles.

CHAPTER 3 details the synthesis of a promesogen-capped β-CD-based star-like polymer (CNBP-21-PAA-β-CD) with well-controlled molecular weight and low PDI produced by a combination of ATRP, CuAAC, and hydrolysis. This star-like polymer is used to template superparamagnetic Fe_3O_4 within the inner poly(acrylic acid) (PAA) core via precursor coordination to produce inorganic nanoparticles with strongly tethered promesogen surface units. This is the first instance of promesogen-capped templated nanoparticles displaying improved solubility in liquid crystal solution comparable to that of other strategies with the added benefit of improved stability. Successful template synthesis and template capability is verified by NMR, chromatography, spectroscopy and microscopy techniques.

CHAPTER 4 details the synthesis of star-like HPG-based polymers possessing a large number of polystyrene arms (HPG-*b*-PS) ranging from 98 to 170. This star-like polymer is used to template functional inorganic nanoparticles including plasmonic Au and Ag and superparamagnetic Fe_3O_4. The inner HPG core is used to coordinate with the inorganic precursors and fix their position where precursors are typically either reduced or hydrolyzed to the final nanoparticle form. This strategy produces fairly uniform polymer-capped organic-soluble nanoparticles possessing excellent solution stability. By varying the solvent type, polymer arm length and number, it was possible to ascertain a

critical molecular weight of the capping arms above which successful templating occurs and below which largescale aggregation and sedimentation occurs. Successful template synthesis, templating capability, and nanoscale property retention of the resulting inorganic nanoparticles is verified by NMR, chromatography, UV-Vis spectroscopy and microscopy.

CHAPTER 5 details the synthesis of star-like azide-functionalized HPG and its light-induced unimolecular crosslinking to form biocompatible wholly-polymeric soft nanoparticles possessing a fairly uniform size and shape. By using both low concentrations and abundant intramolecular azide crosslinking, it is possible to suppress undesirable reactive aziridine crosslinks leading to stable structures as well as small particle sizes. This work serves as a first example of a new, simple, and clean method of template-free soft nanoparticle production offering a large potential for chemical diversification (biotagging, responsive crosslinkers) and many end uses.

CHAPTER 6 summarizes the overall conclusions and broader impacts of the work. In brief, the broader impacts of the work are as follows: (1) the successful demonstration of promesogen-capped star-like polymers as templates for inorganic nanoparticles offers a new route to producing dopants for not only thermotropic liquid crystals (as in displays) but also lyotropic formulations, and shows that inorganic doping of liquid crystals can be further improved for realizing low energy display technology; (2) the synthesis of an HPG-*b*-PS dense arm star-like polymer and its successful use in templating a variety of nanomaterials with excellent stability and solubility paves the way for the production of other useful solution templated nanomaterials including water soluble and stimuli responsive varieties simply by adjusting the polymer capping layer;

(3) the synthesis of wholly polymeric azo-crosslinked HPG simply and without the need for purification demonstrates the immense potential of this biocompatible non-linear polymer in the production of low toxicity drug carriers and potable water treatment materials whose further incorporation with stimuli responsive crosslinkers and preloaded reactive species offer an attractive route to new and interesting soft polymeric structures.

CHAPTER 3. STAR-LIKE POLYMER CLICK-FUNCTIONALIZED WITH SMALL CAPPING MOLECULES: AN INITIAL INVESTIGATION INTO PROPERTIES AND IMPROVING SOLUBILITY IN LIQUID CRYSTALS

This work was published in *RSC Advances* (J. Iocozzia, H. Xu, X. Pang, H. Xia, T. Bunning, T. White, and Z. Lin*, *RSC Advances*, **8**, 2936 (2014))

3.1 Background

Thermotropic liquid crystals (LCs) are a well-known class of matter that forms in certain molecular systems between that of a pure liquid and a pure solid.[165, 166] LCs are prevalent in many technologies and nature.[167, 168] The anisotropy of LC systems, and non-uniform property variations are what make them attractive active media as they selectively respond to myriad perturbations, including deformation, radiation and magnetization.[169] Investigations into the properties of pure or mixed liquid crystalline phases is an ongoing area of research, however the use of LCs as a host species for other chemically-modified active species, such as polymers and nanoparticles, is an emerging area which takes advantage of the unique properties of LCs with the desire to incorporate additional functionality through doping. By far the most common class of material investigated for doping into LCs has been nanoparticles (NPs) of one form or another.[170-177] NPs have been of particular interest because the physics and properties of materials on this scale generally differ from their bulk, macroscopic counterparts.[178, 179]

Parameters such as size, size distribution, and spatial arrangement greatly affect how NPs respond due to properties such as local surface plasmon resonance (LSPR),[173] quantum confinement,[180] and energy level mixing.[181-183] Research into nanoparticle-liquid

crystal composites (NP-LCs) promises a wide spectrum of applications, including advanced display technology,[167, 168, 184] photonics,[169, 185, 186] optics,[167, 169, 181, 187] sensors and metamaterials.[167, 181] Furthermore, the assembly (self or directed) of NP has proven to be successful by many other techniques spanning a broad range of backgrounds.[188]

One specific area of investigation is the use of LCs as a means of assembling dopant species into various arrangements.[171, 172, 175, 189] The idea being that dopants would align within the LC matrix and have an order to their assembly imposed by the LC host. Unfortunately, the realization of this technique has not been easy. A few active research areas on NPs include gold NPs and quantum dots (QDs) variously passivated with alkylthiolate, alkylthiol, or (S)-naproxen ligand species.[171, 172, 176, 177, 180, 181, 190] There are myriad techniques for making NPs (particularly Au,[166, 191] Ag,[165] and metal oxides[192]) variably capped with many species in large yield.[172, 177] However, some techniques yield NPs with non-uniform size and shapes, while the others cannot afford the synthesis of NPs with tunable size (i.e., limited applicability/variability).[20, 172] Furthermore, the degree and nature of ligand coverage on NPs is oftentimes based on coordination or adsorption rather than strong bonding and subsequent processing steps (sonication, heating, reaction) have the potential to change the surface functionality. This change can affect the solubility, and therefore behavior interaction, and organization of NPs, in LC host media.

The development of well-defined living polymerization techniques such as atom-transfer radical polymerization (ATRP)[135, 136, 193] in conjunction with star-like polymer templates[17, 24-26, 194] is an interesting alternative with the potential for producing polymeric and nanocomposite systems with improved solubility in LC media. Living polymerization is an expansive class of polymerization techniques in which the polymer

chains grow uniformly to yield highly monodisperse (low polydispersity index, PDI) and telechelic (end-reactive) polymers capable of further polymerization/reaction. Pioneered by Matyjaszewski et al.,[135, 136] ATRP in particular is of great interest because of the retention of end group reactivity, typically halogen atoms which are excellent leaving groups. Thus, the polymeric materials can be further functionalized with methods such as the burgeoning and versatile class of chemistry known generally as "click" chemistry. First reported by Sharpless et al.,[72] "click" chemistries are generally characterized as simple and robust addition-type reactions which proceed to high yields at moderate conditions with minimal control of temperature or atmospheric conditions required. Many types of click chemistry have been developed with the azide-alkyne reaction of particular interest in this work.[67, 72, 163] More details on the broad field of click chemistry are referred to a comprehensive review.[195]

Here we report a simple and easily systematized approach for producing functional star-like polymers tethered with small molecules that are structurally similar to the common LC 4-cyano-4'-pentylbiphenyl (5CB). ATRP of *tert*-butyl acrylate (*t*BA) was performed on a 21-arm β-cyclodextrin macroinitiator core to produce starlike poly(*tert*-butyl acrylate) (P*t*BA). In a parallel reaction, a small molecule, 4-isocyano-4'-(prop-2-yn-1-yloxy)biphenyl (CNBP), was synthesized which possessed similar chemical structure to 5CB. Ultimately, CNBP was grafted onto star-like P*t*BA via azide-alkyne click chemistry to produce CNBP-capped star-like P*t*BA (i.e., starlike P*t*BA-CNBP) which was subsequently hydrolyzed to yield star-like poly(acrylic acid-CNBP) (PAA-CNBP). The latter can potentially be utilized as template through the coordination interaction between hydrophilic inner PAA blocks and the metal moieties of precursors to

produce NPs[18, 20, 196] with improved solubility in LC host media as the resulting NPs are intimately and permanently linked with LC-like CNBP.[20] The structural properties were investigated by proton nuclear magnetic resonance (^{1}HNMR), gel permeation chromatography (GPC), Raman spectroscopy, Fourier transform infrared spectroscopy (FTIR), dynamic light scattering (DLS) and atomic force microscopy (AFM). This simple synthetic approach serves as an initial investigation into the properties and solubility of NP templates (i.e., star-like PAA-CNBP) derived from the β-cyclodextrin core in LC hosts. Moreover, this approach can be readily generalized to investigate a wide range of chemical and physical parameters which influence solubility.

3.2 Experimental Details

3.2.1 Materials

N,N,N',N'',N''-pentamethyldiethylenetriamine (PMDETA, 99%),2-bromoisobutyryl bromide (2-Br-iBu-Br, 98%), 1-methoxy-2-propanol (M-IPA) (99%), and anhydrous 1-methyl-2-pyrrolidinone (N-methyl pyrrolidinone) (NMP) were purchased from Sigma-Aldrich. Sodium Azide (99.5%), aluminum oxide (neutral), petroleum ether (60/80), calcium hydride (90-95%), sodium bicarbonate (99%), anhydrous magnesium sulfate (99.5%), hexane, trifluoroacetic acid (99%), and 4-cyano-4'-pentylbiphenyl (5CB) were purchased from Alfa Aesar. Propargyl bromide (99%, stabilized with MgO), and 4-hydroxy-4'-biphenylcarbonitrile were purchased from TCI America. Reagent grade chloroform and ethyl acetate were purchased from BDH. Silica gel (mesh 60-200) was purchased from EMD. All abovementioned chemicals were used as received. β-CD (Sigma-Aldrich) was dried and purified as detailed below. CuBr (98%,

Sigma-Aldrich) was purified using a procedure from a previous work.[19] Tertiary butyl acrylate (*t*BA) (99% with 15 ppm 4-methoxyphenol as inhibitor, Alfa-Aesar) was stirred with calcium hydride for 1h and distilled under heat and light vacuum to remove the inhibitor prior to use. Polyimide (PI-2555) was purchased from HD Microsystems. Norland 68 UV curing glue was purchased from Edmund Optics. Glass rod spacers (10 μm thickness) were purchased from Nippon Electric Glass.

3.2.2 Characterization

Absolute molecular weights of polymers and their chemical structures were verified by ^{1}HNMR using a Varian VXR-400 (400 MHz) Unity Innova 500 spectrometer equipped with a Nalorac quad-probe. Samples employed $CDCl_3$ as the deuterated solvent with TMS as internal reference. Molecular weight, polydispersity (PDI) and modality of star-like polymers were measured using a Shimadzu gel permeation chromatography setup (GPC equipped with a RID-10A refractive index detector, LC-20A chromatograph pump, and CTO-20A column oven. Tetrahydrofuran (THF) was used as the eluent at an operating temperature of 35 °C and a flow rate of 1ml/min. Two 5μm phenogel 10E4A columns (molecular weight range: 200 to 2 x 10^6 g/mol) were calibrated using linear polystyrene (PS) standards. Dipolar functional group incorporation was determined using FTIR. FTIR spectra were measured using a Fisher Thermo Scientific Nicolet 6700 spectrometer equipped with an Ever-Glo source (9600-2- cm^{-1}). FTIR samples were prepared in KBr disks. Morphological properties were investigated with a Bruker Dimension Icon atomic force microscope (AFM) with 36 μm^2 scan areas**.** Scans were performed in tapping mode at a scanning rate of 0.5 Hz. AFM samples were prepared on

cleaned silica substrate (cleaning sequence: water-ethanol-water). Concentrated samples of PAA-CNBP (c = 0.2mg/ml) were prepared and spin coated at 3000 rpm (Headway Research, model PWM32) for 30 seconds for AFM measurements. Symmetric (polarizable) functional group incorporation was determined by Stokes-shift Raman scattering. Raman spectra were acquired using a Renishaw inVia Raman microscope equipped with a 785nm laser (5 mW) and MS20 encoded stage (100 nm resolution) on a Leica DM2500 M microscope. Dynamic light scattering (DLS) was performed using a Wyatt DynaPro NanoStar system at 25 °C using a solid-state 785 nm laser and quartz cuvette.

3.2.3 Preparation of High Functionality Macroinitiator β-CD-21Br from β-CD-21OH

In a procedure adapted from Pang et al.[20] β-CD (5.68 g, 5 mmol) was dried by distilling with toluene at 120 °C to completely remove any water. Once dried, β-CD was dissolved in anhydrous polar solvent 1-methyl-2-pyrrolidinone (60 ml) and chilled to 0 °C in an ice bath. Once cooled, 2-bromoisobutyryl bromide (49 ml, 210 mmol) was added dropwise in a 42:1 molar ratio (2-Br-iBu-Br: β-CD-21OH) or equivalently a 2:1 molar ratio (2-Br-iBu-Br: -OH) and allowed to react for at least 2 h at low temperature. The reaction was allowed to run an additional 24-36 h to ensure full reactivity of surface –OH groups. The product was then precipitated in hexane under vigorous stirring and allowed to settle overnight. The supernatant was then collected and redissolved in chloroform. The raw product was then added to a separatory funnel and sequentially washed with saturated aqueous sodium bicarbonate ($NaHCO_3$) solution (until no bubbles evolve) and deionized water. Any residual water was removed with $MgSO_4$, and the

product was then filtered and dried under vacuum for at least 48 h. The final product was obtained by recrystallization in hexane. Its structure was verified using ^{1}HNMR (solvent $CDCl_3$ δ(ppm)): 1.78 (126H, CH_3), 3.45-5.25 (49H); and FTIR ν(cm^{-1}): 2932 (ν_{C-H}), 1735 ($\nu_{C=O}$), 1159 cm^{-1} (ν_{C-O-C}), 1039 and 1106 (ν_{C-C} coupled with ν_{C-O}). Initiation efficiency (conversion of –OH groups to –Br groups) was calculated according to the procedure in a related publication from our group using ^{1}HNMR and was found to be 100%.[19] The same brominated β-CD employed in the previous study was also used in this investigation.

3.2.4 Synthesis of 4-isocyano-4'-(prop-2-yn-1-yloxy)biphenyl Small Molecule Capping Agent (CNBP-alkyne)

Part (I) of **Figure 3.1** details the synthetic pathway for CNBP-alkyne. 4-hydroxy-4'-biphenylcarbonitrile (1 g, 5.12 mmol) and potassium carbonate (1.6 g, 25.6 mmol) were added to a 50 ml three-neck flask equipped with a magnetic stirrer and condenser. The atmosphere was exchanged for argon. Anhydrous acetone (10 ml) was then added via syringe into the flask and allowed to fully mix for 10 min. Diluted in acetone (5 ml), propargyl bromide (0.7312 g, 6.2 mmol) was added dropwise via syringe into the vigorously stirred flask. The flask was then heated to reflux and left to react for 4 days. The raw product was dried for 48 h under vacuum, yielding a bright yellow raw product. It was then dissolved in chloroform and mixed with silica gel until a dry pale yellow colored powder was formed. This was added to a silica gel column prewashed with petroleum ether (PET). A series of solvent mixtures containing petroleum ether (low polarity), ethyl acetate (EtOAc) (medium polarity) and chloroform ($CHCl_3$) (high polarity) were passed through the column, collected, and evaporated. The solvent mixtures were (1:0, 1:2, 2:1, 0:1) (PET: $CHCl_3$, v/v); (9:1, 4:1, 1:1) ($CHCl_3$: EtOAc, v/v).

The pure product was collected with the solvent mixture 9:1 ($CHCl_3$: EtOAc, v/v) ^{1}HNMR (solvent $CDCl_3$ δ(ppm)): 7.60-7.75 (protons from phenylene ring attached cyano group), 7.0-7.6 (protons from phenylene ring attached to oxygen), 4.75 (protons on oxymethylene bridge), and 2.51 (ethynyl proton).

3.2.5 Preparation of 21-Arm Star-like PtBA-Br via Atom-Transfer Radical Polymerization (ATRP)

In a round bottom flask, 200 ml of *t*BA and 20 g of calcium hydride were added. The flask was then attached to a typical distillation setup and allowed to react for approximately 1 h under vigorous stirring (no heat, no vacuum). Then a vacuum and light heat was applied in 5 °C increments until a slow boil was reached. The distillate was collected in a separate container and ready for use. Polymerization of *tert*-butyl acrylate (*t*BA) employed the β-CD-21Br macroinitiator in an ATRP controlled living polymerization. The ATRP synthesis was summarized in part (II) of **Figure 3.1**. A 150 ml threaded cylindrical pressure vessel was sequentially charged with β-CD-21Br (0.1g), *t*BA (14.3 ml), 2-butanone (14.3 ml) (1:1 v/v monomer: solvent), CuBr (0.071 g), and PMDETA (0.1701 g). Upon addition of PMDETA, the contents changed color from a pale, diffuse green to a strong dark green, indicating successful complexation and dispersion of the CuBr/PMDETA co-catalyst. The vessel was then subjected to three freeze-thaw-pump cycles in inert N_2 atmosphere using liquid nitrogen as the freezing agent. The vessel was then set in an oil bath at 90 °C and allowed to react under stirring for 24 h. The raw product was then diluted with acetone to roughly 140 ml total volume and passed through an aluminum oxide column (neutral, pre-washed with acetone) to remove the CuBr salt. The eluent was then precipitated in a mixture of cold methanol and

water (1:1 v/v). This process was repeated three times to ensure removal of linear homopolymer. The contents were then dried with $MgSO_4$, filtered and dried under vacuum for at least 48 h. ^{1}HNMR (solvent $CDCl_3$ δ(ppm)): 1.35-1.55 (tert-butyl protons), 1.25-1.29 (methyl protons on backbone), 2.15-2.35 (proton on tertiary carbon in backbone).

3.2.6 Preparation of Azide Terminated 21-Arm Star-like PtBA-N_3

Purified 21-arm star-like PtBA-Br (1.52 g) was dissolved in dimethylformamide (10 ml) and excess sodium azide (0.7 g) (molar ratio of terminal Br to NaN_3 = 1:30) was then added to the reaction flask. The solution was allowed to react for 60 hours at room temperature while covered with aluminum foil. Excess NaN_3 was removed by filtration. The raw product is then precipitated in cold methanol and water (1:1, v/v). The precipitate was dissolved in chloroform (30 ml) and washed with deionized water (3 × 15 ml). The organic layer was concentrated to remove $CHCl_3$ and re-dissolved in 100 ml acetone before finally being precipitated in cold methanol and water (1:1, v/v). The precipitate was dried in a vacuum oven overnight. Azide functionalization was verified by FTIR ν(cm^{-1}): 2110 ($\nu_{N=N=N}$).

3.2.7 Synthesis of 21-Arm Star-like PtBA-CNBP by Click Reaction

Figure 3.1 details the synthetic pathway for the click reaction. In a dry 150 ml threaded cylindrical pressure vessel star-like P*t*BA-N_3 (300 mg) and 4-isocyano-4'-(prop-2-yn-1-yloxy)biphenyl (CBNP; 90 mg) were dissolved in DMF (15 ml). To this, CuBr (113.5 mg) and PMDETA (136.8 mg) were added. The vessel was then sealed and subjected to three freeze-pump-thaw cycles under inter N_2 atmosphere using liquid

nitrogen as the freezing agent. The contents were then allowed to react at 90 °C for 36 h under stirring in an oil bath. The reaction was quenched by immersing the pressure vessel in liquid nitrogen. The contents were then diluted with THF and passed through an aluminum oxide (neutral) column to remove the copper salt. The product was then precipitated twice in cold methanol and water (1:1, v/v) and dried under vacuum at 50 °C for 24 h to yield a slightly yellowish powder.

3.2.8 Hydrolysis of 21-Arm Star-like PtBA-CNBP into 21-Arm Star-like Poly(acrylic acid)-CNBP (PAA-CNBP)

In a 20 ml vial, 21-arm star-like P*t*BA-CNBP (80mg) was dissolved in dichloromethane (DCM) (12 ml). Next trifluoroacetic acid (4 ml) was added and the solution was stirred for 24 h. 21-arm star-like PAA-CNBP was precipitated out of solution. It was filtered and washed with dichloromethane three times and dried under vacuum for 24 h.

3.2.9 In Situ Synthesis of CNBP-Capped Iron Oxide (Fe_3O_4) Nanoparticles

The star-like PAA-CNBP template was subsequently reacted with iron oxide precursors $FeCl_3$-$6H_2O$ and $FeCl_2$-$4H_2O$ in a 9:1 (v/v) mixture of DMF and benzyl alcohol (BA). The mixture is stirred for 30-60 minutes to completely disperse the precursors and sonicated for an additional 30 minutes. The mixture was then added to a three-neck flask and allowed to reach a temperature of 120 °C. Ammonium hydroxide was then added to form superparamagnetic iron oxide (Fe_3O_4). The mixture was left to react for 30 minutes and then allowed to age (nucleate) for 20 hours at a lower temperature of 80 °C. The templated iron oxide nanoparticles were purified by sequential

precipitation in ethanol, centrifugation, and redispersion in toluene three times. The mixture was then drop-cast onto TEM grids for characterization.

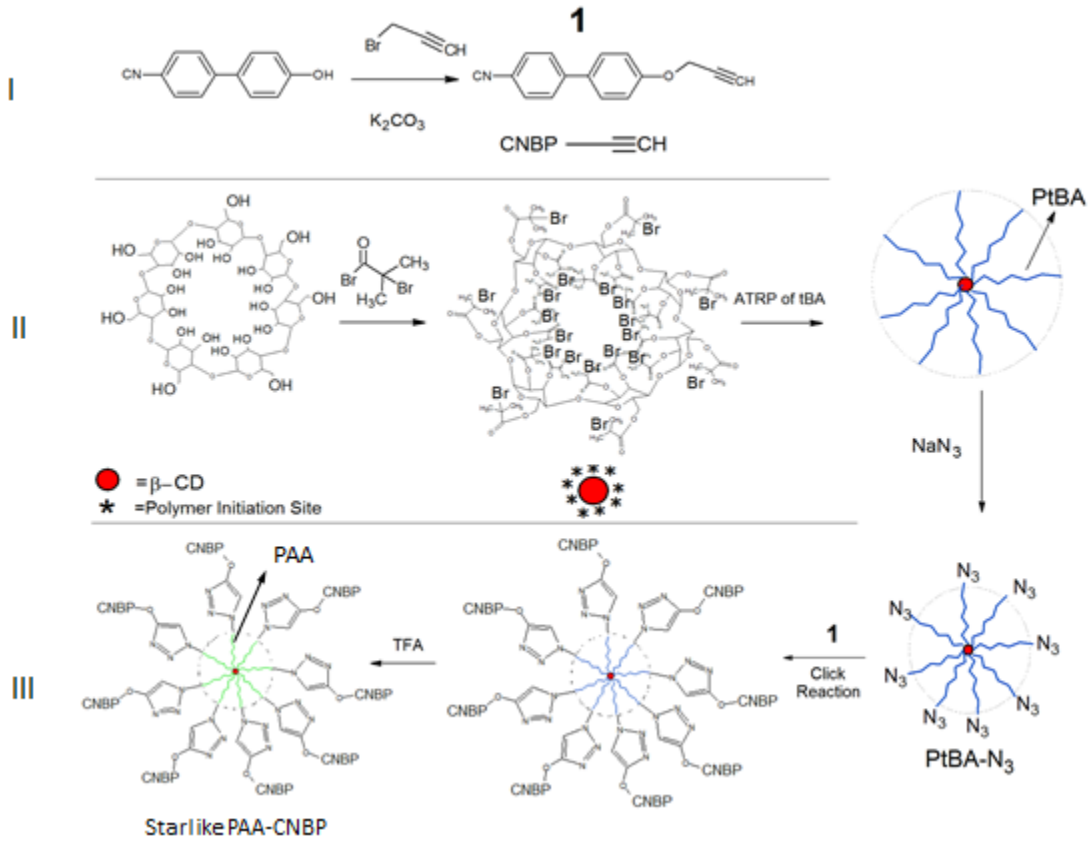

Figure 3.1 Reaction scheme for (I) synthesis of CNBP-alkyne (1) promesogen small molecule capping agent; (II) synthesis of star-like PtBA-Br via ATRP from β-CD-based macroinitiator; (III) synthesis of star-like PAA-CNBP via azide-alkyne click chemistry and subsequent hydrolysis.

3.3 Results and Discussion

The choice of small molecule capping agent, 4-isocyano-4'-(prop-2-yn-1-yloxy)biphenyl (CNBP), was motivated by its structural similarity and potential for compatibility with the LC host (i.e., 4-cyano-4'-pentyl biphenyl; 5CB). The synthesis of CNBP in a nucleophilic substitution reaction was detailed in reaction pathway I in **Figure 3.1**. Essentially, a terminal alkoxide served as a nucleophile which can attack the methylene carbon of propargyl bromide with bromine acting as a leaving group. It was necessary to purify the product via column chromatography. The eluent ratios used are detailed in the Experimental section. Very fine divisions in polarity of the eluents were required to isolate highly pure final product. **Figure 3.2** shows the ^{1}HNMR spectrum of the purified product, verifying the successful alkyne functionalization. The key peaks to note were the alkynyl proton at 2.5 ppm, the two aromatic groupings around 7.8 ppm and 7.05 ppm.

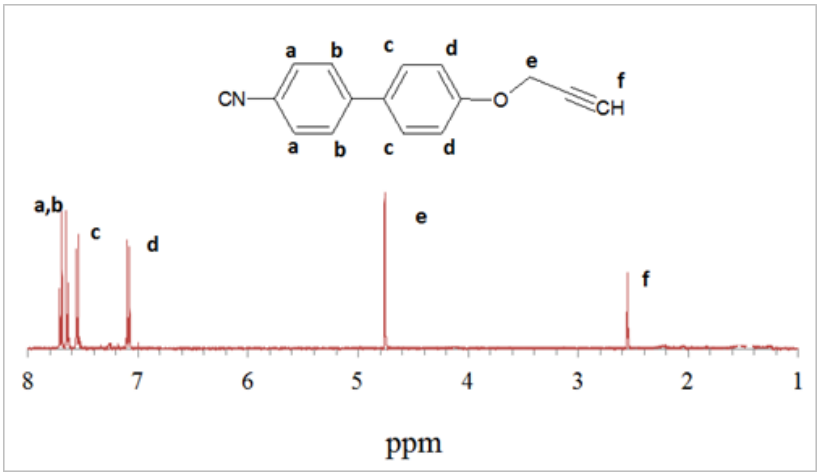

Figure 3.2 ^{1}HNMR spectrum of capping agent (CNBP-alkyne) (solvent $CDCl_3$). Solvent peaks are removed for clarity.

As a verification of alkyne functionalization, Raman spectroscopy was also performed on the capping agent. Raman spectroscopy is complimentary to FTIR in that where one technique affords a weak chemical signature; the other would usually yield a stronger one. Raman gives stronger signals for materials with highly polarizable bonds such as alkenes and alkynes. **Figure 3.3** shows the Raman spectrum for CNBP-alkyne which exhibited the carbon-carbon triple bond vibration mode and the cyano vibration mode at 2127 cm^{-1} and 2226 cm^{-1}, respectively. The relatively weak aromatic peaks were also evident as well as the C-O-C bending mode, which further substantiated that the reaction had occurred (replaced C-O-H bond with C-O-C bond).

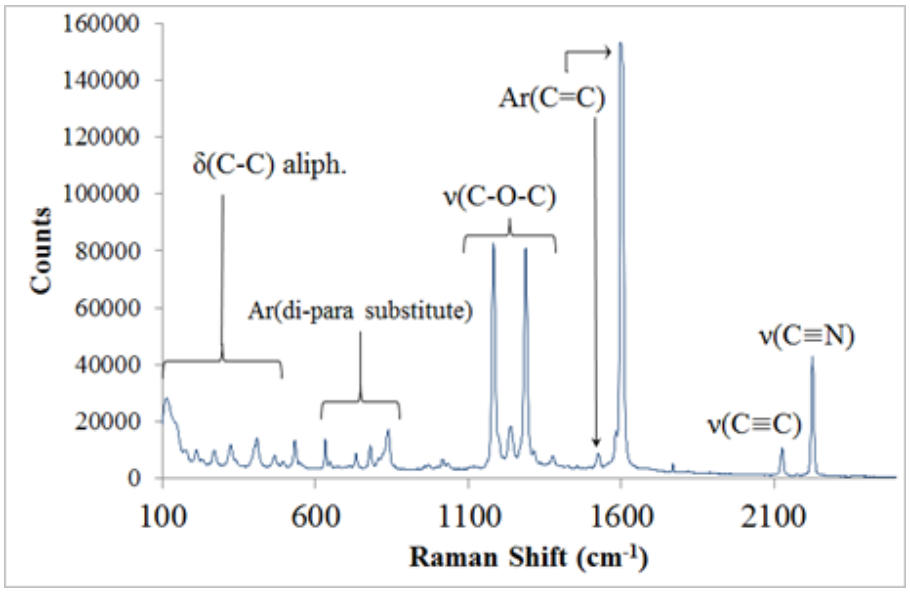

Figure 3.3 Raman spectrum of CNBP-alkyne promesogen capping agent. The separate, resolvable signals from the cyano and alkynyl groups are around 2200 cm^{-1} and 2100 cm^{-1} respectively. Aromatic signals indicate the presence of the biphenyl component. Laser excitation is at 785 nm.

The 21 hydroxyl groups of β-CD were bromine-functionalized via esterification with 2-bromoisobutyryl bromide to yield β-CD-21Br. This served as the macroinitiator for the subsequent polymerization. ATRP was then performed on the macroinitiator through the addition of tert-butyl acrylate monomer at a temperature of 90 °C for 24 h (see Experimental section for more details). A CuBr/PMDETA co-catalyst was used for the polymerization. The resulting polymer was first purified several times by fractional precipitation into a 1:1 (v/v) mixture of cold methanol and water to remove the linear homopolymer which inevitably formed during ATRP. **Figure 3.4** describes the GPC traces showing the removal of both the homopolymer peak and the weak shoulder on the main peak. The pure star-like P*t*BA-Br was then characterized by ^{1}HNMR to obtain an absolute molecular weight. It should be noted that the values obtained from GPC and NMR are not expected to be equal due to the fact that the standards used for calibration were linear PS which possessed different solubility (and favourability) in the eluting solvent (THF) compared to the star-like P*t*BA-Br synthesized herein.

The ^{1}HNMR spectra of the CNBP capping agent (see **Figure 3.2** section for more details) and the unfunctionalized star-like P*t*BA are shown in **Figure 3.5A** and **Figure 3.5B**, respectively. **Figure 3.5C** displays a strong signal of the star-like P*t*BA protons which can be integrated. The characteristically strong signal at δ = 1.4 ppm (peak **a**) corresponded the pendant tertiary butyl protons, and the weaker signal at δ = 1 ppm (peak **b**) can be assigned to the methyl protons at the attachment site on β-CD. The relationship between these respective intensities (normalized to a per proton basis) enabled the length of a single arm to be calculated and thus the total length (i.e., molecular weight) to be

determined. It should be noted that only one arm of the star-like polymer is shown in the inset in **Figure 3.5** for simplicity. In reality there were 21 total polymer arms due to the presence of 21 –OH groups of β-CD capable of reaction.

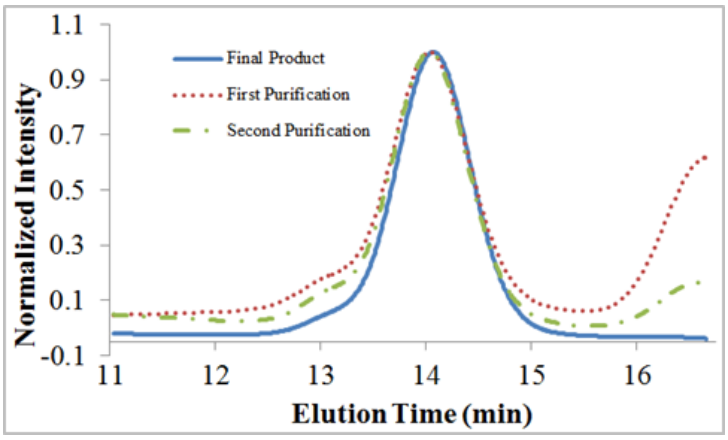

Figure 3.4 GPC traces of star-like P*t*BA-Br in a series of purification steps. Note that the linear homopolymer found at long elution times is gradually removed.

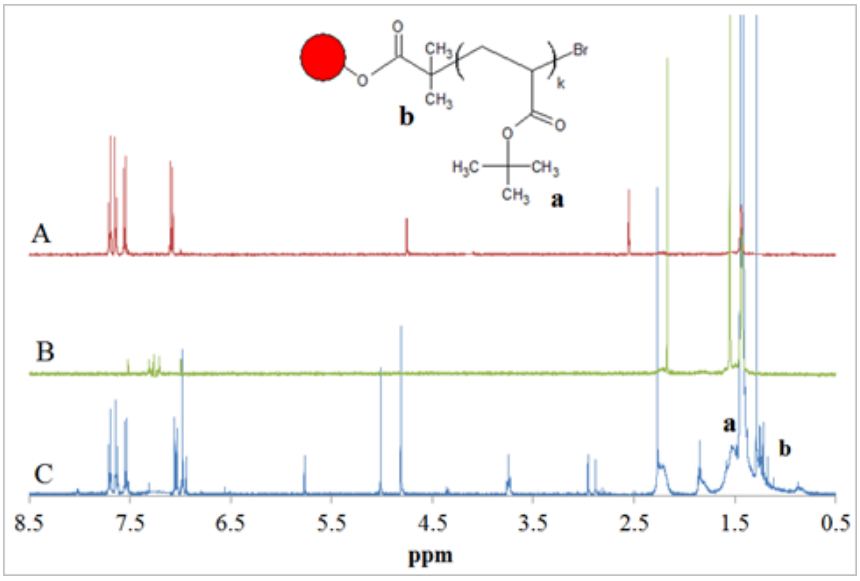

Figure 3.5 ^{1}HNMR spectra of (A) CNBP capping agent (for more detail see **Figure 3.2**), (B) star-like P*t*BA-Br, and (C) star-like P*t*BA-CNBP. Inset shows polymer repeat unit (single arm) and proton matching for P*t*BA (solvent $CDCl_3$). Note the combination of the signals from (A) and (B) in the final product (C) particularly in the aromatic region and the shift of the alkynyl proton after the click reaction. The red circle represents the β-CD macroinitiator core. Solvent peaks are removed for clarity.

In addition to the observation of small molecule peaks in the post-click material, a sizeable ppm shift of the alkynyl proton is evident from 2.5 ppm in (A) to 3 ppm in (C). **Table 3.1** summarizes the results of GPC and ^{1}H-NMR analysis. As expected in ATRP, the PDI of the resulting polymer was low, indicating the formation of polymer with narrow molecular weight distribution.

Table 3.1 Summary of molecular weights for 21-arm starlike PtBA-Br

Sample	Time (h)	$M_{n,GPC}$[a]	PDI[b]	$M_{n,NMR}$[c]
PtBA-Br	24	108,000	1.07	283,500

[a]The number average molecular weight was determined by GPC with PS calibration standards.[b]Polydispersity index (PDI) was determined by GPC. [c]The number average molecular weight of star-like P*t*BA-Br was determined by ^{1}H-NMR (see **Figure 3.3C**) as follows:

$$M_{n,NMR} = \frac{\left(\frac{A_a}{9}\right)}{\left(\frac{A_b}{6}\right)} \times 21\ arms$$

where A_a and A_b are the integrated areas of the pendant backbone methyl protons and main-chain methyl protons from **Figure 3.3C**, respectively.

The last step in reaction pathway II from **Figure 3.1** involves the azidation of the terminal bromines of the star-like P*t*BA via the reaction with sodium azide (NaN_3). FTIR is a useful technique for verifying the successful azidation of the polymer. This is largely due to the ease with which the dipole moment of the N_3 group can be perturbed. **Figure 3.6** compares the FTIR spectra of the pre-click (i.e., azide functionalized star-like PAA-N_3) (**Figure 3.6A**) and the post-click materials (i.e., after azide has reacted with alkynyl

group) (**Figure 3.6B**). The expected stretching signal from ν(-N_3) was clearly observed at 2103 cm^{-1} in **Figure 3.6A**. The click reaction involved the reaction between a terminal azide group and a terminal alkynyl (triple bond) group. This reaction was highly selective so side reactions were not a concern and it can proceed at moderate conditions of temperature and pressure. After the reaction, a stable 1,2,3-triazole ring was formed (five-membered ring containing three nitrogens and two carbons) which did not have a strong IR signal. Thus, a successful click reaction was evidenced by the disappearance of the azide peak in **Figure 3.6B**.

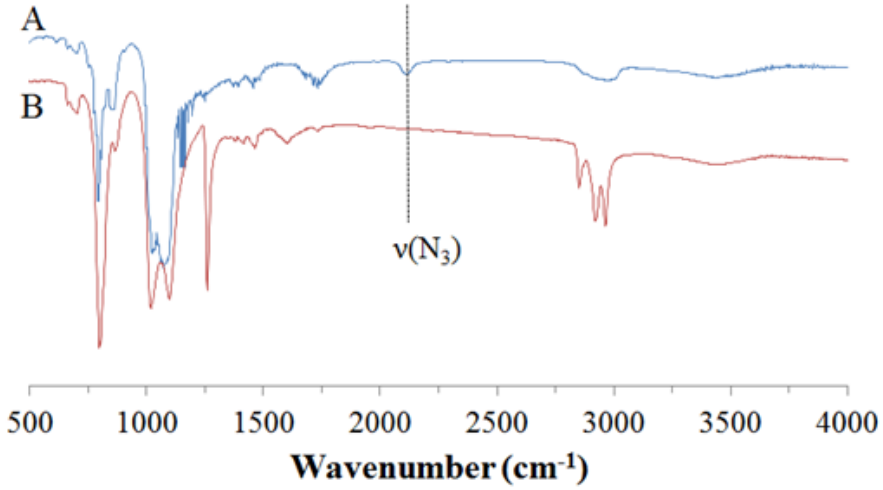

Figure 3.6 FTIR spectra of (A) star-like 21-arm PtBA-N_3 and (B) star-like 21-arm PtBA-CNBP. The signal in (A) at 2100 cm^{-1} indicated the presence of azide functionalization. Its disappearance in (B) confirmed the success of the click reaction between azide and alkyne.

Successful chemical verification of star-like PAA-CNBP allowed for the characterization of material properties. Several characterization techniques were employed, including AFM, DLS and optical microscopy, to investigate the properties of this novel star-like polymer structure.

Investigation into the morphology formation was undertaken by AFM and summarized in **Figure 3.7**. A sample of star-like PAA-CNBP with a concentration of 0.2 mg/ml in dimethylformamide (DMF) was prepared and spin-coated on a silicon wafer. The resulting height profile obtained for this sample is shown in **Figure 3.7A**. Forming an interesting interconnected network, the obtained structure was similar in appearance to structures seen in a previous work on high molecular weight comb block copolymers.[197] The similarity of the observed structure as well as the polymeric nature of the system suggested a similar formation mechanism via the thin-film dewetting.[197] Initially, the solvent created holes in the thin film of PAA-CNBP as solvent evaporated. The holes then expanded outwards and the rims (i.e., concentrated star-like PAA-CNBP) ahead of the holes eventually merged to form interconnected thread-like structures which cannot propagate further. Notably, despite the different polymer architectures investigated, similar morphologies were observed.[197] A line scan of the interconnected network is shown in **Figure 3.7B**. The average height of the threads was between 2 nm and 3 nm with an average thickness of approximately 6.5 nm.

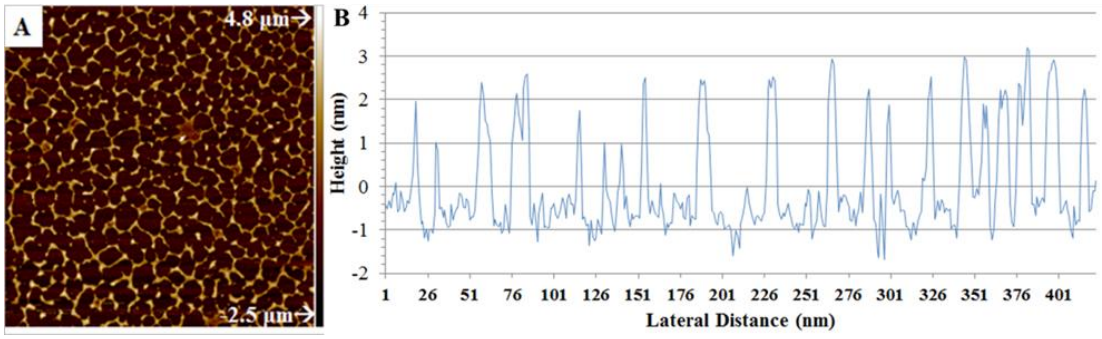

Figure 3.7 (A) AFM height image of 21-arm star-like PAA-CNBP. (B) The corresponding cross sectional analysis of star-like PAA-CNBP in (A). Image size = 2.5 x 2.5 μm^2.

Dynamic light scattering (DLS) was also performed on star-like PAA-CNBP at a concentration of 0.2 mg/ml in methanol (MeOH). Using a multi-arm model, it was found that the peak diameter was approximately 7 nm (**Figure 3.8**). Comparison between DLS and AFM results was challenging given that the structures observed in the latter were more complicated assemblies of individual star polymers, and thus the larger dimensions. However, DLS did verify the production of low polydispersity star polymer, which is a conclusion also supported by GPC and typical of controlled living polymerizations.

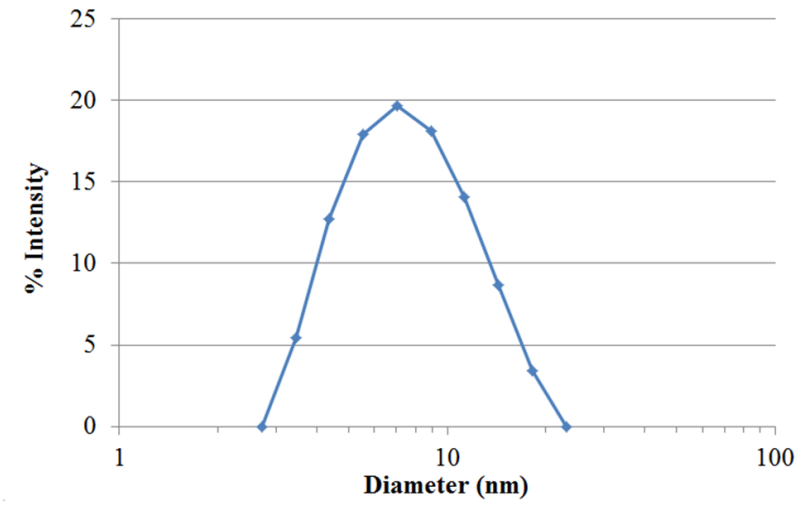

Figure 3.8 Diameter distribution of star-like PAA-CNBP template obtained from DLS. Peak diameter is 7 nm. This is in agreement with sizes expected from similar conditions in a previous publication.[195]

The solubility of the star-like PAA-CNBP in the LC host (i.e., 5CB) was also investigated in two ways. First, samples with from concentrations from approximately 0.3 wt% to 1.76 wt% of PAA-CNBP in 5CB were prepared. The choice of 5CB as the LC host was due to its structural similarity to the capping agent decorating the star-like PAA-CNBP. **Table 3.2** summarizes the different concentrations prepared and their corresponding digital images of the various doped LC samples are shown in **Figure 3.9**.

Table 3.2 Summary of weight percentages of star-like PAA-CNBP samples in 5CB host

Sample	wt%
A	0.32
B	0.54
C	0.72
D	0.99
E	1.09
F	1.28
G	1.42
H	1.76

Samples were heated to 60 °C (above the nematic-to-isotropic transition temperature T_{NI} of 5CB) and sonicated for 5 min. Images of samples A-H were obtained in both the isotropic and nematic states of the 5CB host. It was found that both the isotropic and nematic states for sample A, B, and C yielded clear solutions which were stable after several hours, exhibiting minimal sedimentation of the star-like PAA-CNBP. These corresponded to a peak wt% of 0.72 which was fairly high loading for such systems. Above 0.72 wt% loadings, sedimentation was clearly observed (samples D through H) in **Figure 3.9** in both the isotropic and nematic phases (circled regions). Another notable observation is that even the isotropic phases at higher loading were cloudier, likely indicating a dispersion of the star-like PAA-CNBP in the 5CB host due to thermal and sonic agitations. Additional investigations into the behavior in other LC hosts are necessary to better understand the solubility behavior.

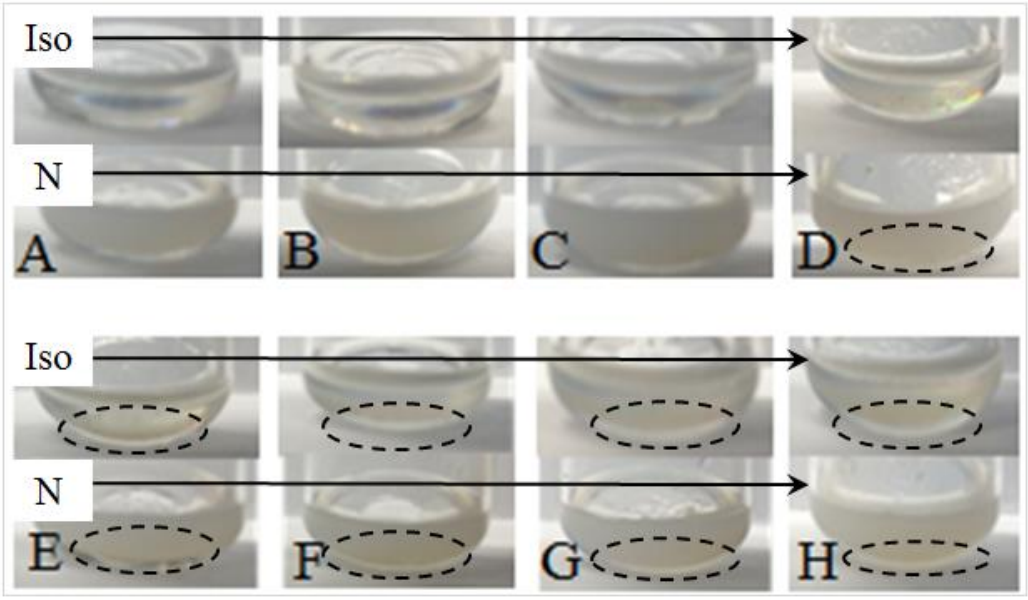

Figure 3.9 Sequence of photographs of star-like PAA-CNBP in 5CB in order of increasing concentration from left to right (0.32 wt% to 1.76 wt% in 5CB). The top series of images in each sequence is in the isotropic state (Iso) ($T>T_{NI}$), and the bottom series is in the nematic state (N) ($T<T_{NI}$). For 5CB, T_{NI} = 35 °C. Images were taken after the same amount of heating and sonication. Dashed circles indicate samples with noticeable sedimentation of PAA-CNBP. Sample A-C showed minimal sedimentation.

The resulting PAA-CNBP template was well-defined and fully functionalized with the CNBP promesogen. The star-like template was shown to successfully template superparamagnetic iron oxide nanoparticles by coordinating with the inner poly(acrylic acid) (PAA) core of the template followed by hydrolysis to preferentially nucleate nanoparticles in within the core of the templates (**Figure 3.10A**). More irregular particles and aggregates also form outside of the template, but these are removed during purification in which the templated particles are precipitated in ethanol, centrifuged and redispersed in toluene. The resulting particles had diameters between 5 and 10 nm and showed minimal aggregation (Figure 3.10B). The template was unsuccessful in templating particles in all trials. This is likely a result of the short capping layer on the

surface of the particles which provides minimal protection from aggregation during nanoparticle growth.

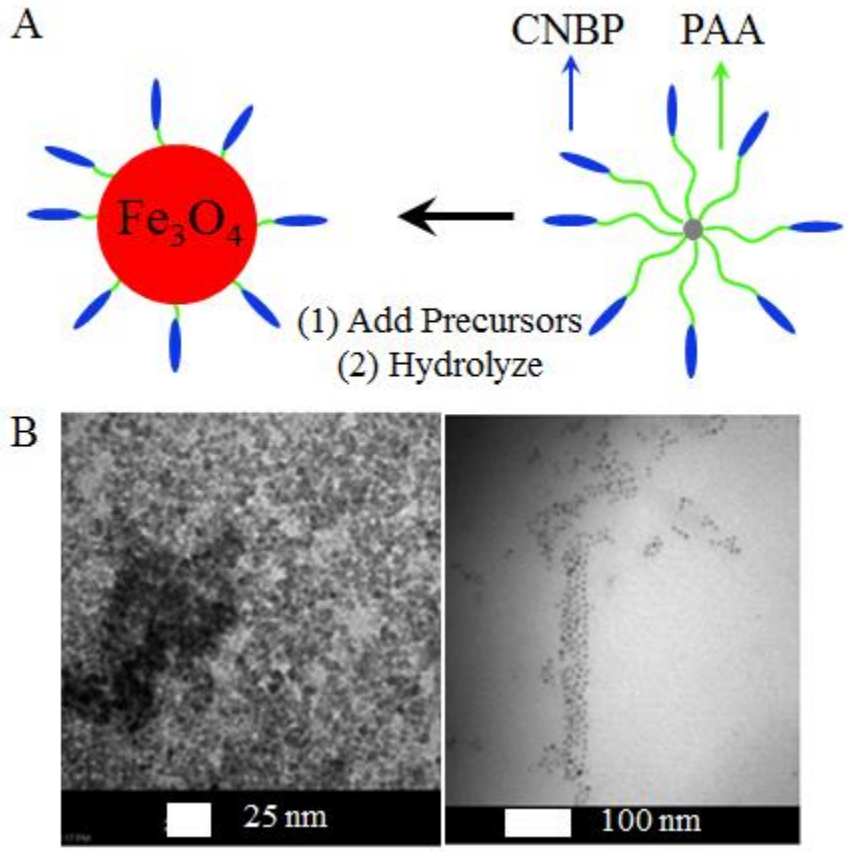

Figure 3.10 (A) The role of star-like PAA-CNBP as a template for nucleating charged iron precursors within the inner PAA core prior to hydrolysis and growth of superparamagnetic iron oxide nanoparticles capped with CNBP. (B) TEM images of particles templated by star-like PAA-CNBP.

3.4 Conclusions

Through a combination of controlled living polymerization (i.e., ATRP) and click chemistry (i.e., azide-alkyne cyclization), a novel star-like PAA-CNBP composed of inner hydrophilic PAA blocks and outer small molecules (i.e., CNBPs) that possessed similar chemical structures to the small molecular LC host

(i.e., 5CB) were synthesized. The uniformity of the resulting star-like polymer was verified by GPC and DLS. The success of click functionalization was verified by ^{1}H-NMR, FTIR, and Raman measurements. The properties of the star-like PAA-CNBP were investigated by AFM and optical imaging. An interesting interconnected morphology was formed, analogous to prior examinations of high molecular weight comb block copolymers. In addition, the star-like PAA-CNBP demonstrated solubility in the canonical nematic liquid crystal host 5CB up to 0.72 wt%. We expect that investigations into the variation of key parameters including the molecular weight of inner polymer blocks, the type of capping agent, and the length of capping agent may increase the solubility of the nanoparticles and facilitate a better understanding of the observed structure and phase behavior. These star-like PAA-CNBP can be employed as templates to produce NPs intimately and permanently connected with CNBP that render the improved solubility in the LC host. The CNBP-capped NPs are formed via the coordination interaction between hydrophilic inner PAA block and the metal moieties of precursors.[20] While the star-like PAA-CNBP successfully demonstrated the ability to template superparamagnetic iron oxide, the reliability remains low. This is due to the nature of the small molecule capping species which provides little protection against aggregation. Incorporating an intermediate outer polymer shielding layer between the PAA core and the outer CNBP promesogen units would likely improve the stability of templated nanoparticles as well as the overall success rate. The ability to harness the dynamism of the LC phase to deliberately and repeatedly control the arrangement of functional nanoscale materials (e.g., NPs, nanorods,

etc.) is the key to enabling for applications in sensing, photonics and flexible electronics among others.

CHAPTER 4. SOLUTION-STABLE COLLOIDAL GOLD NANOPARTICLES VIA SURFACTANT-FREE, HYPERBRANCHED POLYGLYCEROL-*b*-POLYSTYRENE UNIMOLECULAR TEMPLATES

This work was published in *Langmuir* (J. Iocozzia and Z. Lin*, *Langmuir*, **32**, 7180 (2016))

4.1 Background

The production of nanocomposites for various end uses has matured past mere lab scale curiosities to relevant application-driven research. Thus, the question of scalability and cost are two essential factors governing practical research development. Established methods for the production of nanoscale materials include chemical vapor deposition (CVD), atomic layer deposition (ALD) and other sputtering-type approaches. Requiring ultrapure starting materials and cleanroom conditions, these techniques are expensive to employ. Among many alternatives, non-micelle templating of nanostructures via solution chemistry (in the same class as hydrothermal and solvothermal reactions) has emerged as a low-cost, readily scalable approach. Previous work in this area has utilized various biological and synthetic templates (unimolecular and self-assembling) to produce inorganic nanostructures, including viruses,[4, 198, 199] cylindrical polymer bottlebrushes,[75, 200] polyelectrolyte-containing microspheres[201] and polyelectrolyte-containing star-like copolymers,[20] self-assembling bio and inorganic structures,[202-205] and DNA templating.[206-209] It should be emphasized that many more templating strategies exist, but they are dissimilar to those related to this work which focuses on unimolecular, synthetic and non-self-assembly processes.

In the case of star-like polymeric templates, efforts to improve the regularity, arm number and arm type are important for conferring the necessary templating functions as well as stability of the resulting nanocomposite to prevent aggregation, subsequent reaction and degradation. One approach to addressing these requirements is the development of perfect dendrimer templates. Early dendrimeric templating has focused on amino- and imine-containing dendrimers to nucleate catalytically-active metal nanoparticles.[210, 211] While dendrimers afford a more precise template structure, higher molecular weights are challenging to reach due to the generation-based growth which is tedious and time consuming. An alternative to dendrimers employs multi-site initiators, including β-cyclodextrin (containing 21 hydroxyl groups),[20] small polyols (possessing 3-6 hydroxyl groups),[29, 212] and inorganic polyhedral oligomeric silsesquioxane (POSS) (possessing 8 or more hydroxyl groups if bridged aggregates)[213] that have been modified to serve as "grafting-from" initiators for polymerizations. The formation of regular star-like initiators has been greatly improved by the parallel development of controlled polymerization techniques, including atom-transfer radical polymerization (ATRP).[137, 214]

ATRP is a popular choice for producing well-defined polymer chains with low polydispersity. Owing to the low cost of the copper-based catalysts used and the ease of separation from the products via filtration and the mild conditions often required (below 90 °C, and at neutral pH), it is an attractive approach for polymerizations. Since several established, one-step strategies exist for converting polyols to multi-site ATRP initiators (i.e., ATRP macroinitiators), it is a natural approach to use in the production of star-like copolymer templates of diverse compositions. These strategies offer simple approaches to multi-site initiators but the number of initiation sites is typically low (less than 10) and

fixed for any given material class. Thus, it is desirable to have multi-site polyol initiators that can be functionalized for ATRP where the number of initiation sites can also be tuned to any desired value while maintaining a low cost, scalability, and low toxicity. Hyperbranched polyglycerols (HPG) offer such a solution.

Hyperbranched polyglycerols are an attractive class of biocompatible, water-soluble polymers possessing a large number of hydroxyl groups and ether linkages. Unlike dendrimer templating approaches, HPG can be produced in large quantities via single-pot reactions from inexpensive commercially-available materials (glycidol monomer, sodium methoxide base, and TMP initiator) in a relatively simpler fashion. Since their initial discovery, HPGs have been promising for many applications. Much has been done to address the challenges associated with their synthesis via uncatalyzed ring opening multibranching polymerization (ROMBP) of glycidol as detailed in **Figure 4.1**.[85, 86, 95, 129, 215]

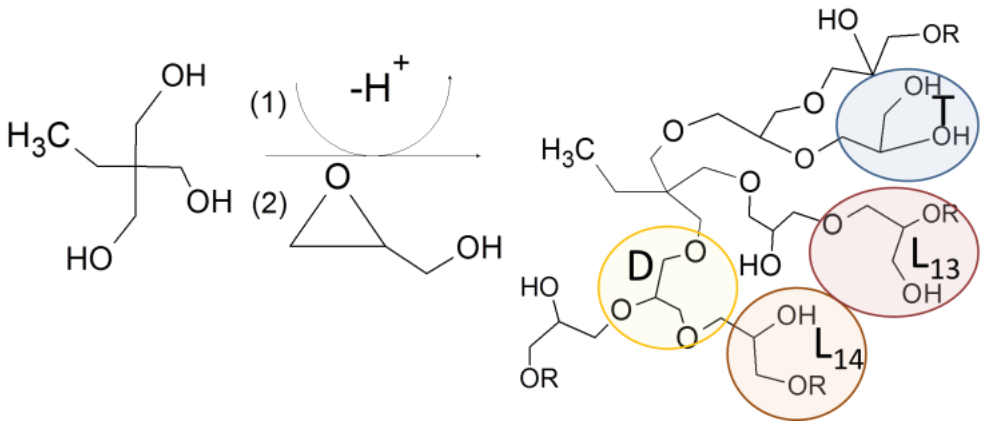

Figure 4.1 The general scheme for the ring opening multibranching polymerization of glycidol monomer into HPG. The 1,1,1-tris(hydroxymethyl) propane (TMP) initiator (left) is deprotonated and the epoxide-containing glycidol monomer is slowly added. How the monomer adds dictates the type of repeat unit formed in the growing HPG structure defined as dendritic (D), terminal (T) and linear-13 (L_{13}) and linear-14 (L_{14}).

The scheme illustrates the complicated structure of a general HPG molecule containing the characteristic core structure and four different repeat units within the polyether-polyol structure denoted terminal (T), dendritic (D) linear-13 (L_{13}) and linear-14 (L_{14}). Frey, Sunder, Brooks et al. have introduced strategies, including slow monomer addition (SMA), improved reactor design and sequential ROMBP,[93] to produce higher molecular weight HPGs with improved degrees of branching (i.e., more terminal and dendritic units and less linear units) while maintaining a low polydispersity index (PDI < 1.5).

In contrast to perfect dendrimers which require tedious, time-consuming and expensive protection/deprotection chemistry, HPG can be produced in large single-pot reactions and is equally amenable to subsequent chemical modification as dendrimers. Moreover, the wealth of chemical modification techniques applied to HPG macroinitiators is impressive. The surface hydroxyl groups can be deprotonated and subjected to additional ring opening reactions to produce hydrophilic HPG-*b*-polyethylene oxide type star copolymers,[119, 216, 217] functionalized with click-moieties[218] or converted to ATRP macroinitiators for the polymerization of many acrylate monomers, leading to amphiphilic star copolymers[219-222] with added functionalities such as cross-linking, hydrogel formation and improved solubility in different solvents (polar, nonpolar, aqueous, etc.). Given the large potential for useful chemical functionality, HPG-based templates have emerged as a natural choice for unimolecular templating of inorganic nanoparticles.

To date, there have been only a handful of reports employing HPG-based templates in the synthesis of inorganic structures. One study focused on the partial

olefinic functionalization of HPG for use in nucleating palladium nanoparticles.[223] The work relies on the coordination of metal precursors to the remaining unreacted hydroxyl groups for subsequent reduction. Partial capping with the relatively small olefinic capping agent is a good approach.[223] However, partial capping is nonspecific. It doesn't readily enable control over the size of the capping layer, and often relies on the random distribution of residual hydroxyl groups to coordinate with metal precursors. Another study grows a layer of HPG on the surface of premade nanoparticles (surface-initiated ROMBP).[127] Subsequently, the hydroxyl groups are modified with an anhydride to produce carboxylic acid-terminated HPG which coordinates with metal ions in a similar fashion to poly(acrylic acid) in other templating materials.[20, 224-229] In two related studies, a linear multi-molecular templating approach is employed that relies on ether chemistry for coordinating with metal precursor ions.[230, 231] Both studies utilize a linear P3HT derivative, 2-2(ethoxyethoxy)ethoxy-modified polythiophene (P3EEET), whose side chains have been converted from hexyl chains to oligomeric ether groups. These ether groups are then used to coordinate with Au or Zn ions for in situ reduction/condensation to the respective metallic and inorganic components. The modified linear P3EEET successfully template particles; however the monomer synthesis procedure is quite tedious and the use of multimolecular linear P3EEET templates reduces the control of size and likely affects the solution stability of the resulting nanocomposites.[224, 225] In another related work, HPG was used to stabilize multiple nanoparticles in aqueous environments during synthesis.[232] This study supports the versatility of HPG-based templating; however this approach may have long term stability issues as well as difficulties with film formation due to multiple particles being stabilized by multiple

HPG molecules in an essentially random fashion. Lastly, a few previous works have investigated HPG-*b*-PS and HPG-*b*-mixed arm polymers possessing lower degrees of ATRP functionalization.[133, 233, 234] The lower degrees of functionalization likely made such polymers less equipped to serve as templates, but nonetheless heavily informed on the present work.

Herein, we report the implementation of ROMBP and ATRP to produce low cost multi-arm hyperbranched polyglycerol-*block*-polystyrene (HPG-*b*-PS) block copolymers which are subsequently investigated for their ability to template the formation of Au nanoparticles as well as other types. Unlike previous linear polymer templating approaches, this work demonstrates, *for the first time*, the use of the unimolecular hyperbranched core in HPG-*b*-PS copolymers to sequester Au ions primarily via polyether coordination and facilitate the in situ reduction into Au nanoparticles capped with PS chains. The resulting system shows excellent long-term solution stability in organic solvents. The effects of the molecular weight of the PS arms and the solvent type were also studied to optimize the reaction conditions and verify the templating capabilities of hyperbranched HPG-*b*-PS. The synthesis procedure for the template and the resulting colloidal nanoparticles is simple, reproducible, and likely generalizable to guiding the nucleation and growth of other metal and metal oxide systems quickly and at low cost. The PS capping layers make such colloidal systems applicable to thin film and interfacial deposition via simple wet deposition techniques such as spin coating and dip coating.

4.2 Experimental Details

4.2.1 Materials

2-bromoisobutyryl bromide (BIBB, 98%), 2,2-bipyridyl (BDY, 99%), 1-methyl-2-pyrrolidinone (N-methyl pyrrolidinone) (NMP, 98%), glycidol (96%), gold (III) chloride hydrate ($HAuCl_4 \bullet 3H_2O$, 99%) were purchased from Sigma-Aldrich and used as received unless otherwise noted. NMP was mixed with CaH_2 overnight and distilled under vacuum prior to use. Glycidol was distilled under vacuum immediately prior to use. Silver (I) nitrate ($AgNO_3$, 99%) Styrene (St, 99% stabilized with 15ppm 4-tert-butyl catechol), sodium methoxide (NaOMe, 98%), borane tert-butylamine complex (BTBA, 97%), benzyl alcohol (BA, 99%) and 1,1,1-tris(hydroxymethyl) propane (TMP, 98%) were purchased from Alfa Aesar and used as received unless otherwise noted. Styrene was distilled to remove polymerization inhibitor prior to use. Dimethylformamide (DMF, solvent grade) and methanol (MeOH, solvent grade) were purchased from BDH and distilled prior to use and stored over activated molecular sieves. Iron (II) chloride tetrahydrate ($FeCl_2 \bullet 4H_2O$), iron (III) chloride hexahydrate ($FeCl_3 \bullet 6H_2O$), bis(methoxyethyl) ether (diglyme, 99%) was purchased from Acros Organic and used as received.

4.2.2 Characterization

Absolute molecular weights of polymers and structural verification were determined by ^{1}HNMR operating on a Varian VXR-400 (400 MHz) Unity Innova spectrometer with a Nalorac quad-probe. T^1-inversion recovery and Inverse-gated carbon NMR (IG ^{13}C NMR) were performed on the same instrument to determine necessary scan

times, determine the structural composition of HPG samples and calculate the degree of branching (DB). Gel permeation chromatography was performed on a Shimadzu GPC setup (RID-10A refractive index detector, CTO-20A column oven and LC-20A chromatograph pump). For HPG polymers only, DMF with LiCl additive was used as the mobile phase (calibrated with linear PEO standards). For HPG-*b*-PS copolymer templates, THF was used as the mobile phase (calibrated with linear PS standards). A phenomenex phenogel linear column with mixed pore size beads was used in GPC measurements (MW range: 200 to 2×10^6 g mol^{-1}). UV-Vis was performed on a Shimadzu UV-2600 spectrometer with quartz cuvettes (10 mm path length). HPG-*b*-PS template and PS-capped Au nanoparticles characterization were performed on a Renishaw inVia Raman microscope with 785 nm excitation wavelength. The elemental composition of Au nanoparticles was verified by x-ray diffraction on a PANalytical XRD with Cu Kα radiation ($\lambda = 0.154$ nm).

4.2.3 Synthesis of Hyperbranched Polyglycerols (HPG)

The ROMBP reactor was prepared by attaching an eternally-powered Teflon stirrer into a Teflon bearing attachment in the top of a three-neck flask and placed in a temperature-controlled oil bath. To the left port of the flask, a syringe pump needle was attached. To the right port, the argon inlet and vent was attached (**Figure 4.2**).

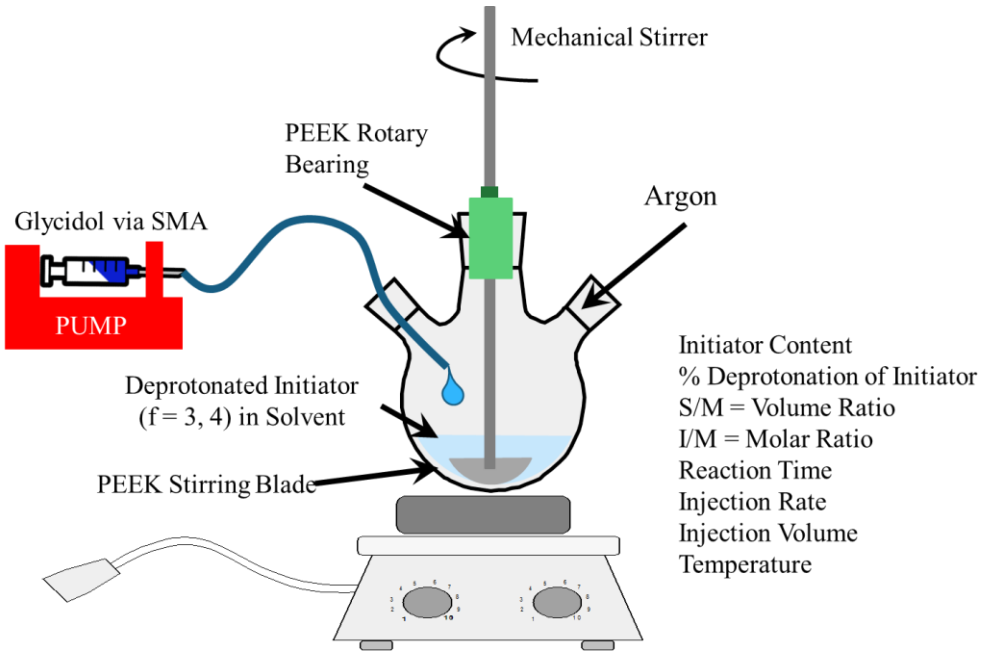

Figure 4.2 Reactor setup for the synthesis of HPG via the slow monomer addition (SMA) approach. Key parameters in HPG synthesis are also included: f, functionality of initiator; S/M, solvent to glycidol monomer volume ratio; I/M, initiator to glycidol monomer molar ratio.

An amount of the TMP initiator and KOMe was added to the reactor and heated to 80 °C to form a melt. This was reacted for 60 minutes to remove residual water and methanol. Benzene was then added and the reactor dried under vacuum to form the initiator. In some experiments, a small amount of diglyme was added to redissolve the activated initiator. In most experiments a measured amount of dry NMP was added to redissolve the initiator. Freshly-distilled glycidol (50/50 weight ratio in dry NMP) was then loaded into the syringe pump and injected into the reactor at a specified rate, temperature and stirrer speed (120 rotations per minute). The reaction then proceeded for a specified period of time under inert argon atmosphere. Since the ROMBP reaction isn't catalyzed like ATRP, precise control over the different reactions parameters is essential to producing low PDI product. After the reaction, NMP was distilled off and the product

was redissolved in methanol. This product was then precipitated in acetone, collected and purified twice more to yield the final HPG product (Yield: 30% for HPG10 and 37% for HPG7). ^{1}HNMR (DMSO-d_6) δ (ppm): 0.91 (s, 3H, methyl group of TMP); 1.45 (s, 2H, —CH_2— bridge group of TMP); 3.4-4.0 (m, 5H, HPG backbone). Inverse-gated carbon NMR, IG ^{13}C NMR, (DMSO-d_6) δ (ppm): 79.5-80.5 (L_{13}); 78-79 (D), 72-73 ($2L_{14}$); 70.5-71.5 (2D, 2T); 68-70 (L_{13}, L_{14}); 62.5-63.5 (T); 61-62.5 (L_{13}). Reaction details for HPG synthesis can be found in **Table 4.1**.

Table 4.1 Summary of reaction details for relevant HPG samples

Sample[a]	TMP(g)[b]	%Dep[c]	Base	M (ml)[d]	Solvent (Vol, ml)	Time (min)	T (°C)	Inj. Rate (ml/hr)
HPG2	0.12	3	KOMe[†]	12	Dioxane (12)	510	95	1.41
HPG7	0.12	10	KOMe‡	12	Diglyme (12)	340	95	4.24
HPG10	0.12	10	KOMe‡	12	Mixed (12)[e]	330	100	4.24

[a]Other samples were also produced (i.e., HPG1, HPG3, etc.) which were not included in this study. The numbers refer to the experimental batch and the reactions conditions associated with each batch. [b]Anhydrous 1,1,1-tris(hydroxymethyl)propane (TMP) is the initiator employed for all ROMBP of HPG. [c]Degree of deprotonation of the TMP initiator. [d]Glycidol monomer content. [e]Mixed denotes a 1:1 (v/v) of NMP and diglyme. [†]Potassium Methylate solution (in methanol). [‡]Potassium methylate powder.

Since the proton signals of HPG are convoluted together in the ^{1}HNMR spectrum, only the degree of polymerization can be evaluated without any detail regarding the overall branching structure of the HPG sample. Since HPG is a pseudorandom structure, every batch is different and the structural types desired may change each time. Inverse-gated ^{13}CNMR enables a quantitative evaluation of the different carbon centers associated with the four different and distinct structural repeat units to be integrated. These percentages can be used to calculate the degree of branching (DB) using equation

2. **Figure 4.3** presents a representative example of the IG ^{13}CNMR spectra for HPG2, and **Table 4.2** has the associated calculation of the repeat unit composition and the degree of branching. Yields for primary HPG synthesis are deliberately low to prevent cross-coupling and increased PDI.

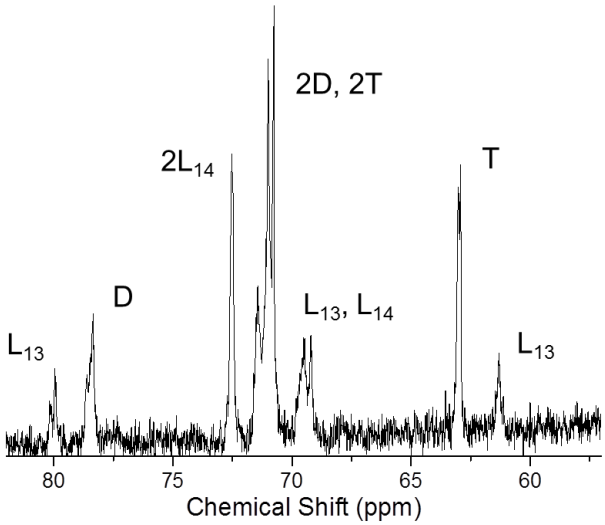

Figure 4.3 The IG ^{13}CNMR spectrum for HPG2 (in DMSO-d_6) showing the different types of repeat units possible during ROMBP.

Table 4.2 Sample calculation of different HPG components from IG ^{13}CNMR data

Component	Relative Integrals	Contribution (%)
L_{13}	10	15
L_{14}	11.2	16
T	31.6	22
D	14.6	47
Sum	67.4	100

4.2.4 Formation of HPG-Br Macroinitiators (MI)

The HPG macroinitiators (i.e., brominated HPG (HPG-Br)) were formed by reacting BIBB with the hydroxyl groups of HPG in an esterification reaction. Different HPG samples were used to prepare HPG-BR macroinitiators (i.e. HPG1, HPG2, and so on) as summarized in **Table 4.1**. In a representative procedure, 4.06 g of HPG7 (0.055 mol –OH) was dried in a vacuum oven overnight followed by azeotropic distillation with 40 ml of toluene. HPG7 was dissolved in dry NMP (20-30 ml) and chilled to 0 °C. 8.12 ml of BIBB (0.066 mol) was added dropwise to HPG7 solution under magnetic stirring over 30 minutes and allowed to react for 24 hours. The crude product was washed with $NaHCO_3$ (5 wt% in DI water) 3-4 times until bubbling stops, washed with DI water 2-3 times, dried overnight with $MgSO_4$, filtered and dried overnight under vacuum (55 °C) to yield a brown highly viscous product (Yield: 75% for HPG10-Br and 81% for HPG7-Br). ^{1}H NMR ($CDCl_3$) δ (ppm): 1.92 (s, 6H, —C(C*H*$_3$)$_2$—Br (primary bromination signal); 4.1-4.2, 4.25-4.4, 4.5-4.6, 5-5.2, 5.25-5.4 (m, 6H, —C*H*$_2$— and –CH$_2$—C*H*(—O—)—CH$_2$— near bromine in HPG backbone). In all HPG brominations, BIBB was added in a 1:1.2 molar ratio –OH:BIBB.

4.2.5 Preparation of Unimolecular HPG-b-PS Copolymer Templates

ATRP of styrene was performed in bulk at 90 °C. A 150 ml Schlenk flask was charged with an amount of HPG-b-PS macroinitiator, 80% of the required amount of freshly distilled and dried styrene monomer, and a magnetic stirrer. In a separate vial, an amount of CuBr co-catalyst was dispersed in the remaining styrene. To this, an amount of PMDETA co-catalyst was added dropwise to the CuBr solution and sonicated to produce the catalyst solution. The catalyst was added to the Schlenk flask and sealed. The flask

then undergoes three freeze-pump-thaw cycles under N_2 atmosphere. The flask reacted at temperature for a given amount of time. The flask was quenched with liquid nitrogen, diluted with THF and passed through a neutral alumina column to remove catalyst. The crude product was precipitated in a cold solution of 50/50 methanol and water. The product was redissolved and precipitated twice more. The purified product was then stirred with $MgSO_4$ overnight, filtered and dried in a vacuum over for 48 hours. Details for the different ATRP experiments are in **Table 4.3**. ^{1}HNMR ($CDCl_3$) δ (ppm): 0.70-0.95 (s, 6H, —C(C*H*$_3$)$_2$—PS); 1.25-2.15 (m, 3H, --C*H*$_2$C*H*— of PS); 2.80-4.0 (m, 5H, —C*H*— and —C*H*$_2$— of HPG core); 4.45-4.65 (d, 1H, CH$_2$—C*H*(Ph)—Br); 6.35-7.35 (m, 5H, —C$_6$*H*$_5$ of PS). The different HPG-*b*-PS samples are usefully labeled based on the molecular weight of the HPG core, the number of PS arms and the length of the PS arms. The molecular weight of the grown chains was determined by cleaving the ester linkages attaching the chains to the HPG core by refluxing the HPG-*b*-PS copolymers in THF under basic conditions. The resulting solutions were precipitated in water, filtered and dried prior to analysis.

Table 4.3 Recipes for HPGX-Br-initiated ATRP of styrene

Product[a]	**M.I.**[b] **g (mmol -Br)**	**CuBr g (mmol)**	**BDY g (mmol)**	**St. (ml)**	**Solvent (ml)**	**T (°C)**	**Time (min)**
HPG12.6k-*b*-117PS3.6k	0.25 (1.12)	0.161 (1.12)	0.175 (1.12)	13.9	bulk	90	45
HPG12.6k-*b*-117PS5k	0.25 (1.12)	0.161 (1.12)	0.175 (1.12)	13.9	bulk	90	150
HPG9.3k-*b*-98PS4.5k	0.25 (1.13)	0.163 (1.14)	0.178 (1.14)	14.1	bulk	90	150
HPG9.3k-*b*-98PS13.4k	0.25 (1.13)	0.163 (1.14)	0.178 (1.14)	14.1	bulk	90	720

[a]Molar ratios for HPG7-Br and HPG10-Br products are 1:1:1:108.3 (HPG7-Br:CuBr:BDY:St). [b]Designates macroinitiator.

Several different templating trials were performed using the same group of HPG-*b*-PS templates under different reaction conditions. These different conditions are summarized in **Table 4.4** and the sample IDs are referenced in the main text.

4.2.6 In Situ Synthesis of PS-Capped Colloidal Au Nanoparticles

Several conditions for templating Au nanoparticles with HPG-*b*-PS copolymers were investigated. In all cases, a molar ratio of 1:7 was maintained between the Au precursor and the borane tert-butylamine complex (BTBA) reducer used to reduce Au ions to metallic Au. The BTBA precursor solution was prepared in small batches by dissolving 0.0393 g of $HAuCl_4 \bullet 3H_2O$ in 1 ml of dry DMF. The reducer solution was prepared in small batches immediately prior to each experiment by dissolving 0.061 g of BTBA in 1 ml of dry DMF. For samples Au1@HPG9.3k-***b***-98PS4.5k, Au2@HPG9.3k-*b*-98PS4.5k, Au3@HPG9.3k and Au4@HPG9.3k, 20 hours of stirring was allowed for precursor incorporation prior to in-situ reduction and allowed to react for 30 minutes prior to termination. For samples Au5@HPG9.3k-*b*-98PS4.5k, Au6@HPG9.3k-*b*-98PS4.5k, Au7@HPG9.3k and Au8@HPG9.3k, 120 hours of stirring was allowed for precursor incorporation into the inner HPG block prior to in-situ reduction and allowed to react for 10 minutes prior to termination. For samples Au9@HPG9.3k-*b*-98PS4.5k, Au10@HPG9.3k-*b*-98PS4.5k, Au11@HPG9.3k-*b*-98PS4.5k, the reaction solvent type was varied from 9:1, to 8:2, to 6:4 DMF:BA (v/v), respectively. Gradually increasing the content of BA gradually reduces the overall solubility of the PS chains of the HPG-*b*-PS templates. Previous work with templating via a different nanoreactor approach also showed the importance of the solvent type in yielding nanoparticles. For samples Au12@HPG9.3k-*b*-98PS7k, Au13@HPG9.3k-*b*-98PS13.4k, Au14@HPG12.6k-*b*-

117PS3.6k and Au15@HPG12.6k-*b*-117PS5k, the length of the arms was varied to investigate its effect. Details of the reaction conditions can be found in **Table 4.3** and **Table 4.4**.

Table 4.4 HPG-*b*-PS Templating Sample Details

Sample ID[a]	**Template Mass (mg)**	**BTBA Reducer Soln. (ml)**[b]	**Precursor Soln. (ml)**[d]	**Vol. (DMF:BA) (v/v)**[e]
Au1@HPG9.3k-*b*-98PS4.5k	100	0.4	0.4	10:0
Au2@HPG9.3k-*b*-98PS4.5k	100	0.1	0.1	10:0
Au3@HPG9.3k**	100	0.4	0.4	10:0
Au4@HPG9.3k**	100	0.1	0.1	10:0
Au5@HPG9.3k-*b*-98PS4.5k	100	0.4	0.4	10:0
Au6@HPG9.3k-*b*-98PS4.5k	100	0.1	0.1	10:0
Au7@HPG9.3k**	100	0.4	0.4	10:0
Au8@HPG9.3k**	100	0.1	0.1	10:0
Au9@HPG9.3k-*b*-98PS4.5k	100	0.4	0.4	9:1
Au10@HPG9.3k-*b*-98PS4.5k	100	0.4	0.4	8:2
Au11@HPG9.3k-*b*-98PS4.5k	100	0.4	0.4	6:4
Au12@HPG9.3k-*b*-98PS7k*	50	0.25[c]	0.25	10:0
Au13@HPG9.3k-*b*-98PS13.4k	50	0.25[c]	0.25	10:0
Au14@HPG12.6k-*b*-117PS3.6k	50	0.25[c]	0.25	10:0
Au15@HPG12.6k-*b*-117PS5k	50	0.25[c]	0.25	10:0
Control 1 (C1)	-	0.4	0.4	10:0
Control 2 (C2)	-	0.4	0.4	10:0

[a]These sample IDs are used throughout the main text and in relevant figures and denote the type of template used as well as the associated reduction conditions. Molar ratio of 1:7 (precursor : reducer) for all samples but the ratio between template and reducer/precursor varies. [b]0.06 g/ml BTBA in DMF. [c]0.048 g/ml BTBA in DMF. [d]0.039 g/ml $HAuCl_4 \bullet 3H_2O$ in DMF. [e]Total volume after addition of all reagents during reaction is 10ml. *This sample showed a polydisperse GPC trace for the HPG-b-PS copolymer whereas all the others showed narrow, monodisperse GPC traces for overall template and cleaved PS chains. **These samples attempted to use only HPG (no PS capping layer) to template particles but were unsuccessful and not further investigated.

4.3 Results and Discussion

4.3.1 Effect of Stoichiometry, Solvent, Co-solvent and Degree of Deprotonation on HPG Structure

Three different molecular weights of HPG were synthesized for use as ATRP macroinitiators after bromination of HPG (see Experimental Section). Ultimately HPG2-Br was not employed as a macroinitiator for this study due to its relatively low number of ATRP initiation sites compared to the other two as well as its relatively low yield during ROMBP. Despite having the longest polymerization time and slowest monomer injection rate, it still had the lowest molecular weight due largely to the low degree of deprotonation of the initiator. It is nonetheless illustrative for the purposes of characterization as it provides clear peaks in IG ^{13}CNMR. With an adjustment of the reaction conditions to include a higher initial degree of deprotonation, faster monomer injection rate and higher proportion of NMP solvent (improved solubility), higher molecular weight HPG7 and HPG10 were obtained (**Table 4.1**). The tradeoff, however, is that when higher molecular weights are attained, there is a pronounced increase in the molecular weight distribution, a reduction in the number of dendritic and terminal units and an increase in the number of linear units as demonstrated for HPG7. A comfortable balance was obtained for HPG10 in which a substantial number of initiation sites were produced without a compromise in the molecular weight. Degree of polymerization (DP) and degree of branching (DB) were calculated by equations (1) and (2) as follows and summarized in **Table 4.5**:

$$DP = \frac{\left(\frac{A_{polyether\ core}}{5} - 2A_{methyl}\right)}{\left(\frac{A_{methyl}}{3}\right)} \qquad (1)$$

$$DB = \frac{2D}{2D + L_{13} + L_{14}} \qquad (2)$$

where $A_{polyether\ core}$ is the integrated area of the HPG backbone proton signals, A_{methyl} is the integrated area of the methyl group of the TMP initiator core, and D, L_{13} and L_{14} are the integrated areas of the IG ^{13}C NMR spectrum of HPG.

Table 4.5 Molecular weight and structural characterization parameters of HPG

Sample	**$M_{n,HNMR}$ (g mol^{-1})[a]**	**$M_{n,GPC}$ (g mol^{-1})[b]**	**$M_{w,GPC}$ (g mol^{-1})[b]**	**PDI**	**OH[a]**	T[c]	D[c]	**L_{13}[c]**	**L_{14}[c]**	**DB[d]**	**Br[e]**
HPG2	7,200	4,200	6,200	1.4	91	47	22	15	16	59	88
HPG7	12,600	5,900	18,000	3.2	170	38	18	12	32	45	69
HPG10	9,300	7,200*	10,000*	1.38*	126	34	23	18	25	52	78

[a]Average value determined by dividing the integrated HPG backbone proton signal by the integrated proton signal of the initiator core using equation (1). [b]DMF GPC mobile phase contains 0.1% LiCl additive and uses linear PEG calibration standards. [c]Percentage of HPG terminal (T), dendritic (D), linear type-1 (L_{13}) and linear type-2 (L_{14}) determined by integrating respective signals obtained in IG ^{13}CNMR spectra (see **Figure 4.3** and **Table 4.2** for a representative spectra and calculation). [d]Degree of branching (DB) calculated by equation (2).[93] [e]Percent esterification via BIBB calculated by equation (3).[133]

Thus, HPG10-Br (i.e., HPG10 after bromination, see Experimental Section) served as the principal macroinitiator for this work. HPG7-Br was also employed to investigate the effects of arm number on the templating of Au nanoparticles. It should be noted that the investigation of the effects of arm number and length are introductory and not the main focus of this work. The long reaction time during bromination enabled a higher percentage of initiation sites to be realized than reported in previous works which

typically focused on lower degrees of esterification.[233, 234] In this work, the degree of esterification (i.e., to yield HPG-Br) was much larger such that most of the hydroxyl groups are converted to ATRP initiation sites. The high degree of bromination was calculated from equation (3) using the ^{1}H NMR signals for the HPG-Br macroinitiators.

$$-Br\ \% = \frac{\left(\frac{A_{Br}}{6}\right)}{\left(\frac{A_{polyether\ core}}{5}\right)} \qquad (3)$$

where A_{Br} is the integral of the methyl group NMR signal on the BIBB-functionalized HPG-Br macroinitiator and $A_{polyether\ core}$ is the integral of the polyether backbone NMR intensity. By multiplying the degree of bromination with the average number of –OH present in each HPG molecule, the number of initiation sites (i.e. PS arms to be grown) can be calculated. For HPG7 and HPG 10 these values were 117 and 98, respectively.

4.3.2 Molecular Weight Control of HPG-b-PS Copolymers

Two points needed to be addressed before using the HPG-*b*-PS copolymers as templates. The first was whether or not ATRP of styrene was initiated by the HPG-Br macroinitiators. The second was whether or not the polymerizations proceeded in a living fashion that can be controlled over various molecular weights. Both points were verified by assuming the macroinitiators worked and growing various PS chain lengths from them (**Figure 4.4a**). We note that HPG7-based macroinitiators had 117 arms and HPG10-based macroinitiators had 98 arms. It was found that a massive increase in the molecular weight of HPG-*b*-PS copolymer occurred, indicating a growth from the macroinitiator as desired. Subsequently, the PS chains were cleaved from the HPG-*b*-PS template and measured via GPC to determine the polydispersity and average size (**Figure 4.4b**). In all cases, a PDI

less than 1.31 and a molecular weight ranging from 3.6 kg/mol up to 13.4 kg/mol per arm were obtained.

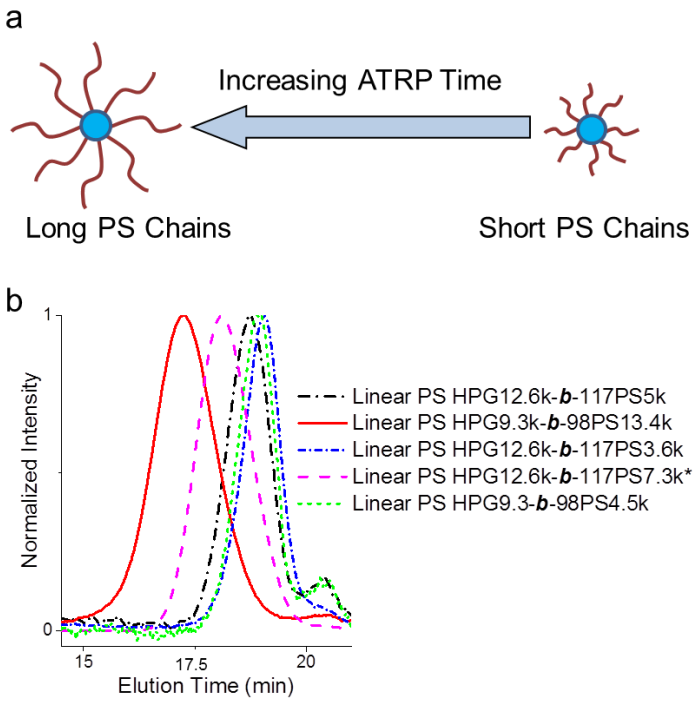

Figure 4.4 (a) Schematic describing the effect of reaction time on the length of the PS arms grown from the HPG-Br macroinitiators. (b) GPC traces of the cleaved linear PS chains grown via ATRP from the various HPG-Br macroinitiators. Samples showed low PDIs and unimodal distributions supporting the expected initiation mechanism and living nature of the polymerizations. The number or arms was either 117 or 98 for HPG7 or HPG10-based macroinitiators, respectively. *This reaction used twice the catalyst compared to the other HPG12.6k-*b*-117PS5k template.

Larger molecular weights of HPG-*b*-PS were avoided due to the greater chance of chain-chain coupling leading to larger polydispersity for the HPG-*b*-PS templates. This effect can already be seen for HPG9.3k-*b*-98PS13.4k (PS polymerization for 720 minutes) whose PDI is greater than 2. Since the number of arms is much larger than most polymers previously investigated, there is a much larger possibility for intra- and inter-

chain coupling in this system.[227, 228] Despite this, the cleaved chains are still quite monodisperse, which supports that the chains are initiated from the HPG-Br macroinitiators as desired and that the chains grow in a living fashion. The detailed molecular weight characterizations of the HPG-*b*-PS samples are summarized in **Table 4.6**. Note the sample names in **Table 4.6** include the molecular weight of the HPG core, the number of initiation sites and the length of the PS arms.

Table 4.6 Summary of parameters for HPG-Br, HPG-*b*-PS and cleaved PS chains

Sample[a]	$\mathbf{M_{n,star}}$ **(g mol^{-1})**[b]	$\mathbf{M_{w,\ star}}$ **(g mol^{-1})**[b]	$\mathbf{PDI_{star}}$	$\mathbf{M_{n,\ PS}}$ **(g mol^{-1})**[c]	$\mathbf{M_{w,\ PS}}$ **(g mol^{-1})**[c]	$\mathbf{PDI_{PS}}$
HPG12.6k-*b*-117PS3.6k	31,000	44,000	1.45	3,600	4,400	1.23
HPG12.6k-*b*-117PS5k	134,000	156,000	1.16	5,000	5,900	1.16
HPG9.3k-*b*-98PS4.5k	32,000	42,000	1.31	4,500	5,100	1.14
HPG9.3k-*b*-98PS13.4k	127,000	274,000	2.16	13,400	17,500	1.31

[a]Star-like copolymer samples HPG12.6k-*b*-117PS3.6k and HPG12.6k-*b*-117PS5k use HPG7-Br macroinitiator and star-like copolymer samples HPG9.3k-*b*-98PS4.5k and HPG9.3k-*b*-98PS13.4k use HPG10-Br macroinitiator. HPG7-Br has 117 initiation sites and HPG10-Br has 98 initiation sites which are reflected in the names of the different samples. [b]THF GPC molecular weight of HPG-b-PS star copolymer. [c]THF GPC molecular weight of linear PS chains cleaved from the HPG macroinitiator.

To further establish that HPG-Br serves as an ATRP initiator in these experiments, ^{1}HNMR was used to ensure high bromination efficiency as well as verify that the core (i.e., HPG) is retained in the template (i.e., HPG-*b*-PS). **Figure 4.5** summarizes the ^{1}HNMR spectra of the HPG samples as well as their macroinitiators (**Figure 4.5a**) and a representative HPG-*b*-PS copolymer sample (**Figure 4.5b**). Consistent results are observed for HPG synthesis as well as their respective brominated macroinitiators (HPG7-Br and HPG10-Br) as shown by the strong peaks found around 1.92 ppm in the NMR spectrum (peak e in **Figure 4.5a**). The low intensity peaks of the

TMP initiator are also observed, thus supporting the proper initiation and ROMBP (peaks c and d in **Figure 4.5a**). In addition, the weak signals of the HPG backbone and macroinitiator core are also preserved in the spectrum for HPG9.3k-*b*-98PS4.5k (peaks f and g **Figure 4.5b**) as well as the PS chain signals (peaks j, i, and h in **Figure 4.5b**). Verification of the retention of the inner HPG core was essential prior to using HPG-*b*-PS as a template for synthesizing Au nanoparticles.

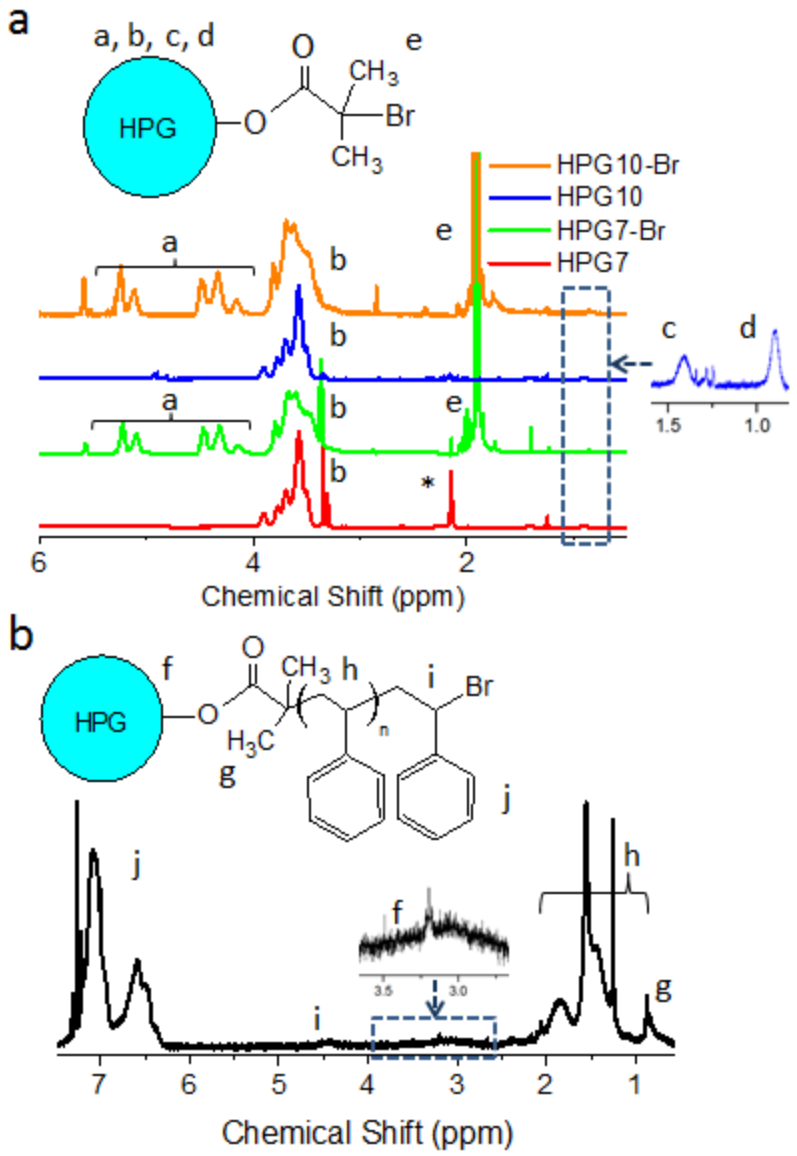

Figure 4.5 (a) [1]HNMR spectra for HPG7, HPG10, their respective brominated macroinitiators, and (b) HPG9.3k-*b*-98PS4.5k, showing both the HPG core signals as well as the PS chains. Residual solvent peaks denoted with *.

4.3.3 Effect of Solvent Conditions on HPG-b-PS Templating of Au Nanoparticles

Investigation into the templating ability of various HPG-*b*-PS copolymers was divided into three sections. In the first section, optimum solvent conditions were employed (pure DMF) and the importance (if any) of the chelation time was investigated.

In the second section, the solvent type was varied to determine if the nanoparticles are in fact being preferentially coordinated with the polyether core and reduced in-situ. In the third section, variation in the length and number of PS arms was scrutinized to examine the effective arm length for separating the different cores during coordination/reduction as well as maintaining long-term, stable nanoparticle dispersions. The success of the various HPG-*b*-PS star-like copolymers in templating inorganic nanoparticles depends on finding a balance between precursor coordination (loading time), aggregation minimization (PS arm length), and reduction time (total reaction time) (**Figure 4.6**). These parameters likely differ when templating different inorganic nanoparticles.

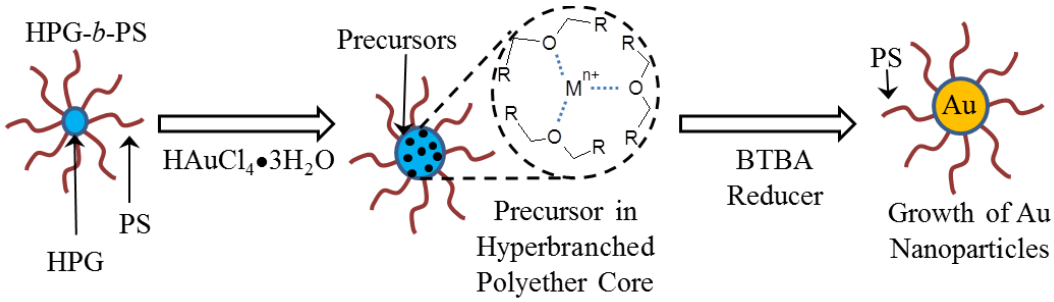

Figure 4.6 Schematic showing the phases of inorganic nanoparticle templating using HPG-*b*-PS star-like copolymers. First, the inorganic precursor (M^{n+}) is allowed to coordinate with the inner HPG ether moieties by diffusing through the outer protective PS layer encasing the HPG core. Second, a reducing agent (borane tert-butylamine complex, BTBA) is added to reduce the precursors preferentially coordinated within the HPG-*b*-PS template. The outer PS core isolates the individual inorganic nanoparticles during growth to prevent aggregation. Note that precursor outside of the template also reacts and is subsequently removed during the purification steps.

It is important to note that the effects of arm length and arm number are of lesser importance than the overall ability to template particles. Samples Au1@HPG9.3k-*b*-98PS4.5k and Au2@HPG9.3k-*b*-98PS4.5k allowed precursor chelation over 20 hours

whereas Au5@HPG9.3k-*b*-98PS4.5k and Au6@HPG9.3k-*b*-98PS4.5k allowed precursor chelation for 120 hours (see Experimental Details). After in situ reduction, it was found that the degree of cluster formation and adjoined particles was greatly reduced for the latter two samples (**Figure 4.7**).

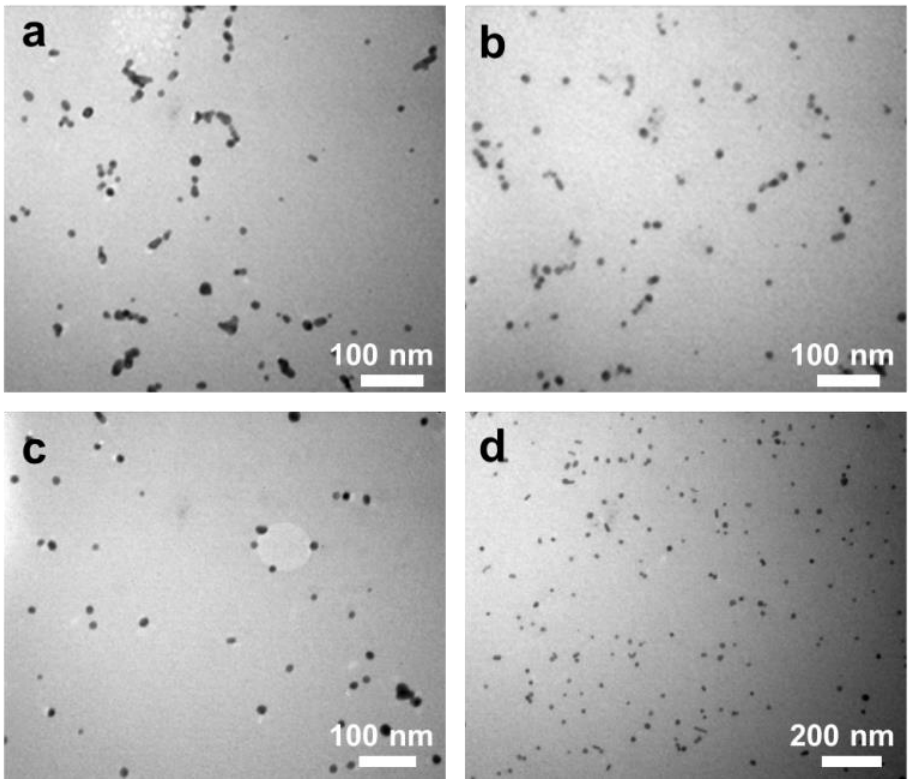

Figure 4.7 TEM images of Au nanoparticles templated by HPG9.3k-*b*-98PS4.5k under different conditions in optimal solvent (DMF only). (a) Au1@HPG9.3-*b*-98PS4.5k and (b) Au2@HPG9.3k-*b*-98PS4.5k were allowed 20 hours for precursor incorporation prior to in situ reduction to produce particles with satisfactory shape and size variation (D_{Au}=13.3±3.1 nm). (c) Au5@HPG9.3k-*b*-98PS4.5k and (d) Au6@HPG9.3-*b*-98PS4.5k were allowed 120 hours for precursor incorporation prior to in-situ reduction with a reduced size variation compared to first trials (D_{Au}=13.1±1.4 nm). Both Au5@HPG9.3k-*b*-98PS4.5k and Au6@HPG9.3-*b*-98PS4.5k successfully templated the formation of Au nanoparticles; however the longer incorporation time improved the shape quality and reduced the formation of clusters.

The overall size and shape of the PS-capped Au nanoparticles did not vary significantly between the four samples which were on the order of 13 nm in diameter. Successful precursor coordination and in-situ reduction is indirectly observed during the purification process of the resulting PS-capped Au nanoparticles via repeated precipitation, centrifugation and dissolution. During precipitation, only Au ions coordinated by the HPG core and subsequently reduced in-situ are integrated into the various HPG-*b*-PS templates. Thus during centrifugation, the particles that form outside the template settle to the bottom and are removed (**Figure 4.8**). This supports the presence of the Au ion-HPG core interaction.

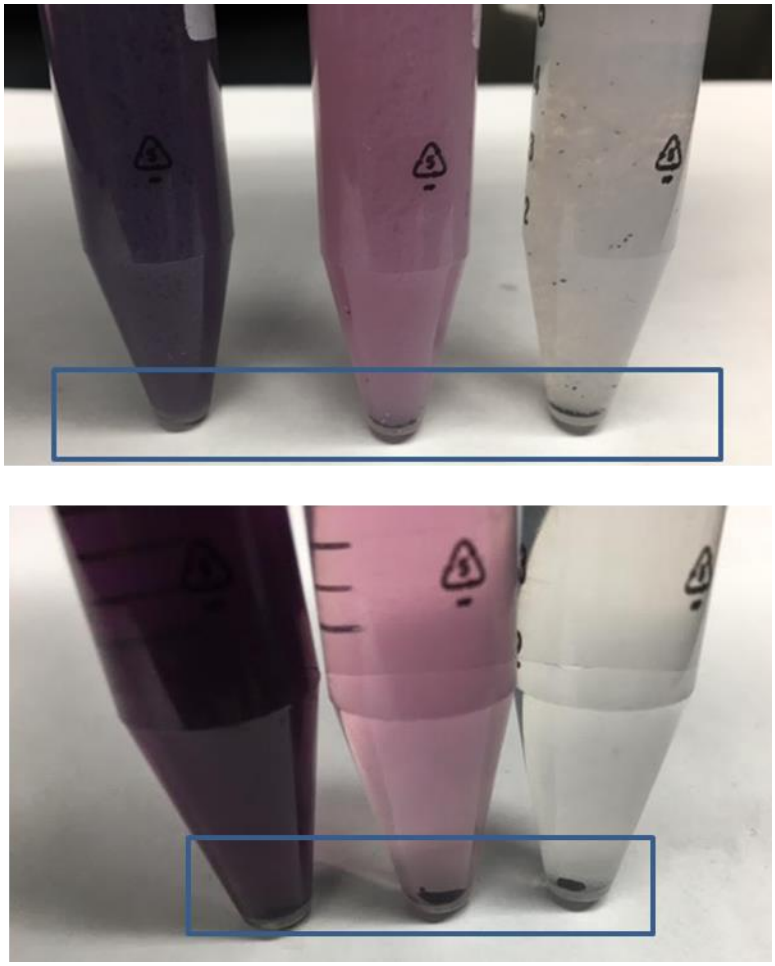

Figure 4.8 (Top) Precipitated PS-capped Au nanoparticles templated by various HPG-*b*-PS templates in (left) 9:1, (middle) 8:2 and (right) 6:4 DMF:BA. Note the color of the precipitate in the tubes indicating the presence of Au ions successfully coordinated and reduced as well as the agregated sediment (in blue rectangle) at the bottom of the tubes representing gold reduced outside the template which subsequently aggregates and settles to the bottom to be removed. (Bottom) PS-capped Au nanoparticles redissolved in THF solution. Note again the aggregated Au particles at the bottom of the tubes (in blue rectangle) which are not soluble in the THF solution

In addition to successful templating of individual Au nanoparticles, the resulting PS-capped Au nanoparticles showed excellent long-term stability in organic solvents with no observable sedimentation. These experiments were all performed in DMF. Prior to the addition of the reducer, the precursor ions were allowed to diffuse into the inner HPG template. The outer PS chains encapsulated the ions during the in-situ reduction and

prevented aggregation and sedimentation of the Au nanoparticle formed within the HPG-*b*-PS template. Additional verification of the formation of Au nanoparticles within the inner HPG core is supported by Raman and XRD experiments (**Figure 4.9** and **Figure 4.10**). Raman spectroscopy supported the formation of Au nanoparticles due to the presence of the characteristic PS signature in the PS-capped Au nanoparticles. XRD measurement showed the characteristic peaks of Au. The success rate for producing Au nanoparticles using the HPG9.3k-*b*-98PS4.5k template is high and the method for purification of the nanocomposites (i.e., PS-capped Au nanoparticles) relies on simple precipitation of the PS capping layer.

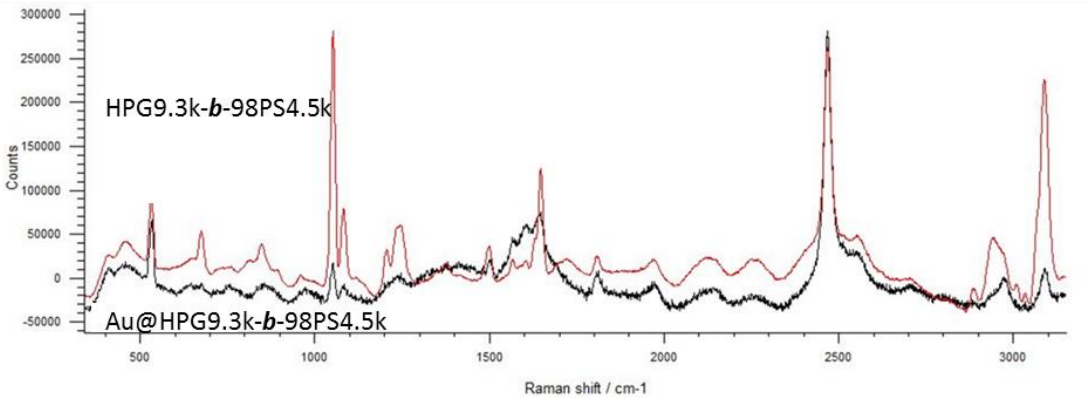

Figure 4.9 Raman spectra of the HPG9.3k-*b*-98PS4.5k template before precursor incorporation (top) and after it is used to template the formation of Au nanoparticles (bottom) in pure DMF. In both cases the characteristic peaks of PS are emerged which supports the role of the HPG-*b*-PS copolymer as a unimolecular template.

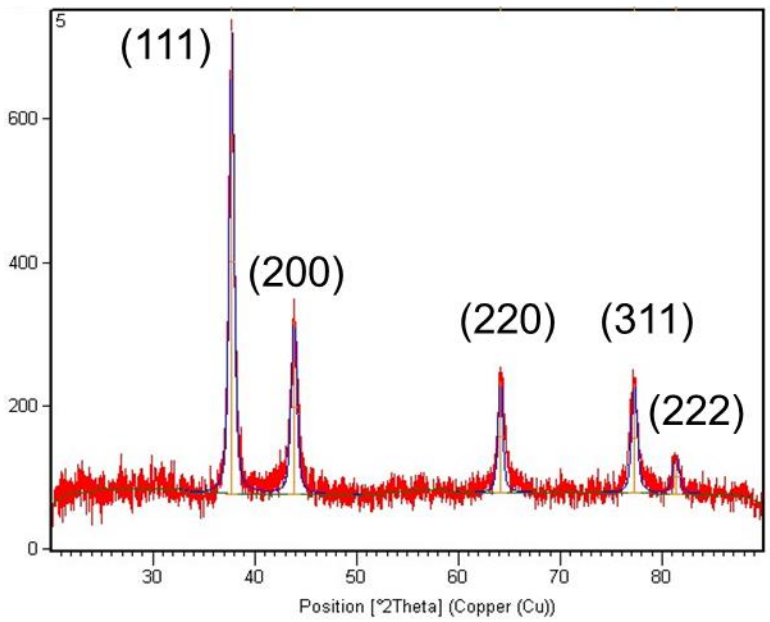

Figure 4.10 Representative powder X-ray diffraction spectrum for Au5@HPG9.3k-*b*-98PS4.5k showing the characteristic peak positions and intensities for Au. The broadening of the peaks is typical for nanoscale crystallographic features.

In order to further support the nature of HPG-*b*-PS copolymers as Au templates, an investigation into the effects of solvent type on templating was also undertaken. These experiments varied the solvent composition from 9:1 DMF:BA, a relatively good solvent mixture for PS, to 6:4 DMF:BA a relatively poor solvent mixture for PS. BA is a bad solvent for PS, the rationale is that the PS chains will collapse inward as the solvent composition worsens, thereby reducing the ability of the metal precursor ions and reducer to diffuse into the inner HPG core. The expected result then is a reduction in the degree of successful templating and/or quality of the resulting nanocomposites. **Figure 4.11** shows TEM images of the templated PS-capped Au nanoparticles under some of the solvent compositions investigated.

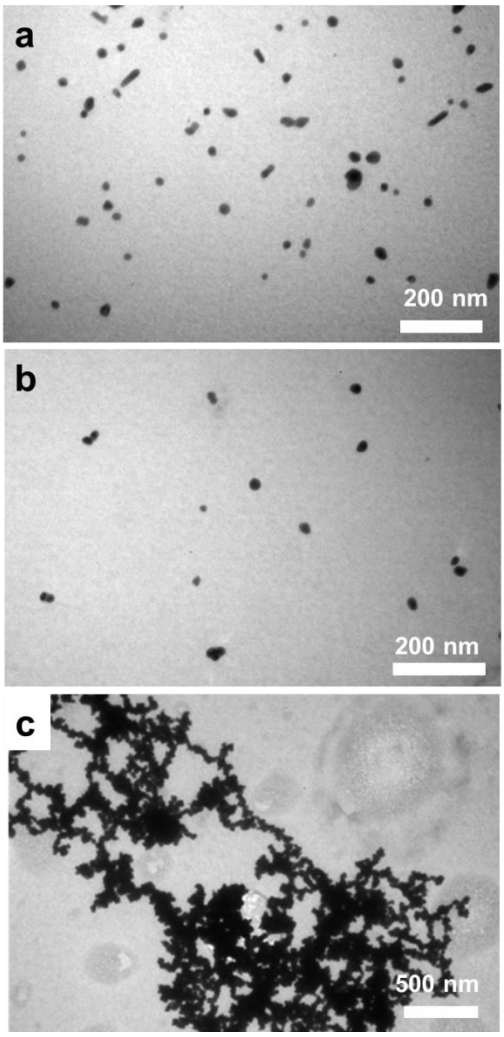

Figure 4.11 TEM images of PS-capped Au nanoparticles templated with HPG9.3k-*b*-98PS4.5k (i.e., HPG10 batch with PS polymerized for 150 minutes from the chain end of HPG) under different solvent conditions. (a) The solvent for Au9@HPG9.3k-*b*-98PS4.5k is 9:1 DMF:BA (v/v) and showed a large number of nanoparticles templated and a larger average particle diameter (D_{Au}=18.0±5.0 nm). (b) The solvent for Au10@HPG9.3k-*b*-98PS4.5k is 8:2 DMF:BA (v/v) and showed some particle templating but a reduced number due to the slightly collapsed PS chains outside of the HPG core and a larger average particle diameter (D_{Au}=20.6±6.4 nm). (c) For comparison, a control experiment was also performed with no template and demonstrated large-scale aggregation and sedimentation. Au11@HPG9.3k-*b*-98PS4.5k (6:4 DMF:BA) also aggregated and settled too quickly to create a TEM grid.

The particles templated in the best solvent mixture for PS (**Figure 4.11a**) resulted in aggregate-free and well-dispersed PS-capped Au nanoparticles on the order of 15 nm which retained the characteristic plasmonic Au peak around 520 nm (**Figure 4.12a**,(1)).

Nanoparticle templating in the intermediate solvent mixture (intermediate PS solubility) (**Figure 4.11b**) showed a reduction in the number of nucleated particles with a noticeable aggregate formation on the bottom of the vial (**Figure 4.12a**, (2)). Templating in the worst solvent mixture DMF:BA = 6:4 was completely ineffective and TEM was unable to be performed. The immediate large-scale aggregation and sedimentation resulted in a complete loss of nanoscale plasmonic properties as demonstrated by the complete disappearance of the characteristic plasmonic Au peak (**Figure 4.12a**, (3)). For comparison, a control experiment was performed in which no template or other surfactant was added (**Figure 4.11c**) to emphasize the importance of the HPG-*b*-PS template. Similar to templating in a bad solvent mixture (i.e., DMF:BA = 6:4), the control experiment also showed large-scale agglomeration and sedimentation. **Figure 4.12b** shows digital images of the PS-capped Au nanoparticles formed in solvent mixtures of different compositions. Notably, the stability of the PS-capped Au nanoparticles is clearly dependent on the solvent mixture conditions.

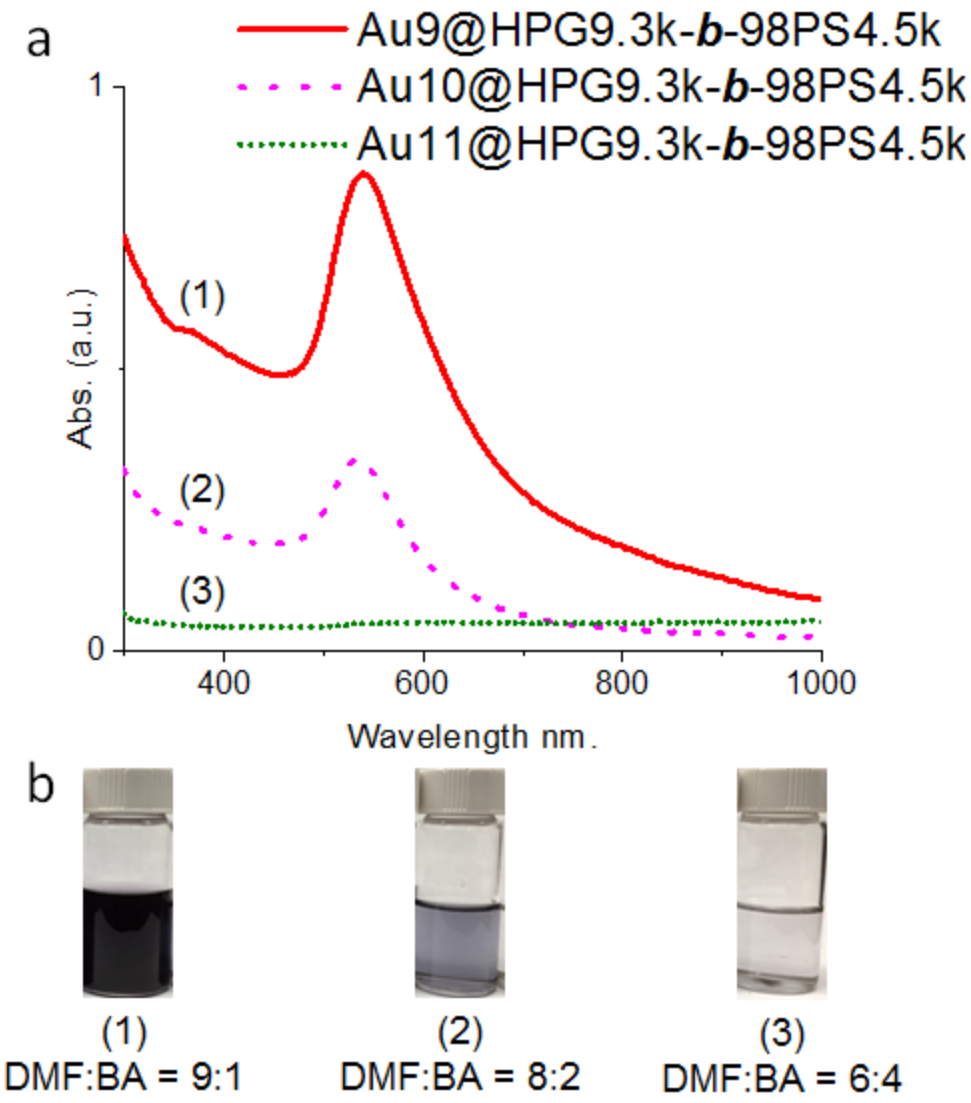

Figure 4.12 (a) Plasmonic absorption of PS-capped Au nanoparticles templated in the best solvent mixture for PS (i.e., Au9@HPG9.3k-*b*-98PS4.5k in DMF:BA = 9:1) showing good long-term solution stability; in intermediate solvent mixture for PS (i.e., Au10@HPG9.3k-*b*-98PS4.5k in DMF:BA = 8:2) showing some particle formation and some sedimentation over time; and in the worst solvent mixture for PS (Au11@HPG9.3k-*b*-98PS4.5k in DMF:BA = 6:4) showing no nanoparticle formation and a large-scale aggregation and sedimentation. (b) Digital images of the corresponding PS-capped Au nanoparticles showing their varied solution stability as a function of solvent mixture composition.

4.3.4 Effect of PS Chain Length on HPG-b-PS Templating of Au Nanoparticles

It is clear that the solvent composition has a pronounced effect on the success of templating by the HPG-*b*-PS copolymer. This supports the essential role of the PS capping layer during all stages of nanoparticle formation. With this understanding in mind, an initial investigation into the effects of the length and number of the PS chains was undertaken. Four different HPG-*b*-PS templates were studied and used to template Au in DMF. Two templates were derived from HPG10-Br with different lengths of PS chains and the two other templates were derived from HPG7-Br with different length of PS chains (**Figure 4.13**). The TEM images demonstrate that the PS chain length does have an effect on the success and quality of templated PS-capped Au nanoparticles. The details of the various PS chain lengths of HPG-*b*-PS templates employed can be found in **Table 4.4**. Au12@HPG9.3k-*b*-98PS7k (**Figure 4.13a**), Au13@HPG9.3k-*b*-98PS13.4k (**Figure 4.13b**) and Au15@HPG12.6k-*b*-117PS5k (**Figure 4.13d**) showed aggregate-free templating of Au nanoparticles as demonstrated by the distinct and separate nanoparticles observed. These three samples had PS chain molecular weights ranging from 4500 g/mol to 13,400 g/mol. Whereas Au14@HPG12.6k-*b*-117PS3.6k, which had PS chains with a molecular weight of 3600 g/mol, it demonstrated large-scale aggregation and sedimentation with no solution stability (**Figure 4.13c**). This difference between the samples lends support to the importance of the PS capping layer length in minimizing the aggregation and maximizing the separation between the resulting PS-capped Au nanoparticles during both formation and dissolution. This is not surprising as short PS chains (i.e., MW = 3600 g/mol) cannot form a compact layer on the surface of the inner HPG core. As a result, more precursors can diffuse into the space occupied by the inner

HPG resulting in the formation of network-like structures via continuous nucleation and growth of PS-capped colloidal Au nanoparticles.

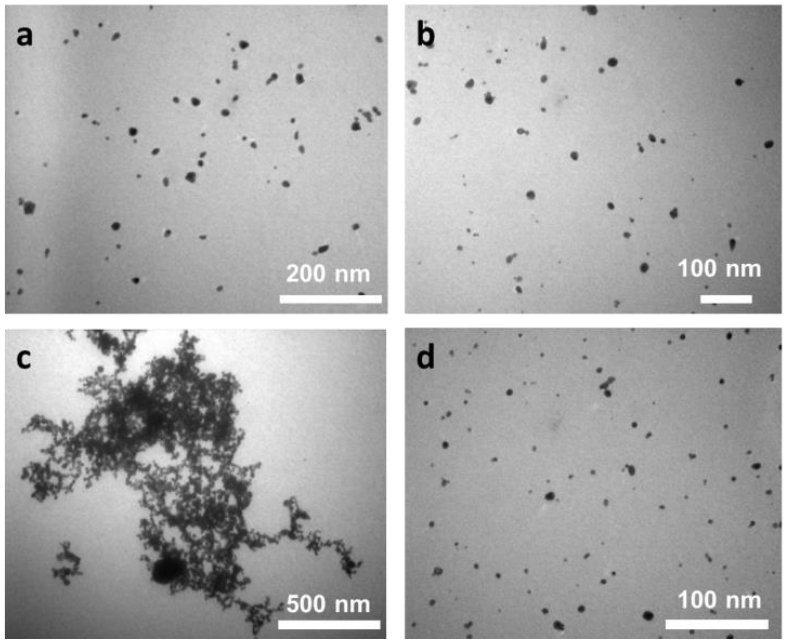

Figure 4.13 TEM images of Au nanoparticles templated by HPG-*b*-PS of different arm numbers and arm lengths. (a) Au@12HPG9.3k-*b*-98PS7k, HPG9.3k-*b*-98PS7k templated Au nanoparticles (D_{Au}=12.6±2.0 nm). (b) Au13@HPG9.3k-*b*-98PS13.4k, HPG9.3k-*b*-98PS13.4k templated Au nanoparticles (D_{Au}=12.9±1.8 nm). (c) Au14@HPG12.6k-*b*-117PS3.6k, HPG12.6k-*b*-117PS3.6k templated Au nanoparticles (aggregated). (d) Au15@HPG12.6k-*b*-117PS5k, HPG12.6k-*b*-117PS5k templated Au nanoparticles (D_{Au}=6.2±1.3 nm). It is notable that the micron-scale aggregation is present in Au14@HPG12.6k-*b*-117PS3.6k. All reactions were performed in pure DMF.

The effect of arm number on the success of templating appears to be of secondary importance to the lengths of the PS chains. It needs to be emphasized that the initiation efficiency of the PS chains could not be verified due to peak convolution in the ^{1}H NMR. However, it is typical to have high initiation efficiencies in these types of systems based on the reaction conditions. Therefore nothing definitive can be said about the effect of arm number. The relative importance of arm number will be the subject of future work.

The successful nanocomposite formation (defined as well-dispersed aggregate-free templated Au nanoparticles) can also be verified by UV-vis measurement and is consistent with the results observed in TEM (**Figure 4.14a**). Specifically, the samples that were well-dispersed showed the expected plasmonic Au peak around 520 nm, whereas the nanoparticles unsuccessfully templated by the short PS chain template produced no such peak and quickly settled out (**Figure 4.14b**).

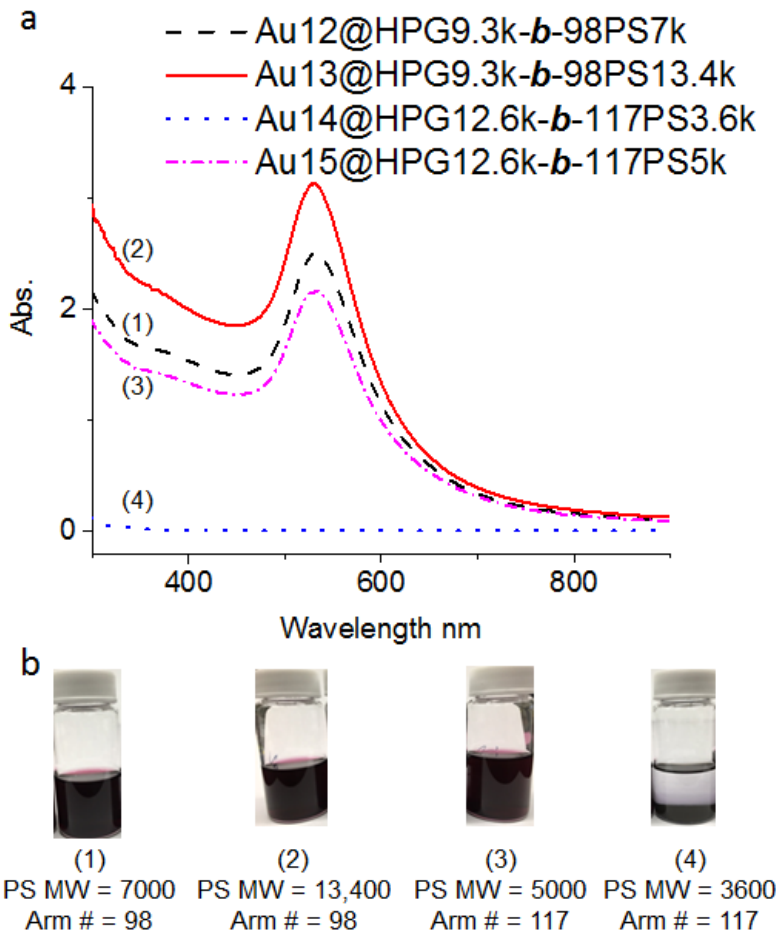

Figure 4.14 Plasmonic absorption of Au nanoparticles with varied PS arm lengths and arm numbers. Au12@HPG9.3k-*b*-98PS7k, Au13@HPG9.3k-*b*-98PS13.4k and Au15@HPG12.6k-*b*-117PS5k all showed characteristic plasmonic Au peaks indicating the successful formation of PS-capped Au nanoparticles with minimal aggregation. Au14@HPG12.6k-*b*-117PS3.6k, which had the shortest PS arm lengths (3600 g/mol),

was unable to template Au nanoparticles thus leading to aggregation and the absence of a plasmonic Au peak.

In addition to the spectroscopic and TEM data, it is immediately apparent from examining the solutions which trials were successful and unsuccessful. Since Au is a heavy material, it settles quickly unless stabilized by a ligand (i.e., CTAB) or long polymer chains. Consequently, particles that are not stabilized quickly aggregate and settle out. In this work, no conventional ligands of any kind were employed and stabilization is only possible when the Au particles are templated using the HPG-*b*-PS template herein devised with relatively long PS chains (MW $\geq$ 4,500 g/mol). The templating capabilities of HPG-*b*-PS star-like copolymer templates have also been extended to other inorganic systems including plasmonic/biocidal Ag nanoparticles (**Figure 4.15**) and superparamagnetic Fe_3O_4 nanoparticles (**Figure 4.16**). It should be noted that the conditions for templating these two materials require further optimization to produce more well-defined nanoparticles. But the results to date demonstrate the generalizability of HPG-*b*-PS templating to different functional nanoparticles. Also being a noble metal, Ag is templated in very much the same way as Au. To ensure minimum aggregation, the HPG9.3k-*b*-98PS13.4k template was used. The longer PS arms ensure separation of neighboring growing Ag nanoparticles. In the case of Ag, the nanoparticle formation occurs rapidly (less than 1 hour) and produces nanoparticles around 20 nm in diameter (**Figure 4.15a**).

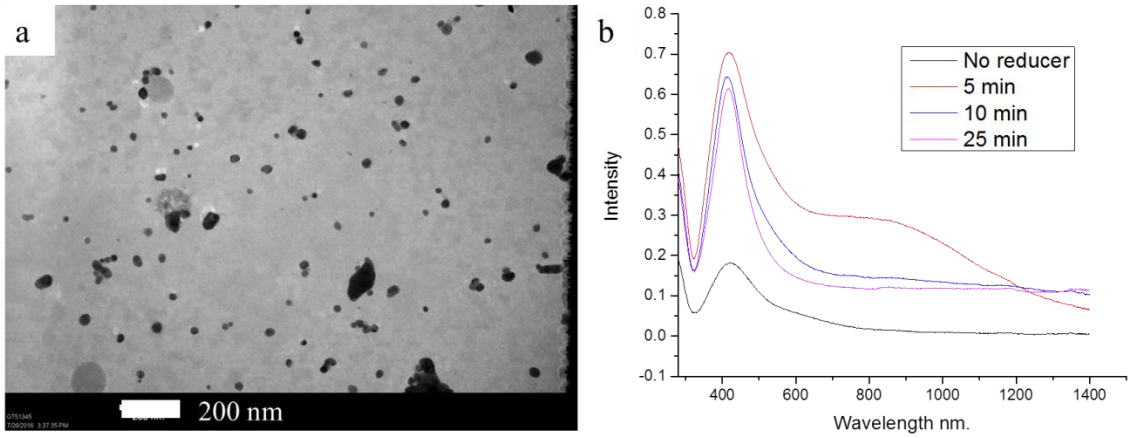

Figure 4.15 (a) Representative TEM of plasmonic Ag nanoparticles templated using HPG9.3k-*b*-98PS13.4k. (b) UV-vis spectra of templated Ag nanoparticles showing the formation of the characteristic plasmonic peak indicative of Ag around 450 nm.

The formation of Ag nanoparticles occurs very rapidly with full onset of plasmonic character is less than 1 hour. Longer reaction times lead to excessive aggregation of Ag formed outside of template and difficulty purifying the templated Ag nanoparticles (**Figure 4.15b**). The templating conditions for Ag nanoparticles can likely be further improved.

In addition to templating noble metals, HPG-based templates have also been investigated for templating useful metal oxide nanoparticles such as superparamagnetic iron oxide (Fe_3O_4). HPG9.3k-*b*-98PS13.4k was used to template Fe_3O_4 in a mild, low temperature process in contrast to the high temperature and pressure hydrothermal methods typically used. The templated particles are larger and less uniform than templated noble metal nanoparticles (**Figure 4.16a**) with diameters around 150-300 nm. The templated particles demonstrate the expected strong response to a magnetic field (**Figure 4.16b**). The right vial shows templated Fe_3O_4 nanoparticles strongly attracted to a magnet (right). For comparison, Fe_2O_3 nanoparticles are also shown. They are far less magnetic and are only weakly attracted to the magnet (left). Much more work is required

to extend the use of HPG-based star-like copolymers to templating other inorganic nanomaterials including metal oxides and metal chalcogenides.

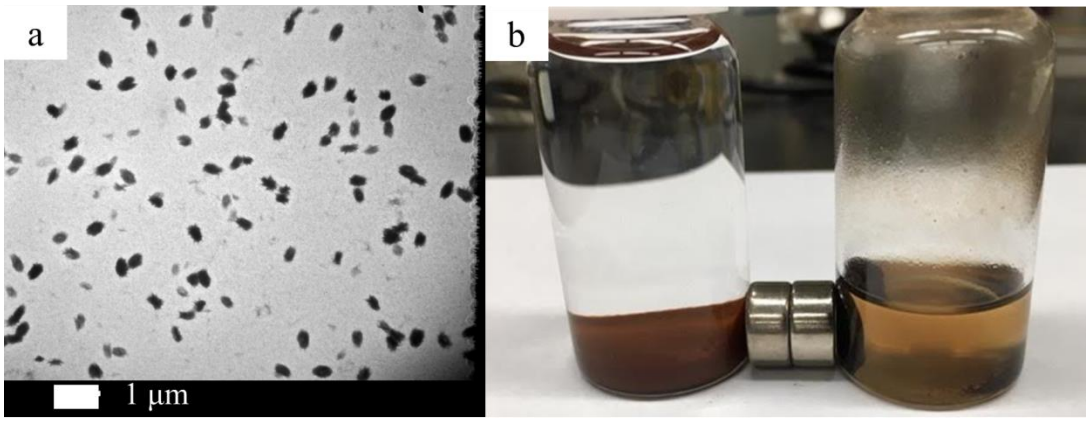

Figure 4.16 (a) TEM of Fe_3O_4 nanoparticles templated by HPG9.3k-*b*-98PS13.4k showing diameters of several hundred nanometers. (b) Photograph of Fe_2O_3 (left) and Fe_3O_4 (right) showing the strong response of superparamagnetic Fe_3O_4 to a magnet.

4.4 Conclusions

A lower-cost and ligand-free method of templating PS-capped colloidal Au nanoparticles capitalizing on rationally-designed unimolecular HPG-*b*-PS copolymers has been devised. The resulting PS-capped Au nanoparticles possessing Au cores below 50 nm in diameter demonstrated excellent solution stability in organic solvents. An investigation of the templating ability of HPG-*b*-PS copolymers was undertaken primarily by tuning the solvent composition and observing the spectroscopic and microscopy data of the resulting PS-capped Au nanoparticles. An initial investigation into the effect of PS arm length was also performed. It was found that the PS arms play an essential role in separating neighboring Au nanoparticles as well as encapsulating the

metal ions during nanoparticle formation. When the solvent quality was deliberately worsened, the PS arms were unable to function as intended and the resulting templating ability of the HPG-*b*-PS was reduced leading to the larger aggregates, sedimentation, and ultimate loss of nanoscale plasmonic properties. The chain length appears to impact the success of Au nanoparticle nucleation and growth. The effect of arm number is likely secondary to the length of the PS chains given that the number of PS arms for all templates investigated is quite large. This simple yet effective strategy for producing colloidal Au nanoparticles validates the use of polyether coordination as an effective approach in unimolecular polymeric templates. Furthermore, its generalizability has been demonstrated in the successful templating of Ag plasmonic nanoparticles and Fe_3O_4 superparamagnetic nanoparticles.

CHAPTER 5. A CLEAN AND SIMPLE ROUTE TO SOFT, BIOCOMPATIBLE NANOCAPSULES VIA UV-CROSSLINKABLE AZIDO-HYPERBRANCHED POLYGLYCEROL

This work was published in Macromolecules (J. Iocozzia and Z. Lin*, *Macromolecules*, **50**, 4906 (2017))

5.1 Background

The development of soft polymeric nanostructures has emerged as a promising approach for drug encapsulation and delivery[235, 236] as well as a passivation layer in hard-soft inorganic nanocomposites.[237] Owing to the wealth of different polymer types, polymerization techniques and post-polymerization chemistries, several strategies for translating polymers into nanostructures have been realized. Largely based on the self-assembly of linear block copolymers including poly(lactic acid), poly(ε-caprolactone), poly(lactic-co-glycolic acid), poly(N-acryloylamide) and poly(ethylene glycol), biocompatible liposomes,[238] vesicles,[239-241] spherical micelles,[238, 242] and cylindrical micelles[243-245] have been realized. However, the stability of micelles in terms of shelf life and against environmental changes such as temperature, pH, concentration, solution and ionicity remains a challenge.[246] One approach to addressing micellar stability involves crosslinking the shape through various means once self-assembled. Specific strategies include photo-crosslinking in nanoscale emulsions,[247-249] interfacial silica sol-gel formation,[250] and bifunctional covalent crosslinking.[251, 252] While these strategies do improve the environmental stability, they often suffer from poor size control, large size

dispersions and additional purification steps as precision control of the crosslinking density and emulsion particle sizes is challenging.

Some of these issues noted above have been addressed by using core templating strategies in which copolymers are organized around a surface and crosslinked with the core subsequently removed. The core is most often a rigid inorganic structure, such as Au[253, 254] and silica,[255] that is amenable to chemical ligation and simple etching strategies. The "core" can also be an inner polymeric block of the self-assembled structure that can be removed from the outer crosslinked polymer blocks[47] as well as preformed polymer spheres.[256, 257] In both templating approaches, the size and shape control of the core is more easily controlled through various established wet nanostructure synthesis procedures such as hot-injection,[258] sol-gel,[259] phase transfer/seeded-growth,[260, 261] mesoporous silica,[262] and hydrothermal/solvothermal processes.[263]

A third approach using unimolecular micelles aims to satisfy both the desire for stable, soft nanostructures with more well-defined shapes while also avoiding the use of templating strategies. This approach entails the formation of large globular unimolecular polymers produced by two main routes. The first utilizes multi-site initiators including low molecular weight polyols,[264, 265] polyester polyol dendrimers,[266] hyperbranched polyglycerols,[267] cyclic sugars (cyclodextrins)[20] and inorganic polyhedral oligomeric silsesquioxane (POSS).[268] The second utilizes multi-generation dendrimers including poly(ethylene imine),[269] poly(propylene imine),[270] and poly(amidoamine)[271] which can be subsequently modified. Among these effective unimolecular approaches, hyperbranched polyglycerol (HPG) is of particular interest.

HPG is a hyperbranched polyether polyol that possesses a large number of hydroxyl groups amenable to post-polymerization modification through various means. Only fairly recently has the molecular weight and polydispersity control of HPG been sufficiently improved to allow for systematic investigation into their properties by several approaches including optimized reaction conditions[85, 86, 95, 129, 272] and sequential polymerization[93] in the non-catalyzed ring opening multibranching polymerization (ROMBP) of epoxide-containing glycidol monomers. HPG is also particularly advantageous when applied in bio-related applications. Because of its excellent biocompatibility (neutral charge and minimal irritation, cytotoxicity and genotoxicity)[273] and drug uptake potential,[274, 275] HPG is ideal for applications related to drug delivery. Similarly, it is beneficial as an antifouling coating for use in the body as it does not bind to proteins or biological materials present in the body or within a cell[125, 276, 277] which when coated onto the surface of various inorganic nanostructures enables the introduction of additional treatment and imaging modes within living systems.[278-281] Owing to its unimolecular shape, biocompatibility, and high degree of functionality, HPG is an ideal candidate for developing soft crosslinked nanostructures. Previous work in this area has largely relied on crosslinking through diacrylate-functionalized HPG[282] with only a few reports describing enzymatic crosslinking.[283] Such chemical and biochemical approaches are fairly complex and require precise control of the chemical crosslinker or enzyme chemistry and often lead to large multi-molecular aggregates of poorly controlled shape. Herein, we report on the synthesis of novel crosslinked azido-hyperbranched polyglycerol nanocapsules through a combination of ROMBP, esterification, and UV-induced azide-azide homocoupling. Notably, the advantage of this strategy is that

azidation and crosslinking require no additional chemical crosslinker, and nanocapsule formation occurs quickly under mild conditions driven only by UV light with only N_2 gas as a byproduct.[284-286] The abundance of surface azide groups present in HPG enables coupling primarily between the nitrene intermediates to create intramolecular azo linkages in contrast to nitrene-double bond coupling to form reactive aziridines.[287] The synthesis of azido-hyperbranched polyglycerol and its subsequent formation into nanocapsules (15-25 nm diameters) is systematically monitored over the course of UV irradiation. This simple, three-step strategy for nanocapsule formation may provide a platform for many promising functionalized derivatives for applications in tailored drug encapsulation and delivery.

5.2 Experimental Details

5.2.1 Materials

4-bromomethylbenzoyl chloride (4BMBC, 98%), 1-methyl-2-pyrrolidone (NMP, 98%), glycidol (96%) were obtained from Sigma-Aldrich and used as received unless otherwise specified. NMP was stirred overnight with CaH_2 and distilled prior to use. Glycidol was vacuum distilled immediately before use. Sodium methoxide (NaOMe, 98%), 1,1,1-tris(hydroxymethyl)propane (TMP, 98%), sodium bicarbonate ($NaHCO_3$, 98%), magnesium sulfate ($MgSO_4$, 98%), sodium azide (NaN_3, 99%) and phosphotungstic acid (97%) were obtained from Alfa Aesar and used as received. Diethyl ether (solvent grade), dichloromethane (DCM, solvent grade), dimethylformamide (DMF, solvent grade), chloroform ($CHCl_3$, solvent grade), tetrahydrofuran (THF, solvent grade)

and toluene (solvent grade) were purchased from BDH and used as received unless otherwise specified. THF was dried by stirring overnight with sodium metal and naphthalene and distilled under vacuum prior to use. Bis(2-methoxyether) ether (diglyme, 98%) was purchased from Acros Organics.

5.2.2 Characterization

The absolute molecular weight of HPG was evaluated by ^{1}HNMR using a Varian VXR-400 Unity Innova spectrometer (400 MHz) with a quad probe from Nalorac. Time inversion recovery and inverse-gated carbon NMR (IG ^{13}CNMR) analyses were performed on the same instrument to determine the necessary scan times, degree of branching (DB) and structural breakdown of HPG. All sample concentrations were 10 mg/ml.

The gel permeation chromatography (GPC) analysis was performed on a Shimadzu system (CTO-20A column oven, LC-20A pump and RID-10A refractive index detector). The mobile phase was DMF stabilized with LiCl and calibrated against linear PEO standards. A Phenomenex linear column with mixed pore sizes (range 20-2×10^{6} g mol^{-1}) was used.

FT-IR spectroscopy measurement was performed on a Shimadzu IRTracer-100. Samples were dispersed in KBr discs.

Transmission electron microscopy (TEM) imaging was performed on a Jeol 100 CX-II (acceleration voltage 100 keV). Samples were drop cast on square mesh copper grids (CF-400) from Electron Microscopy Sciences and stained with phosphotungstic acid (0.2 wt. % aqueous solution).

5.2.3 Synthesis of Hyperbranched Polyglycerol (HPG)

HPG is polymerized through a ring opening multi-branching polymerization (ROMBP) of an epoxide-containing monomer (i.e., glycidol) slowly added to a reactor to minimize the cyclization and coupling of neighboring polymers. As the reaction proceeds, the viscosity of the polymer-containing solution increases rapidly. The ROMBP reactor setup is designed to minimize the impact of viscosity on the molecular weight and PDI control. In a general setup, an external power source was attached to a Teflon stirring rod and placed in a three-port flask in a thermostated oil bath. A syringe pump was attached to the second port charged with a 50/50 (v/v) of dried NMP and glycidol monomer and the third port for argon atmosphere supply. The main reactor was charged with TMP and KOMe basic initiator. The reactor was heated to 80 °C for 1 hr to drive off methanol formed during initiator formation. Benzene was then added and evaporated to remove any residual water. The initiator was then dissolved with NMP and diglyme and stirred at a set speed. Monomer was injected at a specific rate and left to react for a period of time. The crude product was then purified by precipitation dissolution three times in acetone and ethanol, respectively (HPG yield: 30%). IG ^{13}CNMR (DMSO-d_6) δ (ppm): 79.5-80.4 (L_{13}); 78-79 (D); 72-73 ($2L_{14}$); 70.4-71.4 (2D, 2T); 68-70 (L_{13}, L_{14}); 62-63.5 (T); 61-62.5 (L_{13}). ^{1}H NMR (DMSO-d_6) δ (ppm): 0.91 (s, 3H, TMP methyl group); 1.45 (s, 2H, —CH_2— group in TMP); 3.4-4.0 (m, 5H, backbone of pure HPG). Details of reaction conditions can be found in **Table 5.1**.

Table 5.1 Summary of reaction conditions for HPG10

Sample[a]	TMP(g)[b]	% (-H^+)[c]	M[d] (ml)	Base	Solvent	Sol. Vol. (ml)	Time (min)	T (°C)	Inj. Rate (ml/hr)
HPG10	0.12	10	12	KOMe[†]	Mix[e]	12	330	100	4.24

[a]Several other samples were also synthesized but were not included in this work. [b]Anhydrous 1,1,1-tris(hydroxymethyl)propane (TMP) initiator. [c]Degree of deprotonation of TMP. [d]Glycidol monomer volume. [e]Mix denotes a mixture of N-methyl-2-pyrrolidone (NMP) and diglyme (1:1 v/v ratio). [†]Potassium methylate powder.

5.2.4 Synthesis and Purification of Hyperbranched Polyglycerol-4-bromomethyl-benzoyl Ester (HPG-4BMBE)

The brominated HPG nanocapsule precursor is formed by esterification of the hydroxyl groups of HPG with the acid chloride unit of 4BMBC. In a typical reaction, 0.1 g of HPG10 (1.35 mmol –OH) was azeotropically dried with toluene (20 ml) to remove all water. HPG10 was dissolved in dry NMP (10 ml) and cooled in an ice bath (0 °C). Then 0.94 g of 4BMBC (3.38 mmol) dissolved in 6 ml dry NMP was added dropwise to the stirred HPG10 solution over 30-60 min in ice and allowed to react 24 hr at room temperature. The crude product was precipitated in diethyl ether and dissolved in DCM three times. Product was washed with $NaHCO_3$ (5 wt. % in DI water) three times, then pure DI water three times and dried over $MgSO_4$ for 12 hours. Product was filtered and dried overnight (60 °C) to produce a viscous brown liquid (yield: 95% for HPG-4BMBE). The 4BMBC was added in a 1:2.5 molar ratio of -OH:4BMBC. ^{1}H NMR ($CDCl_3$) δ (ppm): 3.2-4 (m, 5H, HPG backbone); 4.2-4.7 (s, 2H, —ph—CH_2—Br); 5.2-5.4, 5.45-5.6 (m, 6H, —RCOO—CH_2— and —CH_2—CH(—COOR)— and RCOO—CH_2—CH(—COOR)—CH_2— protons in HPG backbone near next to esterification sites).

5.2.5 Synthesis of Hyberbranched Polyglycerol-4-azidomethyl-benzoyl Ester (HPG-N_3-MBE)

In a small vial, 0.2 g of HPG-4BMBE (0.93 mmol) was dissolved in 6 ml of dry DMF. To this, 0.12 g of NaN_3 (1.86 mmol) dissolved in 7 ml of dry DMF was added. The mixture was allowed to react under vigorous stirring under ambient conditions for 72 hrs. It was then precipitated in water and, centrifuged and dissolved in DCM, washed with water in a separatory funnel, filtered and dried overnight (60 °C). FT-IR (cm^{-1}): 1050, (—C—O—C—); 1720, —COO—; 2100 (—N_3), which is the indirect evidence of azidation in ^1H NMR where the peak shift of the methylene protons adjacent to the bromine in HPG-4BMBE was seen. This peak shift is consistent with that observed for conversion of benzoyl bromide to benzyl azide.

5.2.6 UV-induced Azide Homocoupling of HPG-4-N_3-MBE

In a small vial, 2 mg HPG-4-N_3-MBE is dissolved in 3 ml of $CHCl_3$ and passed through a 0.45 μm syringe filter. Samples are then vigorously stirred at room temperature and subjected to UV light irradiation (λ = 254 nm) in an enclosed dark container for various times (i.e., no ambient visible light exposure) to generate reactive nitrene intermediates that subsequently couple together to form azo crosslinkers. Samples were then dried and dissolved in dry THF and cast on TEM grids to dry overnight. Samples were also stained with phosphotungstic acid (0.2 wt. % aqueous solution).

5.3 Results and Discussion

Figure 5.1 depicts the synthesis route to crosslinked HPG-4-N_3-MBE nanocapsules in three consecutive steps. The mild and simple reaction steps required are ideal from a safety and energy standpoint, making this route fairly practical and green.

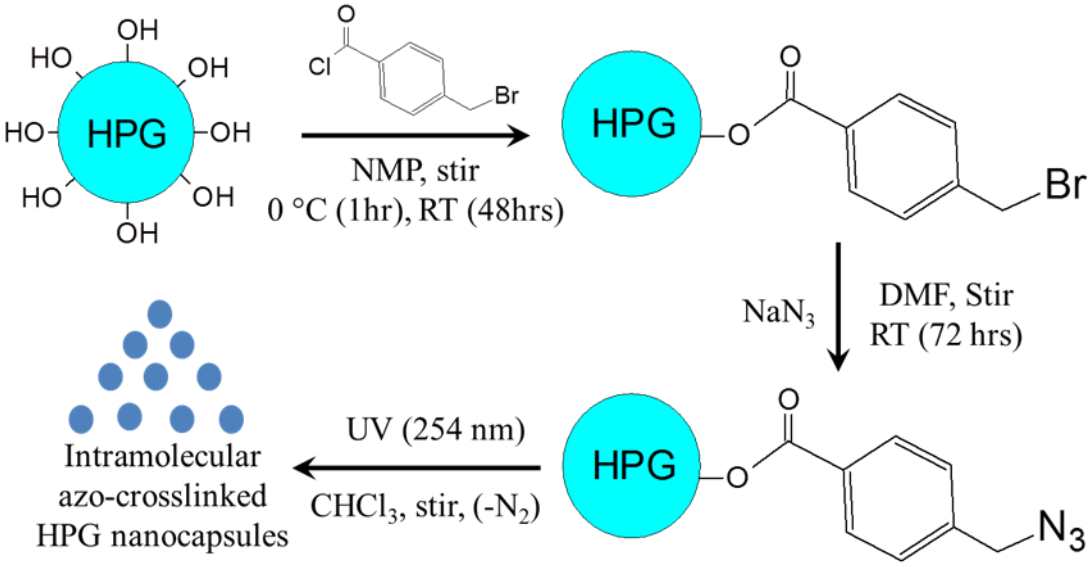

Figure 5.1 Synthesis of UV-crosslinked hyperbranched polyglycerol-4-N_3-methyl benzoyl ether (denoted HPG-4-N_3-MBE) nanocapsules. It is notable that the dilute regime is employed for UV crosslinking to maximize intramolecular azide-azide (i.e., nitrene-nitrene) homocoupling to form azo crosslinks.

5.3.1 HPG Synthesis, Bromination, and Azidation

Among several batches of HPG synthesized, HPG10 was chosen due to its fairly low PDI (1.38), intermediate molecular weight (M_n = 9.3 kg mol^{-1}) and sufficiently large number of hydroxyl groups (n_{OH} = 126 on average). This high degree of -OH and thus azide (N_3) functional groups is ideal for creating intramolecular crosslinks within individual molecules via azide-azide (i.e., nitrene-nitrene) homocoupling. Details of HPG synthesis, including molecular weight, degree of functionalization and structural

breakdown, are summarized in **Table 5.2**. Synthesis details and reaction conditions are summarized in **Table 5.1**.

The degree of polymerization (DP) and degree of branching (DB) were determined using **eqs 1** and **2** with the HPG molecular characterization summarized in **Table 5.2**:

$$DP = \frac{\left(\frac{A_d}{5} - 2A_{methyl}\right)}{\left(\frac{A_{methyl}}{3}\right)} \quad (1)$$

$$DB = \frac{2D}{2D + L_{13} + L_{14}} \quad (2)$$

where A_d is the area of the HPG backbone signal, A_{methyl} is the area of the methyl group from the TMP initiator, and D, L_{13}, and L_{14} are the areas of the peaks in the IG ^{13}CNMR HPG spectrum. Maximizing the dendritic (D) and terminal (T) units at the expense of linear units (L_{13}, L_{14}) is ideal as it raised the degree of branching, enabling a larger number of hydroxyl groups for the same molecular weight as well as a more spherical shape.

Acid halides (typically bromine and chlorine varieties) are advantageous for functionalizing polymers containing hydroxyl groups as they react irreversibly through the formation of HBr or HCl respectively. In this work, bifunctional 4-bromomethyl benzoyl chloride (4BMBC) contains an acid chloride end for attachment to HPG and a primary bromine in the para positon amenable to displacement by azide groups.

Functionalization of HPG with 4-bromomethyl benzoyl chloride (4BMBC) to yield HPG-4BMBE proceeded with high conversion to produce a highly esterified (i.e. brominated) product. HPG-4BMBE is the precursor polymer amenable to intramolecular azide homocoupling possessing a relatively hydrophilic HPG core and relatively hydrophilic crosslinked shell. This esterification is analogous to traditional ATRP functionalization with α-bromoisobutyryl bromide (BIBB) with the major difference being a tertiary bromine amenable to ATRP initiation rather than simple displacement. The high degree of esterification (98%) is attributed to the NMP solvent which served as both a solvent as well as a scavenger for HCl formed during reaction. The successful esterification was verified by ^{1}HNMR (**Figure 5.2**) and clearly shows attachment of the aromatic unit (7-8 ppm) as well as the characteristic methylene peak adjacent to the primary bromine (4.2-4.7 ppm).

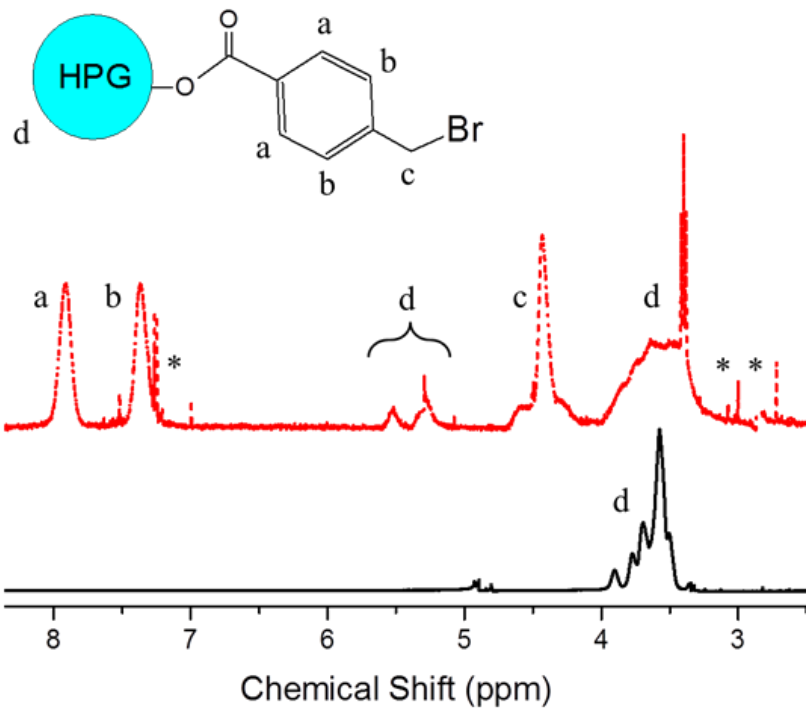

Figure 5.2 [1]HNMR spectra of HPG10 (bottom) and HPG-4BMBE (top) showing functionalization with primary bromine. Residual solvent peaks denoted by an asterisk (*). Inset shows the chemical structure of HPG-4BMBE.

The emergence of new peaks around 5.2-5.7 ppm can be attributed to the shift of HPG protons adjacent to the 4BMBE formation sites. A similar peak appearance is observed when HPG is functionalized with 4BIBB to act as an ATRP macroinitiator. The primary bromine is amenable to displacement by various species, including azide.

The degree of esterification (i.e., bromination) of HPG10 was calculated by **eq 3** based on the [1]HNMR peaks of HPG-4BMBE.

$$\% \, E = \frac{\left(\frac{A_c}{2}\right)}{\left(\frac{A_d}{5}\right)} \tag{3}$$

where A_c is the peak area of the methylene group in HPG-4BMBE, and A_d is the peak area of the HPG10 backbone.

It was found that the degree of esterification was nearly quantitative (98%). This is a necessary condition for having a large number of azide groups for intramolecular crosslinking. Azidation was also quantitative as evidenced by the complete peak shift of nearby proton signals in the formed HPG-4-N_3-MBE (**Figure 5.3**) in conjunction with the excess NaN_3 employed and long reaction time. Having a large number of azide groups is essential for the intramolecular crosslinking to proceed for two reasons: (1) a large number of crosslink sites gives the formed nanocapsules a more rigid shape that can survive through purification and imaging; and (2) a large number of azide groups promotes homocoupling of the azide intermediates (nitrenes) into stable azo crosslinkers rather than other coupling reactions including aziridine formation (nitrene addition to alkenes) which can further react though other pathways.[287, 288]

Table 5.2 Summary of characterization data for HPG10 and hyperbranched polyglycerol-4-bromomethyl benzoyl ester (HPG-4-BMBE)

Sample	$M_{n,\ HNMR}$[a] (g mol^{-1})	$M_{n,\ GPC}$[b] (g mol^{-1})	$M_{w,\ GPC}$[b] (g mol^{-1})	PDI	-OH[a]	D[c]	T[c]	L_{13}[c]	L_{14}[c]	DB[d]	%E[e]
HPG10	9300	7200	10000	1.38	126	23	34	18	25	52	98

[a]Determined by integrating the HPG backbone proton peaks and dividing by integrated initiator peak area using eq 1. [b]Mobile phase is DMF with 0.1 LiCl stabilizer and linear PEG standards. [c]HPG percent dendritic (D), terminal (T), linear type 1 (L_{13}) and linear type 2 (L_{14}) determined by integrating peaks in IG ^{13}CNMR. [d]Degree of branching (DB) is calculated from eq 2.[85] [e]Degree of esterification (i.e., bromination) via 4-bromomethyl benzoyl chloride (4BMBC) is calculated by eq 3.

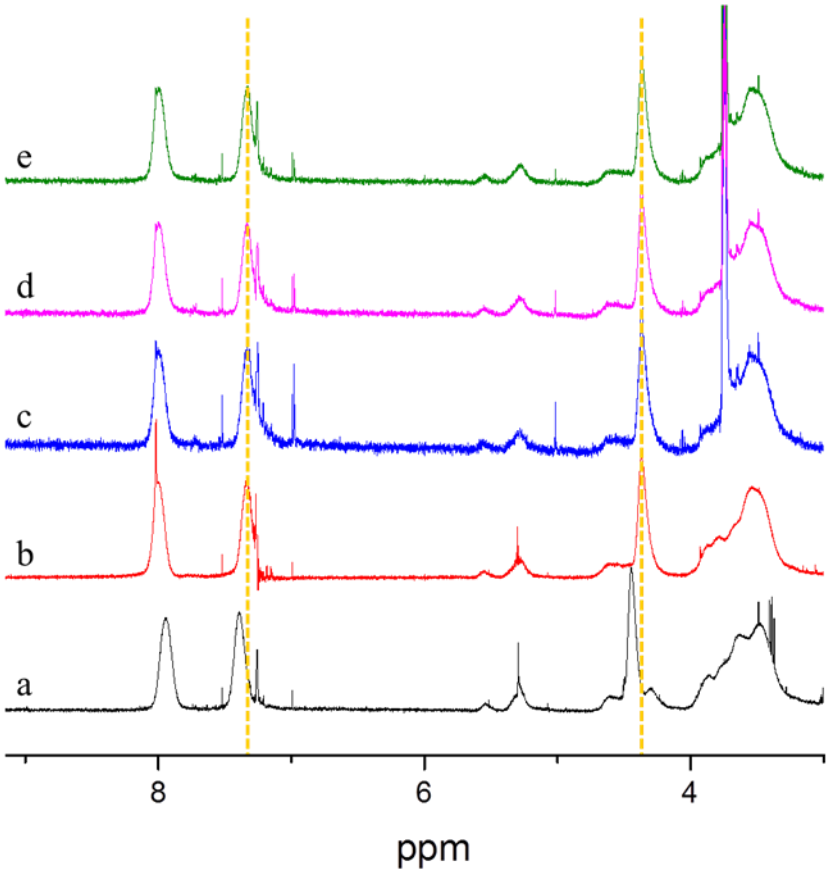

Figure 5.3 ^{1}HNMR plots of hyperbranched polyglycerol-4-bromomethyl benzoyl ester (HPG-4-BMBE) (a), hyperbranched polyglycerol-4-azidomethyl benzoyl ester (HPG-4-N_3-MBE) control (no UV irradiation) (b), and HPG-4-N_3-MBE after UV irradiation for (c) 20 min, (d) 40 min, and (e) 70 min. The slight peak shift suggests the successful azidation and the lack of new peak appearance in the aromatic region signifies nitrene-nitrene coupling as the primary crosslinking route.

5.3.2 UV-Induced Nanocapsule Formation

The primary reaction pathway for the formation of wholly-polymeric HPG-based nanocapsules is though nitrene homocoupling under UV irradiation. The reaction can be followed directly by FT-IR and TEM and indirectly by ^{1}HNMR studies. Since azide has a very distinctive FT-IR absorbance at around 2100 cm^{-1}, it was possible to track the disappearance of azide groups as they react to form azo crosslinks (**Figure 5.4**). Prior to azidation, there is no azide peak detected (**Figure 5.4a**). Nanocapsule formation occurs

over 70 minutes of UV irradiation and the intensity of the azide peak gradually reduces relative to the other unaffected peaks (**Figures 5.4c-4e**).

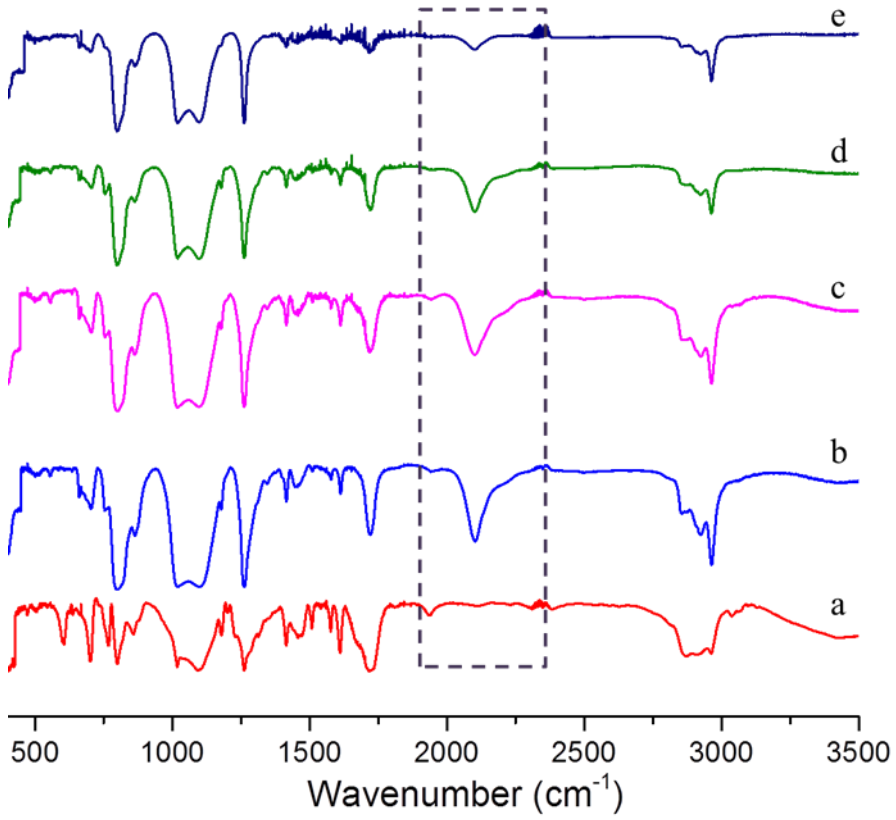

Figure 5.4 FT-IR spectra of HPG-4-N_3-MBE subjected to different UV irradiation times. (a) Hyperbranched polyglycerol-4-bromomethyl benzoyl ester (HPG-4-BMBE), (b) Hyperbranched polyglycerol-4-azidomethyl benzoyl ester (HPG-4-N_3-MBE) control (no UV), and HPG-4-N_3-MBE after UV irradiation for (c) 20 min, (d) 40 min, and (e) 70 min. The outlined region shows the appearance of the characteristic azide peak at 2100 cm^{-1} in HPG-4-N_3-MBE and its gradual disappearance with increasing UV irradiation times as homocoupling reactions occur.

The disappearance of the azide peak is direct evidence of the formation of azo crosslinks through a nitrene-nitrene coupling intermediate. The likely reason for a small remnant azide peak is that not all of the azides were able to couple in the fairly short irradiation time, thus leaving dangling groups.

Further indirect evidence of nanocapsule formation can be found in ^{1}HNMR spectra measured over the same series of irradiation times (**Figure 5.3**). Upon azidation, there is a small shift in the peak positions of the nearest protons (i.e., the methylene protons and aromatic protons of the 4-azidomethylbenzoyl unit). This peak shift is analogous to that observed in the azidation of benzyl bromide, and is consistent with what is expected of the slightly nucleophilic terminal nitrogen of the azide group. Longer irradiation times were not performed as local heating may destroy the formed nanocapsules and possibly lead to some intermolecular coupling. It was also clear that the nitrene-nitrene intermediate coupling was the dominant pathway for crosslinking as there are no additional peaks forming in the aromatic region. If aziridine crosslinking was present, there would be reaction between the phenyl groups of HPG-4-N_3-MBE and nitrene intermediates as well as the potential for additional side reactions through aziridine ring opening (**Figure 5.5**). However, this was not seen.

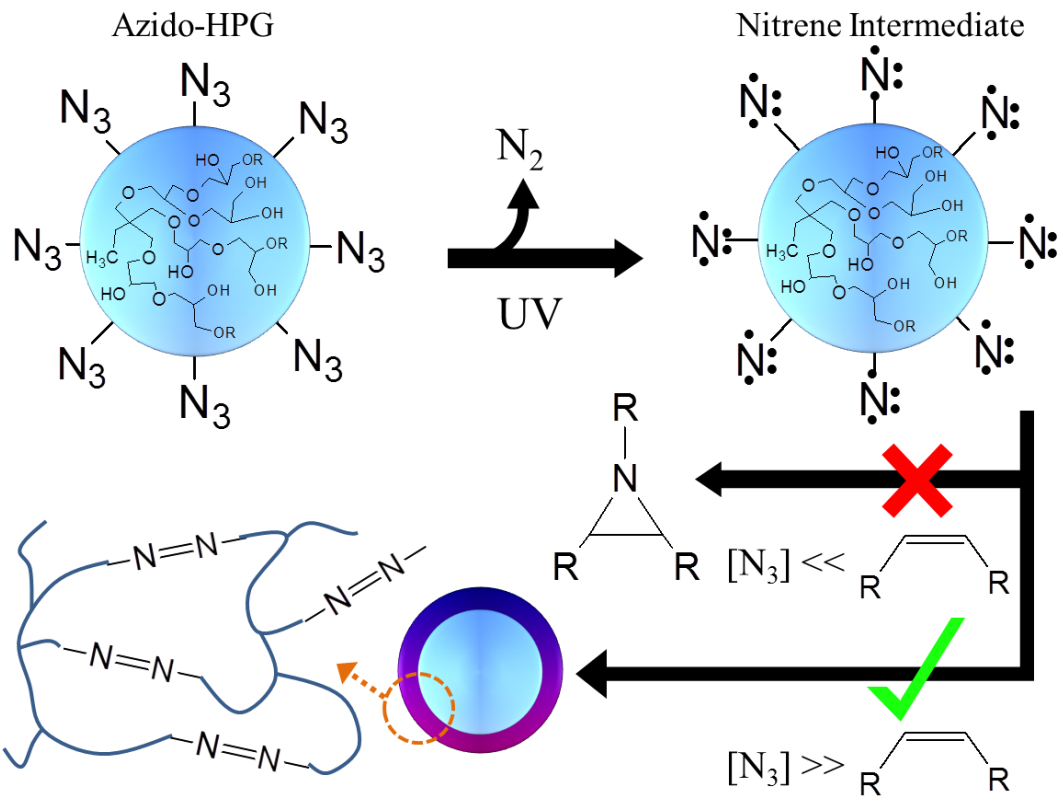

Figure 5.5 Schematic illustration of how azide groups are activated to highly reactive nitrene intermediates by UV irradiation with only gaseous nitrogen as a byproduct. By keeping the concentration of HPG-4-N_3-MBE low, mostly intramolecular nitrene-nitrene coupling occurs leading to soft wholly polymeric crosslinked HPG nanoparticles. By having an abundance of azide groups the formation of aziridine groups is suppressed. Aziridine groups can further react in additional undesirable side reactions.

Direct evidence of nanocapsule formation was also visualized by TEM. Over the course of UV irradiation, nanocapsule formation was clearly present and dominant (**Figure 5.6**). The diameter of the formed nanocapsules was approximately 20 nm with a fairly uniform spherical shape and with no large scale aggregation. There is no apparent change in size or overall shape of the formed nanocapsules between 20-min and 40-min UV irradiation. This further supports that intramolecular crosslinking is primarily occurring during this stage of the reaction (2 mg/ml). With longer irradiation times, larger multimolecular nanocapsules formed as a result of intermolecular crosslinking reactions

(**Figure 5.6c**). For comparison, a TEM control was performed in which HPG-4-N_3-MBE was drop-cast in the dark. As expected, no nanocapsule formation was observed for the control as there was no nitrene intermediate formation. This led to the formation of essentially large film-like regions of uncrosslinked HPG-4-N_3-MBE. The nanocapsules formed rapidly and remained stable in solution for several weeks.

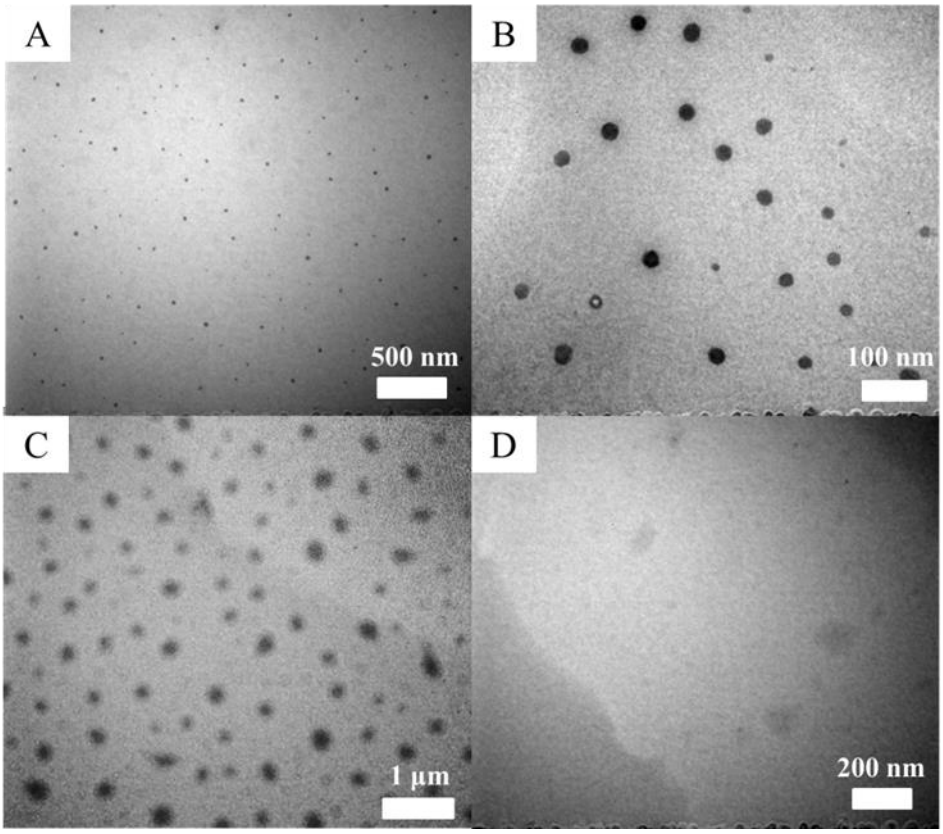

Figure 5.6 TEM images of HPG-4-N_3-MBE subjected to UV irradiation for different times: (a) 20 min, (b) 40 min, (c) 70 min, and (d) control (no UV irradiation). The formation of UV-crosslinked HPG-4-N_3-MBE nanocapsules is clearly evident with only a slight growth in nanocapsule size from 20 minutes to 40 minutes and a noticeable jump at 70 minutes due to the onset of intermolecular crosslinking. The control experiment validates the UV-mediated formation of nanocapsules as no nanocapsules were formed in the absence of UV.

5.4 Conclusions

A simple, clean, and green approach for crafting nanocapsules based on biocompatible hyperbranched polyglycerol (HPG) is described. This three step route to nanocapsules involves the polymerization of well-defined HPG, followed by its esterification with a bromine-containing acid halide (HPG-4BMBE) and subsequent azidation via bromine displacement to produce a new nanocapsule-forming material HPG-4-N_3-MBE. Unlike previous methods of wholly-polymeric nanocapsule synthesis, this approach offers a fast, mild, UV-crosslinkable strategy for forming inexpensive, biocompatible nanocapsules with diameters below 100 nm. When reacted in a dilute regime with brief irradiation times, intermolecular crosslinking can be suppressed. Our strategy requires minimal purification as it avoids the use of chemical crosslinkers and metallic catalysts with only gaseous nitrogen as the byproduct of nanocapsule formation. Taking full advantage of the abundance of azide groups present, the stability of nanocapsules is preserved via preferential intramolecular crosslinking through intermediate nitrene-nitrene coupling to produce azo linkages rather than aziridine linkages which may participate in additional ring-opening reactions. It is interesting to note that HPG-4BMBE may serve as an attractive starting material for creating other UV-crosslinkable nanocapsules for use in drug encapsulation/delivery, waste remediation and surface antifouling coatings.

CHAPTER 6. GENERAL CONCLUSIONS AND BROADER IMPACTS

6.1 General Conclusions

The rapid advancement of controlled living/radical polymerization has enabled the development of increasingly complex polymer architectures with well-defined molecular weight and PDI. When coupled with post polymerization modification strategies such as CuAAC click chemistry, it is possible to easily combine such polymer architectures with useful small molecule species as well as other previously incompatible polymeric materials and in so doing create highly functional materials using only a few robust and extremely useful chemical steps. In parallel with the well-known development of polymerization and coupling techniques highlighted above, the ability to produce HPG with higher molecular weights and lower PDIs has quietly advanced and made them far more useful as macroinitiators. Consequently, the aim of this work is to integrate these three ideas in order to generate useful polymer-based materials for the production of hard and soft nanocomposites by simple means.

In the first section of this dissertation, a combination of controlled living polymerization and CuAAC click chemistry are used to develop a novel promesogen-capped-21-β-CD-PAA star-like polymer. The resulting star-like polymer was found to be highly uniform. The click functionalization was verified by ^{1}HNMR, FT-IR, and Raman measurements and proceeded to near quantitative levels. In addition, the star-like PAA-CNBP demonstrated solubility in 5CB nematic liquid crystal host. Variation and optimization of key parameters including the molecular weight of the inner polymer blocks, the type of capping agent, and the length of the

capping agent may increase the solubility of the nanoparticles. Star-like PAA-CNBP can be employed as a template to produce NPs intimately and permanently connected with CNBP that enable improved solubility in the LC host. While the star-like PAA-CNBP successfully demonstrated the ability to template superparamagnetic iron oxide, the reliability remains low. This is due to the nature of the small molecule capping species that provide little protection against aggregation. The ability to harness the dynamism of the LC phase to deliberately and repeatedly control the arrangement of functional nanoscale materials (e.g., NPs, nanorods, etc.) is essential to finding applications in sensing, photonics and flexible electronics among others. The work in this section represents a starting point for many new and interesting liquid crystal-capped templates that enable doping into LC displays.

In the second section of this dissertation, well-defined polystyrene-capped HPG (HPG-*b*-PS) star-like copolymers are synthesized for use as inorganic nanoparticle templates using a combination of ROMBP and ATRP from a high functionality HPG core. The PS arm numbers varied from 98 to 117 with arm lengths from 3.6 kDa to 13.4 kDa. These star-like polymers successfully templated the growth of Au, Ag with diameters less than 100 nm; and Fe_3O_4 nanoparticles with diameters less than 300 nm. It was found that a critical PS arm length existed (around 4.5 kDa) above which the templated nanoparticles remain well dispersed and retain their nanoscale plasmonic properties and below which there is large scale aggregation and sedimentation. It was found that the PS arms play a key role in separating the templating nanoparticles during their formation and preventing their aggregation in the long term thus improving their

solubility and stability. This simple strategy can be readily extended to other functional nanomaterials with minimal modification of the template composition. It further validates the use of polyether coordination of inorganic precursors as a robust method of nanomaterial coordination.

In the third section of this dissertation, HPG is functionalized with bromine-containing small molecules (HPG-4BMBE) which are converted to azide groups by substitution to produce azide-capped HPG (HPG-4-N_3-MBE) in near quantitative yields. The azide moieties decorating the HPG surface are then crosslinked by UV irradiation under ambient conditions in solution yielding crosslinked nanoparticles requiring no post crosslink purification (N_2 gas is only byproduct). When crosslinking occurs in a dilute regime, it is possible to suppress large scale macromolecular crosslinking and aggregation. Additionally, the abundance of azide groups relative to unsaturated bonds promotes the formation of nonreactive azo crosslinks over reactive aziridine crosslinks conferring overall solution stability. Unlike previous methods of producing polymeric nanocapsules; this approach is fast, simple, and yields biocompatible nanostructures. The HPG-4BMBE polymer can serve as a useful starting point for an array of other crosslinkable materials either by UV or chemical methods with added functionalities. These wholly-polymeric nanoparticles have potential applications in drug encapsulation/delivery, water remediation and surface antifouling coatings.

6.2 Broader Impacts

The efforts detailed in this work offer new and interesting insights into the role of non-linear polymer architectures derived from high functionality polyols in the templating of a wide array of useful inorganic nanomaterials in a simple, low cost, and robust fashion. Furthermore, this work demonstrates the immense control that polymer template-based approaches can have on the properties of resultant hard and soft nanoparticles including solubility, absorption/emission, shape, and size. Ultimately the work presented herein strongly suggests the great potential and applicability of polyol-based polymer templating (specifically HPG and cylodextrins) in the areas of catalysis, drug encapsulation/delivery, surface antifouling, and display technology among many others.

In the first section of this dissertation, the aim was to develop a liquid-crystal like polymer material that could enable improved doping of inorganic species into liquid crystals used in display technology with the ultimate goal of reducing the energy consumption of LC displays. In an effort to realize such a material, promesogen-capped-21-β-CD-PAA star-like polymers were crafted and used to successfully template superparamagnetic Fe_3O_4 nanoparticles in which the promesogen units remained intimately and permanently anchored to their surface. The structural similarity of the promesogen capping species compared to liquid crystals used in displays afforded some improvement in the solubility. This work offers a highly generalizable and stable framework within which other inorganic species can be templated. Furthermore, by using a mix of capping species it is immediately possible to realize systems with mixed

promesogen capping layers of not only thermotropic but also lyotropic liquid crystal types for added functionality, solubility and assembly.

In the second section of this dissertation, HPG-*b*-PS star-like polymers are developed and used to template plasmonic Au and Ag nanoparticles as well as superparamagnetic Fe_3O_4 nanoparticles in solution. The resulting nanoparticles retained their desirable nanoscale properties and long term stability and solubility. In addition, this system can be easily modified to produce water soluble and multi-stimuli-responsive nanoparticles whereby conformation changes in the polymer capping shell can modulate the properties of the inner inorganic core. This work also investigated the impact of the polymer structure on its templating capability and demonstrated that there is a clear minimum requirement in polymer arm length necessary to stabilize particles of a given size and weight. Ultimately, this work serves as an attractive alternative to expensive cleanroom techniques, enabling a wide array of materials to be produce easily and in large quantities using a few templates. Inorganic nanomaterials templated in this fashion are attractive for film, spin coating and other layered processes encountered in photovoltaics, surface antifouling, and functional coatings.

In the third section of this dissertation, azide-functionalized HPG is developed and used to produce wholly polymeric, nanoparticles via UV light-induced crosslinking. This work demonstrates that it is possible to produce uniform, biocompatible, soft nanoparticles possessing stable structures both simply and cleanly (requiring no purification after formation) without the need for tedious self-assembly or sacrificial hard templates. This work can be immediately extended to produce stimuli responsive

nanomaterials for use as responsive drug carriers as well as potable water treatment materials.

Looking forward, the future of work in the area of polymer-based strategies for templating and directing the formation of both inorganic and organic structures is very promising. This is due in large part to the significant development in the types of robust chemistries available that enable the formation of new and more complex polymer architectures.

First, the emergence of more advanced controlled living/radical polymerization techniques based on ATRP and RAFT will enable a greater variety of functional monomers containing latent or overt reactivity in their pendant groups to be polymerized. These new polymers could respond to external stimuli via conformation changes, bond scission or bond rearrangement both reversibly and irreversibly.

Second, the ease with which click moieties can now be incorporated into different chemistries (via CuAAC, metal-free strained cyclooctyne, thiol-ene and Diels-Alder among others) will enable the synthesis of amphiphilic and multifunctional units within polymers such as biological and fluorescent tags, charged species, and initiator sites for additional polymerization. Click-based strategies have also enabled separate and disparate macromolecular structures to be combined which previously could not be easily produced if at all.

Third, in conjunction with the two advancements above, new and complex monomers and macromonomers will also be crafted which once polymerized can directly produce amphiphilic polymer architectures. In such a way, it will be possible to produce

polymers possessing not only multiple functionalities but also spatially controlled functionalities.

The emergence of many robust and generalizable polymerization techniques, complex monomer units, and simple post polymerization modification strategies will enable the production of more complicated structures. For example, in addition to single component particles and rods, it will be possible to produce multicomponent particles and rods and combine these more fundamental structures in more complex hierarchical structures with more interesting nanoscale properties. A particularly promising area to look forward to is the emergence of templated, well-defined metal oxide nanomaterials produced by autoclave-free techniques. The connectivity of such templated structures will also be controllable and responsive to environmental triggers depending on the types of polymers used in templating and connecting the fundamental units.

It is important to emphasize that many of the materials described above can already be made. The innovation is the ease with which similar and new polymer architectures can now be made using more recently developed chemistries thus making them that much more accessible to researchers and industry soon thereafter. The work presented in this dissertation aims to highlight and emphasize the potential and broad applicability of these emerging chemistries in both hard and soft nanomaterials development.

DISSEMINATION OF WORK

This work has been disseminated to the broader researcher community in the following publications and presentation.

Publications

(1) **J. Iocozzia**, Z. Lin*, "A Clean and simple route to soft, biocompatible nanocapsules via UV-crosslinkable azido-hyperbranched polyglycerol," ***Macromolecules***, 2017, 50, 4906-4912.

(2) **J. Iocozzia**, Z. Lin*, "Solution-stable gold nanoparticles via surfactant-free, hyperbranched polyglycerol-*b*-polystyrene unimolecular templates," ***Langmuir***, 2016, 32, 7180-7188.

(3) **J. Iocozzia**, H. Xu, X. Pang, H. Xia, T. Bunning, T. White, Z. Lin*, "Star-like polymer click-functionalized with small capping molecules: an initial investigation into properties and improving solubility in liquid crystals," ***RSC Advances***, 2014, 4, 50212-50219.

(4) Co-first author-J. Mao, **J. Iocozzia**, J. Huang, K. Meng, Y. Lai,* Z. Lin*. "Graphene aerogels for efficient energy storage and conversion," ***Energy & Environmental Science***, 2018, 11, 772.

(5) **J. Iocozzia**, Z. Lin*, "Crafting Multidimensional Nanocomposites: Functional Materials for Applications in Energy Conversion, Energy Storage and Optoelectronics" in the book titled "Nanotechnology: Delivering the Promise," ***ACS Symposia Book Series***, Vol.2, 2016.

(6) **J. Iocozzia**, Z. Lin*, Chapter contribution in "Hybrid Nanocrystal Architectures: Synthesis, Properties, and Applications"—"Semiconductor-Semiconductor and Semiconductor-Metal NCSs (synthesis, characterization and properties)." ***Imperial College Press/World Scientific*** (in press).

(7) **J. Iocozzia**, B. Li, Z. Lin*, "Directing Convection to Pattern Thin Polymer Films: Coffee Rings" in book "Instability-Based Methods for Patterning Polymer Surfaces"—"Directing Convection to Pattern Thin Polymer Films: Coffee Rings." ***Springer Ed.*** (USA), 2015.

(8) X. Li, **J. Iocozzia**, Y. Chen, S. Zhao, X. Cui, W. Wang, H. Yu, S. Lin, Z. Lin*, "From precision synthesis of block copolymers to properties and applications of nanoparticles," ***Angew. Chem. Int. Ed.*** 2018, 2046-2070.

(9) X. Liu, **J. Iocozzia**, Z. Lin*, "Noble Metal—Metal Oxide Nanohybrids with Tailored Nanostructures for Efficient Solar Energy Conversion, Photocatalysis and Environmental Remediation," ***Energy and Environmental Science***, 2017, 10, 402-434.

(10) Y. He, **J. Iocozzia**, Z. Lin*, "Magnetoelectric effect in single-phase multiferroic materials" in book titled "Nano/Micro-Structured Materials for Energy and Biomedical Applictions," ***Springer***, 2017, USA.

(11) M. Wang, **J. Iocozzia**, L. Sun, C. Lin, Z.Lin*, "Inorganic-modified semiconductor TiO2 nanotube arrays for photocatalysis," ***Energy and Environmental Science***, 2014, 7, 2182-2202.

(12) X. Hong, Q. Liu, **J. Iocozzia**, C. Gong, L. Kong, X. Liu, M. Ye*, Z. Lin*. "Needle-leaf-like $Cu_2Mo_6S_8$ Films for Highly Efficient Visible Light Photocatalysis," ***Part. Part. Sys. Char.***, 2018, 35, 1700302-1700308.

(13) M. Ye, Q. Lin, **J. Iocozzia**, X. Hong, X. Liu, Z. Lin, "Polycomponent Electro-Catalysts for Iodine-Mediated Dye-Sensitized Solar Cells," in book titled "Counter Electrodes for Dye-Sensitized and Perovskite Solar Cells," ***Wiley-VCH***, (Germany) 2018.

(14) M. Wang, M. Ye, **J. Iocozzia**, Z. Lin*, Chapter contribution in "Hydrogen Production Technologies"—"Photocatalytic Hydrogen Generation Enabled by Nanostructured TiO_2 Materials," ***Scrivener Publishing LLC***, USA, 2017.

(15) M. Ge, J. Cai, **J. Iocozzia**, C. Cao, J. Huang, X. Zhang, J. Shen, S. Wang, S. Zhang, K. Zhang, Y. Lai*, Z. Lin*, "A review of TiO_2 nanostructured catalysts for sustainable H_2 generation," ***International Journal of Hydrogen Energy***, 2017, 42, 8418-8449.

(16) P. Ye, X. Liu, **J. Iocozzia**, Y. Yuan*, L. Gu, G. Xu, Z. Lin*, "Highly stable non-noble metal Ni_2P co-catalyst for increased H_2 generation by g-C_3N_4 under visible light radiation," ***Journal of Materials Chemistry A***, 2017, 5, 8493-8498.

(17) S. Wu*, C. Han, **J. Iocozzia**, M. Lu, R. Xu, Z. Lin*, "Germanium-Based Nanomaterials for Rechargeable Batteries," ***Angewandte Chemie International Edition***, 2016, 55, 7898-7922.

(18) M. Wang, M. Ye, **J. Iocozzia**, C. Lin*, Z. Lin*, "Plasmon-mediated solar-to-chemical energy conversion via photocatalysis in noble metal/semiconductor composites," ***Advanced Science***, 2016, 3, 1600024.

(19) M. Ye, X. Liu, **J. Iocozzia**, X.G. Liu, Z. Lin*, "Nanostructured materials for high efficiency perovskite solar cells," ***Springer Ed.***, USA, 2016.

(20) X. Meng, C. Yu*, X. Song, **J. Iocozzia**, J. Hong, B. Lu, M. Rager, L. Huang, Z. Lin*, J. Oiu*, "Scrutinizing Defects and Defect Density of Selenium-Doped Graphene for High-Efficiency Triiodide Reduction in Dye-Sensitized Solar Cells," ***Angew. Chem. Int. Ed.***, 2018, DOI: 10.1002/ange.201801337.

(21) Y. Yuan*, W. Xu, P. Ye, **J. Iocozzia**, Z. Lin*, "A general and rapid approach to crystalline metal sulfide nanoparticles for photocatalytic H_2 generation," ***J. Mat. Chem. A***, 2017, 5, 21669.

(22) J. Cai, J. Huang, M. Ge, **J. Iocozzia**, Z. Lin*, K. Zhang, Y. Lai*, "Immobilization of Pt nanoparticles via rapid and reusable electropolymerization of dopamine on TiO_2 nanotube arrays for reversible SERS substrates and non-enzymatic glucose sensors," ***Small***, 2017, 13, 1604240.

(23) R. Liu*, W. Su, C. Shen, **J. Iocozzia**, N. Zhang, C. Wang, Z. Lin*, "Hydrothermal synthesis of hollow SnO_2 spheres with excellent electrochemical performance for anodes in lithium ion batteries," ***Materials Research Bulletin***, 2017, 96, 443-448.

(24) M. Ye*, C. He, X. Hong, **J. Iocozzia**, X. Liu, Z. Lin*, "Recent advances in interfacial engineering of perovskite solar cells," ***J. Phys D: Appl. Phys.***, 2017, 50, 373002-373018.

(25) Y. Yang, C. Han, B. Jiang, **J. Iocozzia**, D. Shi, T. Jiang, Z. Lin*, "Graphene-based materials with tailored nanostructures for energy conversion and storage," ***Materials Science and Engineering-R: Reports***, 2016, 102, 1-72.

(26) S. Wu, R. Xu, M. Lu, R. Ge, **J. Iocozzia**, C. Han, B. Jiang, Z. Lin*, "Graphene-Containing Nanomaterials for Lithium-Ion batteries," ***Advanced Functional Materials***, 2015, 5, 1-40.

(27) M. Ye, X. Wen, M. Wang, **J. Iocozzia**, N. Zhang, C. Lin*, Z. Lin*, "Recent Advances in Dye-Sensitized Solar Cells: From Photoanodes, sensitizers and electrolytes to counter electrodes," ***Materials Today***, 2015, 18, 155.

(28) M. Ye, M. Lv, C. Chen, **J. Iocozzia**. "Design, Fabrication and Modification of Cost-Effective Nanostructured TiO_2 for Solar Energy Applications" in the book titled 'Low-cost Nanomaterials: Toward Greener and More Efficient Energy Applications. Vol. 6. Editors Lin, Wang, ***Springer-Verlag*** (London), 2014. ISBN: 978-1-4471-6472-2.

(29) X. Pang, Y. He, B. Jiang, **J. Iocozzia**, L. Zhao, H. Guo, J. Liu, M. Akinc, X. Tan, N. Bowler, Z. Lin*, "Block Copolymer/ferroelectric nanoparticle nanocomposites," ***Nanoscale***, 2013, 5, 8695-8702.

Presentations

(1) **J. Iocozzia**, Z. Lin*, "Static and stimuli responsive polymer nanogels derived from hyperbranched polyglycerols (HPG): a simple approach for material encapsulation and delivery," Materials Research Society Fall National Meeting Biomaterials Division, Boston, 2017.

(2) **J. Iocozzia**, Z. Lin *, "Synthesizing hyperbranched polyglycerol (HPG) derivatives for use in templating hard inorganic nanostructures, biocompatible nanoparticles and structure-preserving binder materials," American Chemical Society Spring National Meeting POLY Division, San Francisco, 2017.

(3) **J. Iocozzia**, Z. Lin*, "Synthesizing hyperbranched polyglycerol (HPG) derivatives for use in templating hard inorganic nanostructures and stimuli-responsive biocompatible nanoparticles," Southeast Polymer Forum, Macromolecules Innovation Institute, Virginia Tech, Blacksburg, VA, 2017.

(4) **J. Iocozzia**, Z. Lin*, "Synthesis and characterization of hard and soft nanocomposites derived from β-cyclodextrin (β-CD) and hyperbranched polyglycerol (HPG) templates," American Chemical Society Spring National Meeting POLY division, San Diego, 2016.

(5) **J. Iocozzia**, "High functionality polyols for inorganic templating," Kyoto University (Katsura Campus) Japan, 2014.

Awards

National Defense Science and Engineering Graduate Fellowship (NDSEG)
Science and Technology of Advanced Materials and Interfaces Fellowship (STAMI)
NSF East Asian and Pacific Summer Institutes Fellow (NSF-EAPSI)
Graduate Student Presidential Fellow
Bio-nano—enabled Inorganic/Organic Nanostructures and Improved Cognition Fellow
Career, Research and Innovation Development Conference Award (CRIDC)
John Wiley Book Award

APPENDIX A: LETTERS OF PERMISSION

Thesis Figure	License Number	Content Publisher	Publication
1.1	4331470351219	Elsevier	Progress in Polymer Science
1.2a,1.3c	4331471038064	Springer Nature	Nature Nanotechnology
1.2b	4331471402475	Royal Society of Chemistry	Journal of Materials Chemistry
1.2c, d	4336130693658	Elsevier	European Polymer Journal
1.2g	4336131423067	Wiley	Journal of Applied Polymer Science
1.2h	4336140090796	Wiley	Macromolecular Chemistry and Physics
1.2i	4336140247212	Elsevier	European Polymer Journal
1.3a	4331480848292	Wiley	Angewandte Chemie Int. Edition
1.5	4331481172799	Wiley	Macromolecular Chemistry and Physics
1.6	4331490000072	Wiley	Angewandte Chemie Int. Edition
1.7	4331490248636	Royal Society of Chemistry	Nanoscale
1.8b	4331490674364	Springer Nature	The AAPS Journal
1.9	4331491150267	Royal Society of Chemistry	Nanoscale
1.10, 1.11	4331491424791	Wiley	Journal of Polymer Science Part A: Polymer Chemistry
1.13b	4331510655613	Wiley	Journal of Applied Polymer Science
1.13c	4331511153638	Royal Society of Chemistry	Chemical Communications
1.13d	4331511362433	Cambridge University Press	Journal of Materials Research
1.15 (bottom)	4331520165773	The American Association for the Advancement of Science	Science
1.16	4331520818951	Wiley	Journal of Polymer Science Part A: Polymer Chemistry
1.19	4331521103282	Wiley	Macromolecular Symposia
1.24	4331530065223	Elsevier	Progress in Polymer Science
1.27	4331531085568	Royal Society of Chemistry	Chemical Society Reviews
1.28	4331540350361	Royal Society of Chemistry	Chemical Society Reviews

Figure 1.2e

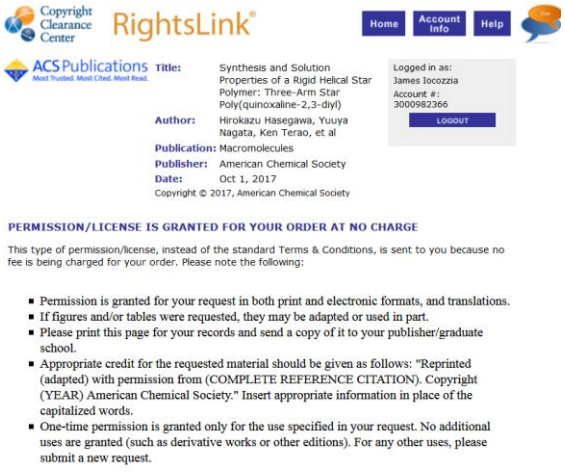

Copyright Clearance Center RightsLink®

Home | Account Info | Help

ACS Publications Most Trusted. Most Cited. Most Read.

Title: Synthesis and Solution Properties of a Rigid Helical Star Polymer: Three-Arm Star Poly(quinoxaline-2,3-diyl)

Author: Hirokazu Hasegawa, Yuuya Nagata, Ken Terao, et al

Publication: Macromolecules

Publisher: American Chemical Society

Date: Oct 1, 2017

Copyright © 2017, American Chemical Society

Logged in as: James Iocozzia
Account #: 3000982366
LOGOUT

PERMISSION/LICENSE IS GRANTED FOR YOUR ORDER AT NO CHARGE

This type of permission/license, instead of the standard Terms & Conditions, is sent to you because no fee is being charged for your order. Please note the following:

- Permission is granted for your request in both print and electronic formats, and translations.
- If figures and/or tables were requested, they may be adapted or used in part.
- Please print this page for your records and send a copy of it to your publisher/graduate school.
- Appropriate credit for the requested material should be given as follows: "Reprinted (adapted) with permission from (COMPLETE REFERENCE CITATION). Copyright (YEAR) American Chemical Society." Insert appropriate information in place of the capitalized words.
- One-time permission is granted only for the use specified in your request. No additional uses are granted (such as derivative works or other editions). For any other uses, please submit a new request.

Figure 1.2f

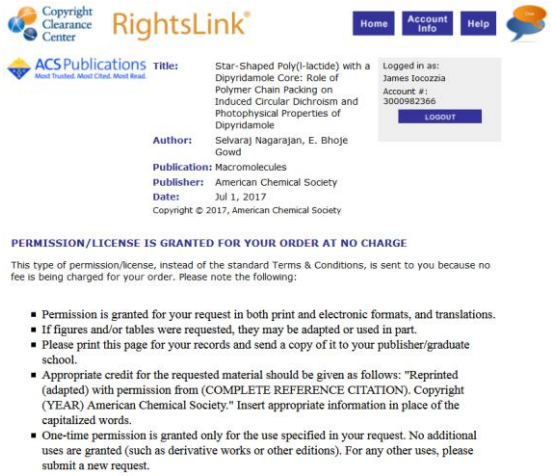

Copyright Clearance Center RightsLink®

Home | Account Info | Help

ACS Publications Most Trusted. Most Cited. Most Read.

Title: Star-Shaped Poly(l-lactide) with a Dipyridamole Core: Role of Polymer Chain Packing on Induced Circular Dichroism and Photophysical Properties of Dipyridamole

Author: Selvaraj Nagarajan, E. Bhoje Gowd

Publication: Macromolecules

Publisher: American Chemical Society

Date: Jul 1, 2017

Copyright © 2017, American Chemical Society

Logged in as: James Iocozzia
Account #: 3000982366
LOGOUT

PERMISSION/LICENSE IS GRANTED FOR YOUR ORDER AT NO CHARGE

This type of permission/license, instead of the standard Terms & Conditions, is sent to you because no fee is being charged for your order. Please note the following:

- Permission is granted for your request in both print and electronic formats, and translations.
- If figures and/or tables were requested, they may be adapted or used in part.
- Please print this page for your records and send a copy of it to your publisher/graduate school.
- Appropriate credit for the requested material should be given as follows: "Reprinted (adapted) with permission from (COMPLETE REFERENCE CITATION). Copyright (YEAR) American Chemical Society." Insert appropriate information in place of the capitalized words.
- One-time permission is granted only for the use specified in your request. No additional uses are granted (such as derivative works or other editions). For any other uses, please submit a new request.

Figure 1.3b

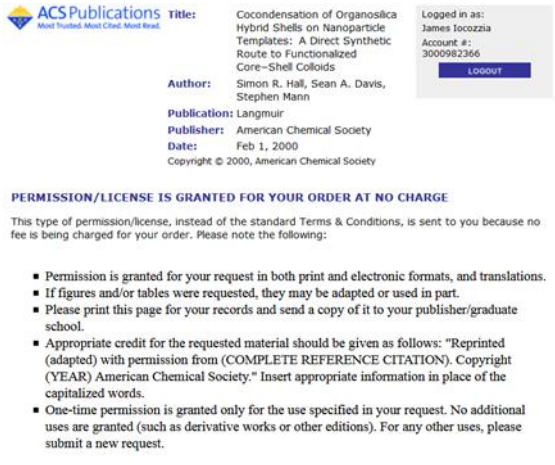

ACS Publications Most Trusted. Most Cited. Most Read.

Title: Cocondensation of Organosilica Hybrid Shells on Nanoparticle Templates: A Direct Synthetic Route to Functionalized Core–Shell Colloids

Author: Simon R. Hall, Sean A. Davis, Stephen Mann

Publication: Langmuir

Publisher: American Chemical Society

Date: Feb 1, 2000

Copyright © 2000, American Chemical Society

Logged in as: James Iocozzia
Account #: 3000982366
LOGOUT

PERMISSION/LICENSE IS GRANTED FOR YOUR ORDER AT NO CHARGE

This type of permission/license, instead of the standard Terms & Conditions, is sent to you because no fee is being charged for your order. Please note the following:

- Permission is granted for your request in both print and electronic formats, and translations.
- If figures and/or tables were requested, they may be adapted or used in part.
- Please print this page for your records and send a copy of it to your publisher/graduate school.
- Appropriate credit for the requested material should be given as follows: "Reprinted (adapted) with permission from (COMPLETE REFERENCE CITATION). Copyright (YEAR) American Chemical Society." Insert appropriate information in place of the capitalized words.
- One-time permission is granted only for the use specified in your request. No additional uses are granted (such as derivative works or other editions). For any other uses, please submit a new request.

Figure 1.8a

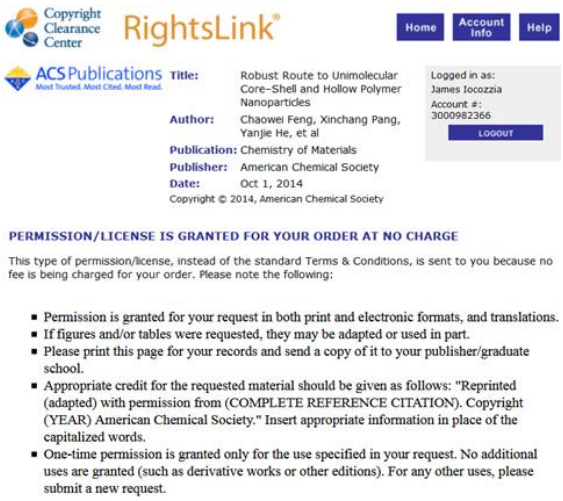

Copyright Clearance Center RightsLink®

Home | Account Info | Help

ACS Publications Most Trusted. Most Cited. Most Read.

Title: Robust Route to Unimolecular Core–Shell and Hollow Polymer Nanoparticles

Author: Chaowei Feng, Xinchang Pang, Yanjie He, et al

Publication: Chemistry of Materials

Publisher: American Chemical Society

Date: Oct 1, 2014

Copyright © 2014, American Chemical Society

Logged in as: James Iocozzia
Account #: 3000982366
LOGOUT

PERMISSION/LICENSE IS GRANTED FOR YOUR ORDER AT NO CHARGE

This type of permission/license, instead of the standard Terms & Conditions, is sent to you because no fee is being charged for your order. Please note the following:

- Permission is granted for your request in both print and electronic formats, and translations.
- If figures and/or tables were requested, they may be adapted or used in part.
- Please print this page for your records and send a copy of it to your publisher/graduate school.
- Appropriate credit for the requested material should be given as follows: "Reprinted (adapted) with permission from (COMPLETE REFERENCE CITATION). Copyright (YEAR) American Chemical Society." Insert appropriate information in place of the capitalized words.
- One-time permission is granted only for the use specified in your request. No additional uses are granted (such as derivative works or other editions). For any other uses, please submit a new request.

Figure 1.12a

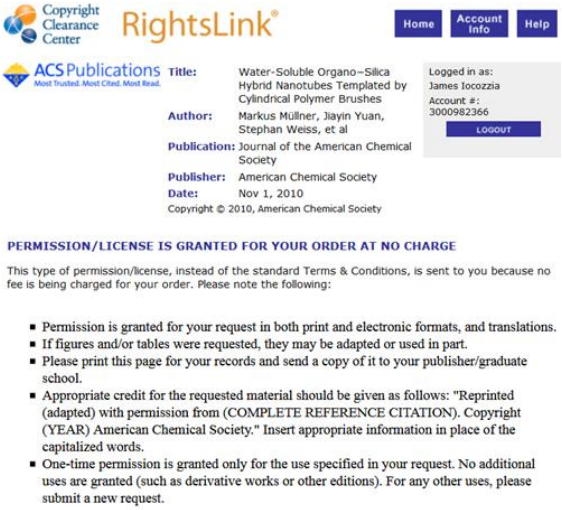

Copyright Clearance Center RightsLink®

Home | Account Info | Help

ACS Publications Most Trusted. Most Cited. Most Read.

Title: Water-Soluble Organo–Silica Hybrid Nanotubes Templated by Cylindrical Polymer Brushes

Author: Markus Müllner, Jiayin Yuan, Stephan Weiss, et al

Publication: Journal of the American Chemical Society

Publisher: American Chemical Society

Date: Nov 1, 2010

Copyright © 2010, American Chemical Society

Logged in as: James Iocozzia
Account #: 3000982366
LOGOUT

PERMISSION/LICENSE IS GRANTED FOR YOUR ORDER AT NO CHARGE

This type of permission/license, instead of the standard Terms & Conditions, is sent to you because no fee is being charged for your order. Please note the following:

- Permission is granted for your request in both print and electronic formats, and translations.
- If figures and/or tables were requested, they may be adapted or used in part.
- Please print this page for your records and send a copy of it to your publisher/graduate school.
- Appropriate credit for the requested material should be given as follows: "Reprinted (adapted) with permission from (COMPLETE REFERENCE CITATION). Copyright (YEAR) American Chemical Society." Insert appropriate information in place of the capitalized words.
- One-time permission is granted only for the use specified in your request. No additional uses are granted (such as derivative works or other editions). For any other uses, please submit a new request.

Figure 1.12b

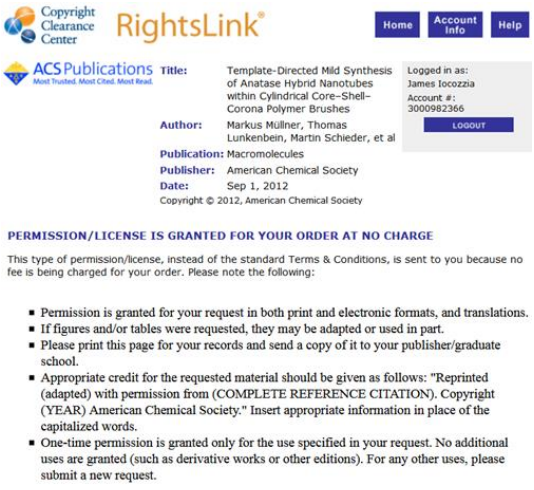

Copyright Clearance Center RightsLink®

Home | Account Info | Help

ACS Publications Most Trusted. Most Cited. Most Read.

Title: Template-Directed Mild Synthesis of Anatase Hybrid Nanotubes within Cylindrical Core–Shell–Corona Polymer Brushes

Author: Markus Müllner, Thomas Lunkenbein, Martin Schieder, et al

Publication: Macromolecules

Publisher: American Chemical Society

Date: Sep 1, 2012

Copyright © 2012, American Chemical Society

Logged in as: James Iocozzia
Account #: 3000982366
LOGOUT

PERMISSION/LICENSE IS GRANTED FOR YOUR ORDER AT NO CHARGE

This type of permission/license, instead of the standard Terms & Conditions, is sent to you because no fee is being charged for your order. Please note the following:

- Permission is granted for your request in both print and electronic formats, and translations.
- If figures and/or tables were requested, they may be adapted or used in part.
- Please print this page for your records and send a copy of it to your publisher/graduate school.
- Appropriate credit for the requested material should be given as follows: "Reprinted (adapted) with permission from (COMPLETE REFERENCE CITATION). Copyright (YEAR) American Chemical Society." Insert appropriate information in place of the capitalized words.
- One-time permission is granted only for the use specified in your request. No additional uses are granted (such as derivative works or other editions). For any other uses, please submit a new request.

Figure 1.12c

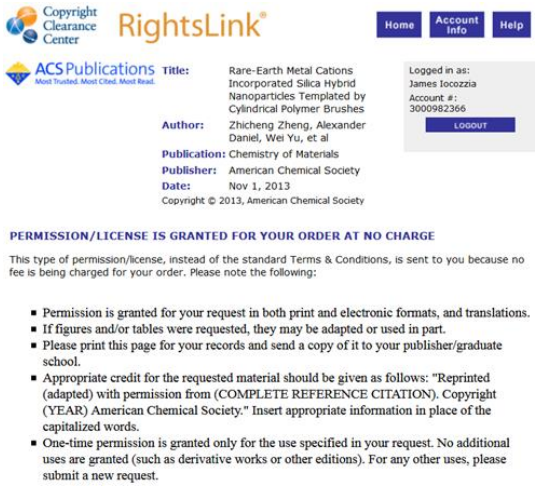

Copyright Clearance Center RightsLink®

Home | Account Info | Help

ACS Publications Most Trusted. Most Cited. Most Read.

Title: Rare-Earth Metal Cations Incorporated Silica Hybrid Nanoparticles Templated by Cylindrical Polymer Brushes

Author: Zhicheng Zheng, Alexander Daniel, Wei Yu, et al

Publication: Chemistry of Materials

Publisher: American Chemical Society

Date: Nov 1, 2013

Copyright © 2013, American Chemical Society

Logged in as: James Iocozzia
Account #: 3000982366
LOGOUT

PERMISSION/LICENSE IS GRANTED FOR YOUR ORDER AT NO CHARGE

This type of permission/license, instead of the standard Terms & Conditions, is sent to you because no fee is being charged for your order. Please note the following:

- Permission is granted for your request in both print and electronic formats, and translations.
- If figures and/or tables were requested, they may be adapted or used in part.
- Please print this page for your records and send a copy of it to your publisher/graduate school.
- Appropriate credit for the requested material should be given as follows: "Reprinted (adapted) with permission from (COMPLETE REFERENCE CITATION). Copyright (YEAR) American Chemical Society." Insert appropriate information in place of the capitalized words.
- One-time permission is granted only for the use specified in your request. No additional uses are granted (such as derivative works or other editions). For any other uses, please submit a new request.

Figure 1.13a

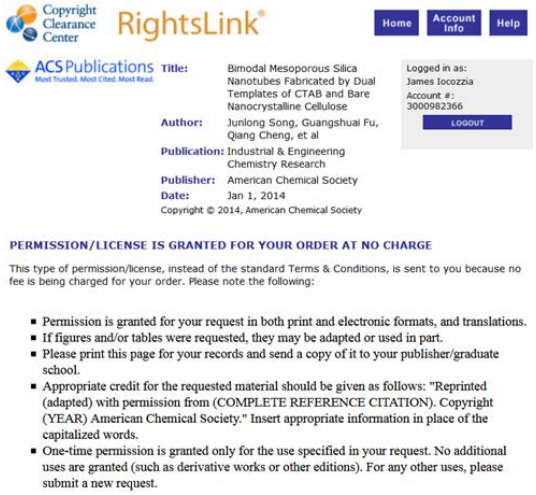

Copyright Clearance Center RightsLink®

Home | Account Info | Help

ACS Publications Most Trusted. Most Cited. Most Read.

Title: Bimodal Mesoporous Silica Nanotubes Fabricated by Dual Templates of CTAB and Bare Nanocrystalline Cellulose

Author: Junlong Song, Guangshuai Fu, Qiang Cheng, et al

Publication: Industrial & Engineering Chemistry Research

Publisher: American Chemical Society

Date: Jan 1, 2014

Copyright © 2014, American Chemical Society

Logged in as: James Iocozzia
Account #: 3000982366
LOGOUT

PERMISSION/LICENSE IS GRANTED FOR YOUR ORDER AT NO CHARGE

This type of permission/license, instead of the standard Terms & Conditions, is sent to you because no fee is being charged for your order. Please note the following:

- Permission is granted for your request in both print and electronic formats, and translations.
- If figures and/or tables were requested, they may be adapted or used in part.
- Please print this page for your records and send a copy of it to your publisher/graduate school.
- Appropriate credit for the requested material should be given as follows: "Reprinted (adapted) with permission from (COMPLETE REFERENCE CITATION). Copyright (YEAR) American Chemical Society." Insert appropriate information in place of the capitalized words.
- One-time permission is granted only for the use specified in your request. No additional uses are granted (such as derivative works or other editions). For any other uses, please submit a new request.

Figure 1.14

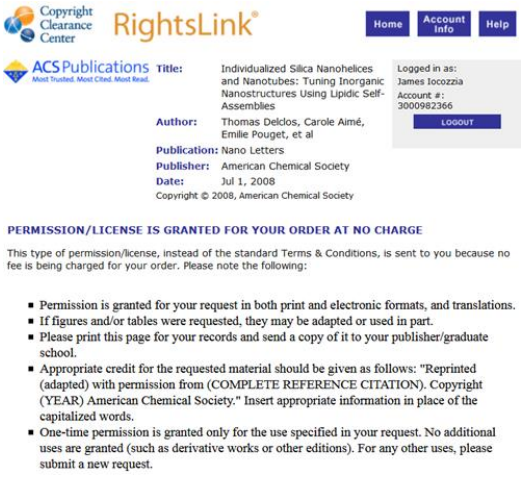

Copyright Clearance Center RightsLink®

Home | Account Info | Help

ACS Publications Most Trusted. Most Cited. Most Read.

Title: Individualized Silica Nanohelices and Nanotubes: Tuning Inorganic Nanostructures Using Lipidic Self-Assemblies

Author: Thomas Delclos, Carole Aimé, Emilie Pouget, et al

Publication: Nano Letters

Publisher: American Chemical Society

Date: Jul 1, 2008

Copyright © 2008, American Chemical Society

Logged in as: James Iocozzia
Account #: 3000982366
LOGOUT

PERMISSION/LICENSE IS GRANTED FOR YOUR ORDER AT NO CHARGE

This type of permission/license, instead of the standard Terms & Conditions, is sent to you because no fee is being charged for your order. Please note the following:

- Permission is granted for your request in both print and electronic formats, and translations.
- If figures and/or tables were requested, they may be adapted or used in part.
- Please print this page for your records and send a copy of it to your publisher/graduate school.
- Appropriate credit for the requested material should be given as follows: "Reprinted (adapted) with permission from (COMPLETE REFERENCE CITATION). Copyright (YEAR) American Chemical Society." Insert appropriate information in place of the capitalized words.
- One-time permission is granted only for the use specified in your request. No additional uses are granted (such as derivative works or other editions). For any other uses, please submit a new request.

Figure 1.15 (Top)

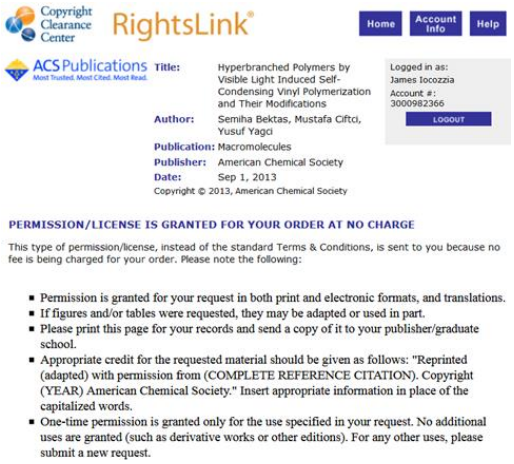

Copyright Clearance Center RightsLink®

Home | Account Info | Help

ACS Publications Most Trusted. Most Cited. Most Read.

Title: Hyperbranched Polymers by Visible Light Induced Self-Condensing Vinyl Polymerization and Their Modifications

Author: Semiha Bektas, Mustafa Ciftci, Yusuf Yagci

Publication: Macromolecules

Publisher: American Chemical Society

Date: Sep 1, 2013

Copyright © 2013, American Chemical Society

Logged in as: James Iocozzia
Account #: 3000982366
LOGOUT

PERMISSION/LICENSE IS GRANTED FOR YOUR ORDER AT NO CHARGE

This type of permission/license, instead of the standard Terms & Conditions, is sent to you because no fee is being charged for your order. Please note the following:

- Permission is granted for your request in both print and electronic formats, and translations.
- If figures and/or tables were requested, they may be adapted or used in part.
- Please print this page for your records and send a copy of it to your publisher/graduate school.
- Appropriate credit for the requested material should be given as follows: "Reprinted (adapted) with permission from (COMPLETE REFERENCE CITATION). Copyright (YEAR) American Chemical Society." Insert appropriate information in place of the capitalized words.
- One-time permission is granted only for the use specified in your request. No additional uses are granted (such as derivative works or other editions). For any other uses, please submit a new request.

Figure 1.17

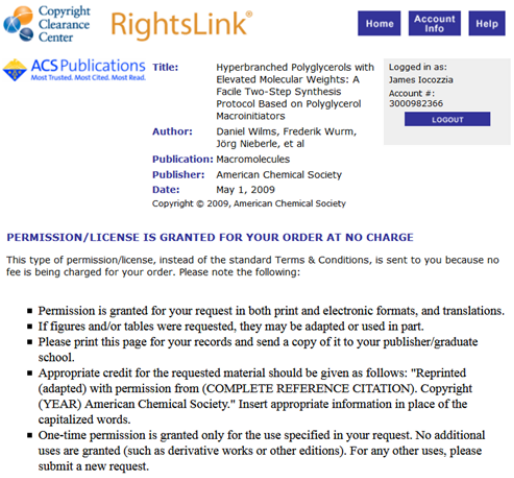

Copyright Clearance Center RightsLink®

Home | Account Info | Help

ACS Publications Most Trusted. Most Cited. Most Read.

Title: Hyperbranched Polyglycerols with Elevated Molecular Weights: A Facile Two-Step Synthesis Protocol Based on Polyglycerol Macroinitiators

Author: Daniel Wilms, Frederik Wurm, Jörg Nieberle, et al

Publication: Macromolecules

Publisher: American Chemical Society

Date: May 1, 2009

Copyright © 2009, American Chemical Society

Logged in as: James Iocozzia
Account #: 3000982366
LOGOUT

PERMISSION/LICENSE IS GRANTED FOR YOUR ORDER AT NO CHARGE

This type of permission/license, instead of the standard Terms & Conditions, is sent to you because no fee is being charged for your order. Please note the following:

- Permission is granted for your request in both print and electronic formats, and translations.
- If figures and/or tables were requested, they may be adapted or used in part.
- Please print this page for your records and send a copy of it to your publisher/graduate school.
- Appropriate credit for the requested material should be given as follows: "Reprinted (adapted) with permission from (COMPLETE REFERENCE CITATION). Copyright (YEAR) American Chemical Society." Insert appropriate information in place of the capitalized words.
- One-time permission is granted only for the use specified in your request. No additional uses are granted (such as derivative works or other editions). For any other uses, please submit a new request.

Figure 1.18

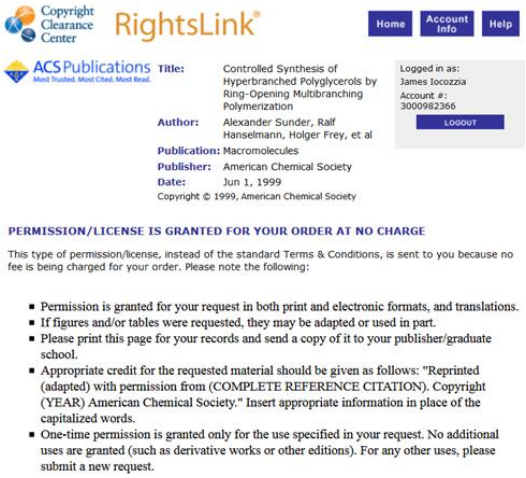

Copyright Clearance Center RightsLink®

Home | Account Info | Help

ACS Publications Most Trusted. Most Cited. Most Read.

Title: Controlled Synthesis of Hyperbranched Polyglycerols by Ring-Opening Multibranching Polymerization

Author: Alexander Sunder, Ralf Hanselmann, Holger Frey, et al

Publication: Macromolecules

Publisher: American Chemical Society

Date: Jun 1, 1999

Copyright © 1999, American Chemical Society

Logged in as: James Iocozzia
Account #: 3000982366
LOGOUT

PERMISSION/LICENSE IS GRANTED FOR YOUR ORDER AT NO CHARGE

This type of permission/license, instead of the standard Terms & Conditions, is sent to you because no fee is being charged for your order. Please note the following:

- Permission is granted for your request in both print and electronic formats, and translations.
- If figures and/or tables were requested, they may be adapted or used in part.
- Please print this page for your records and send a copy of it to your publisher/graduate school.
- Appropriate credit for the requested material should be given as follows: "Reprinted (adapted) with permission from (COMPLETE REFERENCE CITATION). Copyright (YEAR) American Chemical Society." Insert appropriate information in place of the capitalized words.
- One-time permission is granted only for the use specified in your request. No additional uses are granted (such as derivative works or other editions). For any other uses, please submit a new request.

Figure 1.20b

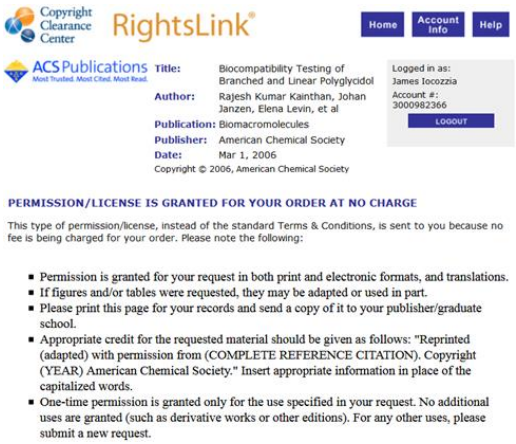

Copyright Clearance Center RightsLink®

Home | Account Info | Help

ACS Publications Most Trusted. Most Cited. Most Read.

Title: Biocompatibility Testing of Branched and Linear Polyglycidol
Author: Rajesh Kumar Kainthan, Johan Janzen, Elena Levin, et al
Publication: Biomacromolecules
Publisher: American Chemical Society
Date: Mar 1, 2006
Copyright © 2006, American Chemical Society

Logged in as: James Iocozzia
Account #: 3000982366
LOGOUT

PERMISSION/LICENSE IS GRANTED FOR YOUR ORDER AT NO CHARGE

This type of permission/license, instead of the standard Terms & Conditions, is sent to you because no fee is being charged for your order. Please note the following:

- Permission is granted for your request in both print and electronic formats, and translations.
- If figures and/or tables were requested, they may be adapted or used in part.
- Please print this page for your records and send a copy of it to your publisher/graduate school.
- Appropriate credit for the requested material should be given as follows: "Reprinted (adapted) with permission from (COMPLETE REFERENCE CITATION). Copyright (YEAR) American Chemical Society." Insert appropriate information in place of the capitalized words.
- One-time permission is granted only for the use specified in your request. No additional uses are granted (such as derivative works or other editions). For any other uses, please submit a new request.

Figure 1.21

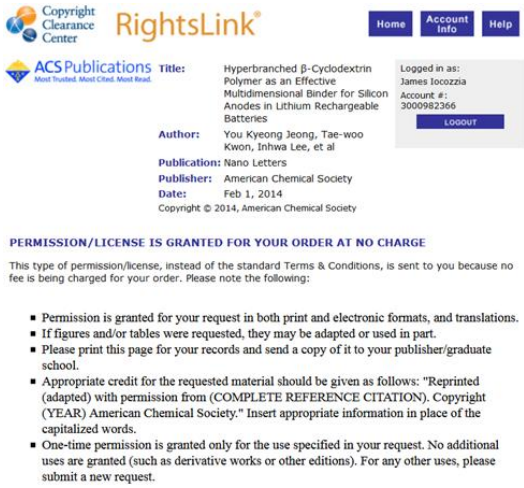

Copyright Clearance Center RightsLink®

Home | Account Info | Help

ACS Publications Most Trusted. Most Cited. Most Read.

Title: Hyperbranched β-Cyclodextrin Polymer as an Effective Multidimensional Binder for Silicon Anodes in Lithium Rechargeable Batteries
Author: You Kyeong Jeong, Tae-woo Kwon, Inhwa Lee, et al
Publication: Nano Letters
Publisher: American Chemical Society
Date: Feb 1, 2014
Copyright © 2014, American Chemical Society

Logged in as: James Iocozzia
Account #: 3000982366
LOGOUT

PERMISSION/LICENSE IS GRANTED FOR YOUR ORDER AT NO CHARGE

This type of permission/license, instead of the standard Terms & Conditions, is sent to you because no fee is being charged for your order. Please note the following:

- Permission is granted for your request in both print and electronic formats, and translations.
- If figures and/or tables were requested, they may be adapted or used in part.
- Please print this page for your records and send a copy of it to your publisher/graduate school.
- Appropriate credit for the requested material should be given as follows: "Reprinted (adapted) with permission from (COMPLETE REFERENCE CITATION). Copyright (YEAR) American Chemical Society." Insert appropriate information in place of the capitalized words.
- One-time permission is granted only for the use specified in your request. No additional uses are granted (such as derivative works or other editions). For any other uses, please submit a new request.

Figure 1.22

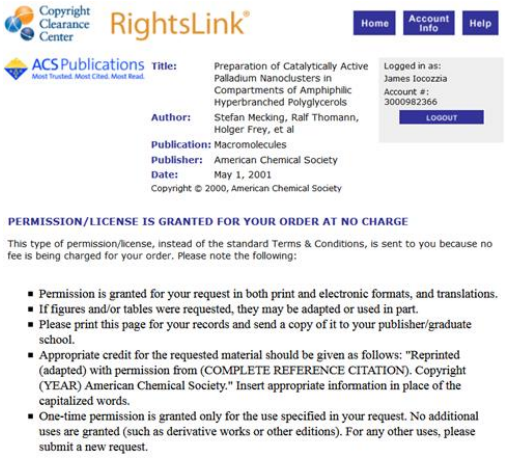

Copyright Clearance Center RightsLink®

Home | Account Info | Help

ACS Publications Most Trusted. Most Cited. Most Read.

Title: Preparation of Catalytically Active Palladium Nanoclusters in Compartments of Amphiphilic Hyperbranched Polyglycerols
Author: Stefan Mecking, Ralf Thomann, Holger Frey, et al
Publication: Macromolecules
Publisher: American Chemical Society
Date: May 1, 2001
Copyright © 2000, American Chemical Society

Logged in as: James Iocozzia
Account #: 3000982366
LOGOUT

PERMISSION/LICENSE IS GRANTED FOR YOUR ORDER AT NO CHARGE

This type of permission/license, instead of the standard Terms & Conditions, is sent to you because no fee is being charged for your order. Please note the following:

- Permission is granted for your request in both print and electronic formats, and translations.
- If figures and/or tables were requested, they may be adapted or used in part.
- Please print this page for your records and send a copy of it to your publisher/graduate school.
- Appropriate credit for the requested material should be given as follows: "Reprinted (adapted) with permission from (COMPLETE REFERENCE CITATION). Copyright (YEAR) American Chemical Society." Insert appropriate information in place of the capitalized words.
- One-time permission is granted only for the use specified in your request. No additional uses are granted (such as derivative works or other editions). For any other uses, please submit a new request.

Figure 1.26

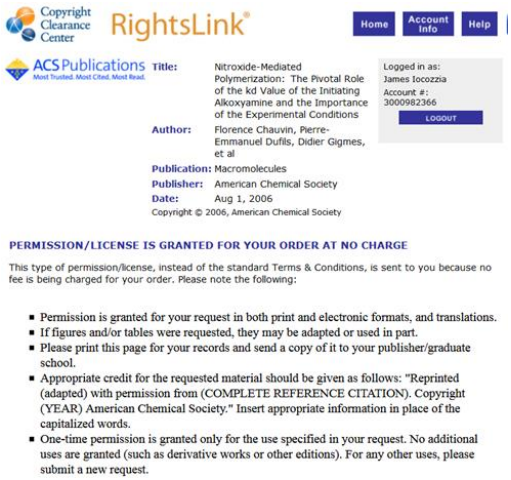

Copyright Clearance Center RightsLink®

Home | Account Info | Help

ACS Publications Most Trusted. Most Cited. Most Read.

Title: Nitroxide-Mediated Polymerization: The Pivotal Role of the kd Value of the Initiating Alkoxyamine and the Importance of the Experimental Conditions

Author: Florence Chauvin, Pierre-Emmanuel Dufils, Didier Gigmes, et al

Publication: Macromolecules

Publisher: American Chemical Society

Date: Aug 1, 2006

Copyright © 2006, American Chemical Society

Logged in as:
James Iocozzia
Account #:
3000982366
LOGOUT

PERMISSION/LICENSE IS GRANTED FOR YOUR ORDER AT NO CHARGE

This type of permission/license, instead of the standard Terms & Conditions, is sent to you because no fee is being charged for your order. Please note the following:

- Permission is granted for your request in both print and electronic formats, and translations.
- If figures and/or tables were requested, they may be adapted or used in part.
- Please print this page for your records and send a copy of it to your publisher/graduate school.
- Appropriate credit for the requested material should be given as follows: "Reprinted (adapted) with permission from (COMPLETE REFERENCE CITATION). Copyright (YEAR) American Chemical Society." Insert appropriate information in place of the capitalized words.
- One-time permission is granted only for the use specified in your request. No additional uses are granted (such as derivative works or other editions). For any other uses, please submit a new request.

REFERENCES

1. Azuri, I., Adler-Abramovich, L. & Gazit, E. Why Are Diphenylalanine-Based Nanostructures So Rigid? Insights from First Principles Calculations. *J. Am. Chem. Soc.* **136**, 963-969 (2014).
2. Castillo, J., Sasso, L. & Svendsen, W.E. Self-assembled peptide nanostrucutres: advances and applications in nanobiotechnology. (Taylor and Francis, CRC Press, Boca Raton, Florida; 2012).
3. Rosi, N.Z., Zhang, P. & Chen, C. A new peptide-based method for the design and synthesis of nanoparticle superstructures: construction of highly ordered gold nanoparticle double helices. *J. Am. Chem. Soc.* **130**, 13555-13557 (2008).
4. Nam, K.T. et al. Virus-enabled Synthesis and Assembly of Nanowires for Lithium Ion Battery Electrodes. *Science* **312**, 885-888 (2006).
5. Belcher, A.M. et al. Virus-based toolkit for the directed synthesis of magnetic and semiconducting nanowires. *Science* **303**, 213-217 (2004).
6. Dragnea, B. et al. Synergistic effects of mutations and nanoparticle templating in the self-assembly of cowpea chlorotic mottle virus capsids. *Nano. Lett.* **9**, 393-398 (2009).
7. Dragnea, B. et al. Nanoparticle-templated assembly of viral protein cages. *Nano Lett.* **6**, 611-615 (2006).
8. Wang, Q. et al. Insights into stabilization of a viral protein cage in templating complex nanoarchitectures: roles of disulfide bonds. *Small* **10**, 536-543 (2013).
9. Yang, H. & Rahman, S. Nanopillar arrays of glassy carbon by anodic aluminum oxide nanoporous templates. *Nano Lett.* **3**, 439-442 (2003).
10. Burkhard, P., Dey, R., Raman, S. & Doll, T. Nanoscale assemblies and their biomedical applications. *J. Royal Soc. Interface* **10**, 1-14 (2013).
11. Gibson, M.I., O'Reilly, R.K., Daniel, L.E., Bremis, K. & Ieong, N.S. The critical importance of size on thermoresponsive nanoparticle transition temperatures: gold and micelled-based polymer nanoparticles. *ChemComm* **47**, 11627-11629 (2011).
12. Hudson, L., Hollamby, M.J. & Eastoe, J. Recent advances in nanoparticle synthesis with reversed micelles. *Adv. Colloid Interface Sci.* **128-130**, 5-15 (2006).
13. Kulkarni, C.V. Lipid crystallization: from self-assembly to hierarchical and biological ordering. *Nanoscale* **4**, 5779-5791 (2012).
14. Mann, S. & Archibald, D.D. Template mineralization of self-assembled anisotropic lipid microstructures. *Nature* **364**, 430-433 (1993).
15. Oda, R. et al. Individualized silica nanohelices and nanotubes: tuning inorganic nanostructures using lipidic self-assemblies. *Nano Lett.* **8**, 1929-1935 (2008).
16. Chen, X.Q. et al. Preparation and characterization of magnetic star-shaped amphiphilic copolymer nanoparticles of S-Fe3O4-PLA-b-MPEG. *Polym. Compos.* **33**, 2134-2139 (2012).
17. Ohno, K., Wong, B. & Haddleton, D. Synthesis of Well-defined Cyclodextrin-Core Star Polymers. *J. Polym. Sci. A Polym. Chem.* **39**, 2206-2214 (2001).
18. Pang, X. et al. Unimolecular micelles composed of inner coil-like blocks and outer rod-like blocks crafted by combination of living polymerization with click chemistry. *Polym. Chem.* **5** (2014).

19. Pang, X.C., Zhao, L., Akinc, M., Kim, J.K. & Lin, Z.Q. Novel Amphiphilic Multi-Arm, Star-Like Block Copolymers as Unimolecular Micelles. *Macromolecules* **44**, 3746-3752 (2011).
20. Pang, X., Zhao, L., Han, W., Xin, X. & Lin, Z. A General and Robust Strategy for the Synthesis of Nearly Monodisperse Colloidal Nanocrystals. *Nat. Nanotechnol.* **8**, 426-431 (2013).
21. Wang, W.P. et al. Synthesis and characterization of star-shaped block copolymers with polyhedral oligomeric silsesquioxane (POSS) core via ATRP. *Polym. Bull.* **65**, 863-872 (2010).
22. Matyjaszewski, K. & Gao, H. Synthesis of functional polymers with controlled architecture by CRP of monomers in the presence of cross-linkers: from stars to gels. *Prog. Polym. Sci* **34**, 317-350 (2009).
23. Ljubic, T.S. et al. Utility of Chromatographic and Spectroscopic Techniques for a Detailed Characterization of Poly(styrene-b-isoprene) Miktoarm Star Copolymers with Complex Architecture. *Macromolecules* **45**, 7574-7582 (2012).
24. Li, J.S., Xiao, H.N. & Kim, Y.S. Synthesis of Water-Soluble Cationic Polymers with Star-Like Structure Based on Cyclodextrin Core via ATRP. *J. Polym. Sci. A Polym. Chem.* **43**, 6345-6354 (2005).
25. Zhang, Q., Guang-Zhao, L., Remzi, B. & Haddleton, D. Cyclodextrin-centered star polymers synthesized via combination of thiol-ene click and ring opening polymerization. *ChemComm* **48**, 8063-8065 (2012).
26. Miura, Y., Narumi, A. & Matsuya, S. Synthesis of Well-Defined AB 20-Type Star Polymers with Cyclodextrin-Core by Combination of NMP and ATRP. *J. Polym. Sci. A Polym. Chem.* **43**, 4271-4279 (2005).
27. Tanaka, K. & Chujo, Y. Advanced functional materials based on polyhedral oligomeric silsesquioxane (POSS). *J. Mater. Chem.* **22**, 1733-1746 (2012).
28. Inoue, K. Functional dendrimers, hyperbranched and star polymers. *Prog. Polym. Sci.* **25**, 453-571 (2000).
29. B., M. & Trzebicka, B. Synthesis and characterization of well-defined poly(*tert*-butyl acrylate) star polymers. *Eur. Polym. J.* **45**, 1979-1993 (2009).
30. Hasegawa, H., Nagata, Y., Terao, K. & Suginome, M. Synthesis and Solution Properties of a Rigid Helical Star Polymer: Three-Arm Star Poly(quinoxaline-2,3-diyl). *Macromolecules* **50**, 7491-7497 (2017).
31. Pahl, P. et al. Core-First Synthesis of Three-Armed Star-Shaped Polymers by Rare Earth Metal-Mediated Group Transfer Polymerization. *Macromolecules* **50**, 6569-6576 (2017).
32. Plietzsch, O. et al. Synthesis and Topological Determination of Hexakis-Substituted 1,4-Ditritylbenzene and Nonakis-Substituted 1,3,5-Tritritylbenzene Derivatives: Building Blocks for Higher Supramolecular Assemblies. *Eur. J. Org. Chem.* **2013**, 283-299 (2013).
33. Nagarajan, S. & Gowd, E.B. Star-Shaped Poly(L-lactide) with a Dipyridamole Core: Role of Polymer Chain Packing on Induced Circular Dichroism and Photophysical Properties of Dipyridamole. *Macromolecules* **50**, 5261-5270 (2017).
34. Ye, W. et al. Six-arm star-shaped polymer with cyclophosphazene core and poly(ε-caprolactone) arms as a modifier of epoxy thermosets. *J. Appl. Polym. Sci.* **134**, 44384 (2017).
35. Huang, X. et al. Star Polymers from Single-Chain Cyclized/Knoted Nanoparticles as a Core. *Macromol. Chem. Phys.* **219**, 1700473-1700477 (2018).
36. Surapati, M., Seino, M., Hayakawa, T. & Kakimoto, M. Synthesis of hyperbranched-linear star block copolymers by atom transfer radical polymerization of styrene using

hyperbranched poly(siloxysilane) (HBPS) macroinitiator. *Eur. Polym. J.* **46**, 217-225 (2010).
37. Odian, G. Principles of Polymerization, Edn. fourth edition. (John Wiley & Sons, New Jersey; 2004).
38. Han, C.C., Hu, Z., Y., L., Niu, Z. & Yang, Z. Template synthesis of inorganic hollow spheres with a tunable cavity onto core-shell gel particles *Angew. Chem. Int. Ed.* **42**, 1943-1945 (2003).
39. Mann, S., Davis, S.A. & Hall, S.R. Cocondensation of organosilica hybrid shells on nanoparticle templates: a direct synthetic route to functionalized core-shell colloids. *Langmuir* **16**, 1454-1456 (2000).
40. Sheng, Y.J., Nung, C.H. & Tsao, H.K. Morphologies of star-block copolymers in dilute solutions. *J. Phys. Chem. B* **110**, 21643-21650 (2006).
41. Matyjaszewski, K., Min, K. & H., G. Synthesis of 3-arm star block copolymers by combination of "core-first" and "coupling-onto" methods using ATRP and click reactions. *Macromol. Chem. Phys.* **208**, 1370-1378 (2007).
42. Heilshorn, S.C., Arunagirinathan, M.A., Schoen, A.P. & Huggins, K.N.L. Multi-site functionalization of protein scaffolds for bimetallic nanoparticle templating. *Adv. Func. Mater.* **24**, 7737-7744 (2014).
43. Jiang, W., Zhu, J., Zhu, Y. & Xu, J. Ultralong gold nanoparticle/block copolymer hybrid cylindrical micelles: a strategy combining surface templated self-assembly and Rayleigh instability. *Nanoscale* **5**, 6344-6349 (2013).
44. Su, W. et al. Iron oxide nanoparticle layer templated by polydopamine spheres: a novel scaffold toward hollow-mesoporous magnetic nanoreactors. *Nanoscale* **7**, 806-813 (2015).
45. Nakahira, T. et al. Preparation of titania hollow particles with independently controlled void size and shell thickness by catalytic templating core-shell polymer particles. *Colloid Polym. Sci.* **291**, 215-222 (2013).
46. Youan, B.C. et al. Hyaluronidase-sensitive nanoparticle templates for triggered release of HIV/AIDS microbicide *in vitro*. *AAPS J.* **16**, 181-193 (2014).
47. Feng, C., Pang, X., He, Y., Li, B. & Lin, Z. Robust Route to Unimolecular Core-Shell and Hollow Polymer Nanoparticles. *Chem. Mater.* **26**, 6058-6067 (2014).
48. Yasar, A.O. & Sahiner, N. Monodispersed p(2-VP) and p(2-VP-co-4-VP) particle preparation and their use as template for metal nanoparticle and as catalyst for H_2 production from $NaBH_4$ and NH_3BH_3 hydrolysis. *Int. J. Hydrog. Energy* **39**, 10476-10484 (2014).
49. Sahiner, N. Soft and flexible hydrgel templates for different sizes and various functionalities for metal nanoparticle preparation and their use in catalysis. *Prog. Polym. Sci* **38**, 1329-1356 (2013).
50. Lin, Z. et al. Block copolymer/ferroelectric nanoparticle nanocomposites. *Nanoscale* **5**, 8695-8702 (2013).
51. Yang, D. et al. Precisely Size-Tunable Magnetic/Plasmonic Core/Shell Nanoparticles with Controlled Optical Properties. *Angew. Chem. Int. Ed.* **54**, 12091-12096 (2015).
52. Oh, J.K. & Park, J.M. Iron oxide-based superparamagnetic polymeric nanomaterials: Design, preparation, and biomedical application. *Prog. Polym. Sci* **36**, 168-189 (2011).
53. Qiao, R., Yang, C. & Gao, M. Superparamagnetic iron oxide nanoparticles: from preparations to in vivo MRI applications. *J. Mater. Chem.* **19**, 6274-6293 (2009).

54. Kim, D.K., Zhang, Y., Voit, W., Rao, K.V. & M., M. Synthesis and characterization of surfactant-coated superparamagnetic monodispersed iron oxide nanoparticles. *J. Magn. Magn. Mater.* **225**, 30-36 (2001).
55. Moore, J., S., White, S.R., Sottos, N.R., Odom, S.A. & Esser-Kahn, A.P. Triggered release from polymer capsules. *Macromolecules* **44**, 5539-5553 (2011).
56. De Smedt, S.C. et al. Intracellularly degradable polyelectrolyte microcapsules. *Adv. Mater.* **18**, 1005-1009 (2006).
57. Chu, L. et al. Multi-stimuli-responsive microcapsules for adjustable controlled-release. *Adv. Func. Mater.* **24**, 3312-3323 (2014).
58. Caruso, F., Barlow, E., Wang, Y. & Yu, A. Mesoporous silica particles as templates for preparing enzyme-loaded biocompatible microcapsules. *Adv. Mater.* **17**, 1737-1741 (2005).
59. Lvov, Y.M. et al. Magnetic switch of permeability for polyelectrolyte microcapsules embedded with Co@Au nanoparticles. *Langmuir* **21**, 2042-2050 (2005).
60. Aktsipetrov, O.A., Kolychek, I.A., Sychev, F.Y. & Murzina, T.V. Tunable ferroelectric photonic crystals based on porous silicon templates infiltrated by sodium nitride. *Appl. Phys. Lett.* **90** (2007).
61. Hur, N.H., Lee, E.K., Kim, J.C., Chi, E.O. & Kim, Y.N. Preparation of ferromagnetic and ferroelectric nanocomposites using the colloidal templating approach. *Solid State Commun.* **128**, 339-343 (2003).
62. Zhang, M. & Muller, A.H.E. Cylindrical polymer brushes. *J. Polym. Sci. A Polym. Chem.* **43**, 3461-3481 (2005).
63. Schmidt, M., Janshoff, A., Zhang, M. & Muthukrishnan, S. New perspectives for the design of molecular actuators: thermally induced collapse of single macromolecules from cylindrical brushes to spheres. *Angew. Chem. Int. Ed.* **43**, 1101-1104 (2004).
64. Zubarev, A.Y., Odenbach, S. & Fleischer, J. Rheological properties of dense ferrofluids. Effect of chain-like aggregates. *J. Magn. Magn. Mater.* **252**, 241-243 (2002).
65. Beers, K.L., Matyjaszewski, K., Wilk, A., Pakula, T. & Rathgeber, S. On the shape of bottle-brush macromolecules: systematic variation of architectural parameters. *J. Chem. Phys.* **122**, 124904-124901-124904-124913 (2005).
66. Brinke, G., Ikkala, O., Szleifer, I. & Saariaho, M. Extended conformations of isolated molecular bottle-brushes: influence of side-chain topology. *Macromol. Theory Simul.* **7**, 211-216 (1998).
67. Kempe, K., Krieg, A., Becer, C.R. & Schubert, U.S. "Clicking" on/with polymers: a rapidly expanding field for the straightforward preparation of novel macromolecular architectures. *Chem. Soc. Rev.* **41**, 176-191 (2012).
68. Grubbs, R.H. et al. Core-Clickable PEG-Branch-Azide Bivalent-Bottle-Brush Polymers by ROMP: Grafting-Through and Clicking-To. *J. Am. Chem. Soc.* **133** (2011).
69. Cappelli, A. et al. Combining spontaneous polymerization and click reactions for the synthesis of polymer brushes: a "grafting onto" approach. *Chem. Eur. J.* **19**, 9710-9721 (2013).
70. Chen, Y., Zhu, W., Shi, Y. & Yan, Y. Highly efficient synthesis of cylindrical polymer brushes with various side chains via click grafting-onto approach. *Polymer* **54**, 5634-5642 (2013).
71. Zhang, X., Wang, Z., Yang, L., Li, F. & Song, Q. Supramolecular polymers synthesized by thio-ene click polymerization from supramonomers. *Polym. Chem.* **6**, 369-372 (2015).
72. Kolb, H.C., Finn, M.G. & Sharpless, K.B. Click chemistry: Diverse chemical function from a few good reactions. *Angew. Chem. Int. Ed.* **40**, 2004-+ (2001).

73. Kozlowski, M.C., Phuan, P. & Xie, X. Novel pathways for the formation of chiral binaphthyl polymers: oxidative asymmetric phenolic coupling alone and in tandem with the glaser-hay coupling. *Angew. Chem. Int. Ed.* **42**, 2168-2170 (2003).
74. Muller, A.H.E., Drechsler, M. & Zhang, M. Template-controlled synthesis of wire-like cadmium sulfide nanoparticle assemblies within core-shell cylindrical polymer brushes. *Chem. Mater.* **16**, 537-543 (2004).
75. Zheng, Z. et al. Rare-earth metal cations incorporated silica hybrid nanoparticles templated by cylindrical polymer brushes. *Chem. Mater.* **25**, 4585-4594 (2013).
76. Muller, A.H.E. et al. Water-soluble organo-silica hybrid nanotubes templated by cylindrical polymer brushes. *J. Am. Chem. Soc.* **132**, 16587-16592 (2010).
77. Muller, A.H.E. et al. Template-directed mild synthesis of anatase hybrid nanotubes within cylindrical core-shell-corona polymer brushes *Macromolecules* **45**, 6981-6988 (2012).
78. Jin, Y., Cheng, Q., Fu, G. & Song, J. Bimodal mesoporous silica nanotubes fabricated by dual templates of CTAB and bare nanocrystalline cellulose. *Ind. Eng. Chem. Res.* **53**, 708-714 (2013).
79. Greil, P., C., Z. & Scheel, H. Luminescent silica nanotubes and nanowires: preparation from cellulose whisker templates and investigation of irradiation-induced luminescence. *J. Mater. Chem.* **24**, 1709-1715 (2009).
80. Qi, L. & Zhang, D. Synthesis of mesoporous titania networks consisting of anatase nanowires by templating of bacterial cellulose membranes. *Chem. Commun.* **0**, 2735-2737 (2005).
81. Wang, H., Zheng, Y., Zhao, S., Chen, S. & Zheng, W. Zinc sulfide nanoparticles template by bacterial cellulose and their optical properties. *J. Appl. Polym. Sci.* **131**, 40874-40881 (2014).
82. Zhang, X., Wang, Z., Ma, Z. & Yang, H. Fabricating covalently attached hyperbranched polymers by combining photochemistry with supramolecular polymerization. *Polym. Chem.* **5**, 1471-1476 (2014).
83. Suzuki, M., Ii, A. & Saegusa, T. Multibranching polymerization: paladium-catalyzed ring-opening polymerization of cyclic carbamate to produce hyperbranched dendritic polyamine. *Macromolecules* **25**, 7071-7072 (1992).
84. Suzuki, M., Yoshida, S., Shiraga, K. & Saegusa, T. New ring-opening polymerization via a pi-allylpalladium complex. 5. multibranching polymerization of cyclic carbamate to produce hyperbranched dendritic polyamine. *Macromolecules* **31**, 1716-1719 (1998).
85. Sunder, A., Hanselmann, R., Frey, H. & Mulhaupt, R. Controlled Synthesis of Hyperbranched Polyglycerols by Ring-Opening Multibranching Polymerization. *Macromolecules* **32**, 4240-4246 (1999).
86. Kautz, H., Sunder, A. & Frey, H. Control of the Molecular Weight of Hyperbranched Polyglycerols. *Macromol. Symp.* **163**, 67-73 (2001).
87. Yagci, Y., Ciftci, M. & Bektas, S. Hyperbranched polymers by visible light induced self-condensing vinyl polymerization and their modifications. *Macromolecules* **46**, 6751-6757 (2013).
88. Frechet, J.M.J. et al. Self-condensing vinyl polymerization: an approach to dendritic materials. *Science* **269**, 1080-1083 (1995).
89. Frey, H., Heinemann, J. & Sunder, A. Controlling the growth of polymer trees: concepts and perspectives for hyperbranched polymers. *Chem. Eur. J.* **6**, 2499-2506 (2000).

90. Blackwell, A.C., Russo, C.L., Vashi, M.R. & Royappa, A.T. A comparison of the cationic ring-opening polymerizations of 3-oxetanol and glycidol. *Macromol. Res.* **21**, 1069-1074 (2013).
91. Frey, H., Berger-Nicoletti, E., Muller, S.S. & Christ, E. Hydroxyfunctional oxetane-inimers with varied polarity for the synthesis of hyperbranched polyether polyols via cationic ROP. *Polym. Chem.* **52**, 2850-2859 (2014).
92. Frey, H., Schull, C. & Schomer, M. Hyperbranched aliphatic polyether polyols. *Polym. Chem.* **51**, 995-1019 (2013).
93. Wilms, D. et al. Hyperbranched Polyglycerols with Elevated Molecular Weights: A Facile Two-step Synthesis Protocol Based on Polyglycerol Macroinitiators. *Macromolecules* **42**, 3230-3236 (2009).
94. Yan, D., Wang, J.W. & Zhou, Z. Kinetic analysis of A2+AB+B3 hyperbranched polymerization approach. *Polymer* **55**, 2952-2958 (2014).
95. Paulus, F. et al. Anionic Ring-Opening Polymerization Simulations for Hyperbranched Polyglycerols with Defined Molecular Weights. *Macromolecules* **46**, 8458-8466 (2013).
96. Frey, H., Kautz, H. & Stiriba, S. Hyperbranched molecular nanocapsules: comparison of the hyperbranched architecture with the perfect linear analogue. *J. Am. Chem. Soc.* **124**, 9698-9699 (2002).
97. Frey, H., Stiriba, S. & Wilms, D. Hyperbranched polyglycerols: from the controlled synthesis of biocompatible polyether polyols to multipurpose applications. *Acc. Chem. Res.* **43**, 129-141 (2010).
98. Thurecht, K., Whittaker, A.K. & Ardana, A. PEG-based hyperbranched polymer theranostics: optimizing chemistries for improved bioconjugation. *Macromolecules* **47**, 5211-5219 (2014).
99. Saltzman, W.M. et al. The effect of hyperbranched polyglycerol coatings on drug delivery using degradable polymer nanoparticles. *Biomaterials* **35**, 6595-6602 (2014).
100. Haag, R. et al. Development of pH-responsive core-shell nanocarriers for delivery of therapeutic and diagnostic agents. *Bioorganic Med. Chem. Lett.* **19**, 1030-1034 (2009).
101. Caruso, F., Li, Q. & Zelikin, A.N. Disulfide-stabilized poly(methacrylic acid) capsules: formation, cross-linking, and degradation behavior. *Chem. Mater.* **20**, 2655-2661 (2008).
102. Frey, H., Mulhaupt, R., Hanselmann, R., Kramer, D. & Sunder, A. Molecular nanocapsules based on amphiphilic hyperbranched polyglycerols. *Angew. Chem. Int. Ed.* **38**, 3552-3555 (1999).
103. Haag, R. et al. pH-responsive molecular nanocarriers based on dendritic core-shell architectures *Angew. Chem. Int. Ed.* **41**, 4252-4256 (2002).
104. Schubert, U.S. et al. Star-shaped block copolymers by copper-catalyzed azide-alkyne cycloaddition for potential drug delivery applications. *Macromol. Chem. Phys.* **213**, 2146-2156 (2012).
105. Tremel, W., Frey, H., Istratov, V., Barriau, E. & Balz, M. Controlled crystallization of $CaCO_3$ on hyperbranched polyglycerol adsorbed to self-assembled monolayers. *Langmuir* **21**, 3987-3991 (2005).
106. Haag, R., Biesalki, M. & Siegers, C. Self-assembled monolayers of dendritic polyglycerol derivatives on gold that resist the adsorption of proteins. *Chem. Eur. J.* **10**, 2831-2838 (2004).
107. Voelcker, N.H., Thissen, H., Vasani, R., Delalat, B. & Moore, E. Patterning and biofunctionalization of antifouling hyperbranched polyglycerol coatings. *Biomacromolecules* **15**, 2735-2743 (2014).

108. Brooks, D.E., Devine, D.V., Levin, E., Janzen, J. & Kainthan, R.K. Biocompatibility testing of branched and linear polyglycidol. *Biomacromolecules* **7**, 703-709 (2006).
109. Inada, Y. et al. PEGylation of proteins and bioactive substances for medical and technical applications. *Prog. Polym. Sci* **23**, 1233-1271 (1998).
110. Kizhakkedathu, J.N. et al. The size-dependent efficacy and biocompatability of hyperbranched polyglycerol in peritoneal dialysis. *Biomaterials* **35**, 1378-1389 (2014).
111. S., A., Haag, R. & Turk, H. Dendritic polyglycerol sulfates as new heparin analogues and potent inhibitors of the complement system. *Bioconjugate Chem.* **15**, 162-167 (2004).
112. Brooks, D.E., Devine, D.V., Kizhakkedathu, J.N., Janzen, J. & Kainthan, R.K. Hydrophobically derivatized hyperbranched polyglycerol as a human serum albumin substitute. *Biomaterials* **29**, 1693-1704 (2008).
113. Choi, J.W. et al. Hyperbranched beta-cyclodextrin polymer as an effective multidimensional binder for silicon anodes in lithium rechargeable batteries *Nano Lett.* **14**, 864-870 (2014).
114. Sunder, A., Frey, H., Thomann, R. & Mecking, S. Preparation of catalytically active palladium nanoclusters in compartments of amphiphilic hyperbranched polyglycerols. *Macromolecules* **33**, 3958-3960 (2000).
115. Haag, R. & Hebel, A. Polyglycerol as a high-loading support for boronic acids with application in solution-phase Suzuki cross-coupling. *J. Org. Chem.* **67**, 9452-9455 (2002).
116. Frey, H., Mulhaupt, R., Quincy, M. & Sunder, A. Hyperbranched polyether polyols with liquid crystalline properties. *Angew. Chem. Int. Ed.* **38**, 2928-2930 (1999).
117. Haag, R., Burakowska, E., Quinn, J.R. & Zimmerman, S.C. Cross-linked glycerol dendrimers and hyperbranched polymers as ionophoic, organic nanoparticles soluble in water and organic solvents. *Angew. Chem. Int. Ed.* **46**, 8164-8167 (2007).
118. Shen, Z., Chen, Y., Barriau, E. & H., F. Multi-arm star polyglycerol-block-poly(tert-butyl acrylate) and the respective multi-arm poly(acrylic acid) stars. *Macromol. Chem. Phys.* **207**, 57-64 (2006).
119. Frey, H. et al. ABA triblock copolymers based on linear poly(oxymethylene) and hyperbranched poly(glycerol): combining polyacetals and polyethers. *Macromolecules* **46**, 8845-8852 (2013).
120. Frey, H., Mulhaupt, R., Neuner, I., Sunder, A. & Burgath, A. Multi-arm star block copolymers based on epsilon-caprolactone with hyperbranched polyglycerol core. *Macromol. Chem. Phys.* **201**, 792-797 (2000).
121. Zentel, R., Frey, H., Schull, C. & Nuhn, L. Combining ring-opening multibranching and RAFT polymerization: multifunctional linear-hyperbranched block copolymers via hyperbranched macro-chain transfer agents. *Macromolecules* **46**, 2892-2904 (2013).
122. Haag, R., Landfester, K., Papp, I. & Sisson, A.L. Functional nanoparticles from dendritic precursors: hierarchical assembly in miniemulsions. *Macromolecules* **42**, 556-559 (2009).
123. Kang, E.T. et al. One-pot reaction for the large-scale synthesis of hyperbranched polyglycerol-grafted Fe_3O_4. *Dalton Trans.* **42**, 13642-13648 (2013).
124. Huang, J., Fu, Q. & Wan, D. Synthesis of a thioether modified hyperbranched polyglycerol and its template effect on fabrication of CdS and CdSe nanoparticles. *J. Appl. Polym. Sci.* **102**, 3679-3684 (2006).
125. Moore, E. et al. Surface-Initiated Hyperbranched Polyglycerol as an Ultralow-Fouling Coating on Glass, Silicon, and Porous Silicon Substrates. *ACS Appl. Mater. Interfaces* **6**, 15243-15252 (2014).

126. Mecking, S., Vogt, D., Schlotterbeck, U. & Sablong, R. Catalysis with soluble hybrids of highly branched macromolecules with palladium nanoparticles in a continuously operated membrane reactor. *Adv. Synth. Catal.* **345** (2003).
127. Zhou, L., Gao, C. & Xu, W. Robust Fe_3O_4/SiO_2-Pt/Au/Pd magnetic nanocatalysts with multifunctional hyperbranched polyglycerol amplifiers. *Langmuir* **26**, 11217-11225 (2010).
128. Kizhakkedathu, J.N., Brooks, D.E., Shenoi, R.A. & Imran ul-haq, M. Solvent-assisted anionic ring opening polymerization of glycidol: toward medium and high molecular weight hyperbranched polyglycerols. *J. Polym. Sci. A Polym. Chem.* **51**, 2614-2621 (2013).
129. Kainthan, R.K., Muliawan, E.B., Hatzikiriakos, S.G. & Brooks, D.E. Synthesis, Characterization, and Viscoelastic Properties of High Molecular Weight Hyperbranched Polyglycerols. *Macromolecules* **39**, 7708-7717 (2006).
130. Lu, J., Morgan, S., Ye, Z. & Xia, X. "Core-first" synthesis of multiarm star polyethylenes with a hyperbranched core and linear arms via ethylene multifunctional "living" polymerization with hyperbranched polyethylenes encapsulating multinuclear covalently tethered Pd-diimine catalysts. *Macromolecules* **43**, 4889-4901 (2010).
131. Lutz, P.J., Knischka, R., Frey, H., Mulhaupt, R. & Sunder, A. Funtional poly(ethylene oxide) multiarm star polymers: core-first synthesis using hyperbranched polyglycerol initiators. *Macromolecules* **33**, 315-320 (2000).
132. Mulhaupt, R., Frey, H., Sunder, A. & Maier, S. Synthesis of poly(glycerol)-block-poly(methyl acrylate) multi-arm star polymers. *Macromol. Rapid. Commun.* **21**, 226-230 (2000).
133. Liu, C., Zhang, Y. & Huang, J. Well-defined star polymers with mixed-arms by sequential polymerization of atom transfer radical polymerization and reverse addition-fragmentation chain transfer on a hyperbranched polyglycerol core. *Macromolecules* **41**, 325-331 (2008).
134. Controlled/Living Radical Polymerization: Progress in ATRP. (American Chemical Society, USA; 2009).
135. Controlled/Living Radical Polymerization: From Synthesis to Materials, Vol. 944. (Oxford University Press, 2006).
136. Controlled/Living Radical Polymerization: Progress in RAFT, DT, NMP, & OMRP. (Oxford University Press, 2006).
137. Matyjaszewski, K. Atom transfer radical polymerization (ATRP): current status and future perspectives. *Macromolecules* **45**, 4015-4039 (2012).
138. Matyjaszewski, K., Pintauer, T. & Coessens, V. Functional polymers by atom transfer radical polymerization. *Prog. Polym. Sci.* **26**, 337-377 (2001).
139. Yagci, Y., Kahveci, M.U. & Tasdelen, M.A. Telechelic polymers by living and controlled/living polymerization methods. *Prog. Polym. Sci* **36**, 455-567 (2011).
140. Hawker, C.J. et al. Metal-free atom transfer radical polymerization. *J. Am. Chem. Soc.* **136**, 16096-16101 (2014).
141. Ding, H. et al. Facile Arm-First Synthesis of Star Block Copolymers via ARGET ATRP with ppm Amounts of Catalyst. *Macromolecules* **49**, 6752-6760 (2016).
142. Min, K., Gao, H. & Matyjaszewski, K. Use of Ascorbic Acid as Reducing Agent for Synthesis of Well-Defined Polymers by ARGET ATRP. *Macromolecules* **40**, 1789-1791 (2007).

143. Kwak, Y., Magenau, A.J.D. & Matyjaszewski, K. ARGET ATRP of Methyl Acrylate with Inexpensive Ligands and ppm Concentrations of Catalyst. *Macromolecules* **44**, 811-819 (2011).
144. Konkolewicz, D. et al. Reversible-Deactivation Radical Polymerization in the Presence of Metallic Copper. A Critical Assessment of the SARA ATRP and SET-LRP Mechanisms. *Macromolecules* **46**, 8749-8772 (2013).
145. Konkolewicz, D. et al. SARA ATRP or SET-LRP. End of controversy? *Polym. Chem.* **5**, 4396-4417 (2014).
146. Krys, P., Wang, Y., Matyjaszewski, K. & Harrisson, S. Radical Generation and Termination in SARA ATRP of Methyl Acrylate: Effect of Solvent, Ligand, and Chain Length. *Macromolecules* **49**, 2977-2984 (2016).
147. Chmielarz, P. et al. Electrochemically mediated atom transfer radical polymerization (eATRP). *Prog. Polym. Sci.* **69**, 47-78 (2017).
148. Chmielarz, P., Krys, P., Park, S. & Matyjaszewski, K. PEO-b-PNIPAM Copolymers via SARA ATRP and eATRP in Aqueous Media. *Polymer* **71**, 143-147 (2015).
149. Cohen-Karni, D. et al. Grafting Challenging Monomers from Proteins using Aqueous ICAR ATRP under Bio-relevant Conditions. *Polym. Chem.* **8**, 3992-3998 (2017).
150. Simakova, A., Averick, S., Konkolewicz, D. & Matyjaszewski, K. Aqueous ARGET ATRP. *Macromolecules* **45**, 6371-6379 (2012).
151. Fantin, M., Isse, A.A., Gennaro, A. & Matyjaszewski, K. Understanding the Fundamentals of Aqueous ATRP and Defining Conditions for Better Control. *Macromolecules* **48**, 6862-6875 (2015).
152. Liu, X., Zhang, L., Cheng, Z. & Zhu, X. Metal-Free Photoinduced Electron Transfer-Atom Transfer Radical Polymerization (ET-ATRP) via a Visible Light Organic Photocatalyst. *Polym. Chem.* **7**, 689-700 (2016).
153. Yan, J. et al. Enhancing Initiation Efficiency in Metal-Free Surface-Initiated Atom Transfer Radical Polymerization (SI-ATRP). *ACS Macro Lett.* **5**, 661-665 (2016).
154. Treat, N.J. et al. Controlled Radical Polymerization of Acrylates Regulated by Visible Light. *ACS Macro Lett.* **3**, 580-584 (2014).
155. Thang, S.H. et al. Living free-radical polymerization by reversible addition-fragmentation chain transfer: the RAFT process. *Macromolecules* **31**, 5559-5562 (1998).
156. Thang, S.H., Rizzardo, E. & Moad, G. Living radical polymerization by the RAFT process. *Aust. J. Chem.* **58**, 379-410 (2005).
157. McCormick, C.L. & Lowe, A.B. Reversible addition-fragmentation chain transfer (RAFT) radical polymerization and the synthesis of water-soluble (co)polymers under homogeneous conditions in organic and aqueous media. *Prog. Polym. Sci* **32**, 283-351 (2007).
158. S., P. et al. Surface-initiated reversible addition-fragmentation chain transfer (RAFT) polymerization from fine particles functionalized with trithiocarbonates. *Macromolecules* **44**, 8944-8953 (2011).
159. Charleux, B. et al. Nitroxide-mediated polymerization. *Prog. Polym. Sci* **38**, 63-235 (2013).
160. Harth, E., Bosman, A.W. & Hawker, C.J. New polymer synthesis by nitroxide mediated living radical polymerization. *Chem. Rev.* **101**, 3661-3688 (2001).
161. Chauvin, F. et al. Nitroxide-Mediated Polymerization: The Pivotal Role of the k_d Value of the Initiating Alkoxyamine and the Importance of the Experimental Conditions. *Macromolecules* **39**, 5238-5250 (2006).

162. C., D., Jerome, R. & Sciannamea, V. In-situ nitroxide-mediated radical polymerization (NMP) processes: their understanding and optimization. *Chem. Rev.* **108**, 1104-1126 (2008).
163. Bock, V.D., Hiemstra, H. & van Maarseveen, J.H. Cu-I-catalyzed alkyne-azide "click" cycloadditions from a mechanistic and synthetic perspective. *Eur. J. Org. Chem.*, 51-68 (2006).
164. Moses, J.E. & Morrhouse, A.D. The Growing Applications of Click Chemistry. *Chem. Soc. Rev.* **36**, 1249-1262 (2007).
165. Zubarev, E.R., Kupstov, S.A., Yuranova, T.I., Talroze, R.V. & Finkelmann, H. Monodomain Liquid Crystalline Networks: Reorientation Mechanism from Uniform to Stripe Domains *Liq. Cryst.* **26**, 1531-1540 (1999).
166. Zubarev, E.R., Talroze, R.V., Yuranova, T.I., Plate, N.A. & Finkelmann, H. Influence of Network Topology on Polydomain-Monodomain Transition in Side Chain Liquid Crystalline Elastomers with Cyanobiphenyl mesogens. *Macromolecules* **31**, 3566-3570 (1998).
167. Liquid Crystals: Frontiers in Biomedical Applications. (World Scientific Publishing Co. Pte. Ltd., 2007).
168. Qi, H. & Hegmann, T. Impact of nanoscale particles and carbon nanotubes on current and future generations of liquid crystal displays. *J. Mater. Chem.* **18**, 3288-3294 (2008).
169. Lagerwall, J.P.F. & Scalia, G. A new era for liquid crystal research: Applications of liquid crystals in soft matter nano-, bio- and microtechnology. *Curr. Appl. Phys.* **12**, 1387-1412 (2012).
170. Basu, R. & Iannacchione, G. Evidence for directed self-assembly of quantum dots in a nematic liquid crystal. *Phys. Rev. E* **80** (2009).
171. Bitar, R., Agez, G. & Mitov, M. Cholesteric liquid crystal self-organization of gold nanoparticles. *Soft Matter* **7**, 8198-8206 (2011).
172. Draper, M. et al. Self-Assembly and Shape Morphology of Liquid-Crystalline Gold Metamaterials. *Adv. Func. Mater.* **21**, 1260-1278 (2011).
173. Hirst, L.S., Kirchhoff, J., Inman, R. & Ghosh, S. in Emerging Liquid Crystal Technologies V, Vol. 7618. (ed. L.C. Chien) (Spie-Int Soc Optical Engineering, Bellingham; 2010).
174. Mitov, M., Bourgerette, C. & de Guerville, F. Fingerprint patterning of solid nanoparticles embedded in a cholesteric liquid crystal. *J. Phys. Condens. Matter* **16**, S1981-S1988 (2004).
175. Payne, J.C. & Thomas, E.L. Towards an understanding of nanoparticle-chiral nematic liquid crystal co-assembly. *Adv. Func. Mater.* **17**, 2717-2721 (2007).
176. Qi, H. & Hegmann, T. Formation of periodic stripe patterns in nematic liquid crystals doped with functionalized gold nanoparticles. *J. Mater. Chem.* **16**, 4197-4205 (2006).
177. Shivakumar, U. et al. Nanoparticles: complex and multifaceted additives for liquid crystals. *Liq. Cryst.* **38**, 1495-1514 (2011).
178. Handbook of Nanophysics: Nanoparticles and Quantum Dots, Vol. 3. (CRC Press, 2011).
179. Handbook of Nanophysics: Principles and Methods, Vol. 1. (CRC Press, 2011).
180. Zhu, M.Z. et al. Chiral Au-25 Nanospheres and Nanorods: Synthesis and Insight into the Origin of Chirality. *Nano Lett.* **11**, 3963-3969 (2011).
181. Kinkead, B. & Hegmann, T. Effects of size, capping agent, and concentration of CdSe and CdTe quantum dots doped into a nematic liquid crystal on the optical and electro-optic properties of the final colloidal liquid crystal mixture. *J. Mater. Chem.* **20**, 448-458 (2010).

182. Slocik, J.M., Govorov, A.O. & Naik, R.R. Plasmonic Circular Dichroism of Peptide-Functionalized Gold Nanoparticles. *Nano Lett.* **11**, 701-705 (2011).
183. Tamborra, M. et al. Optical properties of hybrid composites based on highly luminescent CdS nanocrystals in polymer. *Nanotechnology* **15**, S240-S244 (2004).
184. Qi, H., Kinkead, B. & Hegmann, T. Unprecedented Dual Alignment Mode and Freedericksz Transition in Planar Nematic Liquid Crystal Cells Doped with Gold Nanoclusters. *Adv. Func. Mater.* **18**, 212-221 (2008).
185. Oh, H.S. et al. Chiral Poly(fluorene-alt-benzothiadiazole) (PFBT) and Nanocomposites with Gold Nanoparticles: Plasmonically and Structurally Enhanced Chirality. *J. Am. Chem. Soc.* **132**, 17346-17348 (2010).
186. Alam, M.Z., Yoshioka, T., Ogata, T., Nonaka, T. & Kurihara, S. Influence of helical twisting power on the photoswitching behavior of chiral azobenzene compounds: Applications to high-performance switching devices. *Chem. Eur. J.* **13**, 2641-2647 (2007).
187. Christofi, A., Stefanou, N., Gantzounis, G. & Papanikolaou, N. Giant Optical Activity of Helical Architectures of Plasmonic Nanorods. *J. Phys. Chem. C* **116**, 16674-16679 (2012).
188. Grzelczak, M., Vermant, J., Furst, E. & Liz-Marzan, L. Directed Self-assembly of Nanoparticles. *ACS Nano* **4**, 3591-3605 (2010).
189. Coursault, D. et al. Linear Self-Assembly of Nanoparticles Within Liquid Crystal Defect Arrays. *Adv. Mater.* **24**, 1461-1465 (2012).
190. Gautier, C. & Burgi, T. Chiral Gold Nanoparticles. *Chemphyschem* **10**, 483-492 (2009).
191. Thermal Analysis of Polymers. (Wiley, Hoboken, NJ; 2009).
192. Fan, J., Boettcher, S.W. & Stucky, G.D. Nanoparticle assembly of ordered multicomponent mesostructured metal oxides via a versatile sol-gel process. *Chem. Mater.* **18**, 6391-6396 (2006).
193. Gao, H. & Matjaszewski, K. Synthesis of Star Polymers by a Combination of ATRP and the "Click" Coupling Method. *Macromolecules* **39**, 4960-4965 (2006).
194. Fan, X.W., Lin, L.J. & Messersmith, P.B. Surface-initiated polymerization from TiO2 nanoparticle surfaces through a biomimetic initiator: A new route toward polymer-matrix nanocomposites. *Compos. Sci. Technol.* **66**, 1198-1204 (2006).
195. Moses, J.E. & Moorhouse, A.D. The growing applications of click chemistry. *Chem. Soc. Rev.* **36**, 1249-1262 (2007).
196. Tang, E.J., Cheng, G.X., Ma, X.L., Pang, X.S. & Zhao, Q. Surface modification of zinc oxide nanoparticle by PMAA and its dispersion in aqueous system. *Appl. Surf. Sci.* **252**, 5227-5232 (2006).
197. Zhao, L., Goodman, M., Bowden, N. & Lin, Z. Self-assembly of Ultra-high-molecular-weight Comb Block Copolymer at the Air-Water Interface. *Soft Matter* **5**, 4698-4703 (2009).
198. Douglas, T. et al. Protein Engineering of a Viral Cage for Constrained Nanomaterials Synthesis. *Adv. Mater.* **14**, 415-418 (2002).
199. Uchida, M. et al. Biological Containers: Protein Cages as Multifunctional Nanoplatforms. *Adv. Mater.* **19**, 1025-1042 (2007).
200. Muller, A.H.E. & Zhang, M. Cylindrical polymer brushes. *J. Polym. Sci. A Polym. Chem.* **43**, 3461-3481 (2005).
201. Zhang, J., Coombs, N., Kumacheva, E., Lin, Y. & Sargent, E. A new approach to hybrid polymer-metal and polymer-semiconductor particles. *Adv. Mater.* **14**, 1756-1759 (2002).
202. Kramer, R.M., Li, C., Carter, D.C., Stone, M.O. & Naik, R.R. Engineered Protein Cages for Nanomaterial Synthesis. *J. Am. Chem. Soc.* **126**, 13282-13286 (2004).

203. Ueno, T. et al. Size-Selective Olefin Hydrogenation by a Pd Nanocluster Provided in an Apo-Ferritin Cage. *Angew. Chem. Int. Ed.* **43**, 2527-2530 (2004).
204. Jin, Y. & Gao, X. Plasmonic Fluorescent Quantum Dots. *Nat. Nanotechnol.* **4**, 571-576 (2009).
205. Suzuki, K., Sato, S. & Fujita, M. Template Synthesis of Precisely Monodisperse Silica Nanoparticles within Self-Assembled Organometallic Spheres. *Nat. Chem.* **2**, 25-29 (2009).
206. Naik, R.R., Stringer, S.J., Agarwal, G., Jones, S.E. & Stone, M.O. Biomimetic Synthesis and Patterning of Silver Nanoparticles. *Nat. Mater.* **1**, 169-172 (2002).
207. Braun, E., Eichen, Y., Sivan, U. & Ben-Yoseph, G. DNA-Templated Assembly and Electrode Attachment of a Conducting Silver Wire. *Nature* **391**, 775-778 (1998).
208. Liu, J. et al. Metallization of Branched DNA Origami for Nanoelectronic Circuit Fabrication *ACS Nano* **5**, 2240-2247 (2011).
209. Mertig, M., Ciacchi, L.C., Seidel, R. & Pompe, W. DNA as a Selective Metallization Template. *Nano Letters* **2**, 841-844 (2002).
210. Zhao, M., Sun, L. & Crooks, R.M. Preparation of Cu Nanocluters within Dendrimer Templates. *J. Am. Chem. Soc.* **120**, 4877-4878 (1998).
211. Yeung, L.E., Chechik, V., Sun, L., Zhao, M. & Crooks, R.M. Dendrimer-Encapsulated Metal Nanoparticles: Synthesis, Characterization, and Applications to Catalysis. *Acc. Chem. Res.* **34**, 181-190 (2001).
212. Jankova, K., Bednarek, M. & Hvilsted, S. Star polymers by ATRP of styrene and acrylates employing multifunctional initiators. *J. Polym. Sci. A Polym. Chem.* **43**, 3748-3759 (2005).
213. Doganci, E., Tasdelen, M.A. & Yilmaz, F. Synthesis of miktoarm star-shaped polymers with POSS core via a combination of CuAAC click chemistry, ATRP, and ROP techniques. *Macromol. Chem. Phys.* **216**, 1823-1830 (2015).
214. Wei, H., Wang, C.E., Tan, N., Boydston, A.J. & Pun, S.H. ATRP synthesis of sunflower polymers using cyclic multimacroinitiators. *ACS Macro Lett.* **4**, 938-941 (2012).
215. Christ, E., Muller, S., Berger, N., E. & Frey, H. Hydroxyfunctional Oxetane-Inimers with Varied Polarity for the Synthesis of Hyperbranched Polyether Polyols via Cationic ROP. *J. Polym. Sci. A Polym. Chem.* **52**, 2850-2859 (2014).
216. Sunder, A., Mulhaupt, R. & Frey, H. Hyperbranched polyether-polyols based on polyglycerol: polarity design by block copolymerization with propylene oxide. *Macromolecules* **33**, 309-314 (2000).
217. Klein, R. et al. ABA triblock copolymers based on linear poly(oxymethylene) and hyperbranched poly(glycerol): combining polyacetals and polyethers. *Macromolecules* **46**, 8845-8852 (2013).
218. Sisson, A.L., Papp, I., Landfester, K. & Haag, R. Functional nanoparticles from dendritic precursors: hierarchical assembly in miniemulsions. *Macromolecules* **42**, 556-559 (2009).
219. Chen, Y., Shen, Z., Barriau, E., Kautz, H. & Frey, H. Synthesis of multiarm star poly(glycerol)-block-poly(2-hydroxyethyl methacrylate). *Biomacromolecules* **7**, 919-926 (2006).
220. Sunder, A., Bauer, T., Mulhaupt, R. & Frey, H. Synthesis and thermal behavior of esterified aliphatic hyperbranched polyether polyols. *Macromolecules* **3**, 1330-1337 (2000).
221. Wan, D., Li, Z. & Huang, J. Synthesis of a new type of core-shell particle from hyperbranched polyglycerol. *J. Polym. Sci. A Polym. Chem.* **43**, 5458-5464 (2005).
222. Mesias, R. & Murillo, E. Hyperbranched polyester polyol modified with polylactic acid. *J. Appl. Polym. Sci.* **132**, 41589-41597 (2015).

223. Mecking, S., Thomann, R., Frey, H. & Sunder, A. Preparation of catalytically active palladium nanoclusters in compartments of amphiphilic hyperbranched polyglycerols. *Macromolecules* **33**, 3958-3960 (2000).
224. He, M. et al. Monodisperse Dual-Functional Upconversion Nanoparticles-Enabled Near-Infrared Organolead Halide Perovskite Solar Cells. *Angew. Chem. Int. Ed.* **55**, 4280-4284 (2016).
225. Xu, H. et al. A General Route to Nanocrystal Kebabs Periodically Assembled on Stretched Flexible Polymer Shish. *Sci. Adv.* **1**, 1-11 (2015).
226. Jiang, B., Pang, X., Li, B. & Lin, Z. Organic-Inorganic Nanocomposites via Placing Monodisperse Ferroelectric Nanocrystals in Direct and Permanent Contact with Ferroelectric Polymers. *J. Am. Chem. Soc.* **137**, 11760-11767 (2015).
227. Yang, D. et al. Precisely Size-Tunable Magnetic/Plasmonic Core/Shell Nanoparticles with Controlled Optical Properties. *Angew. Chem. Int. Ed.* **54**, 12091-12096 (2015).
228. Xu, H. et al. An Unconventional Route to Monodisperse and Intimate Semiconducting Organic-Inorganic Nanocomposites. *Angew. Chem. Int. Ed.* **54**, 4636-4640 (2015).
229. Zheng, D. et al. Unconventional Route to Hairy Plasmonic/Semiconductor Core/Shell Nanoparticles with Precisely Controlled Dimensions and Their Use in Solar Energy Conversion. *Chem. Mater.* **27**, 5271-5278 (2015).
230. Lai, C. et al. Highly, luminescent homogeneous ZnO nanoparticles synthesized *via* semiconductive polyalkylthiophene template. *J. Mater. Chem.* **19**, 7284-7289 (2009).
231. Lai, C. et al. Homogeneous, surfactant-free gold nanoparticles encapsulated by polythiophene analogues. *ChemComm* **2009**, 1996-1998 (2009).
232. Zhou, L., Gao, C., Hu, X. & Xu, W. General Avenue to Multifunctional Aqueous Nanocrystals Stabilized by Hyperbranched Polyglycerol. *Chem. Mater.* **23**, 1461-1470 (2011).
233. Jiang, G., Wang, L., Chen, T., Chen, C. & Yu, H. Synthesis of multi-arm star polystyrene with hyperbranched polyester initiators by atom transfer radical polymerization. *J. Appl. Polym. Sci.* **99**, 728-733 (2006).
234. Jiang, G., Wang, L. & Chen, W. Synthesis of multi-arm star polystyrene with hyperbranched polyether core. *Eur. Polym. J.* **42**, 3333-3340 (2006).
235. Huang, S. et al. Development of NIR-II Fluorescence Image-guided and pH-Responsive Nanocapsules for Cocktail Drug Delivery. *Nano. Res.* **8**, 1932-1943 (2015).
236. O'Brien, J., Lee, S., Onogi, S. & Shea, K.J. Engineering the Protein Corona of a Synthetic Polymer Nanoparticle for Broad-Spectrum Sequestration and Neutralization of Venemous Biomacromolecules. *J. Am. Chem. Soc.* **138**, 16604-16607 (2016).
237. Liao, J. et al. Polymer Hybrid Magnetic Nanocapsules Encapsulating IR820 and PTX for External Magnetic Field-Guided Tumor Targeting and Multifunctional Theranostics. *Nanoscale* **9**, 2479-2491 (2017).
238. Musyanovych, A. & Landfester, K. Polymer Micro- and Nanocapsules as Biological Carriers with Multifunctional Properties. *Macromol. Biosci.* **14**, 458-477 (2014).
239. Geng, Q., Xiao, J., Yang, B., Wang, T. & J., D. Rationally Engineering Dual Missions in One Statistical Copolymer Nanocapsule: Bacterial Inhibition and Polycyclic Aromatic Hydrocarbon Capturing. *ACS Macro Lett.* **4**, 511-515 (2015).
240. Kim, M., Dergunov, S.A. & Pinkhassik, E. Directed Assembly of Vesicle-Templated Polymer Nanocapsules under Near-Physiological Conditions. *Langmuir* **31**, 2561-2568 (2015).
241. Lin, W., Sun, T., Xie, Z., Gu, J. & Jing, X. A Dual-Responsive Nanocapsule via Disulfide-Indicued Self-Assembly for Therapeutic Agent Delivery. *Chem. Sci.* **7**, 1846-1852 (2016).

242. Mora-Huertas, C.E., Fessi, H. & Elaissari, A. Polymer-Based Nanocapsules for Drug Delivery. *Int. J. Pharm.* **385**, 113-142 (2010).
243. Li, X. et al. Monodisperse Cylindrical Micelles of Controlled Length with a Liquid-Crystalline Perfluorinated Core by 1D "Self-Seeding". *Angew. Chem. Int. Ed.* **55**, 11392-11396 (2016).
244. Nazemi, A. et al. Monodisperse Cylindrical Micelles and Block Comicelles of Controlled Length in Aqueous Media. *J. Am. Chem. Soc.* **138**, 4484-4493 (2016).
245. Wang, X. et al. Cylindrical Block Copolymer Micelles and Co-Micelles of Controlled Length and Architecture. *Science* **317**, 644-647 (2007).
246. Owen, S.C., Chan, D.P.Y. & Shoichet, M.S. Polymeric Micelle Stability. *Nano Today* **7**, 53-65 (2012).
247. Bazzano, M. et al. Synthesis of Polymeric Nanocapsules by Radical UV-Activated Interface-Emulsion Polymerization. *J. Polym. Sci. A Polym. Chem.* **54**, 3357-3369 (2016).
248. Marturano, V. et al. Photo-Responsie Polymer Nanocapsules. *Polymer* **70**, 222-230 (2015).
249. Tian, H. et al. Growth-Factor Nanocapsules that Enable Tunable Controlled Release for Bone Regeneration. *ACS Nano* **10**, 7362-7369 (2016).
250. Chen, T., Du, B., Zhang, X. & Fan, Z. Fabrication of Polymer Nanocapsules with Controllable Oligo(Ethylene Glycol) Densities, Permeation Properties and Robustly Crosslinked Walls. *ACS Appl. Mater. Interfaces* **5**, 3748-3756 (2013).
251. Kim, D. et al. Direct Synthesis of Polymer Nanocapsules: Self-Assembly of Polymer Hollow Spheres through Irreversible Covalent Bond Formation. *J. Am. Chem. Soc.* **132**, 9908-9919 (2010).
252. Kim, E. et al. Facile, Template-Free Synthesis of Stimuli-Responsive Polymer Nanocapsules for Targeted Drug Delivery. *Angew. Chem. Int. Ed.* **49**, 4405-4408 (2010).
253. Liu, X. & Basu, A. Core Functionalization of Hollow Polymer Nanocapsules. *J. Am. Chem. Soc.* **131**, 5718-5719 (2009).
254. Wajs, E., Nielsen, T., Larsen, K.L. & Fragoso, A. Preparation of Stimuli-Responsive Nano-Sized Capsules Based on Cyclodextrin Polymers with Redox or Light Switching Properties. *Nano. Res.* **9**, 2070-2078 (2016).
255. Yan, L. et al. Selectively Grafting Polymer from the Interior and/or Exterior Surfaces of Bioreducible and Temperature-Responsive Nanocapsules. *Polym. Chem.* **4**, 1243-1249 (2013).
256. Wei, W. et al. Template Synthesis of Hydrogel Composite Hollow Spheres Against Polymeric Hollow Latex. *Colloid Polym. Sci.* **286**, 881-888 (2008).
257. Sheng, D. & Sun, C. Synthesis of Monodisperse Hollow Polyaniline Spheres with Nonsulfonated Latex Template. *Chem. Lett.* **40**, 153-155 (2011).
258. de Mello Donega, C., Liljeroth, P. & Vanmaekelbergh, D. Physiochemical Evaluation of the Hot-Injection Method, a Synthesis Route for Monodisperse Nanocrystals. *Small* **1**, 1152-1162 (2005).
259. Trewyn, B., Slowing, I., Giri, S., Chen, H. & Lin, V. Synthesis and Functionalization of a Mesoporous Silica Nanoparticle Based on the Sol-Gel Process and Applications in Controlled Release. *Acc. Chem. Res.* **40**, 846-853 (2007).
260. Grzelczak, M., Perez-Juste, J., Mulvaney, P. & Liz-Marzan, L.M. Shape Control in Gold Nanoparticle Synthesis. *Chem. Soc. Rev.* **37**, 1783-1791 (2008).
261. Nikoobakht, B. & El-Sayed, M. Preparation and Growth Mechanism of Gold Nanorods (NRs) Using Seed-Mediated Growth Method. *Chem. Mater.* **15**, 1957-1962 (2003).

262. Fukuoka, A. et al. Template Synthesis of Nanoparticle Arrays of Gold, Platinum and Palladium in Mesoporous Silica Films and Powders. *J. Mater. Chem.* **14**, 752-756 (2004).
263. Titirici, M., Antonietti, M. & Thomas, A. A Generalized Synthesis of Metal Oxide Hollow Spheres Using a Hydrothermal Approach. *Chem. Mater.* **18**, 3808-3812 (2006).
264. Jones, M., Ranger, M. & Leroux, J. pH-Sensitive Unimolecular Polymeric Micelles: Synthesis of a Novel Drug Carrier. *Bioconjugate Chem.* **14**, 774-781 (2003).
265. Liu, M., Kono, K. & Frechet, J. Water-Soluble Dendritic Unimolecular Micelles: Their Potential as Drug Delivery Agents. *J. Control. Release* **65**, 121-131 (2000).
266. Li, X. et al. Amphiphilic Multiarm Star Block Copolymer-Based Multifunctional Unimolecular Micelles for Cancer Targeted Drug Delivery and MR Imaging. *Biomaterials* **32**, 6595-6605 (2011).
267. Iocozzia, J. & Lin, Z. Solution-Stable Colloidal Gold Nanoparticles via Surfactant-Free, Hyperbranched Polyglycerol-*b*-Polystyrene Unimolecular Templates. *Langmuir* **32**, 7180-7188 (2016).
268. Zhang, W. & Muller, A. Architecture, Self-Assembly and Properties of Well-Defined Hybrid Polymers Based on Polyhedral Oligomeric Silsesquioxane (POSS). *Prog. Polym. Sci* **38**, 1121-1162 (2013).
269. Liu, H., Yang, P. & Wan, D. The Accessibility of a Unimolecular Micelle's Core to Environmental Ions: Exploration with a Xanthene Dye. *Polym. Phys.* **53**, 566-573 (2015).
270. Fan, X., Li, Z. & Loh, X. Recent Development of Unimolecular Micelles as Functional Materials and Applications. *Polym. Chem.* **7**, 5898-5919 (2016).
271. Liu, G. et al. DACHPt-loaded Unimolecular Micelles Based on Hydrophilic Dendritic Block Copolymers for Enhanced Therapy of Lung Cancer. *ACS Appl. Mater. Interfaces* **9**, 112-119 (2017).
272. Mohammadifar, E. et al. Green Synthesis of Hyperbranched Polyglycerol at Room Temperature. *ACS Macro Lett.* **6**, 35-40 (2017).
273. Xu, Z. et al. Biocompatible Hyperbranched Polyglycerol Modified Beta-Cyclodextrin Derivatives for Docetaxel Delivery. *Mater. Sci. Eng. C Mater. Biol. Appl.* **71**, 965-972 (2017).
274. Kim, Y. et al. Photocrosslinkable Poly(epsilon-caprolactone)-*b*-Hyperbranched Polyglycerol (PCL-*b*-hbPG) with Improved Biocompatibility and Stability for Drug Delivery. *Macromol. Chem. Phys.* **216**, 1161-1170 (2015).
275. Kumar, S. et al. Impact of Structural Differences in Hyperbranched Polyglycerol-Polyethylene Glycol Nanoparticles on Dermal Drug Delivery and Biocompatibility. *Eur. J. Pharm. Biopharm.* **88**, 625-634 (2014).
276. Venkateswaran, S. et al. Fortified Interpenetrating Polymers-Bacteria Resistant Coating for Medical Devices. *J. Mater. Chem. B* **4**, 5405-5411 (2016).
277. Yu, Y. & Frey, H. Controllable Nonspecific Protein Adsorption by Charged Hyperbranched Polyglycerol Thin Films. *Langmuir* **31**, 13101-13106 (2015).
278. Das, P. & Jana, N.R. Highly Colloidally Stable Hyperbranched Polyglycerol Grafted Red Fluorescent Silicon Nanoparticle as Bioimaging Probe. *ACS Appl. Mater. Interfaces* **6**, 4301-4309 (2014).
279. Dong, C. et al. A Highly Photostable Hyperbranched Polyglycerol-Based NIR Fluorescence Nanoplatform for Mitochondria-Specific Cell Imaging. *Adv. Healthcare Mater.* **5**, 2214-2226 (2016).
280. Li, H. & Cooper-White, J.J. Hyperbranched Polymer Mediated Fabrication of Water Soluble Carbon Nanotube-Metal Nanoparticle Hybrids. *Nanoscale* **5**, 2915-2920 (2013).

281. Zhou, L. et al. Multihydroxy Dendritic Upconversion Nanoparticles with Enhanced Water Dispersibility and Surface Functionality for Bioimaging. *ACS Appl. Mater. Interfaces* **6**, 7719-7727 (2014).
282. Steinhilber, D. et al. Hyperbranched Polyglycerols on the Nanometer and Micrometer Scale. *Biomaterials* **32**, 1311-1316 (2011).
283. Wu, C., Bottcher, C. & Haag, R. Enzymatically Crosslinked Dendritic Polyglycerol Nanogels for Encapsulation of Catalytically Active Proteins. *Soft Matter* **11**, 972-980 (2015).
284. Akhrass, S. et al. Design of Crosslinked Hybrid Multilayer Thin Films from Azido-Functionalized Polystyrenes and Platinum Nanoparticles. *Soft Matter* **5**, 586-592 (2009).
285. Bang, J. et al. Facile Routes to Patterned Surface Neutralization Layers for Block Copolymer Lithography. *Adv. Mater.* **19**, 4552-4557 (2007).
286. Yoo, M. et al. Facile Synthesis of Thermally Stable Core-Shell Gold Nanoparticles via Photo-Cross-linkable Polymeric Ligands. *Macromolecules* **43**, 3570-3575 (2010).
287. Albuszis, M., Roth, P.J., Pauer, W. & Moritz, H. Two In One: Use of Azide Functionality for Controlled Photo-Crosslinking and Click-Modification of Polymer Microspheres. *Polym. Chem.* **7**, 5414-5425 (2016).
288. Moon, H.K., Kang, S. & Yoon, H. Aziridine-functionalized Polydimethylsiloxanes for Tailorable Polymeric Scaffolds: Aziridine as a Clickable Moiety for Structural Modification of Materials. *Polym. Chem.* **8**, 2287-2291 (2017).